Investigation of the *Plasmodium falciparum* RH5-Interacting Protein (PfRIPR) as a blood-stage malaria vaccine target



A Thesis submitted in fulfilment of the requirements for the degree of Doctor of Philosophy

Barnabas G. Williams
Nuffield Department of Clinical Medicine
The Jenner Institute
Kellogg College

Hilary term 2021

Prof. Simon Draper
Prof. Matt Higgins

Approximately 48,700 words (excluding References and Appendices)

Abstract

Malaria is an ancient disease that still affects millions of people in endemic regions. Despite ongoing global efforts to produce a vaccine against the malaria parasite, chiefly *Plasmodium falciparum*, an effective vaccine is not yet available. In recent years, new highly conserved blood-stage vaccine candidates have emerged including PfRH5, now being investigated in clinical trials. PfRH5 forms the 'RCR' complex with two other proteins, PfRIPR and PfCyRPA; this essential and highly conserved complex is critical for merozoite invasion of erythrocytes. Here, PfRIPR is investigated as a potential new blood-stage vaccine candidate. PfRIPR is a large and complex protein containing of 10 EGF-like domains. Antibodies raised against full-length PfRIPR are effective at blocking merozoite invasion of erythrocytes *in vitro*, however, beyond this our knowledge is sorely lacking. My work shows that the epitopes of neutralising antibodies fall exclusively within a small region of PfRIPR corresponding to EGF-like domains 5-8. I demonstrate that immunisation with PfRIPR EGF (5-8) protein yields a four-fold improvement in antigen-specific IgG quality compared with full-length PfRIPR. In addition, I show that monoclonal antibodies raised against PfRIPR EGF (5-8) can block merozoite invasion of erythrocytes whereas antibodies that bind outside this region do not. Co-immunisation of PfRIPR with either PfRH5, PfCyRPA, or all three proteins has revealed a complex relationship between the antigens. PfRIPR is the most immunodominant of the three antigens but yields the least potent IgG. These experiments also strongly suggest that co-immunisation leads to inter-antigen synergy which improves the potency of the IgG response. This work provides a platform for second-generation PfRIPR vaccines based on PfRIPR EGF (5-8) to be developed and tested in conjunction with PfRH5 and PfCyRPA.

It is the glory of God to conceal things,

but the glory of kings is to search things out.

Proverbs 25 v2

Acknowledgments

First and foremost, I would like to thank my supervisors Prof. Simon Draper and Prof. Matt Higgins. I would like to especially thank Simon, for taking a risk on an unknown student who emailed him out of the blue looking to move group; I couldn't have asked for a better supervisor or group to work with. I am constantly impressed by your commitment to scientific rigour and quality, following the data wherever it may lead. You bring out the best in the people you mentor and I am grateful to have been given the opportunity to work in your group. To Matt, your calm demeanour and clear insight into this project was always a welcome breath of fresh air. I feel a pang of sadness that the pandemic prevented me from completing the planned structural work in your lab during this DPhil.

To my former managers at OXB, Dr Hannah Stewart and Dr Helen Maunder. Thank you for inspiring me and giving me the confidence to embark upon this DPhil (despite your best efforts to dissuade me!).

Thank you to University of Oxford, Medical Research Council Doctoral Training Partnership for funding this DPhil, and my Oxford college, Kellogg College.

Next, I would like to thank the whole of the Draper group for making the lab such a fun and supportive place to work. I would like to especially thank the post-docs: Kirsty, Martino, David, Carolyn, Lloyd, and Giacomo for sharing their extensive scientific experience and their endless patience with me. Doris and Amelia for running more GIA assays than I can count, Sarah and Jordan for answering every ELISA question, Hannah for providing HEK cells and proteins at all times, Fran and Rob for their camaraderie, humorous science chat and sharing life together. Kate

and Patries for their organisation, answering my never-ending series of questions, and ensuring I get my stipend.

To those outside the Draper group, thank you to Dave M, Katie E and Danielle from TBV for their chat and TC4 rage. The 'kitchen quad squad' Ciaran, Hannah, Jyothi and Fran – sadly broken up by 2m social distancing rules. Danny, Duncan, Dre, Jeremy, Helen, Indra, Sue and Sean & others for making the lab office a fun place to be on any day. Special thanks go to Julie, Mariya, Rhianon and Drew for juggling a thousand tasks to make the Jenner run smoothly. In addition, I would like to thank Kazutoyo Miura at the NIH for his expertise and collaboration.

Thank you to all of those outside the lab bubble: my college friends for all the Monday burgers nights and weekend chats – Bronwyn (aka B-Star), Alex, Simi & Katherine (the MCR dream team), Sarah (and her maddening American positivity), Thea (who is so Canadian she apologised for being supportive), Bastiaan, Jasmine, Ian M, Freddie and Alexa. To my housemates Scott and Ian O for helping me survive lockdown and teaching me how to cook well. My friends from St Ebbe's past and present, in particular Tim Crothers who taught me to relax and enjoy DPhil life in his own sarcastic Northern Irish way, and James Duncan who was always on hand for whatever life threw my way.

Finally, I would like to thank my family. My brothers, Sam and Bo, for all fun times we've had over the years, and my parents, Paul and Julie, for the unending support and encouragement from day one.

Contents

Chapter 1 - Introduction 1

1.1 Malaria 1

1.1.1 The global state of malaria disease 1

1.1.2 Malaria life-cycle and pathogenesis 3

1.1.3 Naturally acquired immunity 6

1.2 Vaccines against malaria 8

1.2.1 Pre-erythrocytic vaccines 12

1.2.2 RTS,S / AS01 12

1.2.3 R21 13

1.2.4 Thrombospondin-Related Adhesion Protein (ME-TRAP) 13

1.2.5 PfCelTOS 14

1.2.6 Transmission blocking vaccines (TBV) 15

1.2.7 Pfs25 15

1.2.8 Pfs230 D1M 16

1.2.9 Pfs48/45 16

1.2.10 Blood stage vaccines 17

1.2.11 Erythrocyte invasion by merozoites 19

1.2.12 PfAMA1/PfRON2 22

1.2.13 *P. falciparum* Reticulocyte-binding protein Homologue 5 (PfRH5) 23

1.2.14 *P. falciparum* Cysteine Rich Protective Antigen (PfCyRPA) 26

1.2.15 *P. falciparum* PfRH5 Interacting Protein (PfRIPR) 28

1.3 Structure based vaccine design 34

1.4 Thesis aims and overview 35

Chapter 2 - Materials and Methods 37

2.1 Chapter 3 methods 37

2.1.1 Expression constructs 37

2.1.2 Construction of PfRIPR fragment plasmids 37

2.1.3 Plasmid preparation and *E. coli* culture 39

2.1.4 Sequencing 39

2.1.5 Cell culture 39

2.1.6 Generating stably transfected S2 cell lines 40

2.1.7 PfRIPR fragment production 41

2.1.8 Removal of monomeric Fc domain 42

2.1.9 Mass Spectrometry 43

2.1.10 Protein quantification 43

2.1.11 SDS-PAGE and western blots 43

2.1.12 Dot blot arrays for non-functional PfRIPR mAbs 44

2.1.13 Protein complex analysis with size exclusion chromatography 44

2.1.14 Peptide ELISA for determining PfRIPR linear epitopes 45

2.1.15 SPR assay for anti-PfRIPR mAbs 45

2.1.16 Production of red blood cell receptors 46
2.1.17 SPR assay for anti-PfRIPR mAbs 46
2.1.18 Rabbit immunisations 47
2.1.19 Purification of IgG from sera 47
2.1.20 Parasite culture and Growth inhibitory activity assay 48
2.1.21 Growth inhibitory activity (GIA) assay 49
2.1.22 GIA reversal assays 49
2.1.23 Statistical analysis 50
2.2 Chapter 4 methods 51
2.2.1 Conjugation to hepatitis B surface antigen (HBsAg) 51
2.2.2 Dynamic light scattering (DLS) 52
2.2.3 Endotoxin testing 52
2.2.4 Mouse vaccination studies 52
2.2.5 Optical density (OD) ELISAs 53
2.2.6 Rat pilot study immunisations 53
2.2.7 Study O1, O2 and O3 rat immunisations. 54
2.2.8 Rat IgG standardised quantitative ELISAs 55
2.2.9 Purification of IgG from rats and mice 57
2.2.10 Growth inhibitory activity assay 57
2.2.11 Growth inhibitory activity assay quality analysis 57
2.3 Chapter 5 methods 58

2.3.1 Mouse immunisations 58
2.3.2 Hybridoma generation 58
2.3.3 Hybridoma culture 60
2.3.4 Monoclonal antibody purification 60
2.3.5 Construction of an PfRIPR protein fragment tetramer 61
2.3.6 Single sorting IgG producing B-cells 61
2.3.7 Variable region PCR and cloning 61
2.3.7.1 In-house PCR method 62
2.3.7.2 PCR method based on Ho et al 62
2.3.7.3 Kappa PCR based on NIH protocols 63
2.3.8 SPR for functional anti-PfRIPR mAbs 64
2.3.9 Depletion of PfRIPR EGF (5-8) antibodies from purified IgG 64
2.3.10 Measure of Synergy in the assay of GIA 64
2.4 Appendix 1 – Primers and sequences 66
2.5 Appendix 2 – Statement on ARRIVE Guidelines 71
Chapter 3 - Investigating PfRIPR neutralising epitopes 73
3.1 Authorship statement 73
3.1 Introduction 74
3.1.1 Production of *P. falciparum* recombinant protein fragments 74
3.1.2 Identification of neutralising epitopes on PfRIPR 77
3.1.3 Anti-PfRIPR monoclonal antibodies 78

3.2 Expression plasmid design and PfRIPR sequence choice 79

3.3 Production of recombinant PfRIPR protein fragments 87

3.4 Reconstitution of the RCR complex with recombinant PfRIPR fragments ... 93

3.5 Characterisation of non-neutralising PfRIPR mAbs 96

3.5.1 Epitope mapping using recombinant PfRIPR fragments 96

3.5.2 Assessment of mouse mAb binding affinities by SPR 100

3.5.3 Non-neutralising mAbs bind the RCR or prevent RCR formation 102

3.6 Investigating potential PfRIPR erythrocyte receptors 105

3.7 Rabbit immunisations and identification of neutralising antibody epitopes on PfRIPR 109

3.7.1 Rabbit immunisations for antigen reversal 109

3.7.2 Antigen reversal GIA assays 111

3.8 Discussion 117

Chapter 4 - PfRIPR vaccine development 122

4.1 Authorship statement 122

4.2 Introduction 122

4.2.1 Virus-like particle vaccines 123

4.2.2 SpyTag-SpyCatcher technology 124

4.3 PfRIPR vaccine design and production 127

4.3.1 PfRIPR-based vaccines 127

4.3.2 PfRIPR-PfCyRPA fusion vaccines 131

4.4 Pilot mouse vaccination study 134

4.4.1 Study design 134

4.4.2 Results 135

4.5 Pilot rat vaccination study 141

4.5.1 Study design 142

4.5.2 Results 143

4.6 Comparing PfRIPR-based vaccines with PfRH5 and PfCyRPA-based vaccines 151

4.6.1 Dose-Ranging Study – Recombinant Protein Approach, Single Component Protein Formulations 151

4.6.2 Study O2 – Recombinant Protein Approach, Single and Multiple Component Protein Formulations 160

4.6.3 VLP-Based Vaccine approaches 170

4.6.4 Summary of outcomes with different antigens used in rat immunisations 176

4.7 Discussion 178

Chapter 5 - Using monoclonal antibodies to aid PfRIPR vaccine design 184

5.1 Authorship statement 184

5.2 Introduction to monoclonal antibody discovery 184

5.3 Monoclonal antibody discovery - hybridomas 188

5.3.1 Antigen choice and immunisation strategies 188

5.3.2 Hybridoma development and antibody production for in-house immunisations 190

5.4 Monoclonal antibody discovery – single cell approaches 191

5.4.1 Development of a flow cytometry protocol for antigen-specific mouse B-cells 192

5.4.2 Development of a single cell RT PCR for mAb isolation 197

5.4.3 Characterisation of mRP021 199

5.4.4 mRP021 and the RCR complex 204

5.4.5 mRP021 binding kinetics 206

5.5 Intra-PfRIPR synergistic antibody effects 207

5.5.1 Failure of mRP021 hybridoma 207

5.5.2 Investigating synergy using non-functional PfRIPR monoclonal antibodies and mRP012 210

5.5.3 Investigating synergy using PfRIPR EGF (5-8) depleted rabbit IgG and mRP012211

5.6 Discussion 216

Chapter 6 - Conclusions and future directions 220

6.1 Summary of output 220

6.1.1 Production of protein PfRIPR fragments 220

6.1.2 Characterisation of anti-PfRIPR antibodies 220

6.1.3 PfRIPR does not bind PfSEMA7A 221

6.1.4 Development of a PfRIPR EGF (5-8) based vaccine 221

6.1.5 Development of GIA positive anti-PfRIPR antibodies 222

6.1.6 Synergistic antibody interactions between the RCR complex proteins and within PfRIPR 222

6.2 Future work 222

6.2.1 Intra-PfRIPR antibody synergy 222

6.2.2 Structural work 223

6.2.3 PfRIPR fusion vaccines 223

6.2.4 Understanding the role of PfRIPR in *P. falciparum* 224

6.3 Prospects of PfRIPR as a blood-stage malaria vaccine candidate 225

6.4 Final remarks 226

Chapter 7 - References 227

Chapter 8 - Appendix 245

8.1 PfRIPR fragments do not form a complex with PfRH5 and PfCyRPA 245

8.2 Non-neutralising mAbs bind and disrupt the RCR complex 248

8.3 Antigen reversal GIA using PfRIPR EGF (5-8) – PfCyRPA fusion protein 250

8.4 Full GIA results from Study O2 251

List of abbreviations

ACTs	Artemisinin-based combination therapies
AdHu5	Adenovirus human serotype 5
AMA1	Apical Membrane Antigen 1
AMIGO2	Adhesion Molecule with Ig like Domain 2
AS01	Adjuvant system 01
BAP	Biotin acceptor peptide
C/IFA	Complete/incomplete Freund's adjuvant
CD4-d3d4	Cluster of differentiation 4, domain 3, 4
CelTOS	*P. falciparum* cell-traversal protein for ookinetes and sporozoites
CFCA	Calibration free concentration analysis
ChAd63	Recombinant Simian Adenovirus 63
CHMI	Controlled human malaria infection
CHO	Chinese hamster ovary
CryoEM	Cryogenic electron microscopy
CSA	Chondroitin sulfate A
CSP	Circumsporozoite protein
DBL	Duffy binding-like
DLS	Dynamic light scattering
DMEM	Dulbecco's modified eagle medium
EBL	Erythrocyte-Binding-Like
EC_{50}	Effective concentration (50%)
EGF	Epidermal-growth factor like domains
ELISA	Enzyme-linked immunosorbent assay
FPLC	Fast protein liquid chromatography
GFP	Green fluorescent protein
GIA	Growth inhibitory activity
GLA-SE	Glucopyranosyl lipid adjuvant-stable emulsion
GPI	Glycosylphosphatidylinositol
GSK	GlaxoSmithKline
HBsAg	Hepatitis B surface antigen
HEK293	Human embryonic kidney 293
HEK293E	HEK293 Epstein-Barr Nuclear Antigen-1
HEK293F	HEK293 Freestyle™
HEK293 GnTI-	HEK293 N-acetylglucosaminyltransferase I-
ICAM1	Intercellular Adhesion Molecule 1
IgG	Immunoglobulin G
IM	Intramuscular
IP	Intraperitoneal
iRBC	Infected red blood cell
IS	Intrasplenic
LLQ	lower limit of quantification
LC-MS/MS	Liquid chromatography-tandem mass spectrometry
mAb	Monoclonal antibody
ME-TRAP	Multiple-Epitope Thrombospondin-Related Adhesion Protein

monoFc	Monomeric fragment crystallizable region
MSP	Merozoite Surface Proteins
MTRAP	Merozoite-specific thrombospondin-related anonymous protein
MVA	Modified Vaccinia Ankara
NAI	Naturally acquired immunity
NIH	National Institute of Health
NMR	Nuclear magnetic resonance
pAb	Polyclonal antibody
Pdi	Polydispersity index
PfCyRPA	*P. falciparum* Cysteine Rich Protective Antigen
PfEMP1	*P. falciparum* Erythrocyte Membrane Protein-1
PfKelch13	*P. falciparum* kelch 13
PfPI3K	*Plasmodium falciparum* phosphatidylinositol-3-kinase
PfRH5	*P. falciparum* Reticulocyte-binding-like protein Homolog 5
PfRIPR	*P. falciparum* RH5 Interacting Protein
Pfs25	*P. falciparum* surface protein 25 kDa
Pfs48/45	*P. falciparum* surface protein 48/45 kDa
PMR	Parasite multiplication rate
qPCR	Quantitative Polymerase chain reaction
QTOF	Quantitative time of flight
RBC	Red blood cell
RCR	RH5, CyRPA, RIPR complex
RH	Reticulocyte-binding-like protein Homolog
RIFIN	repetitive interspersed families of polypeptides
RON2	Rhoptry Neck protein 2
RSV	Respiratory syncytial virus
RT-PCR	Reverse transcription polymerase chain reaction
S2	*Drosophila melanogaster* Schneider 2 cells
SEC	Size exclusion chromatography
SEMA7A	Semaphorin-7A
SPR	Surface plasmon resonance
STEVOR	Subtelomeric Variable Open Reading frame
SURFIN	Surface associated interspersed protein family
TBV	Transmission blocking vaccines
TEM	Transmission electron microscopy
TEV	Tobaccer etch virux
TgMIC1	*Toxoplasma gondii* microneme protein 1
TNFα	Tumour Necrosis Factor Alpha
TRAP	Thrombospondin-Related Adhesion Protein
V_H	Variable heavy
V_L	Variable light
VLP	Virus like particle
VSA	Variant surface antigens
WGCFS	Wheat germ cell-free system
WHO	World health organisation
WRAIR	Walter Reed Army Institute of Research

List of tables

Table 1-1 – Active or recruiting malaria vaccine clinical trials as of March 2021. List compiled from clinicaltrials.gov. 11

Table 1-2 – Table of PfRIPR SNPs above 0.5% frequency 31

Table 1-3 - List of published mAbs for PfRH5, PfCyRPA and PfRIPR with accompanying details..... 32

Table 2-1– Sequence IDs of PfRIPR plasmids used in experiments..... 39

Table 2-2 – Serum volumes and run times for IgG purification 48

Table 2-3 – Study O1 groups and antigens. 54

Table 2-4 - Study O2 groups and antigens. 54

Table 2-5 - Study O3 groups and antigens. 55

Table 2-6 – List of primers used to generate PfRIPR protein fragments 66

Table 2-7 – List of biotinylated PfRIPR 20mer peptides covering non-EGF N-half PfRIPR protein. 67

Table 2-8 – Gamma chain PCR primers for in-house PCR protocol 68

Table 2-9 - Kappa chain PCR primers for in-house PCR protocol 69

Table 2-10 - Gamma chain PCR primers for Ho *et al.* PCR protocol..... 69

Table 2-11 - Kappa chain PCR primers for Ho *et al.* PCR protocol 69

Table 2-12 – Kappa chain PCR primers for NIH PCR protocol..... 70

Table 3-1 –Details for full length PfRIPR sequences used in this thesis 82

Table 3-2 – Table of all PfRIPR fragments made including quality analysis summary 92

Table 3-3 – Summary of non-neutralising mAb data..... 103

Table 4-1 – QTOF results from monoFc cleaved PfRIPR EGF fragments 129
Table 4-2 – EC_{50} values of total purified serum IgG for each group in the mouse pilot study. 138
Table 4-3 – Antigen specific EC_{50} values for each group in the mouse pilot study.. 140
Table 4-4 – EC_{50} values for the four PfRIPR-based vaccines. 150
Table 4-5 - Summary of interpolated EC_{50} values from each immunisation group. 159
Table 4-6 – Summary of interpolated total antigen-specific IgG EC_{50} values from each immunisation group. 169
Table 4-7. Summary of Study O3 GIA Assay Antigen-Specific Rat IgG EC_{50} 175

List of figures

Figure 1.1 – The life cycle of *P. falciparum*.... 4

Figure 1.2 – Anatomy of the merozoite and invasion of an erythrocyte by *P. falciparum*....21

Figure 1.3 – The structure of PfRH5 bound to basigin.....24

Figure 1.4 – Crystal structure of CyRPA.....27

Figure 1.5 – Schematic of PfRIPR.....28

Figure 1.6 – CryoEM structure of the RCR complex.....29

Figure 3.1 – New constructs for PfRIPR fragment expression and purification. 80

Figure 3.2 –PfRIPR N-half fragment expression and optimisation. 85

Figure 3.3 - TEV protease digestion of PfRIPR EGF (5-6) monoFc.....87

Figure 3.4 – PfRIPR fragment design and production of PfRIPR fragments.....89

Figure 3.5 – Representative QTOF plots for monoFc bound PfRIPR fragments. 91

Figure 3.6 – PfRIPR EGF (3-6) does not form a complex with PfCyRPA or PfCyRPA and PfRH5.....95

Figure 3.7 – Single cycle GIA assay using dilution curves of the seven original anti-PfRIPR mAbs used in this thesis. 96

Figure 3.8 – Dot blots of non-neutralising mAbs against different PfRIPR fragments. 98

Figure 3.9 – PfRIPR Peptide screen for linear epitopes.....99

Figure 3.10 – Multi-cycle kinetic SPR sensorgrams of the five characterised non-functional anti-PfRIPR mAbs. 101

Figure 3.11 - Non-neutralising mAbs prevent formation of and bind the RCR complex. 104
Figure 3.12 – Investigating the binding of PfRIPR to SEMA7A-CD4d3+4. 107
Figure 3.13 – Multi-cycle kinetic SPR sensorgrams using PfRIPR on a CM5 chip. ... 108
Figure 3.14 – GIA assay results using sera from rabbits immunised at Genscript... 110
Figure 3.15 – GIA assay results from the NIH & CRB rabbits. 111
Figure 3.16 – Assessment of anti-PfRIPR full-length IgG GIA reversal using Genscript rabbit purified IgG. 112
Figure 3.17 – Anti-PfRIPR purified IgG titration. 114
Figure 3.18 - Assessment of anti-PfRIPR full-length IgG GIA reversal using NIH and CRB rabbit purified IgG. 115
Figure 3.19 – Antigen reversal titrations using PfRIPR EGF-like domains. 116
Figure 4.1 – Virus like particles and nanoparticles in vaccine design. 124
Figure 4.2 – SpyCatcher and SpyTag VLP platform. 125
Figure 4.3 – Schematic of new SpyTag expression construct. Restriction sites are indicated by black arrows. 128
Figure 4.4 – Production and quality analysis of the PfRIPR based VLP vaccines. 130
Figure 4.5 – Production and example quality analysis of PfRIPR – PfCyRPA fusion vaccines. 133
Figure 4.6 – Mouse pilot study design. 135
Figure 4.7 – ELISA results mouse serum from day 35. 136
Figure 4.8 – Single cycle GIA assay with dilution curve of purified IgG from mice using *P. falciparum* clone 3D7 138
Figure 4.9 – Single cycle GIA using *P. falciparum* 3D7 clone with dilution curve of purified IgG. Graph plotted against antigen specific ELISA titres. 140

Figure 4.10 – Study design for rat immunisations. 143
Figure 4.11 – Anti-PfRIPR standardised IgG ELISA titres. 145
Figure 4.12 – Anti-HBsAg ELISA on day -2 and day 55. A) Day -2 B) Day 70. 145
Figure 4.13 – Single cycle GIA assay results for the five antigen groups using *P. falciparum* clone 3D7. Dilution curves of purified IgG from rats. 148
Figure 4.14 – Quality analysis of the different PfRIPR-based vaccines. 150
Figure 4.15 – Study O1 Design. 152
Figure 4.16 – Standardised IgG ELISAs for Study O1. 154
Figure 4.17 – Single cycle GIA assay with dilution curve of purified IgG from rats using *P. falciparum* clone 3D7. 156
Figure 4.18 – Quality analysis of Study O1 GIA data. 159
Figure 4.19 - Study O2 design. 162
Figure 4.20 – Antigen-specific standardised ELISAs on Study O2 samples. 164
Figure 4.21 – Single cycle GIA assay with dilution curve of purified IgG from rats in Study O2 using *P. falciparum* clone 3D7. 167
Figure 4.22 – Single cycle GIA assay with dilution curve of purified IgG from immunisations with full-length PfRIPR and PfRIPR EGF (5-8) protein in Study O2 using *P. falciparum* clone 3D7. 168
Figure 4.23 - Quality analysis of GIA data from immunisations with full-length PfRIPR and PfRIPR EGF (5-8) protein. 169
Figure 4.24 - Study O3 design. 171
Figure 4.25 - Anti-PfRIPR specific standardised ELISA titres for HBsAg-PfRIPR EGF (5-8) immunised rats. 172
Figure 4.26 – GIA results from rats immunised with different doses of HBsAg PfRIPR EGF (5-8). 174

Figure 4.27 - Comparison of interpolated EC_{50} values from Study O3. 175

Figure 4.28 – Summary of interpolated EC_{50} values from the four rat studies in this Thesis. 177

Figure 5.1 – Mouse immunisation plan schedules. 189

Figure 5.2 - OD ELISA titre for HBsAg-PfRIPR EGF (5-6) and HBsAg-PfRIPR EGF (7-8) immunised mice 190

Figure 5.3 – Gating strategy for IgG producing B-cell isolation. 193

Figure 5.4 – Schematic of fluorophore conjugated PfRIPR EGF (7-8) probes 194

Figure 5.5 – PfRIPR EGF (7-8) probe verification on CompBeads bound to purified IgG from mice immunised with HBsAg PfRIPR EGF (7-8). 195

Figure 5.6 – Representative flow cytometry results. 196

Figure 5.7 – Schematic representing the mAb cloning workflow. 197

Figure 5.8 – Basic structure of an IgG molecule 198

Figure 5.9 – Dot blot to determine the location of mRP021 binding 200

Figure 5.10 – Titration of the new anti-PfRIPR mAbs. Single-cycle growth inhibitory activity assay using *P. falciparum* 3D7 clone. 200

Figure 5.11 – SEC chromatograms of mRP021 binding to PfRIPR EGF (5), EGF (5-6), and EGF (8). 202

Figure 5.12 - SEC chromatograms of mRP021 binding to PfRIPR EGF (5-6) and PfRIPR EGF (5-8). 203

Figure 5.13 – SEC chromatograms of mRP021 binding to the RCR complex. 205

Figure 5.14 - Multi-cycle kinetic SPR sensorgrams of mRP021. 207

Figure 5.15 – Original and new mRP021 batches tested by GIA assay and SPR. 208

Figure 5.16 – Characterisation of anti-PfRIPR mAb mRP012. 209

Figure 5.17 – GIA data of mRP012 tested in combination with non-neutralising anti-PfRIPR antibodies. 211
Figure 5.18 – Schematic of PfRIPR EGF (5-8) antibody depletion from polyclonal anti-PfRIPR antibodies. 212
Figure 5.19 – Depletion and dot blot array of polyclonal antibody mixtures. 213
Figure 5.20 - GIA data of mRP012 tested in combination with PfRIPR EGF (5-8) depleted IgG. 215
Figure 8.1 – SEC chromatograms of the Nhalf and Chen3 PfRipr fragments. 245
Figure 8.2 - SEC chromatograms of the EGF (3-6) and EGF (7-10) PfRipr fragments. 246
Figure 8.3 - SEC chromatograms of the Chen1/2 and C-terminal domain (CTD) PfRipr fragments. 247
Figure 8.4 – mRP006 and mRP013 binding to the RCR complex. 248
Figure 8.5 - mRP017 and mRP003 binding to the RCR complex. 249
Figure 8.6 - Antigen reversal of anti-PfCyRPA purified IgG held at 3mg/mL with a titration of PfRIPR-EGF (5-8) – PfCyRPA fusion starting at 0.31μM 250
Figure 8.7 - Single cycle GIA assay results for Study O2 groups using *P. falciparum* clone 3D7. 251

Chapter 1 - Introduction

1.1 Malaria

1.1.1 The global state of malaria disease

Malaria is a disease that has afflicted humanity since antiquity. Despite multiple global eradication attempts 298 million cases of malaria were reported in 2018 with an estimated 459,000 deaths[1], the majority of those were children under five years old. In addition to the human cost, malaria causes substantial economic loss in endemic countries with one study estimating that the economic loss to Uganda due to malaria morbidity was US $50,000,000 per year[2].

Malaria is a disease caused by species of parasitic protozoan. Six species are known to cause malaria disease in humans: *Plasmodium falciparum, Plasmodium vivax, Plasmodium ovale curtisi, Plasmodium ovale wallikeri, Plasmodium malariae* and *Plasmodium knowlesi*. Of these, *P. falciparum* is responsible for the majority of malaria cases and deaths, especially in sub-Saharan Africa, whereas *P. vivax* is more prevalent in South-East Asia. For simplicity in this Thesis, references to "malaria" and "malarial disease" are referring to *P. falciparum* unless otherwise stated.

Prevention and treatment of malaria has historically relied on two key pillars: vector control and small molecule drugs. Although mosquito eradication is unlikely to be a viable option[3], vector control methods such as insecticide treated bed nets and indoor residual spraying have been credited with reducing the number of malaria cases by nearly 70% since 2010[4].

Vector control methods can successfully reduce transmission in urban areas[5], however the success of insecticides and insecticide treated bed nets has been tempered by the rapid spread of insecticide resistance in mosquito populations[6]. In the latest WHO report[1], 73 countries reported resistance to at least one of the four insecticide classes and 28 reported resistance to all main insecticide classes. Resistance to the pyrethroids, the only insecticide class used in insecticide treated bed nets, is also widespread being detected in 70% of sites. This problem is likely to be more serious than reported as 57% of countries that use indoor residual spraying did not report insecticide resistance status[1]. In response to these reports, researchers have been developing new methods of vector control including CRISPR/Cas9-engineered knockout mosquitos that are refractory to *P. falciparum* infection[7], the introduction of non-pathogenic commensal bacteria that inhibit malaria development in the midgut[8], and using fungi modified with spider toxins to kill mosquitos[9]. These new strategies are exciting however, at the time of writing, none of these interventions are ready for large scale implementation.

For treatment of uncomplicated malaria, a combination of artemisinin-based compounds and a second drug such as mefloquine are routinely used; these treatments are referred to as artemisinin-based combination therapies (ACTs). Compounds such as mefloquine can also be used as a prophylactic for travellers to endemic regions. For now ACTs are reported to be 98% effective in the WHO African region[1], however resistance to ACTs is an ongoing concern for those working to eradicate malaria. Resistance to ACTs was first reported in Cambodia in 2008[10] and it has since spread to SE Asia[11], experts have warned that resistance could spread to sub-Saharan Africa hampering eradication efforts[12]. Although there is no consensus

target of the artemisinins, mutations in *P. falciparum* Kelch13 (PfKelch13) that increase the levels of *P. falciparum* phosphatidylinositol-3-kinase (PfPI3K) have been shown to increase the levels of artemisinin resistance[13]. PfKelch13 mutations are not the only path to ACT resistance[14] and therefore long term use of ACTs without novel control strategies is likely to induce resistance hampering global eradication efforts.

1.1.2 Malaria life-cycle and pathogenesis

Malaria is transmitted by female *Anopheles* mosquitos, such as *Anopheles gambiae,* in sub-Saharan Africa. After a mosquito bite, sporozoites move quickly into the blood then migrate to the liver. The sporozoites typically invade hepatocytes within an hour of the bite and begin to replicate (Figure 1.1). This stage is referred to as the pre-erythrocytic stage. Mature merozoites are released from the ruptured hepatocyte into the blood. The merozoites then enter the asexual or blood stage whereby they invade erythrocytes, replicate, then lyse the cells releasing an average of 16 new merozoites per erythrocyte[15]. This replication cycle lasts between 36 and 72 hours and leads to the characteristic cyclic fever associated with malaria. A small portion of the merozoites differentiate into male and female gametocytes. These gametocytes are then taken up into a new mosquito during a blood meal. The final stage of the malaria lifecycle, oocyst formation and sporozoite development, occur in the midgut wall of the mosquito.

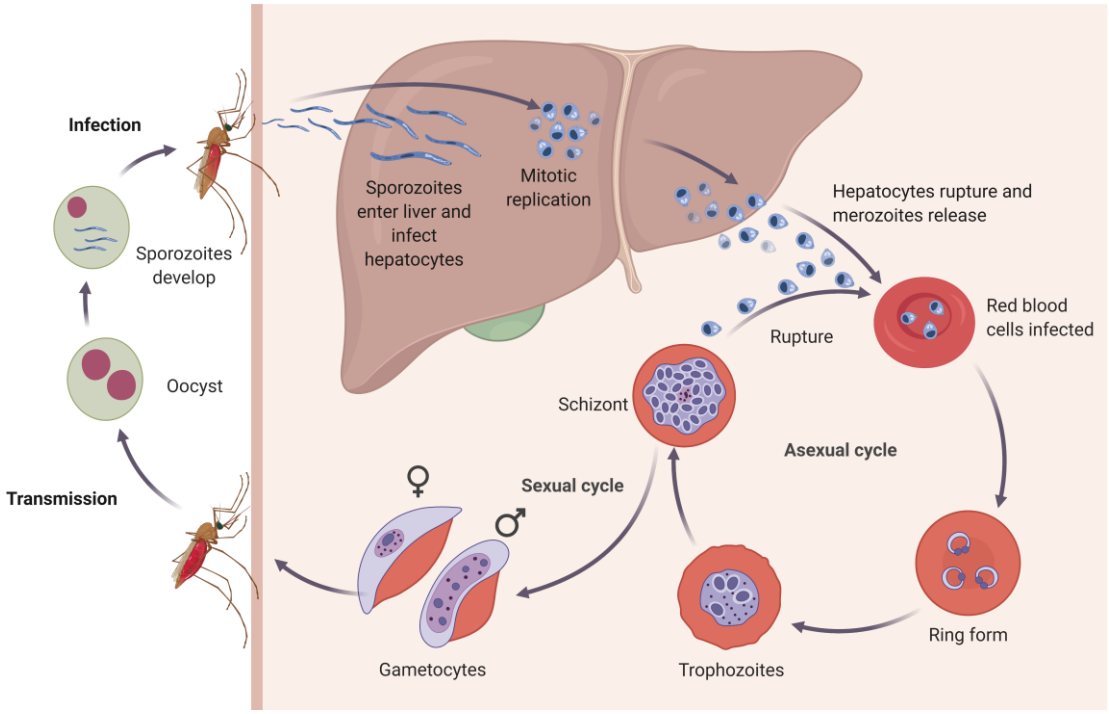


Figure 1.1 – The life cycle of *P. falciparum*.
The complete life cycle requires both a mosquito host and a human host. The three main stages of the lifecycle; pre-erythrocytic, asexual stage and sexual stages are all potential targets for vaccine development. Created with BioRender.com

Symptoms of malaria are typical of most infectious diseases; usually including fever, headaches, chills, diaphoresis, abdominal pain, nausea and tachycardia[16], which often delays accurate diagnostic of malarial disease. The blood stage of infection is responsible for these clinical symptoms; the symptoms coincide with the rupturing of infected erythrocytes to release merozoites leading to the production of cytokines such as TNFα, interleukin-6 and interleukin-1β which cause inflammation, chills and fever[17]. The severity of disease has been associated with the parasite multiplication rate (PMR). PMR is the rate of parasite numbers increasing over time, it is determined by the number of erythrocytes successfully invaded by merozoites and is therefore influenced by the number of merozoites produced by each schizont and the ability of those merozoites to invade erythrocytes. A high PMR has been associated with

increased risk of severe malaria[18] however this relationship has not always bene observed[19] suggesting that our knowledge of malaria pathogenesis is incomplete.

Severe malaria and complications can present in numerous ways including cerebral malaria, severe anaemia, renal failure, pulmonary oedema, acidosis and hypoglycaemia[16]. These severe and life-threatening complications are thought to be the result of several processes – notably cytoadhesion of infected red blood cells (iRBC) to the vascular endothelium[20] leading to damage and vascular leakage; 'erythrocyte rosetting'[21–25] where iRBCs binds to uninfected erythrocytes leading to clumps, or 'rosettes', of erythrocytes sequestering in deep tissues; and platelet-mediated autoagglutination of iRBCs where iRBCs aggregates are bound together by activated platelets[26,27]. The exact mechanism of rosetting and the erythrocyte receptors involved are still contentious[25] and studies are difficult given that most laboratory adapted *P. falciparum* strains, e.g. 3D7, show little to no rosetting *in vitro*. Studies linking these mechanisms to malaria pathology often rely on correlating the presence rosettes or platelet-mediated autoagglutination of iRBCs with the clinical outcome of infection which is not sufficient in itself to demonstrate a causative link, however, there has been substantial research to uncover the underlying molecular mechanisms behind these pathologies. Sequestration of iRBCs in the deep tissues is thought to prevent clearance of iRBCs by the spleen, increasing parasite burden and causing organ damage through multiple mechanisms such as vascular leakage. In the case of cerebral malaria it is likely that the pathology is caused by a combination of parasite factors, such as rosette induced hypoxia[28], and host factors such as neuronal damage by the immune response[29]. Cerebral malaria has a mortality rate of 15-25% and there is currently no effective treatment[30]. The primary mediator of iRBC

cytoadhesion is the *P. falciparum* Erythrocyte Membrane Protein-1 (PfEMP1)[31]. PfEMP1 coats the surface of the iRBC and can bind to various adhesins such as CD36, ICAM1 and CSA. PfEMP1 is not a single protein, rather it is a large family of proteins encoded by 60 *var* genes. Parasites can selectively express different PfEMP1 variants allowing parasites to continually evade the host immune response. Different PfREMP1 variants have different receptor binding tropisms leading to the variety in severe malaria symptoms and outcomes[32].

1.1.3 Naturally acquired immunity

Naturally acquired immunity (NAI) to malaria was observed long before the basis of infection and immunity were understood; early European colonists in Africa understood that they were more susceptible to malaria disease than those born in endemic areas. The physician Robert Koch first reported in 1900 that adults in high transmission areas had lower parasitaemia than children in high transmission areas, whereas in low transmission areas adults and children had comparable parasite numbers. It could be inferred that NAI was induced by continuous exposure to the parasite throughout life and could be lost when exposure ended, ironically leading to a potential increase in symptomatic cases with a decrease in malaria transmission[33].

In the 1950s, antibodies against malaria were uncovered as the key driver for NAI by Cohen and MacGregor[34]. Further work showed that it was the antibodies that targeted blood stage parasites and iRBCs that mediated the acquired immunity with pre-erythrocytic and anti-gametocyte antibodies having a negligible impact. Antibodies against variant surface antigens (VSAs) such as PfEMP-1, discussed earlier, and the more recently identified families RIFINs[35], SURFINs[36] and STEVORs[37], are believed to mediate parasite clearance and prevent cytoadherence of iRBCs in deep tissues

guarding against severe malaria. However, this is far from a complete picture and no single correlate of natural immunity is known for malaria[38]. *P. falciparum* is known to shift expression of different PfEMP-1 proteins as an immune evasion mechanism, this was long assumed to be the primary reason why NAI was slow to develop, as an array of antibodies against many different VSAs are required for protection. However, studies of infected infants have shown that antibody responses decline within four months of infection[39] suggesting that there are more factors than antigenic variability hampering immunity. Indeed, several points of weakness in the immune response to the malaria parasite have been identified, these include production of atypical B-cells that inefficiently produce antibodies[40], induction of exhausted T-cell phenotypes[41] and reduction in memory T-cell responses[42]. Recent advances in technology such as systems immunology, which combines transcriptomic and proteomic data, may be an exciting opportunity for unravelling the human immune responses to malaria[43] and enable vaccine developers to circumvent some of the limitations of NAI.

An additional component of NAI against malaria that is often overlooked is anti-disease immunity, this contrasts with 'anti-parasitic' immunity[44]. Anti-parasitic immunity is what we would intuitively call immunity – immune responses, typically antibody responses, aimed at directly reducing parasite load and therefore preventing the onset of clinical symptoms. Anti-disease immunity involves a reduction in the immunopathology of malaria, for example by lowering proinflammatory marker expression through a decrease in T-cell functionality[45] thus reducing clinical disease and inducing a malaria tolerance. Anti-disease immunity may not be informative for vaccine design, since a vaccine should not simply induce

tolerance to a disease, however understanding its role will help us better characterise the host response to repeated malaria challenge.

1.2 Vaccines against malaria

It is unlikely that vector control and small molecule drugs will lead to the eradication of malaria despite a steady decline in malaria case numbers since 2010[46]. This is why the third pillar of malaria eradication, vaccination, is tipped to play a greater role in the malaria eradication strategy. Vaccines are considered to be one of the best and most cost-effective methods of disease control and a vaccine to malaria is sorely lacking. The WHO Malaria Vaccine Technology Roadmap[47] outlines two main strategic goals to be reached by 2030:

1. "Development of a licensed malaria vaccine(s) with protective efficacy of at least 75 percent against clinical malaria (over at least 2 years) suitable for administration to appropriate at-risk groups in malaria endemic areas"[47]

And

2. "Development of malaria vaccines that reduce transmission of the parasite … Vaccines to reduce transmission should be suitable for administration in mass campaigns."[47]

This two-pronged approach should simultaneously reduce the incidence of clinical malaria, reduce the economic burden, and interrupt transmission leading to lower levels of transmission with a goal of eradication.

Early malaria vaccine work is built on experiments in the 1940s using inactivated *Plasmodium gallinaceum* to immunises domestic fowl[48]. This was followed up in 1966

by HW Richards who demonstrated protection in birds against using UV attenuated *P. gallinaceum* sporozoites[49]. Nussenzweig in 1967 used radiation attenuated sporozoites to immunise mice[50], these irradiated sporozoites delivered by mosquito bite would migrate to the liver but not complete the liver development stage. This was sufficient to provoke a protective immune response against malaria challenge. This work led to several human trials of radiation attenuated sporozoites[51–55] in the 1970's and 1980's which succeeded in protecting human volunteers against challenge with *P. falciparum* and *P. vivax*. Volunteers were also protected against heterologous strain challenge indicating that the antigenic variation may be a more tractable challenge for sporozoite vaccines than asexual stage vaccines. These successes were attenuated by several challenges faced by irradiated sporozoite vaccines: firstly, volunteers required 6-8 exposures, or 450 to 1,000 parasites, to develop protective immunity[52]. Secondly, radiation attenuated sporozoites are difficult to make in the quantities required for vaccination programmes. Thirdly, irradiated sporozoites had to be delivered either by mosquito bite or by intravenous injection. These challenges have historically rendered attenuated sporozoite vaccines impractical for mass vaccination strategies.

Over the last three decades, vaccination with attenuated sporozoites has been championed by Sanaria, USA. Sanaria's PfSPZ vaccine (radiation attenuated, aseptic, purified, cryopreserved *Plasmodium falciparum* [Pf] sporozoites [SPZ]) is manufactured to meet GMP compliance with a phase 3 trial planned for 2021. PfSPZ has been consistently shown to be safe and well tolerated in vaccinated individuals[56–61] with protection against malaria infection lasting for more than one year in some individuals[56]. PfSPZ can also induce protection against a heterologous malaria

challenge (87% at 3 weeks post vaccination)[60] . Despite these advances, the current immunisation regime for PfSPZ requires 5 doses[58] of PfSPZ; It remains to be seen how the logistics of this vaccines will work in a real world setting. Aside from attenuated sporozoites, the majority of vaccine efforts have focused on recombinant-protein/adjuvant or vector-based strategies. These vaccines will be the primary focus of this review.

In an ideal scenario, conserved antigens are identified then tested for immunogenicity and cross strain protection, although this does not always occur. Each subunit vaccine typically targets a particular life cycle stage, such as the blood stage or sexual stage. There are many new vaccines currently being evaluated in clinical trials; active clinical trials are summarised in Table 1-1 and a detailed look at some of the vaccine candidates is given in subsequent sections.

Table 1-1 – Active or recruiting malaria vaccine clinical trials as of March 2021. List compiled from clinicaltrials.gov.

Life cycle stage	Identifier	Phase	Antigen and adjuvant used	Sponsor	Collaborators (abridged)
Pre-erythrocytic	NCT03143218 & NCT04319380	III	Pf CSP (207-395) & HepBsAg, AS01	London School of Hygiene and Tropical Medicine	MRTC (Mali), IRSS-URCN (Burkina Faso)
	NCT03580824	Ib/II	CSP – HbsAg, Matrix-M™ 1	University of Oxford	Kenya Medical Research Institute, EU
	NCT03896724	I/II	CSP – HbsAg, Matrix-M™ 1	University of Oxford	IRSS-URCN (Burkina Faso), EU
	NCT03806465	IV	RTS,S/AS01	World Health Organization	-
	NCT03084289	I	TRAP + ME epitopes	University of Oxford	-
	NCT03867331	I	CSP-iαVLP, alum	VLP Therapeutics	Walter Reed Army Institute of Research
	NCT03917654	II	Radiation Attenuated NF54 Sporozoites	National Institute of Allergy and Infectious Diseases (NIAID)	National Institutes of Health Clinical Center (CC), NIAID
	NCT03510481	I	Radiation Attenuated NF54 Sporozoites	NIAID	CC, NIAD
	NCT03952650	I/II	Radiation Attenuated NF54 Sporozoites with Chloroquine	NIAID	CC, NIAD
	NCT03589794	I	CSP, Glucopyranosyl Lipid A, Quillaja saponaria 21 formulation	NIAID	-
	NCT04268420	I	CSP fragment with ALFQ	U.S. Army	Walter Reed Army Institute of Research (WRAIR)
	NCT04296279	I	CSP fragment with ALFQ	U.S. Army	WRAIR
Blood-stage	NCT04318002	I/II	PfRH5.1, Matrix-M™	University of Oxford	Ifakara Health Institute Clinical Trial Facility, Tanzania
Sexual stage/ Transmission blocking	NCT03917654	II	Pfs230, Pseudomonas aeruginosa ExoProtein A, AS01	NIAID	-
	NCT02942277	I	Pfs25, PfS230, EPA, AS01,	NIAID	CC, NIAD
	NCT04130282	Ia	Pfs25-IMX313, Matrix-M™ 1	University of Oxford	
Multi-stage	NCT00392015	I/2a	CSP & PfAMA1 / adenovector	U.S. Army	USAID, (MIDRP), Naval Medical Research Center

1.2.1 Pre-erythrocytic vaccines

Pre-erythrocytic vaccines can target two distinct phases of the malaria life cycle. The first target is the sporozoites as they enter the skin and migrate to the liver. The second is targeting infected hepatocytes before merozoites rupture the cells and begin the blood stage of infection. The pre-erythrocytic stages are an attractive target for vaccination as complete protection would yield sterilising immunity by preventing the sporozoites from starting the lifecycle in humans. In addition, there are fewer parasites that need to be eliminated compared to the blood stage theoretically making clearing the parasite more manageable. Pre-erythrocytic vaccines include the most advanced malaria vaccine candidates; these are discussed below.

1.2.2 RTS,S / AS01

The most advanced malaria candidate to date is RTS,S/AS01, or Mosquirix, originally developed by GlaxoSmithKline (GSK) in 1987. This vaccine is now in pilot implementation trials post phase III. This vaccine uses amino acids 207 - 398 from the circumsporozoite protein (CSP) C-terminus corresponding to 19 tetrapeptide NANP/NVDP repeat region C-terminal flanking region. This peptide is fused to the hepatitis B surface antigen (HBsAg) and co-expressed with unmodified HBsAg in yeast to generate a virus-like particle (VLP) mix of HBsAg and CSP-HBsAg[62] at a ratio of 4 to 1. The vaccine uses GSK's proprietary adjuvant AS01 to deliver robust humoral and cellular immune responses. Results from a large phase III trial show that initial efficacy was between 27 & 45% for different age groups but protection waned with time[63]. Despite the low efficacy, a recent analysis suggested that widespread use of the RTS,S/AS01 vaccine could prevent between 31,000 - 160,000 cases of clinical

malaria and prevent between 200-800 deaths per 100,000 children vaccinated[64]. The widespread implementation of this vaccine may therefore make a significant contribution to both malaria reduction and our understanding of disease response to large interventions in endemic areas.

1.2.3 R21

A RTS,S/AS01 biosimilar vaccine, called R21, is rapidly progressing through clinical trials. R21 was developed to improve the immunogenicity of the RTS,S/AS01 vaccine and reduce the anti-HBsAg immune response observed in RTS,S clinical trials[65]. R21 contains the same CSP repeat region as RTS,S fused to HBsAg but it forms a single CSP-HBsAg VLP, rather than a mix of CSP-HBsAg and HBsAg[66]. In mice, this vaccine elicited minimal anti-HBsAg titres and was protective in a murine transgenic *P. berghei* challenge[66]. In follow up phase I studies, dosing with 10μg R21 with Matrix-M™ adjuvant from Novavax performed comparably to dosing with 50μg of RTS,S/AS01[67]. The developers hope that R21 will show greater efficacy in larger phase II and III trials with a lower production cost due to the lower dosing and simpler adjuvant required.

1.2.4 Thrombospondin-Related Adhesion Protein (ME-TRAP)

Thrombospondin-Related Adhesion Protein (TRAP) is required for sporozoite motility and hepatocyte invasion[68]. TRAP is also presented by HLA class I molecules on the surface of infected hepatocytes[69] making infected cells vulnerable to cytotoxic CD8+ T-cell killing. Parasites replicate in hepatocytes for several days increasing the window of time in which a vaccine can have an effect as compared to targeting sporozoites which migrate from the mosquito bite to the liver, often within minutes.

TRAP has been fused to 20 T and B-cell epitopes[70], termed 'ME' for multiple epitope[71], to create the antigen ME-TRAP. ME-TRAP has been delivered using multiple vectors including DNA vectors[70] and Pox virus vectors[72] in both pre-clinical and clinical studies. Early on in development, modified vaccinia virus Ankara (MVA) vectors[73] were used alone, these were subsequently employed alongside recombinant chimpanzee adenovirus serotype 63 (ChAd63)[74] vectors in a heterologous prime-boost strategy. This strategy has been tested in clinical trials in Gambian and Kenyan adults where the heterologous prime boost strategy was shown to be safe and induce a strong T-cell response[75]. T-cell responses in malaria exposed infants (aged 5-17 months) were more subdued with no significant efficacy observed over the follow up period[76]. Researchers have also conducted trials of ChAd63/MVA-ME-TRAP in combination with RTS,S/AS01, a combination which should target both pre-erythrocytic lifecycle stages and therefore provide a stronger basis for protection. Results were initially positive[77] however a reduction in immunogenicity was observed in one study[78] indicating that immunisation dose and vaccination schedule will require further research.

1.2.5 PfCelTOS

The *P. falciparum* cell-traversal protein for ookinetes and sporozoites (CelTOS) is a microneme protein that mediates parasite invasion into both the liver and mosquito midgut and is therefore a potential multistage vaccine candidate[79]. Work in mouse models has yielded mixed results with one study showing robust protection using recombinant CelTOS with Montanide ISA against heterologous *P. berghei* challenge[80]. No protective efficacy was observed using a heterologous ChAd63-MVA prime-boost vaccination scheme with transgenic *P. berghei* challenge[81]. Subsequent studies have

found that recombinant CelTOS is poorly immunogenic but when given with a potent adjuvant such as glucopyranosyl lipid adjuvant-stable emulsion (GLA-SE)[82], toll-like receptor (TLR)-based adjuvants[83], or Monophosphoryl Lipid A (MPL)[84], robust cellular and humoral responses are observed. No human trial data has been published to date however one phase I clinical trial has been completed (Clinicaltrials.gov NCT02174978).

1.2.6 Transmission blocking vaccines (TBV)

Transmission blocking vaccines are a unique class of vaccine for parasitic diseases. The vaccines do not help the infected individual by providing direct immunity, but they may protect populations by preventing onward transmission of the disease aid eradication efforts. TBV vaccines typically focus on raising antibody responses to gametocyte and/or ookinete antigens. These antibodies are taken up in the mosquito blood meal and prevent the malaria parasite from completing its sexual lifecycle in the mosquito.

1.2.7 Pfs25

Pfs25 was the first TBV candidate antigen to progress to clinical trials and remains the most developed antigen to date. The protein is found on the surface of zygotes and ookinetes[85] and was first identified using mAbs that had potent TBV activity[86]. An early clinical trial of Pfs25 with Montanide ISA 51 had to be halted due to severe reactogenicity[87] however, data from patients receiving two 5 μg doses of Pfs25/ISA 51 showed that it was possible to induce transmission blocking antibodies through Pfs25 immunisation. Immune responses to Pfs25 were improved by conjugating the antigen to a VLP or nanoparticle, for example IMX313[88]. Pfs25 and Pfs25-IMX313 expressed from ChAd63 and MVA vectors yielded significantly better immune

responses that recombinant Pfs25 alone[89]. Pfs25-IMX313 is now progressing to phase I clinical trials (ClinicalTrials.gov: NCT04130282) and there is promising evidence that Pfs25-IMX313 can be combined with RTS,S/AS01 with no reduction in immunogenicity of either vaccine[90].

1.2.8 Pfs230 D1M

The *P. falciparum* 230-kDa sexual stage protein (Pfs230) forms a complex with Pfs48/45 (discussed below) on the surface of sexual stage parasites. Pfs230 domain 1 with no His_6 tag (referred to as Psf230 D1M) developed by the NIH is the current clinical lead[91] however other variants of the protein have been manufactured[92,93] for clinical trials. Clinical trials for Pfs230 have been planned, however no complete preclinical or clinical data has yet been published.

1.2.9 Pfs48/45

Pfs48/45 is one of the newest TBV candidates. Pfs48/45 contains a GPI moiety which anchors the Pfs48/45 - Pfs230 complex to the gametocyte surface[94]. Pfs48/45 is exposed when the gametocyte enters the mosquito midgut[95] and blocking its activity prevents gametocyte fertilization[96]. Transmission blocking antibodies are detected in between 20-30% of individuals in endemic areas[97] suggesting that a Pfs48/45 vaccine could benefit from natural boosting by parasite infection. Pfs48/45 is comprised of an N-terminal 6-cysteine domain, a central domain, and a C-terminal 6-cysteine domain. The 16 cysteine residues have historically made Pfs45/48 a difficult antigen to manufacture however recent progress has been made making a Pfs45/48 fusion with the R0 region of the blood start antigen Glutamate Rich Protein (GLURP) in *Lactococcus lactis*[98,99]; or as a soluble recombinant protein in the baculovirus

systems[100] and *Drosophila* Schneider-2 (S2) cells[101]. The neutralising epitopes in Pfs45/48 correspond to B-cell epitopes[102] present in the C-terminal domain and central domain. The current vaccine constructs undergoing pre-clinical trials correspond to the C-terminal and Central domains, 10C, and the C-terminal domains, 6C, named after the number of cysteines in each region, with the most potent known epitopes being located in the C-terminal 6C region[101]. Pfs45/48 is soon to enter clinical trials with pre-clinical trials in rhesus macaques yielding positive results[103].

1.2.10 Blood stage vaccines

The asexual blood stage of infection is the target of NAI and therefore may be a good target for vaccine-mediated immunity. Benefits of a blood stage vaccine include vaccination against clinical disease, if not generating sterile immunity, reducing mortality and morbidity of malaria and reducing parasite transmission by lowering the number of parasites in the blood. Blood stage vaccines have been criticised because they may allow asymptomatic carriers to continue transmission of the parasite, however, a blood stage vaccine would almost certainly be used as part of a multistage vaccine to provide the vaccinated individual a second layer of protection should some parasites successfully complete the lover stage of infection. In addition, with regulatory approval still a long way away for blood stage vaccines, there is time to research and properly quantify this possible risk at a later date.

Blood stage vaccine development benefits from an established standardised *in vitro* growth inhibitory activity (GIA) assay[104,105]. The GIA assay measures the ability of antibodies to inhibit merozoite invasion of erythrocytes in a controlled setting. GIA assays generally do not contain complement or F_c receptor expressing cells limiting the assay measurements to direct blocking of invasion. GIA however does not

necessarily correlate with NAI and protection against clinical disease[106], probably due to the complex interplay of immunological factors and anti-disease immunity discussed earlier. This is not necessarily a problem since NAI would be very difficult to replicate with a single vaccine and, given that NAI wanes with time and the parasite has evolved to evade NAI, it is not a desirable response to mimic. The GIA assay strictly measures anti-parasitic humoral immunity which may be seen as an 'unnatural' yet useful measure of protection for vaccine design[107]. Work to quantify the relationship between vaccine efficacy and *in vitro* GIA led to the development of the 'GIA_{50} titre' in challenge studies with *Aotus* monkeys[108]. GIA_{50} titre is a plasma dilution factor calculated by taking the total plasma IgG concentration and dividing it by the total purified IgG GIA EC_{50}. A GIA_{50} titre of 5 or higher was correlated with protection in *Aotus* monkeys, *i.e.* if the plasma can be diluted 5-fold and still shows 50% GIA or higher, then the animal was protected. This system was verified by passively transferring a known quantity of an anti-PfRH5 mAb, 2AC7, to *Aotus* monkeys followed by *P. falciparum* challenge[109]. Groups given 100 mg/kg of IgG, with GIA_{50} titres ranging from 14-20, were protected from challenge. Groups given 33 mg/kg were not protected with the highest GIA_{50} titre calculated as 4. *In vivo* growth inhibition (IVGI) can also be determined by calculating the percentage reduction in the parasite multiplication rate (PMR); here IVGI and *in vitro* GIA were found to correlate well further validating the *in vitro* GIA assay as an important tool for vaccine development[108]. Further work will be needed to determine if the same correlation remains true in humans however initial data indicate that the correlate is transferable to humans[110].

Once a blood stage vaccine candidate progresses to human trials the efficacy can be tested using controlled human malaria infection (CHMI)[111,112]. Volunteers are given a known number of *P. falciparum* iRBC intravenously after vaccination, normally 400 – 800 parasites per volunteer. Regular qPCR assays on blood samples can accurately determine the number of parasites in the blood on each subsequent day. From these data the parasite PMR can be calculated and used to determine the vaccine efficacy. When a defined endpoint is reached, subjects are treated with antimalarial drugs to clear the parasites. The blood-stage CHMI model bypasses the liver stage and enables a more controllable dose of parasite challenge than mosquito bite.

Despite these advantages blood stage vaccines face two main technical hurdles. Firstly, polymorphic merozoite surface antigens such as MSP1 have been used to generate effective blood stage vaccines in animal models[113], however, the responses have not translated into an effective vaccine in humans[114]. After decades of work, novel antigens that are highly conserved across strains have been identified, these will be discussed in the proceeding sections. Secondly, the speed of erythrocyte invasion leaves very little time for the immune system to block erythrocyte invasion. Live cell imaging shows that a merozoite takes 60 seconds to invade a new erythrocyte[115] with crucial antigens exposed for only a portion of this time.

1.2.11 Erythrocyte invasion by merozoites

Erythrocyte invasion by merozoites is a complex and coordinated process; insights into this process have uncovered several essential vaccine targets therefore a brief overview of the process is warranted. *In vitro* studies have shown that merozoites rapidly lose their ability to invade erythrocytes, with an invasive half-life of around 5 minutes[116]. This half-life is likely to be shorter *in vivo* due to pressure from the

immune system. It is therefore imperative that merozoites invade a new erythrocyte host and form the parasitophorous vacuole as soon as possible. To this end merozoites are highly specialised. Merozoites are polarized cells with the microneme and rhoptry bulb organelles (Figure 1.2A) primed with proteins required for entry into a new erythrocyte. Invasion occurs in several distinct phases[117] (Figure 1.2B) each mediated by different protein effectors.

The initial attachment between the RBC and merozoite is likely mediated by the Merozoite Surface Proteins (MSPs) however there is some evidence that they are not essential for invasion[118]. MSP1 appears to be the most important of the MSP family; MSP1 forms a complex with MSP3, MSP6, MSP7, MSPDBL1 and MSPDBL2[119] which interacts with the RBC plasma membrane through unknown receptors. Although the role of MSP1 in RBC invasion is still contentious there are many reports that MSP1 is one of the major targets for NAI[120]. In addition, MSP1 is also required for parasite egress from RBCs[118] indicating that the MSPs may play a multifaceted role in the asexual cycle.

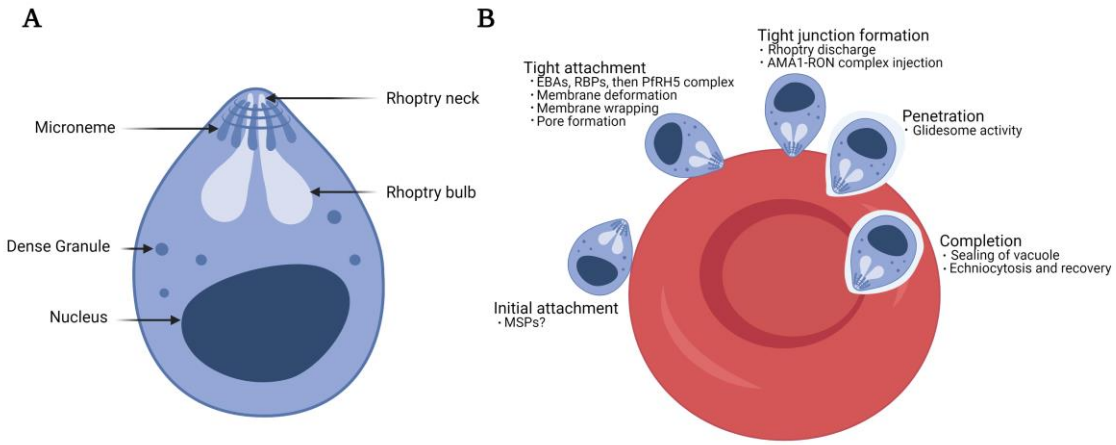


Figure 1.2 – Anatomy of the merozoite and invasion of an erythrocyte by *P. falciparum*.
A) The *P. falciparum* merozoite is a polarized cell with the apical organelles stacked and ready to release proteins required for erythrocyte invasion. **B)** Invasion requires several discrete steps: Initial attachment, tight junction formation, penetration using the actin-myosin motors, and parasitophorous vacuole formation. Image based on Cowman *et al.* 2017[121], created with BioRender.com.

The next step in invasion involves the Erythrocyte-Binding-Like (EBL) proteins and the Reticulocyte-binding-like protein Homolog (RH) proteins. This binding pathway was sometimes referred to as the alternative pathway due to the high degree of redundancy shown amongst the proteins. The evidence suggests that the function of the RH proteins is required, even if individually the proteins are not[122]. The exception to this rule is PfRH5, which is absolutely required for invasion. PfRH5 forms a ~200 kDa 'invasion complex' with Cysteine Rich Protective Antigen (PfCyRPA)[123], PfRH5 Interacting Protein (PfRIPR)[124], and PII3[125]; these proteins will be addressed in subsequent sections. The role of the EBLs and RH proteins has been thoroughly reviewed in Cowman *et al.* 2017[121] however, we expect that proteins from other protein families that play a role in invasion will be discovered in the future as knowledge of other apicomplexan parasites grows[126]. Binding of the EBAs and RH proteins leads to deformation of the erythrocyte membrane, reorientation of the merozoite, and wrapping of the RBC plasma membrane[127]. During this event, binding

of PfRH5 to its receptor basigin is followed by a Ca^{2+} influx into the RBC that is of uncertain function[128]. Shortly following this event a tight junction is formed by Apical Membrane Antigen 1 (PfAMA1) and Rhoptry Neck Protein 2 (PfRON2)[129]. PfRON2 is released by the rhoptries into the RBC plasma membrane to act as a receptor for PfAMA1[130] through a conserved 49 amino acid peptide termed PfRON2L[131]. The formation of the tight junction commits the merozoite to invasion of the RBC[132]. This junction has been targeted by both small molecule drugs[133] and peptides[134] in an attempt to find novel therapeutics against malaria. Finally the merozoite is pulled into the RBC by the 'glidosome', an actomyosin motor[135], forming the parasitophorous vacuole whilst shedding the outer merozoite membrane proteins.

1.2.12 PfAMA1/PfRON2

PfAMA1 was an early blood stage vaccine candidate antigen that showed a lot of promise in early non-human primates studies[136], however it was noted that protection was strain specific and required high antibody titres. Subsequent analysis has estimated that five variants of PfAMA1 may be required in a single vaccine[137] to achieve cross strain protection. This early optimism has now been tempered by a string of Phase I/II clinical trial failures[138–141] where no efficacy was observed against homologous parasite challenge by CHMI or against natural exposure in field efficacy trials. Recent strategies have shifted away from using PfAMA1 in isolation and now focus on immunisation with the PfAMA1/PfRON2 complex. Immunisation with PfAMA1-PfRON2L in a *P. yoelii* murine model induced complete protective immunity against homologous challenge whilst protection was not observed in animals immunised with individual antigens[142]. The induced antibody response however was not sufficient to protect against heterologous challenge, consistent with previous

studies demonstrating the importance of using multiple PfAMA1 variants. In this study immunisation with PfAMA1-PfRON2L complex induced qualitatively better antibodies than PfAMA1 alone due to a shift in antibody production towards the conserved loops surround the PfRON2L binding site in PfAMA1. This result was not replicated in rabbits in a separate study that found that immunisation with PfAMA1 with PfRON2 did not improve potency of PfAMA1 IgG responses[143]. In addition, no significant difference in GIA was observed and no improvement in antibody quality was found between vaccine groups. Further studies are thus needed to verify the utility of PfAMA1/PfRON2 complex vaccines, however with new and more promising vaccine candidate antigens emerging it is hard to see PfAMA1/PfRON2 vaccines progressing further clinically.

1.2.13 *P. falciparum* Reticulocyte-binding protein Homologue 5 (PfRH5)

For many years it was unclear why *P. falciparum* was able to invade mature erythrocytes whilst its close relative, *P. vivax*, could only invade reticulocytes. This difference is thought to be the primary driver of *P. falciparum's* increased virulence compared to *P. vivax.* Work to identify novel proteins involved in erythrocyte invasion led to the discovery of *P. falciparum* reticulocyte-binding protein homologue 5 (PfRH5)[144]. PfRH5 is a unique RH protein, it is smaller than its homologs, lacks a transmembrane domain or GPI anochor[144], and has so far only been identified in one human malaria species - *P. falciparum.* Invasion of erythrocytes by *P. falciparum* requires PfRH5 to bind to basigin (CD147)[145], this interaction is essential and PfRH5 knockouts are not viable. Recent work suggests that PfRH5 is the result of an introgression event from other closely related *Laverania* species[146], such as *P. praefalciparum*[147], which causes disease in gorillas. Subsequent mutations restricted

PfRH5 binding to human basigin[148] separating *P. falciparum* from other *Laverania* species. The exact role of PfRH5 in invasion remains unknown; its potential functions include cytoskeletal remodelling and inducing a calcium influx[117,128]. There is also an N-terminal processing step[144] of unclear function. The structure of PfRH5 (Figure 1.3) reveals a kite like structure[149] with little similarity to other known structures. Antibodies against PfRH5 are associated with protection against clinical malaria[61,150–152] in endemic areas, IgG3 antibodies in particular were associated with protection[153]. In addition PfRH5 is remarkably well conserved across *P. falciparum* isolates with only five SNPs identified at above 10% frequency in 227 field isolates[154] suggesting that PfRH5 would make a good vaccine target and hopefully circumventing the need for a mixed allele vaccine.

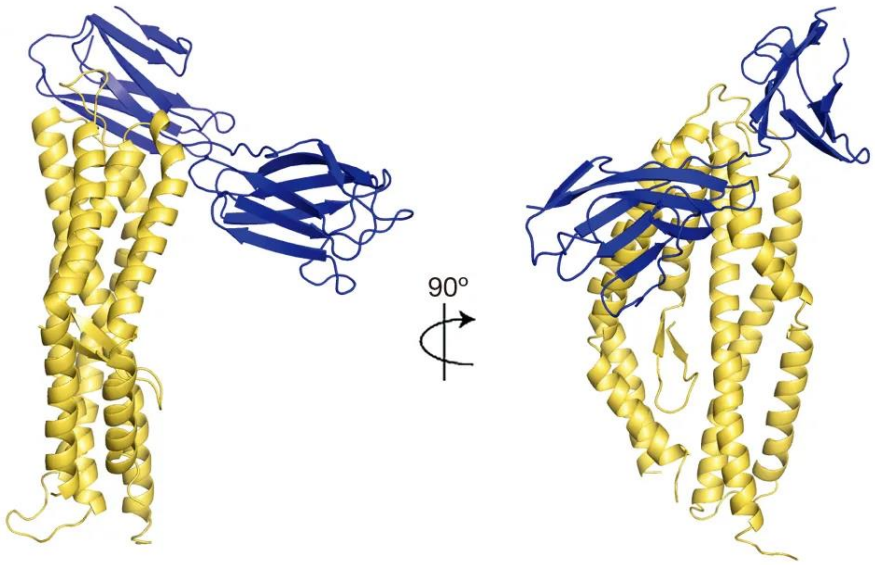


Figure 1.3 – The structure of PfRH5 bound to basigin.
PfRH5ΔNL (yellow) forms a kite like structure and binds to basigin (blue) through the tip of the kite. PfRH5ΔNL lacks the disordered amino terminus to enable crystallisation. Figure from Wright *et al.* 2014[149].

Monoclonal antibodies directed against PfRH5 can block invasion of erythrocytes by merozoites[154,155]. Some mAbs, such as QA1, QA5 and R5.004 overlap with the basigin binding site on PfRH5[149,156] whereas 9AD4, which does not block basigin binding *in*

vitro, still shows potent parasite neutralisation[155]. Further structural work showed that 9AD4 and R5.016, another potent PfRH5 mAb, overlap with the binding of one conformation of basigin and each other[156] suggesting that steric hindrance of the PfRH5-basigin interaction is likely the primary mediator of anti-PfRH5 mAb neutralising activity. A full list of published mAbs against PfRH5, PfCyRPA and PfRIPR is given in Table 1-3**.** The serendipitous discovery of a non-neutralising PfRH5 mAb that potentiates the activity of neutralising mAbs[156] raises intriguing questions for vaccine design and the functional role of PfRH5. R5.011, a mAb with no GIA activity *in vitro*, improved neutralising activity of functional mAbs by 10-fold. This was achieved by slowing the invasion of the merozoite from 25 seconds to >60 seconds presumably allowing more time for other neutralising mAbs to bind.

Initial vaccine studies with PfRH5 used viral vectored vaccines including replication-deficient adenovirus human serotype 5 (AdHu5) and MVA[157]. Subsequently full length recombinant PfRH5 was made in several expression systems including HEK293E cells[154,157] and insect cells[158,159]. A thermostable version has also been developed[160] which can be produced in *E. coli* and features 18 mutations to improve stability. The use of PfRH5 as a vaccine candidate was firmly established when a PfRH5 vaccine was found to be protective against a heterologous *P. falciparum* challenging in *Aotus* monkeys[108]. PfRH5 has quickly progressed to clinical stage testing with some promising results. A Phase Ia clinical trial[161] in UK adults using ChAd63 and MVA encoding PfRH5 induced anti-PfRH5 antibodies with cross-strain functional growth inhibition activity. A follow up trial in Tanzanian adults, children and infants has recently been completed with results expected soon (ClinicalTrials.gov: NCT03435874). A third trial using recombinant PfRH5 protein PfRH5.1/AS01$_B$ with

CHMI challenge has now completed human trials in the UK with initial results showing a reduction in parasitaemia in vaccinated volunteers[110].

1.2.14 *P. falciparum* Cysteine Rich Protective Antigen (PfCyRPA)

PfRH5 does not act in isolation. PfRH5 forms a 1:1:1 200kDa complex called the RCR (PfRH5/PfCyRPA/PfRIPR) complex. Other proteins may be involved; however, their identities and functions are unknown. PfCyRPA was identified as part of a screen of *P. falciparum* open reading frames[162] and later confirmed as a binding partner of PfRH5 and PfRIPR by co-immunoprecipitation of the RCR complex with anti-PfRH5 antibodies[123]. PfCyRPA acts as the central protein in the RCR complex binding both PfRH5 and PfRIPR[163]. PfCyRPA performs an essential role in the invasion process functioning prior to PfAMA1-PfRON2 binding but after the calcium influx triggered by PfRH5-basigin binding[128], however its exact role has not yet been elucidated. Similar to PfRH5, antibodies raised against recombinant PfCyRPA had GIA activity against multiple strains of *P. falciparum*[123,164]. Antibodies against PfCyRPA were also found to be additive[165] and synergistic[166,167] when combined with antibodies against additional blood stage antigens suggesting that a multiple antigen blood stage vaccine could be very potent.

PfCyRPA has a 6-bladed β-propeller structure (Figure 1.4) resembling a sialidase yet lacking sialidase activity[168]. The 6-bladed propeller shape enables PfCyRPA to bind PfRH5 through the blade 4 and blade 5 connecting loop and to PfRIPR through blade 6[163] (Figure 1.6). None of the proteins in this complex have membrane bound domains or GPI anchors so it is currently not known how the complex is secured to the membrane – if at all. A number of anti-PfCyRPA mAbs that inhibit parasite growth have been identified (full list in Table 1-3). Structural work has determined that mAb

C12 binds between blades 2 and 3[168] whereas mAb 8A7 binds blade 1[165]. Interestingly mAb 8A7 displaces PfRH5 binding[165], supposedly through blocking the PfRH5 C-terminal interaction with blade of PfCyRPA[163] however this seems odd given that the binding of 8A7 on blade 1 does not overlap with the PfRH5-PfCYRPA interface. Two other mAbs: 5B12 and 3D1 have invasion blocking activity yet do not disrupt the CyRPA-PfRH5 complex, therefore their invasion blocking mechanism remains unknown.

Monoclonal antibodies against PfCyRPA have shown that there is a promising future for PfCyRPA as a vaccine candidate however anti-PfCyRPA antibodies are not found in endemic region populations[169] suggesting that PfCyRPA is poorly immunogenic in natural infection. Further work establishing the immunogenicity of PfCyRPA in humans will be crucial moving forward.

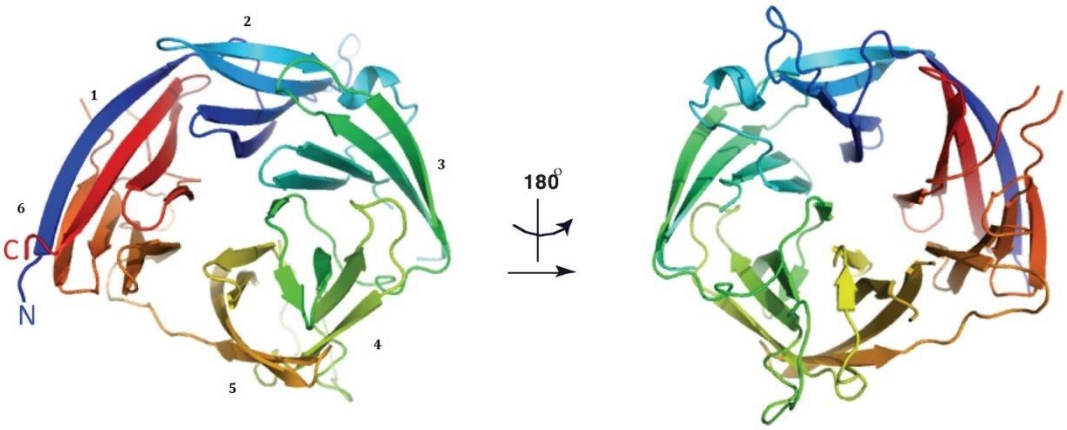


Figure 1.4 – Crystal structure of CyRPA.
Ribbon representation of CyRPA coloured from Blue (N-terminus) to red (C-terminus) with blade numbers labelled. Figure adapted from Chen *et al.* 2017[165]

1.2.15 *P. falciparum* PfRH5 Interacting Protein (PfRIPR)

P. falciparum PfRH5 interacting protein (PfRIPR) is the third member of the RCR complex and the primary subject of this Thesis. PfRIPR is a ~120 kDa protein that was found to co-immunoprecipitate with PfRH5[124] and later found to form the RCR complex with PfRH5 and PfCyRPA[128,170]. PfRIPR is a large complex protein containing ten epidermal-growth factor like (EGF) domains (Figure 1.5) with 87 cysteine residues implying a structure bound by extensive disulphide bridging. The protein is cleaved into two ~60kDa halves by plasmepsin X (PMX)[171], these two halves remain tightly associated[124], the functional significance of this cleavage event is unclear. Like the other members of the RCR complex, PfRIPR is highly conserved with only 19 SNPs above 0.5% frequency identified in analysed populations, 3 above 10% frequency. A list of SNPS is given in Table 1-2.

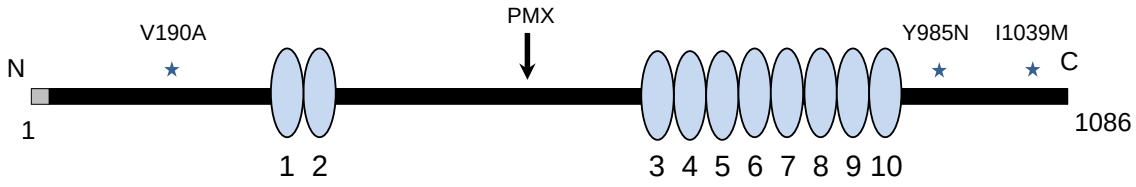


Figure 1.5 – Schematic of PfRIPR.
The protein contains 10 epidermal-growth factor like domains, blue ovals, these are numbered 1-10 from N to C terminus. The putative plasmepsin X cleavage site is indicated with a black arrow. The location of SNPs above 10% frequency are highlighted with blue stars (MalariaGen).

The cysteine rich nature of PfRIPR has made the recombinant full-length protein difficult to make. PfRIPR fragments have been made using *E. coli*[124], baculovirus-infected Sf21 cells, and *Pichia pastoris*[166] with full length PfRIPR only being produced in *Drosophila* Schneider 2 cells[163], albeit at low yields[163]. The structure of PfRIPR has also been refractory to study, likely due to the protein's flexible nature. A low-

resolution cryoEM structure was produced in complex with PfRH5 and PfCyRPA[163] (Figure 1.6) however at least half of the protein could not be resolved. The structure did suggest that the C-terminus was predominantly loops and β-strands, consistent with the EGF domain structural prediction; in addition, two α-helices in the N-terminus (residues 196–211 and 364–373) were identified. The α-helix at 196-211 and a β-strand of unknown sequence, possibly from EGF domains 1-2, interact with PfCyRPA blade 6[163]. PfRIPR is not known to bind directly to PfRH5, despite its name.

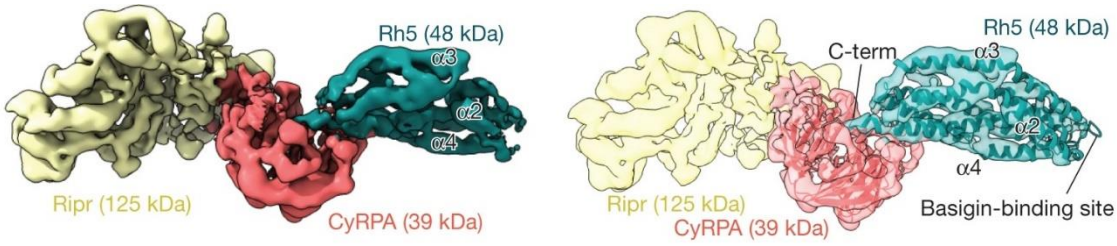


Figure 1.6 – CryoEM structure of the RCR complex.
The three proteins form an elongated complex with PfCyRPA at the centre. The amino terminus half of PfRIPR interacts with PfCyRPA through an α-helix found prior to the first two EGF domains. The carboxy terminus half of PfRIPR could not be resolved in the structure probably due to its flexibility; from Wong *et al.* 2018[163]

PfRIPR is located in the apical microneme of the merozoite but co-localises with PfCyRPA and PfRH5 at the plasma membrane during invasion of erythrocytes[123,124,128]. The precise role of PfRIPR in invasion is vaguely defined; the RCR complex triggers a Ca^{2+} release on PfRH5-Basigin binding[128] before the PfAMA1 /PfRON2 tight junction forms, however the role of PfRIPR in this process has not been elucidated. Insights into the function of PfRIPR may be drawn from the study of other malaria species. PfRH5 is not present in *P. knowlesi* and *P. vivax* yet both of these species have RIPR and CyRPA orthologues that are essential for survival[172]. No complex involving PkCyRPA was detected in *P. knowlesi*, however PkRIPR was found

to form a novel triple complex with thrombospondin-related apical membrane protein (PkTRAMP) and cysteine-rich, small, secreted protein (PkCSS)[172]. This PkTRAMP-PkRIPR-PkCSS complex may be functioning in an analogous way to the RCR complex in *P. falciparum* and therefore insights into each of the protein's functions may help elucidate the role of RIPR in *P. falciparum.*

Antibodies against PfRIPR have been shown to inhibit the growth of multiple strains of *P. falciparum*[123,124,128,166,173] with two neutralising monoclonal antibodies, 1G12 and 5G6, recently published[166]. Both of these antibodies bind PfRIPR EGF-like domain 7, the structure of which could unfortunately not be seen in the cryo-EM structure of the RCR complex. These antibodies bind the RCR complex to form a quaternary complex and may block insertion of PfRIPR into the erythrocyte membrane, however this theory, as proposed by Wong *et al*[163]., is contentious (M. Higgins personal communication). An additional study published in 2020 further highlighted the importance of the C-terminal EGF domains[174]. Rats vaccinated with a PfRIPR fragment corresponding to PfRIPR EGF (5-9) produced GIA positive sera, unlike rats immunized with other fragments. These initial studies, combined with studies that demonstrate that there is little natural immune response to PfRIPR[175], suggest that PfRIPR may be a strong candidate for a next generation blood stage vaccine.

Table 1-2 – Table of PfRIPR SNPs above 0.5% frequency

MAF_Global	Mutant Name	Mutant Type	ref	Non-ref	ancestral
0.396741*	Y985N	N	A	T	T
0.131053*	V190A	N	A	G	A
0.10834*	I1039M	N	T	C	T
0.091343	A755G	N	G	C	C
0.079706	H511R	N	T	C	C
0.069326	L673V	N	A	C	C
0.032609	V883L	N	C	A	C
0.031003	A1003S	N	C	A	C
0.027887	N144K	N	A	T	A
0.019936	D995E	N	G	T	G
0.015474	N228K	N	A	C	A
0.015406	H524L	N	T	A	-
0.014606	N66Y	N	T	A	T
0.014307	T327A	N	T	C	T
0.013912	Y184S	N	T	G	T
0.013836	G341R	N	C	T	T
0.006422	N1060S	N	T	C	T
0.005907	V281A	N	A	G	G
0.004905	L199S	N	A	G	A

*denotes SNPS above 10% frequency
N = non-synonymous

Table 1-3 - List of published mAbs for PfRH5, PfCyRPA and PfRIPR with accompanying details

Antigen	Name	Growth inhibition	GIA EC_{50} or result	Binds or blocks formation of the RCR	K_D	Structure	Notes	Reference
PfRH5	2AC7	✓	15 µg/ml	Disrupts[166]	3.2×10^{-10}	-	One cycle GIA	Douglas *et al.* 2014[155]
	9AD4	✓	62 µg/ml	Binds	6.4×10^{-10}	Wright *et al.* 2014[149]		
	QA1	✓	38% at 500µg/mL	Disrupts	1.4×10^{-09}	Wright *et al.* 2014[149]		
	QA5	✓	63% at 500µg/mL	Disrupts	1.2×10^{-09}	-		
	6BF10	✓	30% at 500µg/mL	Disrupts	-	-		
	8BB10	×	-	Binds		-		
	4BA7	×	-	Binds		-		
	RB3	×	-	Binds		-		
	R5.001	×	-	-	1.62×10^{-09}	-	One cycle GIA	Alanine *et al.* 2019[156]
	R5.002	×	-	-	1.27×10^{-08}	-		
	R5.003	×	-	-	1.09×10^{-09}	-		
	R5.004	✓	22.3 µg/mL	-	6.36×10^{-10}	Alanine *et al.* 2019[156]		
	R5.005	×	-	-	-	-		
	R5.006	×	-	-	3.46×10^{-09}	-		
	R5.007	✓	50% at 3mg/mL	-	8.63×10^{-09}	-		
	R5.008	✓	69.5 µg/mL	-	8.86×10^{-10}	-		
	R5.009	×	-	-	5.31×10^{-10}	-		
	R5.010	×	-	-	4.63×10^{-10}	-		
	R5.011	×	-	-	1.03×10^{-11}	Alanine *et al.* 2019[156]		
	R5.012	×	-	-	-	-		
	R5.013	✓	184.0 µg/mL	-	7.79×10^{-11}	-		
	R5.014	×	-	-	$<9.21 \times 10^{-13}$	-		
	R5.015	×	-	-	6.73×10^{-011}	-		
	R5.016	✓	9.6 µg/mL	-	4.28×10^{-10}	Alanine *et al.* 2019[156]		
	R5.017	✓	26.6 µg/mL	-	2.01×10^{-10}	-		
	R5.018	✓	496.6 µg/mL	-	1.58×10^{-11}	-		
	R5.019	✓	31.0 µg/mL	-	1.54×10^{-10}	-		
PfCyRPA	C02	✓	-	-	5.57×10^{-11}	-	mAbs inhibit *P. falciparum* growth in the NOD-*scid* IL2Rγ^{null} mouse model	Dreyer *et al.* 2012[162]
	C04	✓	-	-	1.11×10^{-09}	-		
	C05	×	-	-	1.13×10^{-11}	-		
	C06	✓	-	-	1.34×10^{-10}	-		
	C08	✓	-	-	1.83×10^{-08}	-		
	C09	✓	-	-	3.01×10^{-11}	-		
	C10	✓	-	-	7.65×10^{-12}	-		
	C12	✓	-	-	1.00×10^{-09}	Favuzza *et al.* 2017[168]		
	C13	×	-	-	-	-		

Table 1.3 (continued)

Antigen	Name	Growth inhibition	GIA EC_{50} or result	Binds or disrupts the RCR	K_D	Structure	Notes	Reference
PfCyRPA	SB1.5	×	-	-	-	-	-	Favuzza *et al* 2016[164]
	SB1.6	✓	64% at 500µg/mL	-	-	-		
	SB2.1	✓	55% at 500µg/mL	-	-	-		
	SB2.3	✓	40% at 500µg/mL	-	-	-		
	SB2.4	×	-	-	-	-		
	SB2.5	×	-	-	-	-		
	SB3.3	✓	40% at 500µg/mL	-	-	-		
	SB3.8	×	-	-	-	-		
	SB3.9	×	-	-	-	-		
	3D1	✓	~70% at 2mg/mL	Binds	6.5 (±0.6) x 10^{-10}	-	2 cycle GIA	Chen *et al.* 2017[165]
	8B9	×	-	-	-	-		
	7A6	×	-	-	-	-		
	8A7	✓	~70% at 2mg/mL	Disrupts	5.7 (±2.0) x 10^{-10}	Chen *et al.* 2017[165]		
	5B12	✓	~70% at 2mg/mL	Binds	2.7 (±0.3) x 10^{-9}	-		
PfRIPR	1C4	×	-	Binds	-	-	2 cycle GIA	Healer *et al.* 2019[166]
	1G12	✓	0.35 mg/mL	Binds	4.0 (±1.6) x 10^{-11}	Binds PfRIPR EGF (7)		
	3C3	×	-	Unknown	2.1 (±0.7) x 10^{-10}	-		
	4A8	×	-	Unknown	2.4 (±0.6) x 10^{-10}	-		
	5G6	✓	0.8 mg/mL	Binds	6.4 (±0.9) x 10^{-11}	Binds PfRIPR EGF (7)		

1.3 Structure based vaccine design

The majority of licenced vaccines were developed without structural information on the target antigens or the location of the neutralizing epitopes. Vaccines were commonly live-attenuated or inactivated virus or bacteria which generate a broad immune response to multiple antigens. Although this strategy has been very effective, the 'low hanging fruit' of vaccine development has all been taken. In contrast, these approaches have been poorly efficacious for "difficult" diseases such as influenza, HIV, and malaria. Even when a subunit vaccine is used inducing a broad range of neutralising and non-neutralising antibodies, the non-neutralising antibodies can be neutral or detrimental to the development of protection[176,177]. Structure based design can therefore be used to design better immunogens and therefore improve vaccines for some of the most difficult infectious diseases. Some of the best examples in structure-based vaccine design come from viral diseases. Many viruses use class I fusion proteins to facilitate cell invasion, these proteins are often present in a metastable pre-fusion conformation that undergoes a conformational shift into a more stable post-fusion conformation on host cell receptor binding. The respiratory syncytial virus (RSV) fusion protein F is one such protein. The infectious virus almost exclusively displays the pre-fusion conformation. The RSV vaccine, RSV inactivated with formalin (FI-RSV), caused severe respiratory disease in vaccinated individuals when initially tested[176]. It was found that the FI-RSV has little or no protein F in the pre-fusion state[178] meaning that it did not accurately reflect the epitopes of the infectious virus. Protein engineering was then used to create a stabilised pre-fusion subunit vaccine which is capable of generating a strong neutralising humoral response[179]. This approach has now been applied to several viral diseases included

SARS-CoV-2[180]. In addition to stabilised fusion proteins, both protein scaffolds[181] and self-assembling nanoparticles[181] can improve vaccine efficacy. All of these structure-based design methods could be used to generate new malaria vaccines especially since the structures of proteins such as PfRH5 and PfCyRPA bound to neutralising mAbs are now known.

1.4 Thesis aims and overview

PfRIPR is a promising new blood stage vaccine candidate, however very little is known about the protein and few neutralising antibodies are available. In this Thesis I aim to identify neutralising epitopes on PfRIPR, progress PfRIPR into a viable blood stage vaccine candidate, and develop new neutralising anti-PfRIPR monoclonal antibodies.

Chapter 2 details the materials and methods used in this Thesis.

Chapter 3 describes efforts to produce a number of PfRIPR protein fragments that were used as tools to identify the targets of GIA negative antibodies. Using these protein fragments, in an antigen reversal GIA assay, I identified the regions of PfRIPR that are targeted by GIA positive antibodies from purified anti-PfRIPR rabbit IgG. I also examined whether non-neutralising anti-PfRIPR mAbs can bind to the RCR complex, and investigated a potential PfRIPR erythrocyte receptor.

In Chapter 4 I took the insights from Chapter 3 and developed a new, smaller PfRIPR vaccine based on the identified epitopes. Various versions of this vaccine were tested in mice and rats, this includes virus-like particle and fusion vaccines. I also investigated the immune response to co-immunisation with multiple antigens in the RCR complex.

Chapter 5 describes attempts to generate new GIA positive monoclonal antibodies against PfRIPR. I also investigate synergy between GIA negative and positive anti-PfRIPR antibodies leading to potential designs of an improved PfRIPR vaccine.

Chapter 6 summarises this work and discusses the future work that can build upon this Thesis.

Chapter 2 - Materials and Methods

2.1 Chapter 3 methods

2.1.1 Expression constructs

PfRIPR constructs were cloned into custom expression plasmids based on the commercially available pENTR4 expression vector (ThermoFisher). pENTR4LP contains the kanamycin resistance gene for selection in *E. coli* and a modified long version of the CMV promoter incorporating intron A. A gene string containing a mouse IgG signal sequence, cloning site, linker and C-tag was inserted into Jenner Institute plasmid #4965 (based on pENTR4LP), a plasmid developed in house by Dr David Pattinson, via HindIII and BbcVI restriction enzyme sites. This new plasmid was designated #5251. A second gene string containing a monomeric Fc (monoFc)[182], tobacco etch virus (TEV) protease cleavage sequence, mouse IgG signal sequence, cloning site, linker and C-tag was also inserted into #4965 using the same enzyme to create a second expression plasmid designated #5252. Both plasmids have a CMV immediate early promoter containing an intron and a bovine growth hormone (BGH) polyA tail.

2.1.2 Construction of PfRIPR fragment plasmids

The PfRIPR construct used for fragment production was based on the 3D7 clone *P. falciparum* sequence with eleven mutations introduced to ablate N-linked glycosylation and a C-terminal 4-amino acid C-tag (EPEA). Each fragment was genetically fused to the monoFc using a G4S linker to improve solubility and expression.

PfRIPR fragment sequences were isolated by PCR using OneTaq® Hot Start Quick-Load® 2X Master Mix with Standard Buffer (NEB). PfRIPR full-length target sequence plasmid IDs were given in Table 2-1, primers used were given in Table 2-6 in section 0. Plasmid #5285 was used for all PfRIPR fragments except the following: PfRIPR N-half: #3133, PfRIPR C-half, produced in S2 cells, #4093.

Thermal cycling conditions:

94°C for 30s, 30 cycles [94°C for 30s; Tm°C for 20s, 68°C for 30s per kbp], 68°C for 5 min.

PCR products were digested with BamHI-HF and KpnI-HF for 1h at 37˚C then cleaned with MinElute Reaction Cleanup Kit (Qiagen). Plasmids #5251 and #5252 were linearised with BamHI-HF and KpnI-HF and the digests run on a 1% agarose gel. Plasmid #5251 and #5252 backbones were isolated using a gel extraction kit (Qiagen). 100ng of #5251 or #5252 was ligated with T4 DNA Ligase (NEB) at a 1:1 or 1:3 ratio backbone to insert. Ligations were transformed into One Shot™ TOP10 Chemically Competent *E. coli* and plated on Lysogeny broth (LB) agar plates with kanamycin at 50µg/mL and incubated at 37˚C overnight. 'No ligase' and 'no insert' controls were included. Colonies were picked and incubated in 5mL LB-kanamycin cultures at 37˚C and 220rpm overnight. Plasmid DNA was isolated using Qiagen miniprep kit according to manufacturer's instructions. Plasmid DNA was digested with BamHI and KpnI to ensure the PfRIPR fragment insert was present. Correct cultures were used to seed a 200mL LB Kanamycin, at 50µg/mL, culture and incubated overnight at 37˚C and 220rpm. Plasmid DNA was isolated using Qiagen Maxiprep plus kits according to the manufacturer's instructions. Plasmid DNA was quantified using the Nanodrop 2000 and stored at -20˚C.

Table 2-1– Sequence IDs of PfRIPR plasmids used in experiments

Jenner PfRIPR Sequence number	Codon optimised	N-X-T/S Glycosylation sites	Notes
3133	Mammalian	Intact	Based on NCBI accession sequence: XP_001351305
4093	S2	mutated N-Q	
4797	Mammalian codon harmonised	S/T - A	Developed by WRAIR
5825	Mammalian	mutated N - Q	Based on 3133

2.1.3 Plasmid preparation and *E. coli* culture

1µg of plasmid DNA was used to transform chemically competent *E. coli* (NEB® 5-alpha). 1µg was added to 25µL of competent cells, these were then incubated on ice for 30 minutes. The cells were heat-shocked at 42˚C for 30 seconds followed by a 2-minute incubation on ice. 250µL of pre-warmed SOC media was then added and the cells incubated at 37˚C at 225 rpm for one hour. Cells were plated on LB-agar plates containing the appropriate antibiotic. After 24 hours a single colony was used to seed an appropriate volume of LB with antibiotic and incubated at 37°C and 225rpm for approximately 18 hours. Plasmid DNA was then prepared using Plasmid Plus mini or maxi kits (Qiagen) as per the manufacturer's instructions.

2.1.4 Sequencing

All sequencing was carried out by GATC-biotech, now Eurofins, by Sanger (dye-termination) sequencing.

2.1.5 Cell culture

Suspension HEK293F cells were cultured in disposable non-baffled Erlenmeyer flasks (Corning) and passaged in serum-free Gibco Expi293™ medium (Life Technologies). Cells were cultured at 37˚C, 130rpm and 8% CO_2. Cells were passaged twice weekly

at a density of 3.5 x 10^5 cells/mL or when required. Cell counts were determined using disposable haemocytometers (FastRead).

Suspension Schneider 2 (S2) cells were cultured in disposable non-baffled Erlenmeyer flasks (Corning, USA) in Ex-cell 420 Insect serum free medium (Sigma) supplemented with pen-strep to a final concentration of 100 U/ml penicillin, 0.1 mg/ml streptomycin (Sigma). Flasks were seeded at 8 x 10^6 cells/mL and passaged twice a week, once by dilution and once by centrifugation at 300xg for 3 minutes followed by resuspension in fresh media. Cell counts were determined using a Casy Counter (OLS OMNI Life Science).

2.1.6 Generating stably transfected S2 cell lines

Protocols for the stable transfection of S2 cell lines were provided by ExpreS^{2}ion Biotechnologies. A summary is provided below.

Day 1: S2 cells were split by centrifugation (300g, 3 minutes) and resuspend at 5 x 10^6 cells / mL in complete medium (Ex-cell 420 Insect serum free medium, 100 U/ml penicillin, 0.1 mg/ml streptomycin, 10% FBS) and incubated at 115rpm, 25°C for 24 hours. Day 2: Cells were centrifuged (300g, 3 minutes) and resuspended in incomplete media (Ex-cell 420 Insect serum free medium, 100 U/ml penicillin, 0.1 mg/ml streptomycin) at 2 x10^6 cells / mL. 5mL of cell suspension was transferred to a non-vented T25 followed by 50 µL ExpreS^2 Insect-TR reagent, 12.5 µg of DNA was then added to the flask. Flasks were incubated at 25°C for 2-4 hours prior to adding 1mL FBS to a final volume of 6mL. Day 3: 4000 µg/mL of G418 was added for selection. Day 5: Cells were diluted to 1 x 10^6 cells / mL. Day 6 onwards: Cells were counted every 3-4 days splitting cultures down to 1 x 10^6 cells / mL when appropriate. Week 3: Cells were counted every 3-4 days. When the cells reach a density of ≥ 3 x 10^6

cells/mL they were transferred to a T75 with an additional 4mL of complete media. Cells were recounted 4 days later, if the cells were again ≥ 3 x 10^6 cells/mL another 5mL of complete media was added. Cells were continually passaged and counted until they reach ≥ 8 x 10^6 cells/mL. Cells were then centrifuged and resuspended to 8 x 10^6 cells/mL in incomplete medium in a new shake flask.

2.1.7 PfRIPR fragment production

Each PfRIPR protein fragment was expressed as a secreted protein from HEK293F cells using the Expi293™ Expression System (Thermo Fischer). Briefly, HEK293F cells were seeded on day 0 at 1E06 cells/mL. On day 1 cells were transfected with a mix of DNA (1µg/mL) ExpiFectamine™ 293 transfection reagent and OptiMEM (Life Technologies, UK). DNA and ExpiFectamine™ 293 transfection reagent were mixed and incubated at room temperature for 20 minutes before being added to the cells. After 16 hours, ExpiFectamine™ 293 enhancer 1 and 2 were added according to manufacturer's instructions. Supernatants were harvested after a further 56-hour incubation.

Supernatants were processed by centrifugation at 500g for 5 minutes then 3200g for 15 minutes. Supernatants were then filtered through a 0.22µm Steritop™ (Merck). Proteins were then purified using FPLC on an ÄKTA pure (GE Lifesciences) using a 10ml CaptureSelect™ C-tag affinity matrix (Thermo Fischer Scientific) followed by a final polishing step on a Superdex™ 200 Increase 10/300 GL or Hiload 16/600 size exclusion column (SEC, GE Healthcare). Appropriate fractions were pooled, quantified on the Nanodrop 2000, aliquoted and finally snap frozen in liquid nitrogen. Proteins were stored at -80˚C.

The PfRIPR N-half was generated using the 3D7 clone *P. falciparum* sequence with N-linked glycosylation left intact (plasmid number #3133). The PfRIPR N-half was produced in HEK293F cells using the Expi293™ Expression System (Thermo Fisher) in the presence of 5μM kifunensine (Abcam ab215116). Following affinity purification with CaptureSelect™ C-tag affinity matrix (Thermo Fischer Scientific) the purified protein was incubated overnight in 5L TBS buffer in a 3.5 kDa Dialysis cassette Slide-A-Lyzer (Thermo), with a 1 to 50 ratio of purified protein to EndoH (Promega V4875.). After treatment the EndoH was removed on a Superdex™ 200 Increase 10/300 GL size exclusion column (SEC, GE Healthcare).

2.1.8 Removal of monomeric Fc domain

Before any PfRIPR fragments were used in *in vivo* for immunisations the monoFc, which was added to improve expression and solubility, was removed using TEV protease. 5mg of purified PfRIPR protein fragment was incubated with TEV protease (Sigma/promega) at a 1:10 v/v ratio overnight at 4˚C on a rolling mixer. The sample was then centrifuged at 10,000 g in a benchtop centrifuge to remove any aggregated protein before affinity purification on a 1mL CaptureSelect™ C-tag affinity matrix. The cleaved monoFc and TEV protease lack a C-tag so were found in the column flow through. Cleaved and un-cleaved PfRIPR fragment bind to the C-tag column and were eluted. The un-cleaved mono-Fc PfRIPR fragment was removed from the cleaved PfRIPR fragment using a Superdex™ 75 Increase 10/300 GL size exclusion column (SEC, GE Healthcare).

2.1.9 Mass Spectrometry

Liquid chromatography-tandem mass spectrometry (LC-MS/MS) and intact mass analysis were performed at the Centre for Medicines Discovery (CMD) under the guidance of Dr Rod Chalk and Tiago Moreira.

2.1.10 Protein quantification

Proteins were quantified using Pierce™ BCA Protein Assay Kit (Thermo Scientific), a colorimetric assay based on the reduction of Cu^{+2} to Cu^{+1}, according to manufacturer's instructions.

2.1.11 SDS-PAGE and western blots

1 µg of protein was made up to 11µL with PBS and 4 µL of laemmli buffer (BioRad). For reducing conditions 10x NuPAGE LDS reducing sample (Thermo Fisher) was added followed by heating to 95˚C for 10 mins. Samples were loaded onto a NuPAGE Bis-Tris 4-12% midi gel (Thermo Fisher) including NEB Colour Prestained Protein Standard, Broad Range (11–245 kDa), and run for 45 mins at 200V in MES buffer. Gels were washed in diH_2O and placed in 20 mL SimplyBlue SafeStain (ThermoFisher) for 1 h. The gel was washed once with diH_2O then left in diH_2O overnight to de-stain.

For western blots 100-200ng of protein was prepared and run on a gel in the manner described above. The gel was washed in diH_2O then the proteins transferred to a nitrocellulose membrane using the Trans-Blot® Turbo™ Transfer System (BioRad). The gel was loaded using pre-soaked Nitrocellulose transfer packs and run using a manufacturer specified 'turbo' programme. The iBind Western Systems (Thermo Fisher) were used for the blocking, primary and secondary antibody steps. The primary Capture select Biotin anti-C-tag conjugate (Thermo Fisher) and secondary, streptavidin alkaline phosphatase conjugate (Thermo Fisher) antibodies were diluted

in iBind™ Flex Solution and drawn over the membrane by the iBind flex card overnight. Detection was carried out using SIGMA FAST™ BCIP/NBT (5-Bromo-4-chloro-3-indolyl phosphate/Nitro blue tetrazolium), one tablet wash dissolved in 10mL water then poured over the membrane. The reaction was stopped by washing the membrane in water after the protein bands became visible.

2.1.12 Dot blot arrays for non-functional PfRIPR mAbs

200ng of full-length PfRIPR, monoFc-GFP (negative control), and PfRIPR protein fragments were pipetted onto a 0.2 μm nitrocellulose membrane and allowed to air dry. Immunoblotting was performed using the Invitrogen iBind Western System according to manufacturer's instructions with each primary mAb diluted to 2 μg/mL. Alkaline phosphatase conjugated Goat Anti-Mouse IgG, Fc specific, (Sigma-Aldrich) diluted to 1:2000 was used for detection with Sigmafast BCIP/NBT alkaline 405 phosphatase substrate at 1 mg/mL (Sigma-Aldrich).

2.1.13 Protein complex analysis with size exclusion chromatography

Protein-protein interactions were initially screened using size exclusion chromatography (SEC). First, 30 μg of each individual protein was made up to 500μL in TBS pH7.4. Samples were then injected onto a Superdex™ 200 Increase 10/300 GL column. Protein amounts were optimised for each assay to give a 3-4 mAU peak on the UV trace for better resolution. To test protein-protein interactions, an equimolar amount of each protein, with one protein held constant at 30μg, were mixed and made up to a final volume of 500μL in TBS pH7.4 and incubated for 18 hours at 4°C. Samples from each chromatogram peak were run on an SDS-PAGE gel to identify which proteins were present.

2.1.14 Peptide ELISA for determining PfRIPR linear epitopes

A set of sixty-two biotinylated 20-mer peptides of PfRIPR overlapping by 12 amino acids (Table 2-7) were synthesised (Mimotopes). The peptides correspond to amino acids 21-247 and 364-648 of PfRIPR as these were the only regions that could not be made in HEK293 cells. Peptides included an N-terminal biotinylated linker peptide (biotin-SGSG). Peptides were resuspended in 1mL DMSO to an average concentration of 1.7 mg/mL. Streptavidin-coated 96-well plates (Pierce; Cat #15125) were coated with 50µL peptide diluted to 5 µg/mL in DPBS and then stored for 18 hours at 4°C. Plates were washed with PBS/T and then blocked for 1 hour with 200 µL of Blocker™ Casein (ThermoFisher) followed by washing five times with PBS/T. 50 µL of mAb was added at an initial concentration of 2 µg/mL and incubated for 2 h. After washing, 50 µL of an anti-mouse whole IgG specific alkaline phosphatase-conjugated secondary antibody (Sigma-Aldrich) diluted to 1:1000 was added. Plates were incubated for a further 60 minutes. Plates were washed five times with PBS-T before being developed with 100 µL of PNPP alkaline phosphatase substrate for 20 minutes and read at 405 nm on an Infinite 50 plate reader (Tecan).

2.1.15 SPR assay for anti-PfRIPR mAbs

Data were collected using a Biacore X100 (GE healthcare, now Cytiva). Experiments were performed at 25°C in SPR running buffer (PBS + 0.05% Polysorbate-20, Cytiva). 1500 RU PfRIPR was amine-coupled to a CM5 chip (Cytiva) using standard N-Hydroxysuccinimide (NHS)/ ethyl(dimethylaminopropyl) carbodiimide (EDC) coupling chemistry. PfRIPR mAbs were diluted in running buffer to a final concentration of 0.5 µM. mAbs were injected at a flow rate of 10 µL/min for 60s. Running buffer was injected at a flow rate of 10 µL/min for 240 s to allow the mAbs

to dissociate. The surface was regenerated with 10 mM glycine pH 1.5 at a flow rate of 10 µL/min for 30 s. Binding values were measured manually in the Biacore X100 control software. The kinetic parameters of the non-functional mAbs were determined using the Biacore X100 evaluation software by fitting to a 1:1 Langmuir binding model.

2.1.16 Production of red blood cell receptors

SEMA7A and AMIGO2 were produced in HEK293 cells according to the protocol in section 2.1.7. Plasmids for both receptors were obtain from Addgene: Semaphorin7A-CD4d3+4-bio and AMIGO2-CD4d3+4-bio were gifts from Gavin Wright (Addgene plasmid #73115 and #73103). Both plasmids were cut with NotI and EcoRI to excise the receptor sequence from #73115 and #73103, these were ligated into Jenner plasmid #5619 which contains a C-tag for purification.

2.1.17 SPR assay for anti-PfRIPR mAbs

Data were collected using a Biacore X100 (GE healthcare, now Cytiva). Experiments were performed at 25°C in SPR running buffer (PBS + 0.05% Polysorbate-20, Cytiva). 1500RU PfRIPR was amine-coupled to a CM5 chip (Cytiva) using standard NHS/EDC chemistry. SEMA7A and PfCyRPA were diluted in running buffer to a final concentration of 2.0 µM. Proteins were injected a flow rate of 10 µL/min for 60s. Running buffer was injected at a flow rate of 10 µL/min for 240 s to allow the proteins to dissociate. The surface was regenerated with 10 mM glycine pH 1.5 at a flow rate of 10 µL/min for 30 s. Binding values were measured manually in the Biacore X100 control software. The kinetic parameters of the protein-protein interactions were determined using the Biacore X100 evaluation software by fitting to a 1:1 Langmuir binding model. An anti-PfRIPR mAb was included in the assay as a positive control.

2.1.18 Rabbit immunisations

Rabbit immunisations were first outsourced to GenScript, USA. 20 µg protein was used to immunise 4 rabbits via intramuscular injection (IM) in complete Freund's adjuvant on day 0 and incomplete Freund's adjuvant on days 14, 28 and 42. Pre-immune blood samples were taken on day -2 and final bleed and serum harvest was taken on day 56. Subsequent rabbit studies were outsourced to Cambridge Research Biochemicals (CRB), UK. Two rabbits were immunised IM with 50 µg antigen on day 0, 21 and 42 in Montanide ISA720 adjuvant. Pre-immunisation bleeds were taken at day -2 and final bleeds were taken at day 64. Four rabbits were immunised at the National Institute of Allergy and Infectious Diseases (NIAID, USA) by Dr Kazutoyo Miura. 50 µg of antigen was given IM in complete Freund's adjuvant on day 0 and incomplete Freund's adjuvant on day 21 and 42. Pre-immunisation bleeds were taken at day -2 and final bleeds were taken at day 64.

2.1.19 Purification of IgG from sera

IgG purification is based on the NIH MVDU Protocol IM-6018-00. 10 mL polypropylene columns (Pierce Cat. No. 29924) were packed with 2mL Immunopure Plus Immobilized Protein G Gel (Pierce Cat. No. 22852) and stored in 70% ethanol. Before use, columns were degassed manually to ensure consistent flow rates. 10 mL of diH_2O was run over the column to remove the 70% ethanol, followed by 10 mL binding buffer (Immunopure IgG Binding buffer, Pierce, Cat. No. 21011), 10mL elution buffer (0.1 M glycine pH2.7) and finally 20 mL binding buffer to equilibrate the column. Serum samples were first diluted with binding buffer to a final volume of 10 mL. The serum was then applied to the column, the flow through collected and applied to the column again according to Table 2-2 below:

Table 2-2 – Serum volumes and run times for IgG purification

Species	Minimum volume (mL)	Maximum volume (mL)	Number of times to run over the column	Expected yield (mg)
Mouse	1.3	2	4	0.3 – 2
Rat	1	2	4	3 – 6
Rabbit	1	4	2	2 - 5

The column was washed twice with binding buffer followed by elution with 10mL elution buffer into a tube containing 350 µL 1 M Tris pH9. The column was finally washed with 20 mL elution buffer, 20 mL binding buffer, 10 mL diH_2O and 10 mL 70% ethanol. If the purified IgG was to be used in the GIA assay, the IgG was futher buffer exchanged with a 30kDa Amicon centrifugal filter, first into RPMI 1640 then incomplete media (IMC, RPMI 1640 supplemented with 25 mM HEPES, 35µM hypoxanthine, 2 mM L-glutamine). Prior to use in GIA assay, RBC adsorption is required. To each purified IgG sample, 50 µl of 100% haematocrit human O+ RBCs was added per 1 ml of original serum sample and mix at 1200 rpm for one hour at room temperature. Samples were then centrifuged at 5000 xg for 2 minutes to pellet the RBCs. Samples were then transferred to a sterile filtration tube and centrifuged at 5000 xg. IgG can then be quantified using the Nanodrop 2000 and stored at -20 °C.

2.1.20 Parasite culture and Growth inhibitory activity assay

Parasites were cultured using standard protocols[105]. Briefly, parasites were grown in complete culture medium at 2% haematocrit using O+ red blood cells. Complete culture medium comprised RPMI 1640 supplemented with 10% heat-inactivated pooled human serum, 25 mM HEPES, 35µM hypoxanthine, 2 mM L-glutamine, and 20 µg/mL gentamycin. Culture flasks were gassed with a gas mixture of 5% O_2, 5% CO_2 and 90% N_2, and kept at 37°C.

Parasite cultures were synchronized the day before GIA assay set up using 5% sorbitol. Sorbitol kills late stage parasites by osmotic lysis whilst young parasites and uninfected RBCs (which are not sorbitol permeable) remain unaffected. Synchronised parasites were returned to culture until GIA assay set up the following day.

2.1.21 Growth inhibitory activity (GIA) assay

GIA assays were performed to the protocol of the international GIA reference centre at NIAID, NIH, USA[183]. Parasite cultures were synchronised using treatment with 5% sorbitol on the day before GIA assay set up.

Synchronised *Plasmodium falciparum* parasite cultures (3D7 clone) at the trophozoite/early schizont stage were cultured with test samples for 40-44 hours at 1% haematocrit at a starting parasitaemia of 0.4%. Endpoint parasitaemia was quantified by measurement of parasite lactate dehydrogenase activity read using a Varioskan flash plate reader (ThermoFisher) at a 650nm wavelength. Percent GIA was calculated using the following equation:

$$\%\ \text{GIA} = 100 - \frac{100(\text{Sample}_{A650} - \text{Uninfected RBC}_{A650})}{(\text{Infected control}_{\text{A650}} - \text{Uninfected RBC}_{A650})}$$

Assays were quality-controlled by inclusion of the anti-RH5 mAb 2AC7[155] as an in-plate control, and the anti-RH5 mAbs 2AC7, QA5, 9AD4 as external plate controls. 5mM EDTA is included as a positive control and a Zaire Ebolavirus glycoprotein-reactive IgG1 mAb (EBL040)[184] was used as a negative isotype control for mAb samples.

2.1.22 GIA reversal assays

The GIA activity of a mAb or purified IgG can be reversed by the addition of a protein that binds the antibodies in the assay. The GIA assay is set up as previously described but with the addition of a protein of interest, in ICM, added to the plate at a starting concentration of 1.0μM. For titrations, the starting concentration can be up to 20μM and serially diluted down the plate. Proteins were also tested in the absence of mAb or purified IgG to ensure that the protein itself did not cause GIA.

2.1.23 Statistical analysis

Statistical analysis was conducted using GraphPad Prism. All GIA curves were fitted with a Richard's five-parameter dose-response curve with no constraints. EC_{50} values were interpolated from each curve. A 5-parameter curve was chosen since the GIA curves are not symmetrical around the midpoint and are therefore modelled more accurately using a 5-parameter curve. In some cases, the data was not of sufficient quality to use a 5-parameter curve therefore a 4-parameter curve was used instead. This will be indicated in the figure legend.

For GIA reversal assays, significance was determined by Kruskal-Wallis test with Dunn's multiple comparisons test against the control 10 mg/mL anti-PfRIPR pool. The threshold for statistical significance (α) was set at 0.05

2.2 Chapter 4 methods

2.2.1 Conjugation to hepatitis B surface antigen (HBsAg)

A SpyTag fused PfRIPR protein fragment and then HBsAg-SpyCatcher were thawed and left to equilibrate on ice for at least 15 minutes. An equimolar amount of the antigen and HBsAg VLP were mixed in a 2mL tube and incubated overnight at 4˚C. After incubation the tube was examined by eye for precipitation, if precipitation had occurred the contents were centrifuged at 14,000g for 10 minutes. The free antigen and fused HBsAg-Antigen were separated using fast protein liquid chromatography (FPLC) on a Superose 6 10/300 GL column (GE healthcare). The appropriate fractions corresponding to the HBsAg-Antigen peak were combined and quantified using the BCA assay. The VLP was then aliquoted, snap frozen using liquid nitrogen and stored at -80˚C.

Conjugation efficiency was measured by densitometry. 1µg conjugated VLP was made up to 11 µL with PBS, 4 µL of laemmli buffer (BioRad), and 1.5 µL 10x NuPAGE LDS reducing sample (Thermo Fisher). Samples were heated to 95˚C for 10 minutes. Samples were loaded onto a NuPAGE Bis-Tris 4-12% midi gel (Thermo Fisher) including NEB Colour Prestained Protein Standard, Broad Range (11–245 kDa), and run for 45 minutes at 200V in MES (2-[N-morpholino]ethanesulfonic acid) buffer (ThermoFisher). Gels were washed in diH_2O and placed in 20mL SimplyBlue SafeStain (ThermoFisher) for 1 hour. The gel was washed once with diH_2O then left in diH_2O overnight to de-stain. The density of the larger MW conjugated HBsAg-Antigen band and smaller HBsAg was measured using image J software and a percentage conjugated VLP was calculated.

2.2.2 Dynamic light scattering (DLS)

The size of conjugated HBsAg samples were checked by DLS using the Zetasizer Nano ZSP machine. 50 µL of sample volume was analysed in a quartz cuvette at 25°C. Measurements were performed in triplicate with 10-15 readings taken per sample. The Z-average and polydispersity index were calculated by the Zetasizer software.

2.2.3 Endotoxin testing

Endotoxin testing was carried out using ToxinSensor™ Chromogenic LAL Endotoxin Assay Kit (GenScript).

2.2.4 Mouse vaccination studies

BALB/c mice were immunised with an equimolar amount of each antigen normalised to 2 µg full-length PfRIPR. For VLP immunisations, the conjugation efficiency for each VLP was determined and used to calculate an equimolar dose of conjugated antigen. Each sample was made to a volume of 25 µL with sterile DPBS then mixed with 25 µL Addavax™ adjuvant (Invitrogen) to a final volume of 50 µL. The 50 µL was administered via IM injection to the quadriceps of mice anaesthetised with vaporized isofluorane with 25 µL injected into each leg. Two immunisations at 14-day intervals were given with blood sampling via tail bleeds taken the day before immunisation. Blood was harvested at the end of the study by cardiac puncture under terminal anaesthetic.

All animal experiments and procedures were performed according to the UK Animals (Scientific Procedures) Act Project Licence (PPL: PA7D20B85) and approved by the Oxford University Local Ethical Review Body.

2.2.5 Optical density (OD) ELISAs

OD ELISA was carried out by coating PfRIPR or PfRIPR protein fragments at 2 µg/mL in 50µL on Maxisorp flat-bottom 96-well ELISA plates (Nunc). Plates were incubated at 4 °C overnight. Plates were washed six times with (phosphate-buffered saline with 0.05% Tween 20 (PBS-T) and blocked with 200 µL Blocker™ Casein (ThermoFisher) or 10% milk powder for 1 hour at room temperature. After another six washes with PBS-T, 50 µL of rabbit serum diluted 1 in 100 in Blocker™ Casein was added to each well and the plate incubated for 2 hours at room temperature. The plate was washed six times with PBS-T followed by addition of 50 µL of a 1 in 1000 dilution in blocking agent of goat anti-rabbit IgG (whole molecule) or goat anti-mouse IgG (Fc specific) alkaline phosphatase-conjugated secondary antibody (Sigma-Aldrich). After a 1 h incubation at room temperature the plates were washed six times with PBS-T. The plates were developed with 4-nitrophenylphosphate substrate at a final concentration of 1 mg/mL (Sigma-Aldrich) in water and diethanolamine and read on an Infinity F50 plate reader at 405 nm (Tecan).

2.2.6 Rat pilot study immunisations

Rat immunisations were carried out by Noble Life Sciences, Inc, USA. Rats were immunised with an equimolar dose of antigen normalised to 2 µg of full length PfRIPR with 25 µg of Mtrix-M™ adjuvant (Novavax, USA). The conjugation efficiency of the VLP vaccines was considered when the normalisation calculations were conducted. Rats were immunised on days 0, 28 and 56 with blood samples taken on days -2, 27 and 55 with a terminal bleed at day 70.

2.2.7 Study O1, O2 and O3 rat immunisations.

Rat immunisations were carried out by Noble life sciences, USA, using a standard regime. Wistar Rats (a commonly used outbred laboratory rat) were immunised IM on days 0, 28 and 56 with antigen in 25 µg of Matrix-M™ adjuvant (Novavax). Blood samples were taken at day -2, 42 and a final cardiac bleed at day 70. Each study used a different combination of antigens, these are detailed in the tables below.

Table 2-3 – Study O1 groups and antigens.

Group	Antigen	Dose (µg)	Group size
1	RH5.1	2.00	6
2	RH5.1	0.20	6
3	RH5.1	0.02	6
4	CyRPA	2.00	6
5	RIPR	2.00	6
6	Matrix-M Only	0	6
7	Negative Control	0	3

Table 2-4 - Study O2 groups and antigens.

Group	Antigen	Antigen Doses						Group size
		PfRH5.1 (µg)	PfCyRPA (µg)	PSRIPR (µg)	RCR (µg)	Other (µg)	Total (µg)	
1	PfRH5.1	2					2	6
2	PfCyRPA		20				20	6
3	PfRIPR			20			20	6
4	PfRH5.1 + PfRIPR	2		20			22	6
5	PfRH5.1 + CyRPA	2	20				22	6
6	PfRIPR + PfCyRPA		20	20			40	6
7	PfRH5.1 + PfCyRPA +	5.36	3.51	11.11			20	6
8	PfRH5.1 + PfCyRPA +	2	20	20			42	6
9	Reconstituted RCR				20		20	6
10	Matrix-M Only						NA	3
11	PfRIPR-EGF (5-8)					3.97	3.97	6

Table 2-5 - Study O3 groups and antigens.

Group	Antigen	Dose (µg)	Conjugation efficiency	Group size
1	HBsAg RH5.1	2	67%	6
2	HBsAg RH5.1	0.2		6
3	HBsAg RH5.1	0.02		6
4	HBsAg PfCyRPA	20	86%	6
5	HBsAg PfCyRPA	2		6
6	HBsAg PfRIPR-EGF (5-8)	20	44%	6
7	HBsAg PfRIPR-EGF (5-8)	2		6
8	HBsAg	20		6

2.2.8 Rat IgG standardised quantitative ELISAs

Nunc Immuno 96 well ELISA plates were coated with 50µL of 2 µg/mL PfRIPR, PfRH5 or PfCyRPA diluted in DPBS and incubated overnight at 4°C. Plates were then washed 6 times with PBS/T followed by blocking with 200 µL of Starting Block T20 for 1 h. After another 6 washes, 50 µL of samples in triplicate and standards diluted in starting block were added as follows:

PfRIPR: 1:128,000 dilution of reference control serum, a standard curve starting at 1:8000 dilution of reference serum followed by 2-fold dilutions, and a blank control.

PfRH5: 1:64,000 dilution of reference control serum, a standard curve starting at 1:4000 dilution of reference serum followed by 2-fold dilutions, and a blank control.

PfCyRPA: 1:3,200 dilution of reference control serum, a standard curve starting at 1:100 dilution of reference serum followed by 2-fold dilutions, and a blank control.

The plate layout is as follows:

	1	2	3	4	5	6	7	8	9	10	11	12
A	S1	S2	S3	S4	S5	S6	S7	S8	S9	S10	S11	S12
B	S1	S2	S3	S4	S5	S6	S7	S8	S9	S10	S11	S12
C	S1	S2	S3	S4	S5	S6	S7	S8	S9	S10	S11	S12
D	Internal control	S13	S14	S15	S16	S17	S18	S19	S20	S21	S22	Internal control
E	Internal control	S13	S14	S15	S16	S17	S18	S19	S20	S21	S22	Internal control
F	Internal control	S13	S14	S15	S16	S17	S18	S19	S20	S21	S22	Internal control
G	Blank	1	2	3	4	5	6	7	8	9	10	Blank
H	Blank	1	2	3	4	5	6	7	8	9	10	Blank

After a 1 h incubation the plates were washed and 50 µL of the secondary antibody, 1:1000 dilution of goat anti-rat IgG (whole molecule) Sigma A8438, was added to each plate. After the final wash, 100µL of development buffer, 1x diethanolamine and 4-nitrophenylphosphate at a final concentration of 1mg/mL, was added. The plate was read using Bio-tek ELx808 Microplate Reader with Gen5 ELISA software. The plate was developed until the internal control developed to either 128, 000 PfRIPR AU, 64,000 PfRH5 AU or 3,200 PfCyRPA AU, depending on the assay. The assay was accepted if the R^2 value for the standard curve was >0.994, the Abs405 of the blank wells was 0.15, and the reference value is within 20% of 128,000. Any reading that was below the linear portion of the standard curve at a 1:100 dilution was regarded as negative. Any readings that were above the linear portion of the standard curve were repeated in another ELISA assay at higher dilution. PfRIPR AU was converted to PfRIPR IgG µg/mL using the conversion factor developed by Sarah Silk using calibration free concentration analysis (CFCA): RIPR = 7.046ng/mL per 1 AU (Draper

group, unpublished). Therefore, AU datasets are multiplied by 0.007046 to give μg/mL.

2.2.9 Purification of IgG from rats and mice

Purification of IgG from sera was carried out as detailed in section 2.1.19.

2.2.10 Growth inhibitory activity assay

GIA assays were carried out as detailed in section 2.1.21.

2.2.11 Growth inhibitory activity assay quality analysis

GIA curves are plotted as GIA (%) against total purified IgG (mg/mL). The amount of PfRIPR-specific IgG can be quantified by performing the standardised ELISA (section 2.2.8) on the purified IgG samples used in the GIA assay. The GIA data can then be plotted as GIA (%) against PfRIPR IgG (μg/mL) to give a GIA (%) per μg of PfRIPR IgG.

2.3 Chapter 5 methods

2.3.1 Mouse immunisations

BALB/c and CD1 mice were immunised IM with 2μg of HBsAg-EGF (5-6) or 2μg HBsAg-EGF (7-8) in Addavax™. Each sample was made to a volume of 25μL with sterile DPBS then mixed with 25μL of Addavax™ adjuvant (Invitrogen) to a final volume of 50μL. The 50 μL was administered via IM injection to the quadriceps of mice anaesthetised with vaporized isofluorane with 25μL injected into each leg. Immunisations were carried out on days 0, 14, 28 and 42 with blood samples taken by tail bleed on days -1, 7, 21 and 35. Cardiac bleeds and spleens were taken on day 46.

2.3.2 Hybridoma generation

Hybridomas were generated using StemCell™ technologies' polyethylene glycol (PEG) protocol, media C, D and E were purchased form StemCell technologies.

SP2/0 cells were cultured in media A for at least 1 week prior to fusion. SP2/0 cells were passaged every 2-4 days and seeded at $5x10^4$ cells/mL.

Spleens from immunised mice were crushed through a cell strainer into a 50 mL falcon tube containing 10 mL of media D0 (DMEM supplemented with 2 mM L-glutamine, 100 U/mL penicillin, 0.1 mg/mL streptomycin). 30mL media D0 was added to each tube and the cells counted using the Casy Counter (OLS OMNI Life Science). 1 x 10^8 cells and 2 x 10^7 SP2/0 cells were washed 3 times in media D0 by centrifuging for 5 minutes at 1350 rpm with the splenocytes and SP2/0 cells added together for the final spin. The cell pellet was disrupted and 1 mL of PEG added dropwise. The mix was stirred continuously for 1 min followed by the addition of 4

mL media D0. Samples were then stirred for 4 minutes. 10 mL media B was added and the mix incubated at 37°C for 15 minutes. The cell fusion mix was washed three times with 30mL of media D10 (DMEM supplemented with 10% FBS, 2mM L-glutamine, 100 U/mL penicillin, 0.1 mg/mL streptomycin) before resuspending the pellet in media C and transferring to a T75 flask. Flasks were incubated for 24 hours at 37°C. After incubation, cells were centrifuge at 400g for 5 minutes and resuspend in 8.5mL of media C. Cells were then added to 90mL of semi-solid media D and mixed by inverting several times. The bottle was allowed to stand for 15 minutes to allow air bubbles to rise to the top. A blunt end needle and 20 mL syringe was used to add 17 mL of cell suspension to Nunc omnitrays. Plates were placed in a plastic container with a layer of sterile distilled water to maintain moisture and incubated at 37°C for 10-14 days. Hybridoma colonies were picked into 200 µL media E using the ClonePix 2 Mammalian Colony Picker (Molecular Devices). 10-14 days after colony picking, plates were screened for positive colonies by anti-PfRIPR EGF (5-8) ELISA. Positive colonies were expanded to 24 then 12 well plates and re-screened by ELISA. Positive colonies were then single cell sorted by Drew Worth using the MoFlo cell sorter (Beckman Coulter). Cells were sorted into Media E supplemented with 1x BM Condimed H1 (Sigma). After 7-10 days plates were screened by ELISA and the top 6 colonies were picked and expanded to 6 well plates. Colonies were then adapted to media A (without BM Condimed H1) by splitting cells continuously into media A for two weeks. Roughly 50% of colonies did not survive the adaption process. Surviving colonies were frozen and stored in liquid nitrogen.

Hybridoma production was also outsourced to CRB. Hyrbidomas were generated from mice immunised with 2 µg HBsAg-PfRIPR-EGF (5-8). Briefly: mice were

immunised by sub-cutaneous injection of HBsAg-PfRIPR-EGF (5-8) in CFA on day 0. Mice were immunised again on days 14, 28 and 42 by intraperitoneal injection. Serum was analysed by anti-PfRIPR EGF (5-8) ELISA on day 45. The mouse with the highest ELISA response was immunised again on day 76 by intrasplenic injection. Splenectomy and hybridoma fusion were carried out on day 79. Individual clones were screened by ELISA against PfRIPR EGF (5-8). The most promising clone was isolated by limiting dilution cloning to produce sister hybridoma clones.

2.3.3 Hybridoma culture

Hybridomas were maintained in High glucose DMEM (Sigma-Aldrich) supplemented with 2mM L-glutamine, 100U/mL penicillin, 0.1mg/mL streptomycin and 10% ultra-low IgG foetal bovine serum (Thermofischer). When the hybridomas reached confluence in a T75 flask, cells were transferred to a CELLine two-compartment bioreactor (Integra biosciences) for large scale production. Supernatants were harvested weekly and frozen at -20˚C.

2.3.4 Monoclonal antibody purification

Monoclonal antibodies were purified using a 5mL Protein G HP column (GE Healthcare) on an ÄKTA Pure FPLC system (GE healthcare). Equilibration and wash steps were performed with TBS pH 7.4 and mAbs were eluted in 0.1M citrate pH 3.0. The eluates were pH equilibrated to 7.4 using 1.0M Tris HCl pH 9.0, the eluent peaks were pooled and further purified on a Hiload 16/600 size exclusion column (SEC, GE Healthcare). Purified mAb was then concentrated using an Amicon ultra centrifugal concentrator (Millipore) with a molecular weight cut-off of 30 kDa.

2.3.5 Construction of an PfRIPR protein fragment tetramer

A BAP tag (ASGLNDIFEAQKIEWHE)[185] was added to the C-terminal end of EGF domains 7-8 (amino acids 817-897) immediately upstream of the C-Tag. The biotinylated PfRIPR-EGF fragment was produced as previously described in section 2.1.7 however the PfRIPR-EGF-BAP plasmid was co-transfected with a plasmid encoding the Biotin ligase BirA at a 1:1 ratio. The resulting biotinylated protein was purified and the MonoFc cleaved off as previously described. Probes were generated on the day of flow cytometry by mixing a 4:1 molar ratio of biotinylated PfRIPR EGF (7-8) to the streptavidin conjugated fluorophores PE or APC (BioLegend).

2.3.6 Single sorting IgG producing B-cells

Spleens from immunised mice were processed by standard methods and enriched for B-cells using the EasySep™ Mouse B Cell Isolation Kit (StemCell). These B-cells were stained with the viability stain FVS780, anti-mouse IgG-FITC, anti-B220-PECy7, and with fluorophore-conjugated tetramers described previously. Stained B-cells were single-cell sorted using a MoFlo cell sorter (Dako cytomation) into 96-well PCR plates containing 10 µL 10 mM Tris HCl buffer and RNase inhibitor (Promega) at 40 U/mL. These plates were stored at -80˚C.

2.3.7 Variable region PCR and cloning

One-step RT-PCR was carried out with a QIAGEN Sensiscript RT kit (Qiagen) using 50 µM of random hexamers as primers. Plates were incubated for 1 hour after which the cDNA could be frozen at -20°C or used directly for PCR.

Several sets of primers were used for variable region PCR. These PCR reactions were used in a number of combinations in an attempt to amplify the variable chains, none

of these were successful. Rather than list every attempted combination the conditions and primers of each base PCR reaction are given below.

2.3.7.1 In-house PCR method

Primers and conditions were based on "Jenner Protocol J432 Production of Monoclonal Antibodies from mouse hybridomas v1". For the Gamma chain PCR 10 µL of each forward primer 100 µM primer stock and 20 µL of each reverse 100 µM stock were mixed (primers given in section 0, Table 2-8). 10µL of 2x Phusion master mix (NEB), 1µL of Gamma primer mix and 8 µL of H_2O are required for each PCR reaction. 19 µL of PCR master mix was dispensed into a PCR plate with 1 µL cDNA.

For the Kappa chain PCR, 15 µL of each forward primer 100 µM stock and 45 µL of the one reverse 100 µM primer stock were mixed (primers given in section 0, Table 2-8). 10µL of 2x Phusion master mix (NEB), 1µL of Gamma primer mix, 1 µL DMSO and 7 µL of H_2O were required for each PCR reaction. 19 µL of PCR master mix was dispensed into a PCR plate with 1 µL cDNA.

The following PCR cycler conditions were used for both the Kappa and Gamma chain PCR reactions: 98°C for 2mins, [98°C for 10s, 72°C for 60secs] for 10 cycles, [98°C for 10s, 71-65°C for 30s, 72°C 30s] 5 cycles at each annealing temperature, 1°C increments; 72°C for 600s.

2.3.7.2 PCR method based on Ho et al.

The second PCR method is based on the publication by Ho *et al*. 2016[186]. For the Gamma chain: 20 µL of 100 µM MsVHE primer and 6µL of Cy1, Cy2b, and Cy2c 100

µM primers were mixed with 262 µL H_2O to form a primer mix. Primer sequences are given in section 0

Table 2-10. 2 µL of primer mix, 10µl of 2x Phusion master mix (NEB), 0.5 µL DMSO and 6.5 µL H_2O is required for each PCR reaction with 1 µL cDNA. PCR cycling conditions were as follows:

98°C for 30s, [98°C for 10s, 70°C for 30s, 72°C 60s] for 40 cycles, 72°C for 600s.

For the Kappa chain: 30 µL of each 100 µM reverse primer stock were mixed with 30 µL H_2O to form a 10 µM primer mix. Primer sequences are given in section 0

Table 2-11. 2 µL of primer mix, 10µl of 2x Phusion master mix (NEB), 0.5 µL DMSO and 6.5 µL H_2O was required for each PCR reaction with 1 µL cDNA. PCR cycling conditions were as follows:

98°C for 30s, [98°C for 10s, 74-69°C for 30s, 72°C 60s] 6 cycles at each annealing temperature, 1°C increments; 72°C for 600s.

2.3.7.3 Kappa PCR based on NIH protocols

Only the Kappa variable chain PCR was attempted using the NIH protocol. 10 µl of each 100 µM stock of forward primer were mixed to generate a 10 µM working stock. 10 µl of 100 µM reverse stock was mixed with 30 µl H_2O to generate a reverse primer working stock. Details of primers given in section 0 Table 2-12. For each PCR reaction 36.1 µl H_2O, 5 µl cDNA, 5 µl 10x buffer, 1 µl 10 µM dNTP, 0.5 µl $MgCl_2$, 1 µl forward primer mix, 1 µl reverse primer mix and 0.4 µl of HotStarTaq Plus (Qiagen) was required. PCR cycling conditions were as follows:

95°C for 5 mins, [95°C for 3s, 58°C for 30s, 72°C 60s] for 50 cycles, 72°C for 600s.

2.3.8 SPR for functional anti-PfRIPR mAbs

SPR analysis was conducted as detailed in section 2.1.15.

2.3.9 Depletion of PfRIPR EGF (5-8) antibodies from purified IgG

Serum from rabbits immunised with PfRIPR in section 2.1.18 was taken and the IgG purified as per section 2.1.19.

MonoFc-PfRIPR-EGF (5-8) was coupled to an HiTrap NHS-Activated HP affinity column (Cytiva) using standard amide coupling as per manufacturer's instructions using the AKTA pure system. Briefly: The column was washed with 30mL ice cold 1mM HCl followed by 10mg MonoFc-PfRIPR-EGF (5-8) at 2mg/mL in TBS pH 7.4. The column was allowed to stand for 30 minutes at room temperature. The column was then washed and deactivated by alternate washes with buffer A (0.5 M ethanolamine, 0.5 M NaCl, pH 8.3) and buffer B (0.1 M sodium acetate, 0.5 M NaCl, pH 4). The column was finally equilibrated with TBS pH 7.4.

The purified IgG, in TBS, was flowed over the column at 1 mL/min and the flow through collected. Bound IgG was eluted with 1mM glycine pH 2 and the eluate pH equilibrated to 7.4 using 1.0M Tris HCl pH 9.0. The column was equilibrated with TBS and the collected IgG flow-through sample was reapplied to the column to ensure all anti-PfRIPR EGF (5-8) antibodies were bound to the column. Flow-through and eluent samples were buffer exchanged into ICM, concentrated and sterile filtered prior to GIA assay analysis.

2.3.10 Measure of Synergy in the assay of GIA

Experiments to assess synergy between mAbs or PfRIPR EGF (5-8) depleted purified IgG were set up as described in section 2.1.21. However, instead of one mAb or IgG

sample in each assay, two samples were added. mRP012 was held constant at 2 mg/mL to generate GIA at ~30%, the second mAb or purified IgG sample was also held at 2 mg/mL. Each mAb or purified IgG sample was also run in isolation so that the additive or synergistic effects could be calculated.

2.4 Appendix 1 – Primers and sequences

Table 2-6 – List of primers used to generate PfRIPR protein fragments

Name	Sequence	Target	Enzyme sites	FW/RV
NhalfCoFW	gatcggatccGATCTGATCGAGGGCATCTT	Codon optimised (3133) Nhalf (NH)	BamHI	FW
NhalfCoRV	gatcggtaccaccGTTAGAGTTGGTGTGGGGGT	Codon optimised (3133) Nhalf (NH)	KpnI	RV
NhalfChFW	GATCGGATCCGCCATTGACCTGATCGAGGG	Codon harmonised (4797) Nhalf	BamHI	FW
NhalfChRV	GATCGGTACCACCGTTGCTGTTGGTATGGGGGT	Codon harmonised (4797) Nhalf	KpnI	RV
NhalfS2FW	GATCGGATCCGATCTGATCGAGGGCATCTT	S2 codon optimised (4093) Nhalf	BamHI	FW
NhalfS2RV	GATCGGTACCACCGTTCGAGTTGGTGTGGGGAT	S2 codon optimised (4093) Nhalf	KpnI	RV
BGWP004	gatcggtaccaccGTAGTTCTCTTCGCACACAT	CO PfRIPR (5285) N-Terminal	KpnI	RV
BGWP007	gatcggatccAATATCAACAACATGAATAT	CO PfRIPR (5285) Chalf region	BamHI	FW
BGWP008	gatcggtaccaccGTTCTGGTTGGAGTAATAGA	CO PfRIPR (5285) Chalf region	KpnI	RV
BGWP009	gatcggatccCGGTGCACCCAGGACATCTG	CO PfRIPR (5285) EGF(1-2)	BamHI	FW
BGWP010	gatcggtaccaccGTAGCACTTGTTGTTGTGGT	CO PfRIPR (5285) EGF(1-2)	KpnI	RV
BGWP011	gatcggatccACCAAGAACGATCTGGAACT	CO PfRIPR (5285) Middle Domain	BamHI	FW
BGWP012	gatcggtaccaccGTAGGACACGAACAGGTACT	CO PfRIPR (5285) Middle Domain	KpnI	RV
BGWP013	gatcggatccAACCTGTGCAACAAGTGTCA	CO PfRIPR (5285) EGF(3-10)	BamHI	FW
BGWP014	gatcggtaccaccCACGCAGCTGTCGTCCTTGT	CO PfRIPR (5285) EGF(3-10)	KpnI	RV
BGWP015	gatcggatccCCCAACACCAACGAGTACGACGA	CO PfRIPR (5285) C-terminal	BamHI	FW
BGWP018	gatcggtaccaccTTCCAGATCGTTCTTGGTGT	CO PfRIPR (5285) NTBD region	KpnI	RV
BGWP019	gatcggatccAACATCCAGTACCAGTGCAT	CO PfRIPR (5285) Chen3	BamHI	FW
BGWP020	gatcggatccAACGAAGAGACAGACATCGT	CO PfRIPR (5285) Chen1/2	BamHI	FW
BGWP021	gatcggtaccaccATCTTCCAGCACGCACTTCC	CO PfRIPR (5285) Chen1/2	KpnI	RV
BGWP022	gatcggtaccaccATTCAGGATGCACTCGCCTC	CO PfRIPR (5285) (EGF3-6)	KpnI	RV
BGWP023	gatcggatccGACTACTGCAAGGACATCAA	CO PfRIPR (5285) EGF (7-10)	BamHI	FW
BGWP027	ctagctcgagcAACATCAACAACATGAATAT	S2 4093 C-half cloning	XhoI	FW
BGWP028	ctagggatccGTTCTGGTTGCTGTAGTAAA	S2 4093 C-half cloning	BamHI	RV
BGWP033	ctagctcgag**c**ACCAAGAACGATCTGGAGCT	S2 4093 middle domain	XhoI	FW
BGWP034	ctagggatccGTAGGACACGAACAGGTACT	S2 4093 middle domain	BamHI	RV
BGWP037	GCGCCGGAGTATAAATAGAGG	Sequencing primer for S2 scaffold	N/A	FW
BGWP038	ctagctcgag**c**GATCTGATCGAGGGCATCTT	S2 4093 N-half cloning	XhoI	FW
BGWP039	ctagggatccGTTCGAGTTGGTGTGGGGAT	S2 4093 N-half cloning	BamHI	RV
BGWP040	ctagggatccGTAGTTCTCCTCGCACACAT	S2 4093 N-Terminal	BamHI	RV
BGWP042	gatcggtaccaccCACGCATTTGCCCTTCACGT	CO PfRIPR (5285) EGF(3-4)	KpnI	RV
BGWP043	gatcggatccCCCGATAACAAGTGCGACCT	CO PfRIPR (5285) EGF (5-6)	BamHI	FW
BGWP044	gatcggtaccaccCACGCACTTCCCGTTCACGG	CO PfRIPR (5285) EGF (7-8)	KpnI	RV
BGWP045	gatcggatccCTGGAAGATAAGTGCGTGCA	CO PfRIPR (5285) EGF (9-10)	BamHI	FW
BGWP046	TGGAGGGCAGTGTAGTCTGA	Sequencing Primer 5251	NA	FW
BGWP047	TTCAGCTGCAGCGTGATG	Sequencing Primer 5252	NA	FW
BGWP048	TAGTCAGATATCGATCGATC	S2 sequencing reverse	NA	RV
BGWP049	GCAACTAGAAGGCACAGTCG	5251 and 5252 Sequencing primer	NA	RV
BGWP052	gcgcttgaaaggagtgtgta	S2 sequencing	NA	RV
BGWP054	gatcggtaccaccGTTTTTGGCAATGCAGTTGA	CO PfRIPR (5285) EGF 5	KpnI	RV
BGWP055	gatcggatccAAGTGCAAGCGGAAAGAGTA	CO PfRIPR (5285)EGF 6	BamHI	FW
BGWP056	gatcggtaccaccATAGATGCACTCCCCCTTGT	CO PfRIPR (5285) EGF 7	KpnI	RV
BGWP057	gatcggatccGAGAACAGCTGCCTGATCAA	CO PfRIPR (5285) EGF 8	BamHI	FW
BGWP060	atatGGTACCGGTGGTTCGGACAGCCGGCACGTGTTCAT	E78D, CyRPA	KpnI	FW
BGWP061	atatGGTACCACCCTCGTAGTTGGCGTAGTAGA	E78D, CyRPA	KpnI-G	RV
BGWP062	AACAGCTGCCTGATCAACG	CyRPA cloning orientation check	NA	FW
BGWP063	CTCGCGCTTGTAGATGAAGA	CyRPA cloning orientation check	NA	RV
BGWP064	GATCGCTGAGGTCATCAAGC	N-linked SpyTag-Ctag	BbvCI	RV
BGWP065	GATCAAGCTTGCCACCATGG	N-linked SpyTag-Ctag	HindII	FW
BGWP066	acacgAAGCTTGCCACCATG	C-linked SpyTag-Ctag	HindII	FW
BGWP067	TCCAAGCTGAGGTCATCAAG	C-linked SpyTag-Ctag	BbvCI	RV
BGWP068	gatcggatccGCCAAAAACAAGTGCAAGCG	CO PfRIPR (5285) EGF 6	BamHI	FW
BGWP069	gatcggtaccaccGTCATTCAGGATGCACTCGC	CO PfRIPR (5285) EGF 6	KpnI	RV
BGWP070	gatcggatccCTGAATGACTACTGCAAGGA	CO PfRIPR (5285) EGF 7	BamHI	FW
BGWP071v2	gatcggtaccaccGTTCTCATAGATGCACTCCC	CO PfRIPR (5285) EGF 7	KpnI	RV
BGWP072	gatcggatccTATGAGAACAGCTGCCTGAT	CO PfRIPR (5285) EGF 8	BamHI	FW
BGWP073	gatcggtaccaccATCTTCCAGCACGCACTTCC	CO PfRIPR (5285) EGF 8	KpnI	RV
BGWP074	gatcggatccCTGGAAGATAAGTGCGTGCA	CO PfRIPR (5285) EGF 9	BamHI	FW
BGWP075	gatcggtaccaccATTCTGGATCAGGCACACGC	CO PfRIPR (5285) EGF 9	KpnI	RV
BGWP076	gatcggtaccaccGGTGAAGCTCTCGTCGTACT	CO PfRIPR (5285) EGF 10	KpnI	RV
BGWP083	CGTTGCTGTAGAACCGGTGG	CyRPA reverse sequence middle	NA	RV
BGWP085	gatcggatccATCAGCACCCACGACACCTG	MTRAP FW	BamHI	FW
BGWP086	gatcggtaccaccCAACCCTTTGGATAAAACCT	MTRAP RV	KpnI-G	RV

Table 2-7 – List of biotinylated PfRIPR 20mer peptides covering non-EGF N-half PfRIPR protein.

1 - IDLIEGIFYEKNEIDKLTFS	22 -RSVHVHTHNAILQQETLTYI	43 - TSDKNSHLHSNIPSLYQSSI
2- YEKNEIDKLTFSLDHRVRDN	23 -NAILQQETLTYIKNLCDGKN	44 - HSNIPSLYQSSILPDIQKSK
3 -LTFSLDHRVRDNLKTDLILN	24 - LTYIKNLCDGKNNCKFDFDS	45 - QSSILPDIQKSKFHLISRNS
4 -VRDNLKTDLILNNNGENDYA	25 - DGKNNCKFDFDSIKYEQKSL	46 - QKSKFHLISRNSRTNQYPHN
5 - LILNNNGENDYAYLNKYVYT	26 - DFDSIKYEQKSLTHYLFFIN	47 - SRNSRTNQYPHNQISMLEIQ
6 - NDYAYLNKYVYTILNRDSTE	27 - EQKSLTHYLFFINIQYQCIS	48 - YPHNQISMLEIQNEISSHNS
7 - YVYTILNRDSTEKIKTFFSH	28 - TKNDLELLAIKIEPHKKEKF	49 - LEIQNEISSHNSNQFSTDPH
8 - DSTEKIKTFFSHNKDMKSCD	29 - AIKIEPHKKEKFYKNNLYQG	50 - SHNSNQFSTDPHTNSNNINN
9 - FFSHNKDMKSCDYFISKEYQ	30 - KEKFYKNNLYQGKALKPEYI	51 - TDPHTNSNNINNMNIKKVEI
10 - KSCDYFISKEYQSSDKTNQI	31 - LYQGKALKPEYIFMQCENGF	52 - NINNMNIKKVEIFRSRFSSK
11 - KEYQSSDKTNQICYKKTFCG	32 - PEYIFMQCENGFSIEVINAY	53 - KVEIFRSRFSSKLQCQGGKI
12 - TNQICYKKTFCGVVIPNSEE	33 - ENGFSIEVINAYVSCYRVSF	54 - FSSKLQCQGGKINIDKAILK
13 - TFCGVVIPNSEEIKTNKITN	34 - INAYVSCYRVSFNLNKLKYV	55 - GGKINIDKAILKGGEGCNDL
14 - NSEEIKTNKITNDKLYCAHF	35 - RVSFNLNKLKYVTESLKKMC	56 - AILKGGEGCNDLLLTNSLKS
15 - KITNDKLYCAHFQSTHIIIY	36 - LKYVTESLKKMCDGKTKCAY	57 - CNDLLLTNSLKSYCNDLSEC
16 - CAHFQSTHIIIYYISQPLLL	37 - KKMCDGKTKCAYGNTIDPID	58 - SLKSYCNDLSECDIGLIYHF
17 - IIIYYISQPLLLEPHVVYEE	38 -KCAYGNTIDPIDDLNHHNIC	59 - LSECDIGLIYHFDTYCINDQ
18 - PLLLEPHVVYEETFFEKGKN	39 - DPIDDLNHHNICNNFNTIFK	60 - IYHFDTYCINDQYLFVSYSC
19 - VYEETFFEKGKNDQINCQGM	40 - HNICNNFNTIFKYDYLCVFN	61 - INDQYLFVSYSCSNLCNKCH
20 - KGKNDQINCQGMYISLRSVH	41 - TIFKYDYLCVFNNQQITSDK	62 - DQYLFVSYSCSNLCNKCHNN
21 -CQGMYISLRSVHVHTHNAIL	42 - CVFNNQQITSDKNSHLHSNI	

Table 2-8 – Gamma chain PCR primers for in-house PCR protocol

Name	Sequence
J3403_27-Age (RV)	TAGCAACTGCAACCGGTGTACATAGTGAKRTRCAGCTTMAGGAGTC
J3404_28-Age (RV)	TAGCAACTGCAACCGGTGTACATAGTGAGKTYCAGCTBCAGCAGTC
J3405_29-Age (RV)	TAGCAACTGCAACCGGTGTACATAGTCAGGTGCAGMTGAAGSAGTC
J3406_30-Age (RV)	TAGCAACTGCAACCGGTGTACATAGTGAGRTCCAGCTGCAACARTC
J3407_31-Age (RV)	TAGCAACTGCAACCGGTGTACATAGTCAGGTYVAGCTGCAGCAGTC
J3408_32-Age (RV)	TAGCAACTGCAACCGGTGTACATAGTCAGGTYCARCTGCAGCAGTC
J3409_33-Age (RV)	TAGCAACTGCAACCGGTGTACATAGTGAGGTGMAGCTGGTGGAATC
J3410_34-Age (RV)	TAGCAACTGCAACCGGTGTACATAGTGAVGTGMWGCTSGTGGAGTC
J3411_35-Age (RV)	TAGCAACTGCAACCGGTGTACATAGTGARGTGCAGCTGKTGGAGWC
J3412_36-Age (RV)	TAGCAACTGCAACCGGTGTACATAGTGAGGTGAAGCTGATGGAATC
J3413_37-Age (RV)	TAGCAACTGCAACCGGTGTACATAGTGAGGTGCAGCTTGTTGAGTC
J3414_38-Age (RV)	TAGCAACTGCAACCGGTGTACATAGTGAGGTGAAGCTTCTCRAGTC
J3415_39-Age (RV)	TAGCAACTGCAACCGGTGTACATAGTGAAGTGAARMTTGAGGAGTC
J3416_40-Age (RV)	TAGCAACTGCAACCGGTGTACATAGTCAGGTTACTCWGAAAGWGTCTG
J3417_41-Age (RV)	TAGCAACTGCAACCGGTGTACATAGTCAGGTCCAACTGCAGCAGCC
J3418_42-Age (RV)	TAGCAACTGCAACCGGTGTACATAGTGATGTGAACCTGGAAGTGTC
J3419_43-Age (RV)	TAGCAACTGCAACCGGTGTACATAGTCAGATCCAGTTSGTRCAGTC
J3420_44-Age (RV)	TAGCAACTGCAACCGGTGTACATAGTGAGGTRCAGCTKGTAGAGAC
J3421_45-Age (FW)	TACATCATTGGTCGACGCCGAGGAGACGGTGACCGTGGTCc
J3422_46-Age (FW)	TACATCATTGGTCGACGCCGAGGAGACTGTGAGAGTGGTGC
J3423_47-Age (FW)	TACATCATTGGTCGACGCCGCAGAGACAGTGACCAGAGTCC
J3424_48-Age (FW)	TACATCATTGGTCGACGCCGAGGAGACGGTGACTGAGGTTC

Table 2-9 - Kappa chain PCR primers for in-house PCR protocol

Name	Sequence
J3270_3-Bsa (FW)	tgactggtctcACAGCSAAAWTGTKCTCACCCAGTC
J3271_4-Bsa (FW)	tgactggtctcACAGCGAWATTGTGCTMACTCAGTC
J3272_5-Bsa (FW)	tgactggtctcACAGCGACATTGTGCTRACACAGTC
J3273_6-Bsa (FW)	tgactggtctcACAGCGACATTGTGATGACMCAGTC
J3274_7-Bsa (FW)	tgactggtctcACAGCGAYATCMAGATRAMCCAGTC
J3275_8-Bsa (FW)	tgactggtctcACAGCGAYATCCAGATGAYTCAGTC
J3276_9-Bsa (FW)	tgactggtctcACAGCGATATCCAGATGACACAGAC
J3277_10-Bsa (FW)	tgactggtctcACAGCGACATTGTGCTGACCCAATC
J3278_11-Bsa (FW)	tgactggtctcACAGCGACATYSTRATGACCCARTC
J3279_12-Bsa (FW)	tgactggtctcACAGCGATRTTKTGATGACYCARAC
J3280_13-Bsa (FW)	tgactggtctcACAGCGAYATTGTGATGACBCAGKC
J3281_14-Bsa (FW)	tgactggtctcACAGCGATATTGTGATAACCCAGGA
J3282_15-Bsa (FW)	tgactggtctcACAGCGACATCYTGCTGACYCAGTC
J3283_16-Bsa (FW)	tgactggtctcACAGCGAAAWTGTGYTGACCCAGTC
J3284_17-Bsa (FW)	tgactggtctcACAGCGAAACAACTGTGACCCAGTC
J3285_18-Bsa (FW)	tgactggtctcACAGCGACATTRTGATGWCACAGTC
J3286_19-Bsa (FW)	tgactggtctcACAGCGACATCCAGMTGACMCARTC
J3287_20-Bsa (RV)	TGACtGGTCTCAAGATGGATACAGTTGGTGCAGCATCAGCCC

Table 2-10 - Gamma chain PCR primers for Ho *et al.* PCR protocol

Name	Sequence
5MsVHE	GGGAATTCGAGGTGCAGCTGCAGGAGTCTGG
3Cy1 outerIgG1	GGAAGGTGTGCACACCGCTGGAC
3Cy2b outerIgG2b	GGAAGGTGTGCACACTGGAC
3Cy2c outerIgG2c	GGAAGGTGTGCACACTGCTGGAC

Table 2-11 - Kappa chain PCR primers for Ho *et al.* PCR protocol

Name	Sequence
5VK3	TGCTGCTGCTCTGGGTTCCAG
5VK4	ATTWTCAGCTTCCTGCTAATC
5VK5	TTTTGCTTTTCTGGATTYCAG
5VK6	TCGTGTTKCTSTGGTTGTCTG
5VK689	ATGGAATCACAGRCYCWGGT
5VK14	TCTTGTTGCTCTGGTTYCCAG
5VK19	CAGTTCCTGGGGCTCTTGTTGTTC
5VK20	CTCACTAGCTCTTCTCCTC
3MCK	GATGGTGGGAAGATGGATACAGTT

Table 2-12 – Kappa chain PCR primers for NIH PCR protocol

Name	Sequence
Forward	
1mFK_I	RGTGCAGATTTTCAGCTTCCTGCT
1mFK_II	TGGACATGAGGGCYCCTGCTCAGT
1mFK_III	CTSTGGTTGTCTGGTGTTGAYGGA
1mFK_IV	GTTGCTGCTGCTGTGGCTTACA
1mFK_V	GTATCTGGTACCTGTGG
1mFK_VI	TGCCTGTTAGGCTGTTGGTGCT
1mFK_VII	GCTCAGTTCCTTGGTCTCCTGTTGC
1mFK_VIII	TGGGTGCTGCTGCTCTGGGT
1mFK_IX	CAGTTCCTGTTTCTGTTARTGCTCTGG
1mFK_X	TGCTCTGGTTATATGGTGCTGATGGG
Reverse	
1mRK*	ACTGAGGCACCTCCAGATGTT

2.5 Appendix 2 – Statement on ARRIVE Guidelines

All animal experiments were conducted under the project licence number PA7D20B85.

The ARRIVE guidelines (Animal Research: Reporting of *In Vivo* Experiments) specify two criteria for reporting sample size as part of the 10 essential criteria. These are -

> 2a - Specify the exact number of experimental units allocated to each group, and the total number in each experiment. Also indicate the total number of animals used.

And

> 2b - Explain how the sample size was decided. Provide details of any a priori sample size calculation, if done.

The number of animals used as required in criteria 2a is detailed in the relevant sections of chapter 2.2.

Group sizes in mouse experiments were chosen to provide sufficient power to assess statistical differences in the immune response of interest, for example antibody titre, magnitude or functional activity between two groups immunised with different vaccine immunogens. The specific group size per experiment depends on the variance of the measured outcome (e.g. magnitude of a given vaccine-induced antibody response) and the expected effect size. Previous experiences with a malaria protein vaccination in BALB/c mice have shown that:

For an antibody IgG mean ELISA response of 1600 antibody units with a standard deviation (SD) of 950 (n = 6), the number of mice required to show a 2-fold

improvement in vaccine IgG immunogenicity (an effect size known to have an impact on functional activity in vitro at these levels of response) with 80% power (1-β) (2-tailed test) at a significance level (α) of P = 0.05, group sizes of n = 6 would be required in the proposed study. The same SD was assumed in the test (unknown) group. Power calculations performed using G* power software to determine.

For rabbit experiments between 2 and 4 animals were immunised. Power calculations were not carried out since these animals were used to generate pools of anti-PfRIPR purified IgG as tools for GIA reversal studies, not for statistical comparison of different vaccine groups. Groups of 2 & 4 animals were chosen based on the capacity of our collaborators to perform the immunisations and the requirement for sufficient serum for multiple experiments. Currently serum from four rabbits has met the experimental requirements for 4 years with no plans to immunise more animals.

Prior to starting this project, the Draper group had no experience with working with rats and therefore group sizes were based on the previous calculations for mouse experiments. The four rat experiments described in this thesis served an important role in determining immunisation schedule and dose for each of the three antigens. Future experiments should use this data set to re-evaluate the group sizes of future pre-clinical studies in rats.

Chapter 3 - Investigating PfRIPR neutralising epitopes

3.1 Authorship statement

The GIA assay is standardised to minimise variability and enable direct comparison between different projects ongoing in the lab, all GIA assays were carried out by one of two dedicated research associates: Dr Doris Quinket and Amelia Lias. This includes both regular parasite maintenance and the assay set-up and read-out. Full length PfRIPR, PfRH5, and PfCyRPA protein was produced by either Dr David Pulido-Gomez or Hannah Davies. Dr Rod Chalk and Tiago Moreira from the Centre for Medicines Discovery (CMD) performed the tandem mass spectroscopy (MS/MS) and assisted with the intact mass analysis. Dr Lea Barfod made the PfRIPR hybridomas for mRP003, mRP004, mRP006, mRP013, mRP016, mRP017 and mRP018. Dr David Pulido-Gomez assisted with the anti-PfRIPR mAbs and RCR binding analysis (Section 3.5.3). Expression plasmids for AMIGO2, SEMA7A, and MTRAP were gifts from Gavin Wright (Section 3.6). Rabbit immunizations (Section 3.7) were performed by GenScript Inc, Cambridge Research Biologics, and Dr Kazutoyo Miura National at the Institute of Allergy and Infectious Diseases (NIAID, USA).

3.1 Introduction

P. falciparum RH5 interacting protein (PfRIPR) is a recently discovered[124] conserved protein that forms a triple complex with PfRH5 and PfCyRPA. The complex is essential for merozoite invasion of erythrocytes[123,128]. Antibodies raised against PfRIPR fragments have produced strain transcending neutralising antibodies[124,173] however, at the time of project commencement no group had produced full length PfRIPR or identified the neutralising epitopes on the protein. The work in this chapter details the production of recombinant PfRIPR fragments that were used to identify neutralising epitopes in PfRIPR and provide further characterisation of the protein.

3.1.1 Production of *P. falciparum* recombinant protein fragments

Plasmodium proteins have traditionally been very difficult to produce recombinantly. However, recent advances in cell culture and protein production have made the problem of *Plasmodium* protein production more tractable than 10 years ago. *Plasmodium* proteins have several characteristics that make them particularly difficult to make recombinantly; these characteristics and some practical solutions are outlined in the following paragraph. The genomes of some *Plasmodium* species have a very low G+C content, between 17 and 19%[187,188]. This means that codon usage does not reflect the heterologous system used for expression, such as *E. coli* or mammalian cell systems, which typically have ~50% G+C content. The widespread use of *in silico* codon optimisation[189] has largely negated the G+C content problem as large sections of DNA can now be ordered cheaply from commercial suppliers with codon usage biases changed to reflect the target expression system. More recently, codon harmonisation has been used to express multiple *Plasmodium* proteins to high levels[190]. Codon harmonisation relates codon usage to known protein secondary

structures and includes infrequently used codons at domain junctions to slow translation and allow the protein to fold correctly. Unfortunately, 'harmonising' the DNA sequence does not overcome many other protein folding issues encountered with *Plasmodium* proteins. Many *Plasmodium* proteins contain long disordered regions that are prone to aggregation[191,192]. As such, some proteins must be made by co-expression with *Plasmodium* heat shock proteins such as HSP70[193] to aid folding. Occasionally the protein sequences are so repetitive that they are unstable in DNA vectors[194] let alone as proteins. A further currently unresolved issue for *Plasmodium* protein production is the glycosylation states of different *Plasmodium* proteins. The degree to which *Plasmodium* species glycosylate proteins is a contentious issue[195]. The Glycosylphosphatidylinositol (GPI) anchor is the only glycan consistently found in parasite proteins with N and O-linked glycans largely absent at the asexual stage, however one 2019 study did detect N and O-linked glycans on MSP-1[196]. Most *Plasmodium* proteins contain the consensus N-linked glycosylation sequence (N-X-S/T) but parasites lack nearly all of the glycosyltransferases involved in early N-glycosylation pathways[197]. As such, N-linked glycosylation sites are normally removed prior to protein production in higher expression systems to prevent glycans obscuring potentially neutralising epitopes.

Many *Plasmodium* proteins were initially made in bacterial systems such as *E. coli,* this includes the first fragments of PfRIPR[124]. *E. coli* are cheap and simple to culture however, they are a particularly poor system for *Plasmodium* protein production. For example, one study could only solubly express 5 out of 95 *Plasmodium* proteins[198] in *E. coli*. *E. coli* is also particularly poor at producing proteins rich in disulphide bonds[199] since it lacks an oxidising compartment required for disulphide bond

formation such as the endoplasmic reticulum found in eukaryotic cells. Reported PfRIPR fragments made in *E. coli* were thus purified from inclusion bodies and re-folded[124,166] which may produce a substantial amount of misfolded protein. This problem has also been encountered with studies using PfRH5; PfRH5 produced *E. coli* failed to elicit neutralising antibodies, presumably due to misfolding of important conformational epitopes[200]. PfRIPR contains 87 cysteine residues, the majority forming disulphide bonds in EGF like domains, therefore the successful production of full length PfRIPR protein and larger fragments in *E. coli* seemed unlikely.

Several other heterologous protein expression systems have been used to produce *P. falciparum* proteins with some success. The wheat germ cell-free system (WGCFS) was used to produce a 717 amino acid fragment of PfRIPR[173] comprising K279 – D995, this is roughly from the start of EGF domain 1-2 until the end of EGF domains 9-10, however some contaminating proteins were observed. PfRIPR produced using the WGCFS is also likely to be misfolded. PfRIPR protein produced in another study using the WGCFS[174] exhibited extremely tight binding to PfRH5 by SPR, a protein that it is known to not interact with despite its name, suggesting that the PfRIPR was misfolded and so non-specifically interacting with PfRH5. An alternative system that has been used to produce GMP grade PfRH5 is the *Drosophila melanogaster* Schneider 2 (S2) cell system[159,201]. Prior to starting this project, full-length PfRIPR had just been successfully produced in S2 cells for the first time (S. Draper, unpublished data), although at very low yield. However, protein production from S2 cells requires the production of stable cell lines, and this is a time-consuming process that limits screening of multiple antigens.

Consequently, I elected to initially try a third approach that has been successfully used by multiple groups. This is the HEK293 (Human Embryonic Kidney 293) mammalian cell transient transfection platform, the primary system used for the work in this chapter. Notably, a 2019 study used HEK293E (HEK293 Epstein-Barr Nuclear Antigen-1) cells to produce 20 out of 55 *Plasmodium* proteins in small quantity[202]. Similarly, an earlier study[175] could express ~40% *Plasmodium* proteins tested using the HEK293 system; a vast improvement on other previously tested expression systems. The HEK293 system can also be used for rapid screening of candidates with transient expression and for stable cell line generation once an antigen/construct of interest has been established. The HEK293 system also permits the use of solubility tags such as recombinant mono-biotinylated rat CD4-d3d4[203] to aid the solubility and folding of proteins; this could allow for the production of PfRIPR fragments that could otherwise not be made in isolation. However, as a mammalian system, HEK293 cells do N-glycosylate proteins therefore *Plasmodium* proteins regularly have the N-linked glycosylation sequons (N-X-S/T) mutated threonine/serine to alanine (S/T-A) or asparagine to glutamine (N-Q) to ablate potential glycosylation sites. Strategies have not been devised to remove O-linked glycosylation sites from the DNA sequences as O-linked glycosylation sites do not have a consensus sequence.

3.1.2 Identification of neutralising epitopes on PfRIPR

The production of high-quality recombinant *Plasmodium* protein fragments is equally as important as production of full-length protein. Protein fragments can be used to see if different sections of a protein can reverse antibody-mediated GIA *in vitro* on purified IgG from serum generated from natural infection and/or immunisation with full length protein. This experimental approach can be used to identify important

domains for immunity against a pathogen. For example, clinical immunity against pregnancy associated-malaria is correlated with antibodies against VAR2CSA. This is a large complex protein containing six Duffy binding-like (DBL) domains. One study preincubated purified IgG from multigravida women from malaria endemic regions with recombinant DBL1, DBL2, DBL3, DBL4ε, DBL5ε, and DBL6ε. Three domains (DBL2χ, DBL3χ, and DBL5ε) significantly reduced opsonisation of VAR2CSA-expressing infected erythrocytes by human monocytes indicating that they are the targets of functional antibodies and therefore likely key mediators of clinical immunity[204]. PfRIPR is also a large, complex, and difficult to produce protein that comprises discrete domains, suggesting that antigen reversal experiments could be an effective tool for identifying domains that are the targets of nAbs. At the start of this project no information was known regarding the location and nature of neutralising epitopes on PfRIPR.

3.1.3 Anti-PfRIPR monoclonal antibodies

Monoclonal antibodies (mAbs) provide a useful tool for epitope mapping and structural studies. These reagents can complement antigen reversal experiments by providing more specific epitope structural/functional data. They are also potential prophylactics for travellers or military personnel due to their specificity and high affinity for target proteins. Monoclonal antibodies have informed vaccine antigen design by the identification of neutralising epitopes[178]. A panel of anti-PfRIPR monoclonal antibodies were isolated by Dr Lea Barfod in the Draper group (unpublished data) prior to the start of this project, however none of these antibodies showed functional *in vitro* GIA against *P. falciparum*. This was surprising since anti-PfRIPR polyclonal antibodies routinely show strong GIA. A second aim of the work in

this chapter was to therefore characterise the epitopes/domains bound by these non-functional mAbs in order to better understand this observation.

3.2 Expression plasmid design and PfRIPR sequence choice

Before I could perform an expression screen of multiple PfRIPR protein fragments in mammalian HEK293 cells, I elected to design and test new expression plasmids to try and maximise chances of success with this difficult protein. These new constructs contained the C-terminal C-Tag for affinity purification (that had been successfully employed by the group with PfRH5[205]) and enzyme sites for rapid replacement of the PfRIPR fragment by restriction cloning. Two new plasmid scaffolds, 5251 and 5252 (Figure 3.1), were designed and inserted into the pENTR4LP plasmid backbone, one scaffold contained the monomeric Fc domain[182] (monoFc) which was reported to improve the solubility/expression of fused proteins. The monoFc is cleavable using TEV protease which would allow purification of soluble fragments for future immunisation studies. Both 5251 and 5252 were initially cloned with a 'stuffer' DNA sequence in place of a PfRIPR fragment. This sequence was the first half of the GFP protein. This sequence was chosen as it is allowed the monoFc to be expressed bound to a non-*P. falciparum* protein which could then be used as a monoFc control in experiments. The GFP is known to be not toxic to HEK293 cells when expressed in large quantities so would not cause problems during production.

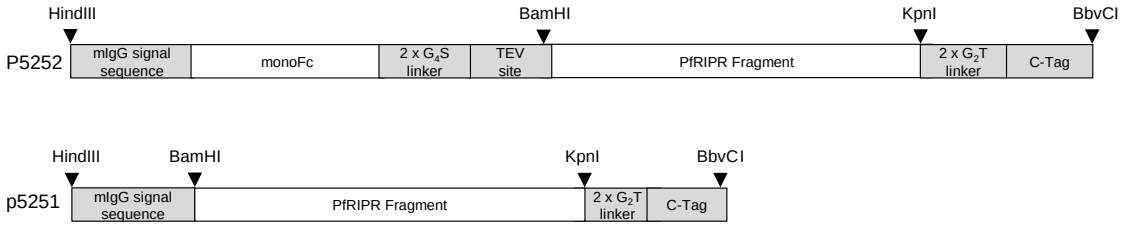


Figure 3.1 – New constructs for PfRIPR fragment expression and purification.
Schematic of the two expression constructs: p5252 contains the monoFc with a TEV protease site fused to the fragment of interest. Both p5252 and p5251 have a linker before the C-Tag which contains the KpnI site. 5252 contains an additional GS moiety after the TEV cleavage site which contains the BamHI site whereas the BamHI site was added to the end of the mIgG signal sequence in 5251.

Having confirmed successful generation of the new expression plasmids by DNA sequencing, I proceeded to focus on the design of the gene sequence encoding PfRIPR. Here, again, a number of options were assessed, with the aim of maximising chances of success of more difficult/larger fragments of PfRIPR. Three full length PfRIPR DNA sequences were initially available for me to use: 1) a human codon optimised sequence by GeneArt, 2) a codon harmonised version (designed by a collaborator: E. Angov, WRAIR, USA), and 3) an insect codon optimised version by GeneArt. A summary of each sequence's features is given in Table 3-1. In order to screen these genes, I elected to assess expression of the 'N-half' fragment of PfRIPR, amino acids 1-553, since low but detectable levels of the N-half fragment had previously been produced by transient transfection of HEK293E cells in a pilot experiment using the human codon optimised version described above (O. Lyth, unpublished data). The N-half sequence of each of the three PfRIPR variants was cloned into 5251 and 5252. 50µg of each of these six plasmids, the three PfRIPR sequences with and without the monoFc, was used to transfect 50 mL cultures of HEK293F cells as described in chapter 2.1.4. After 72 hours the supernatants were processed using C-Tag chromatography. The eluted peaks were quantified using the nanodrop and the peaks

run on a protein gel. Detectable levels of expression could only be obtained from the human codon optimised plasmid (Figure 3.2A) in a 50mL culture, although encouragingly expression was greater from the monoFc bound construct (0.77mg/mL against 0.32mg/mL following C-Tag purification). These data suggested the human codon optimisation sequence should be used for future experiments since no expression was seen from the other constructs. In addition, the monoFc improved yields of the protein fragment and was therefore used when generating further PfRIPR fragments. The expression of N-half from the human codon optimised PfRIPR led to the presence of multiple bands on the protein gel (Figure 3.2A), each bigger than the 88 kDa expected. This was attributed to aggregation and glycosylation, both of these had to be addressed before the N-half fragment could be used in further studies.

The human codon optimised PfRIPR sequence chosen for future experiments contains 11 intact N-linked glycosylation sites. The full length PfRIPR protein, manufactured in-house in S2 cells using the insect codon optimised sequence, has these N-linked glycan sequons mutated asparagine to glutamine (N-Q) resulting in an N-linked glycan free protein. In an ideal setting the PfRIPR protein fragments produced should match the full-length protein's glycosylation pattern and amino acid sequence. The presence of N-linked glycans on the PfRIPR N-half protein produced from the human codon optimised was thus examined using the enzyme PNGase F which efficiently removes all N-linked glycans from a protein. Incubation of the N-half protein fragment with PNGase F led to a mass shift from 135kDa to 90kDa (Figure 3.2B) on a protein gel. The expected mass of Nhalf PfRIPR bound to the monoFc is 88.5 kDa, therefore the N-half protein appears to be heavily glycosylated.

These glycans may obscure potential targets of neutralising epitopes. To mitigate this risk the human codon optimised sequence was thus altered to mutate the N-linked glycosylation sites. The N-linked sequons were mutated N-Q to match the S2 produced full length PfRIPR.

Table 3-1 –Details for full length PfRIPR sequences used in this thesis

Group Sequence number	Codon optimisation	N-linked glycan mutations	Use in thesis
3133 / 5259	Human	None - Native sequence	Production of Nhalf only
4797 / 5260	Human harmonised	S/T - A	Not used
4093	Insect (Drosophila)	N - Q	Production of full length PfRIPR in S2 cells
5285	Human	N-Q	Production of remaining PfRIPR protein fragments. Based on 3133

A new N-half plasmid was generated using the new codon optimised sequence with mutated N-linked glycan sites. This plasmid was based on the monoFc containing plasmid #5252. This new sequence was used to transfect 50mL of HEK293 cells alongside the original N-half codon optimised version to ensure that expression was consistent across constructs. Unfortunately, the new glycan mutated sequence failed to express at detectable levels (Figure 3.2C). This was unexpected because the new glycan mutated sequence was being used to successfully generate new PfRIPR fragments in parallel to this experiment (see section 3.3). It is known that glycosylation forms part of the quality control system for proteins as they fold and pass through the endoplasmic reticulum and Golgi apparatus[206]. Therefore, the most likely explanation for the lack of N-half expression is that the absence of glycosylation

on the large N-half fragment causing the cell to flag the protein for degradation either directly due to missing glycans or indirectly due to misfolding.

The success of producing smaller PfRIPR fragments, particularly those containing EGF like domains, using the new glycan mutated codon optimised sequence suggested that the expression problems with the N-half were directly caused by the lack of glycans on the N-half protein rather than the DNA sequence. A N-linked glycan free N-half fragment was still required for further study since it was possible that the heavy glycosylation of the protein will interfere with important epitopes. Consequently, two strategies were used to produce glycan free N-half. The first was to express the original codon optimised sequence, with glycan sequons intact, in GNT^{1-} HEK293F cells. This cell line lacks the N-acetylglucosaminyltransferase enzyme that modifies the N-linked glycans in the Golgi apparatus[207]. This leads to the production of proteins uniformly linked to the smaller $(GlcNAc)_2Man5$ which can then be cleaved with the enzyme EndoH. Expression using this cell line was very poor (data not shown) therefore a second strategy was tried. The second strategy used the original codon optimised sequence, with glycan sequons intact, expressed in standard HEK293F cells but in the presence of kifunensine, a mannosidase I inhibitor, followed by treatment with EndoH to remove the remaining glycans. Briefly, 100mL of HEK293F cells were transfected with 100 µg of N-half expression plasmid. After 24 hours the cells were centrifuged, and the media removed. The media was then replaced with media containing 5µM kifunensine. After a further 56 hours the N-half fragment was purified using the C-Tag. The purified protein was incubated overnight in 5L TBS buffer in a 3.5 kDA Dialysis cassette Slide-A-Lyzer, with a 1 to 50 ratio of purified protein to EndoH enzyme. The final product was then purified with SEC to isolate the non-

aggregated protein. This process produced acceptable yields of N-linked glycan free N-half protein however a lot of aggregation was seen (Figure 3.2D) which reduced the final amount of product. A quality control step with PNGase F confirmed the production of glycan free N-half (Figure 3.2E). Due to the low yield of N-half, the presence of glycans on this fragment could not be verified by intact mass analysis (Table 3-2).

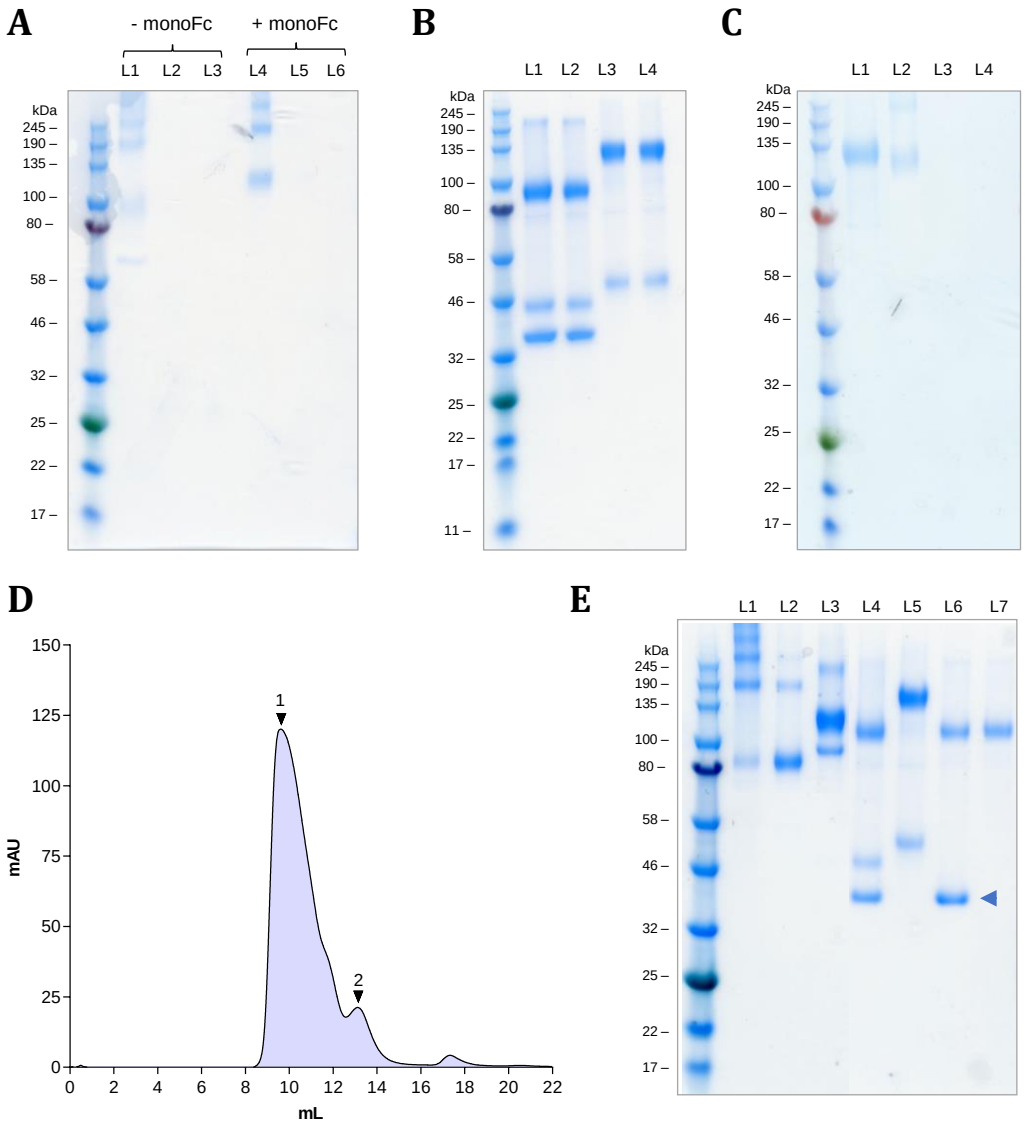


Figure 3.2 –PfRIPR N-half fragment expression and optimisation.

A) Evaluating expression of different PfRIPR N-half DNA sequences with or without the monoFc. Lane 1 & 4: Human codon optimised N-half PfRIPR gene sequence. Lane 2 & 5: Codon harmonised N-half PfRIPR gene sequence. Lane 3 & 6: Insect codon optimised N-half PfRIPR gene sequence. Expected MW 88kDa. **B)** PNGase digest of N-half protein. L1 & L2: Digested N-half fragments, expected MW 88 kDa for N-half and 35 kDa for PNGase F. L3 & L4: Control undigested N-half, expect MW ~135 kDa. **C)** Expression test of N-Half fragment from human codon optimised N-half gene sequence with glycans (L1 & L2) expected MW 135 kDa, and human codon optimised gene sequence with glycans removed (L3 & L4), expected MW 88 kDa. **D)** SEC UV trace of purified N-half produced with kifunensine after overnight dialysis and digestion with EndoH. Peak 1: aggregated N-half. Peak 2: monomeric N-half. **E)** PNGase F digest test on various N-half fragments. L1: Aggregated N-half from panel D peak 1. L2: monomeric N-half from panel D peak 2, expected MW 88 kDa. L3: Nhalf produced with kifunensine prior to EndoH digest, expected MW 120 – 135 kDa. L4: Reduced N-half produced with full N-linked glycans digested with PNGase F, expected MW 88 kDa. L5: Reduced N-half produced with full N-linked glycans & incubated without EndoH, expected MW 135 kDa. L6: Reduced N-half produced with kifunensine and digested with EndoH after PNGase F digest. Expected MW 88 kDa. L7: Reduced N-half produced with kifunensine and digested with EndoH incubated without PNGase F. Expected MW 88 kDa. Blue arrow indicates PNGase F enzyme.

Now that the sequence PfRIPR gene sequence choice had been confirmed, the final test was to determine whether the PfRIPR fragment could be released from the monoFc by TEV protease. The fragment PfRIPR EGF (5-6) was chosen for this test as it could be expressed in high quantities with little aggregation (Section 3.3). 5mg of the protein fragment was incubated overnight with TEV protease. The resulting digest was then purified on a C-Tag column to remove the TEV protease and cleaved monoFc. The elution peak was then polished on a size exclusion chromatography column. The digest led to the production of clean PfRIPR EGF (5-6) (Figure 3.3) that will be suitable for experiments such as immunisations. This success was tempered by the low yield of final product. From 5 mg of starting product only 1 mg of final cleaved protein could be purified. This would be enough for some experiments such as mouse immunisations however it was deemed impractical and expensive to use TEV cleaved protein for all experiments. The majority of experiments would therefore use monoFc bound fragments and a control protein (GFP-monoFC) to ensure the monoFc does not affect the results. It should be noted that most of the proteins produced from PfRIPR ran at larger than expected sizes on protein gels, however this is addressed in the mass spectrometry section in section 3.3.

With the new expression plasmids created and validated and the choice of PfRIPR gene sequence set, the focus shifted to producing protein fragments that covered the whole of PfRIPR.

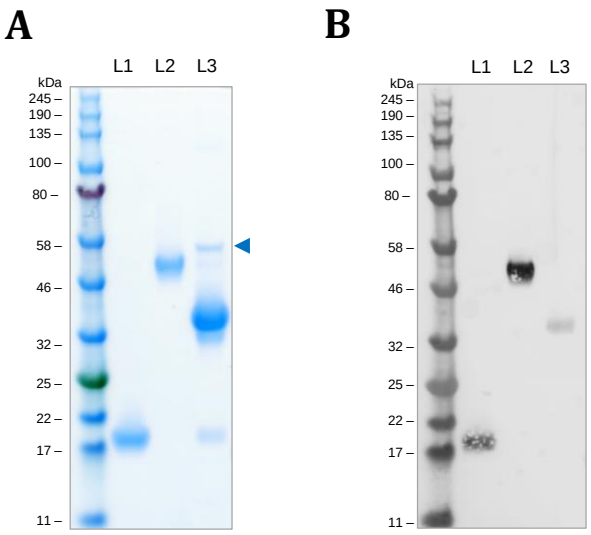


Figure 3.3 - TEV protease digestion of PfRIPR EGF (5-6) monoFc.
A) Protein gel of TEV protease digested PfRIPR EGF (5-6). L1: C-Tag and SEC purified cleaved PfRIPR EGF (5-6) expected MW 12.5 kDa. L2: PfRIPR EGF (5-6) monoFc prior to digest, expected MW 38 kDa. L3: C-Tag column flow through. Blue arrow indicates TEV protease, prominent band is cleaved monoFc and some digested PfRIPR EGF (5-6) is seen. **B)** Western blot of the same samples using anti-PfRIPR rabbit serum.

3.3 Production of recombinant PfRIPR protein fragments

Having defined a plasmid construct and PfRIPR gene coding sequence to use in the mammalian cell expression platform, I next proceeded to attempt expression of a panel of different PfRIPR protein fragments/regions. No structure of PfRIPR was available, therefore the protein sequence was analysed using POODLE-L[208], PONDR[209], and FUGUE[210] to identify domains and inform PfRIPR fragment design. POODLE-L uses the physio-chemical properties of amino acids to predict disordered regions within a protein. PONDR performs a similar disorder-based analysis using an algorithm trained on known ordered and disordered proteins. FUGUE is a structural prediction algorithm based on sequence homology. A significant site of disorder from N520 to F544 was identified with all of the tools corresponding to the putative

protease site[171]. The 10 EGF-like domains were reliably predicted with some disordered sequences likely corresponding to loops between pairs of EGF-like domains. The N-terminal region gave no hits to known proteins. The C-terminal region has some homology to the C-terminal domain of the *Toxoplasma gondii* micronemal protein 1 (TgMIC1). Using these data, I designed an initial set of PfRIPR fragments, amplified them by PCR from the human codon optimised PfRIPR gene sequence and cloned them into the new vectors containing the monoFc for expression in HEK293E cells (Figure 3.4A-C). Included in this screen were "PfRIPR1/2" and "PfRIPR3" from the original PfRIPR paper by Chen *et al.*[124]; these fragments were called Chen1/2 and Chen3.

PfRIPR fragment expression was tested by transient expression in 50mL HEK293F cultures. Culture supernatants were purified on C-Tag columns between 72 and 96 hours after transfection. Any C-Tag elution peaks were screened by SDS-PAGE under reducing and non-reducing conditions and western blot with anti-PfRIPR rabbit serum.

Four out of the 19 protein fragments could not be expressed in HEK293F cells to any detectable level by SDS-PAGE or western blot. One fragment, PFRIPR EGF (3-10), showed detectable expression by western blot but was too aggregated to be used (these five proteins are labelled in red in Figure 3.4A). In particular, these protein fragments covered the N-half of the protein and/or the protease cleavage site. Four other fragments expressed at low levels or showed high levels of aggregation (labelled in blue) and eight expressed well (labelled in black). Notably, these eight mostly spanned the structured EGF domains.

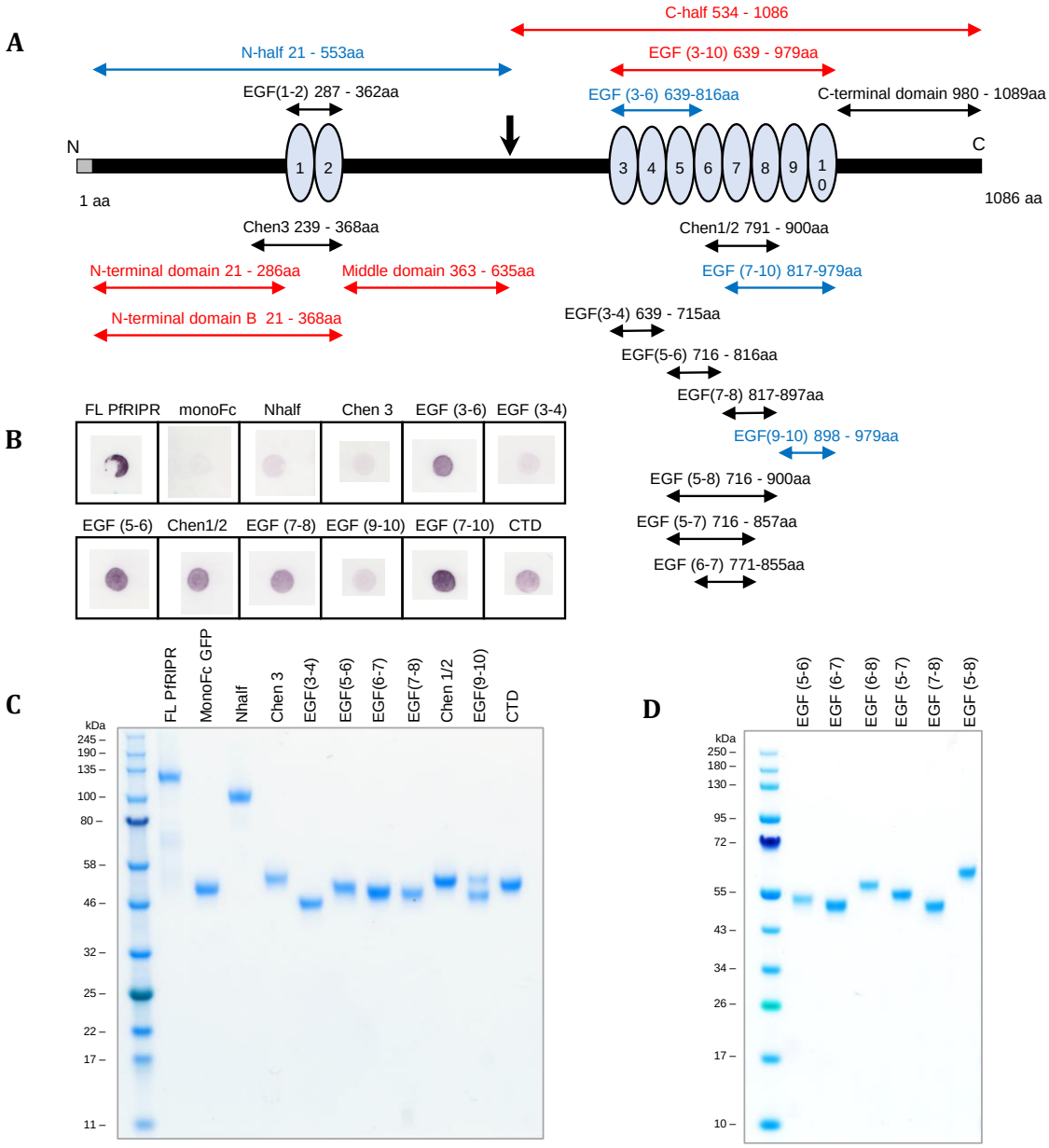


Figure 3.4 – PfRIPR fragment design and production of PfRIPR fragments
A) Protein fragments that could not be made are labelled red, those that expressed poorly are blue, and well expressing proteins are in black. **B)** Dot blot of the initial set of PfRIPR fragments using anti-PfRIPR rabbit serum. **C)** Reducing SDS-PAGE of initial set of PfRIPR protein fragments fused to the monoFc. **D)** Reducing SDS-PAGE of all of the C-terminal EGF-like domain containing fragments fused to the monoFc.

Following expression trials, each protein that could be made was produced from at least 200 mL of HEK293F cells with the bound monoFc and purified using C-Tag columns followed by a polishing step by SEC. This included 9 of the protein fragments plus N-half as described above. These proceeded to further QC testing, along with a monoFc-GFP control protein and full-length PfRIPR protein (which I could produce in

small amounts from the previously described *Drosophila* S2 stable cell line). All proteins were run on a reducing SDS-PAGE and showed bands of expected sizes with good purity and little aggregation (Figure 3.4C). One protein fragment, PfRIPR EGF (9-10) produced a double band on SDS-PAGE, this was also seen with the fragment PfRIPR EGF (7-10) (data not shown). PfRIPR EGF-like domains 9-10 seem to misfold and produce 2 species when produced recombinantly, these could not be separated by size exclusion chromatography. All of these proteins were checked for reactivity against anti-PfRIPR (full-length) rabbit serum (Figure 3.4B) by dot blot and were positive. One protein fragment, PfRIPR EGF (1-2), could be expressed at a high level however it was not used in the project as the fragment Chen3 contained the whole of EGF (1-2) with some additional N-terminal sequence. Rather than effectively repeat experiments, PfRIPR EGF (1-2) was dropped and Chen3 was used exclusively.

The initial panel of eight proteins were made early in the project. However, new fragments were made continually throughout the project to meet the demands of different assays and/or to confirm various results, for example EGF (5-7). Ultimately, I focussed on the region encoding EGF-like domains 5-8 and made multiple combinations of the recombinant domains in a similar manner (Figure 3.4D).

In the above experiments, I was unable to express the entire C-half of PfRIPR. I thus attempted to make the C-half fragment in *Drosophila* S2 cells, however only a very small quantity could be made, this was contaminated with chaperones and highly aggregated (data not shown). I therefore did not use this in subsequent experiments.

A full list of proteins and summary of QC analyses is given in Table 3-2. Each protein was sent for tandem mass spectroscopy (MS/MS) to verify the protein identity. Furthermore, since each PfRIPR fragment ran larger than expected on SDS-PAGE gels

each protein was analysed by intact mass analysis to determine the exact size of each protein (Figure 3.5). Intriguingly, even though the PfRIPR fragments were made from a sequence with mutated N-glycan sites, the QTOF data showed that all the fragments were bound by two N-linked glycans. Investigation showed that these glycans are linked to the monoFc solubility tag, and when these were removed by enzymatic digest each of the PfRIPR protein fragments with monoFc matched their predicted size. The two glycans on the monoFc are required to prevent the Fc regions dimerising and therefore enable the 'mono' Fc. The only protein that could be made to sufficient quantity that did not yield good QC data was EGF domains 9-10. Although correct identity was reported by MS/MS, the QTOF data suggested that the protein had degraded. This was consistent with my previous observation that any protein that contains EGF domains 9-10 did not run as clean bands on an SDS-PAGE gel (Figure 3.4C).

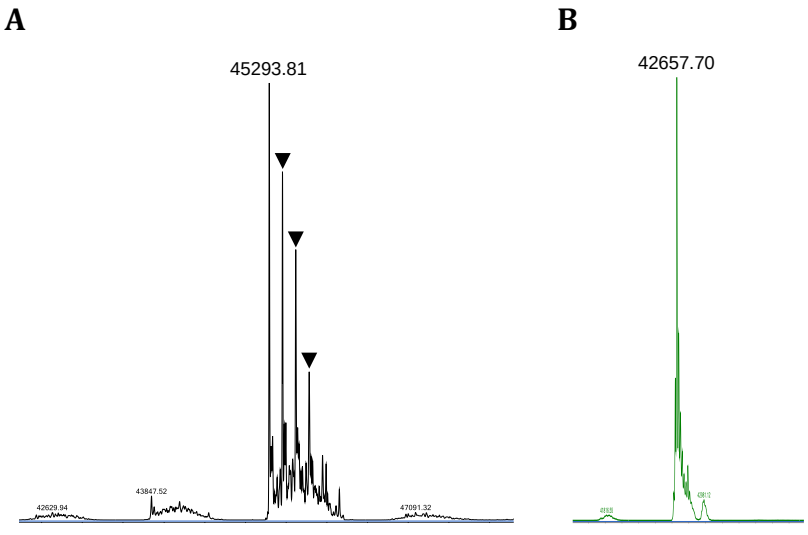


Figure 3.5 – Representative deconvoluted intact mass analysis plots for monoFc bound PfRIPR fragments.

A) Deconvoluted intact mass analysis plot for PfRIPR EGF (5-7) with fused monoFc. Black arrows correspond to 162 Da differences which are proteins bound to different numbers of hexose moieties. **B)** PfRIPR EGF (5-7) after deglycosylation. The different glycosylation variants have now resolved into a single smaller peak.

Finally, each PfRIPR fragment produced in HEK293F cells was fused to the monoFc via a TEV cleavage site. Data showed that the monoFc was indispensable; and the protein fragments could not be produced in HEK293 cells in its absence (data not shown). For future experiments, the monoFc could be easily cleaved by TEV protease if required, however substantial protein losses were observed during the cleavage and purification due to aggregation. Future results indicate when the monoFc was cleaved, otherwise it was present and monoFc control protein was included as necessary.

Table 3-2 – Table of all PfRIPR fragments made including quality analysis summary
All proteins are bound to the monoFc.

PfRIPR fragment description	Amino acids	Expression in HEK293F cells	Expected size / Da	Intact mass ΔM / Da	Deglycosylated Intact mass ΔM / Da	MS/MS verified
monoFc + GFP	N/A	✓	35045	4076	-11	✓
N-half	21-553	✓	88557	Not found	Not found	✓
N-terminal domain	21-286	×	NA*	NA*	NA*	NA*
N-terminal domain B	21-368	×	NA*	NA*	NA*	NA*
Chen3	239-368	✓	41192	2617	-23	✓
EGF domains 1 - 2	287-362	✓	NA†	NA†	NA†	NA†
Middle domain	363-635	×	NA*	NA*	NA*	NA*
EGF domains 3-10	639-979	×	NA*	NA*	NA*	NA*
EGF domains 3-6	639-816	✓	46,000	NA*	NA*	✓
Chen1/2	791-900	✓	39001	2766	4	✓
EGF domains 7-10	817-979	✓	44,000	NA*	NA*	✓
EGF domains 3-4	639-715	✓	35129	2646	0	✓
EGF domains 5-6	716-816	✓	37840	2646	1	✓
EGF domains 6-7	771-855	✓	36370	1473	-82	✓
EGF domains 7-8	817-897	✓	35542	2647	4	✓
EGF domains 9-10	898-979	✓	36935	1674	-1295	✓
EGF domains 5-8	716-900	✓	47431	2664	4	✓
EGF domains 5-7	716-857	✓	42630	2664	4	✓
C-terminal domain	980-1086	✓	39028	-23	-4	✓
C-half (non monoFc)	534-1086	×	NA*	NA*	NA*	✓

*Proteins could not be made to sufficient quality/quantity for mass spectrometry analysis

†PfRIPR-EGF(1-2) was replaced by Chen3 so mass spectrometry was not carried out on PfRIPR-EGF(1-2)

3.4 Reconstitution of the RCR complex with recombinant PfRIPR fragments

PfRIPR forms a complex with PfRH5 and PfCyRPA[123,128] (the "RCR complex"). At the time of starting this project, there was little/no information reported on how this complex formed. Given it was possible that only one domain/region of PfRIPR interacts with PfCyRPA, I proceeded to assess whether the formation of the RCR complex could be recapitulated *in vitro* without the full-length PfRIPR protein present. Here an experimental approach was used based on SEC-FPLC. Each individual component of the complex can be run on a SEC column which shows a single peak corresponding to the protein. PfRH5, PfCyRPA and PfRIPR will spontaneously form the RCR complex when incubated at an equimolar ratio. The complex normally forms in 30 minutes however experiments are normally performed at 4°C overnight to ensure consistency between experiments. The incubated mix can then be run on a SEC column where a single larger peak that elutes at an earlier time point representing the complex is visible (Figure 3.6B). The proteins present in each SEC peak can be verified on an SDS-PAGE gel.

The protein fragments N-half, Chen3, EGF (3-6), EGF (7-10), Chen1/2, C-terminal domain, and EGF (3-6) in combination with EGF (7-10) were all tested for binding to CyRPA and complex formation. These fragments cover most of the full-length protein; the only section not covered is the area immediately surrounding the protease cleavage site. Each PfRIPR protein fragment was incubated overnight with an equimolar volume of CyRPA, or CyRPA + RH5 and then analysed using size exclusion chromatography (full results in Appendix 8.1). A representative example is shown in Figure 3.6A. None of the protein fragments were able to bind to CyRPA or form a

complex with CyRPA + RH5. In contrast, full-length PfRIPR could reproducibly form a complex with CyRPA or CyRPA + RH5; these larger complexes eluted in an earlier SEC fraction than each individual component (Figure 3.6B). In short, it was not possible to identify a smaller sub-domain/region of PfRIPR that could interact with CyRPA and/or RH5 to form a larger complex as seen with the full-length molecule.

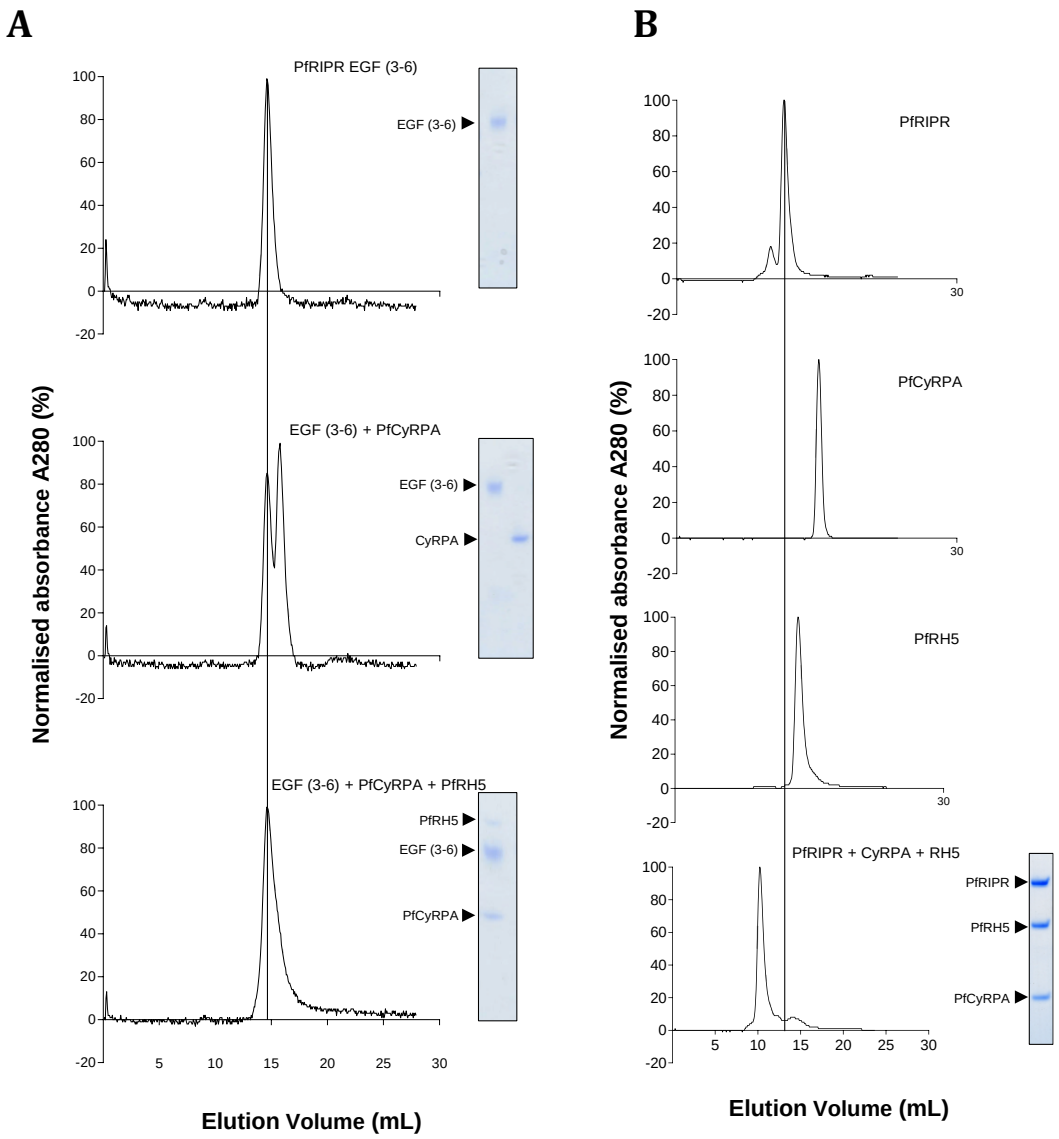


Figure 3.6 – PfRIPR EGF (3-6) does not form a complex with PfCyRPA or PfCyRPA and PfRH5.

A) SEC trace of purified monoFc fused PfRIPR EGF (3-6) individually and as a complex. SDS-PAGE gels are shown to the right. Top panel: PfRIPR EGF (3-6), expected MW 46 kDa. Middle panel: EGF (3-6) (peak 1) and PfCyRPA (peak 2), expected bands 46 kDa and 42 kDa respectively. Bottom panel: EGF (3-6), PfCyRPA and PfRH5, expected band sizes 46 kDa, 42kDa and 58 kDa. The shift in the bottom panel shows that CyRPA and RH5 interact as expected but not with PfRIPR EGF (3-6). A straight line is added for clarity to show the peak of PfRIPR EGF (3-6), which does not shift in any experiment. **B)** SEC trace of PfRIPR full-length, CyRPA, RH5 individually and as a complex. Expected band sizes; PfRIPR: 125 kDa, PfRH5: 58 kDa, PfCyRPA 42 kDa. All three proteins interact to form a triple complex as evidenced by the shift in the bottom trace. The black line corresponds to the size of the PfRIPR peak in all B) panels.

3.5 Characterisation of non-neutralising PfRIPR mAbs

3.5.1 Epitope mapping using recombinant PfRIPR fragments

Having produced recombinant regions of PfRIPR, I next sought to tackle the question of where functional growth inhibitory antibodies may bind on the molecule. At the time of starting this project, a panel of seven anti-PfRIPR mouse mAbs had previously been produced in the Draper group (Lea Barford, unpublished data. Table 3-3). Somewhat surprisingly, none of these mAbs showed *in vitro* GIA (Figure 3.7), and it was therefore useful to better understand where they bind.

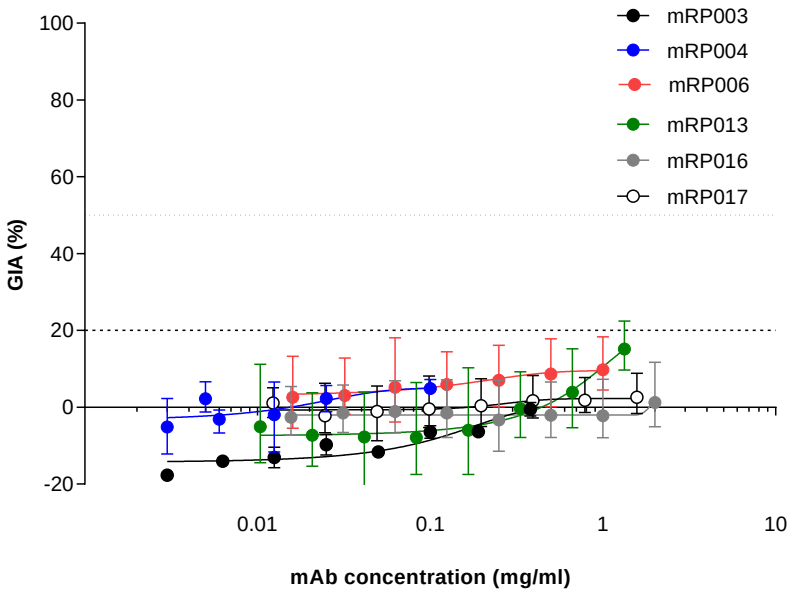


Figure 3.7 – Single cycle GIA assay using dilution curves of the seven original anti-PfRIPR mAbs used in this thesis.
Dashed line at 20% represents the lower cut-off of the assay. A dash line is added at 50% GIA for clarity. Error bars are SEM, points are median values. N = 3.

The recombinant PfRIPR protein fragments were used in a dot blot array to identify which section of PfRIPR contains these non-neutralising epitopes (Figure 3.8A, B). Importantly, all mAbs bound the positive control (PfRIPR full-length) and none to the monoFc negative control. Otherwise, 6/7 of these non-neutralising epitopes were consistently identified in the N-half domain or in EGF (3-4); this covers a substantial portion of the protein. The epitope region for one mAb, mRP013, could not be identified. It is possible that this mAb binds between the protease cleavage site and EGF (3-4) as this is the only section not covered by the protein fragments. I also assessed whether any of these epitopes were conformational by performing a dot blot array with full length PfRIPR and denatured full length PfRIPR (Figure 3.8C). PfRIPR was denatured by heating the protein to 90°C for 10 minutes. Due to the loss of two of the hybridomas only five mAbs could be tested in this array. Of the five, two consistently recognised conformational epitopes on PfRIPR.

In summary these data indicated that potentially the first two-thirds of the molecule may not contain neutralising epitopes. It was also clear that I lacked mAb reagents binding from around EGF5 onwards limiting investigations for nearly half of the protein.

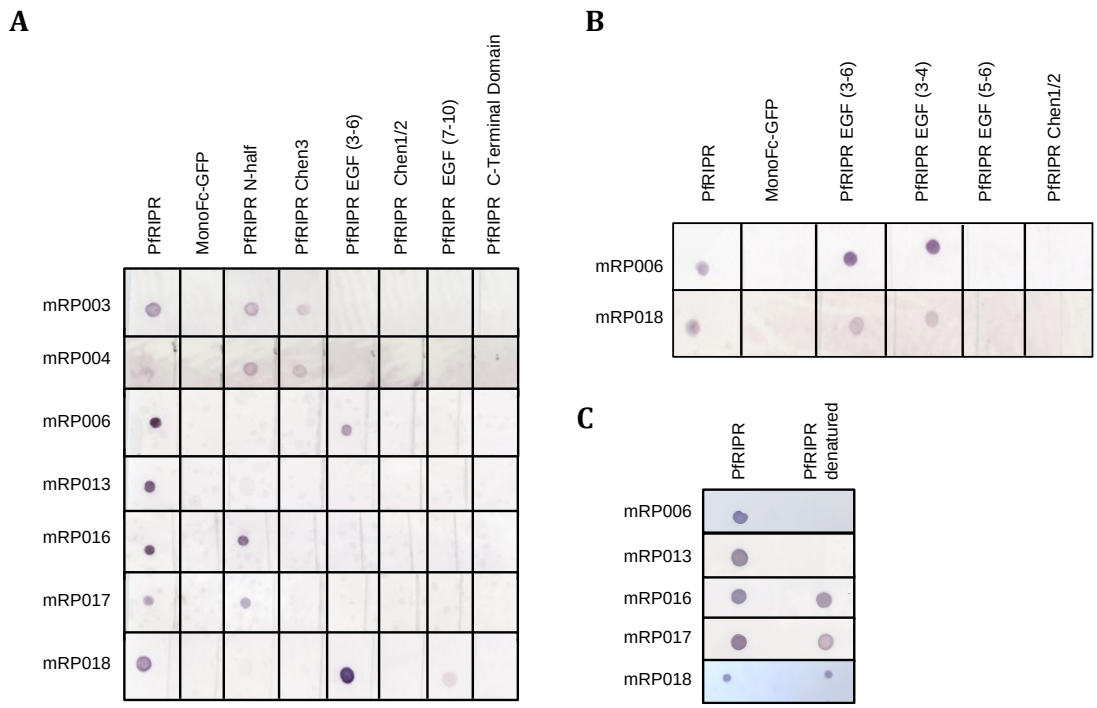


Figure 3.8 – Dot blots of non-neutralising mAbs against different PfRIPR fragments. **A)** Identification of mAb binding region, only the epitope for mRP013 could not be traced to a specific region of PfRIPR. All mAbs bound full length PfRIPR and none bound the monoFc-GFP control **B)** Further characterisation of mRP006 and mRP018 with protein fragments made later in the project, both of these mAbs bind to EGF (3-4). **C)** Determining whether the mAbs bind a linear or conformational epitope. PfRIPR was denatured by heating to 90°C for 10 minutes. mRP003 and mRP004 could not be tested in this screen due to loss of the hybridomas.

The binding sites of mRP013, mRP016 and mRP017 were only very roughly pinpointed by this assay – the binding site of mRP013 was still completely unknown, whilst mRP016 and mRP017 bound within the 400 amino acid N-half region. Since mRP016 and mRP017 appeared to bind linear epitopes, a peptide screen was next used to try and identify the binding epitopes. Peptide 20mers offset by 12 amino acids were thus designed to cover the non-EGF regions of the N-half and the domain surround the protease recognition sequence (Figure 3.9A). Using this library in an ELISA, it was found that mRP016 and mRP017 both bind to peptide 1, sequence IDLIEGIFYEKNEIDKLTFS, at the very N-terminus of PfRIPR (Figure 3.9B). A concentration titration of mRP016 and mRP017 in the ELISA peptide binding assay

suggested that they have different binding properties (Figure 3.9C) with mRP017 likely to have a higher affinity. This was further explored using surface plasmon resonance in section 3.5.2.

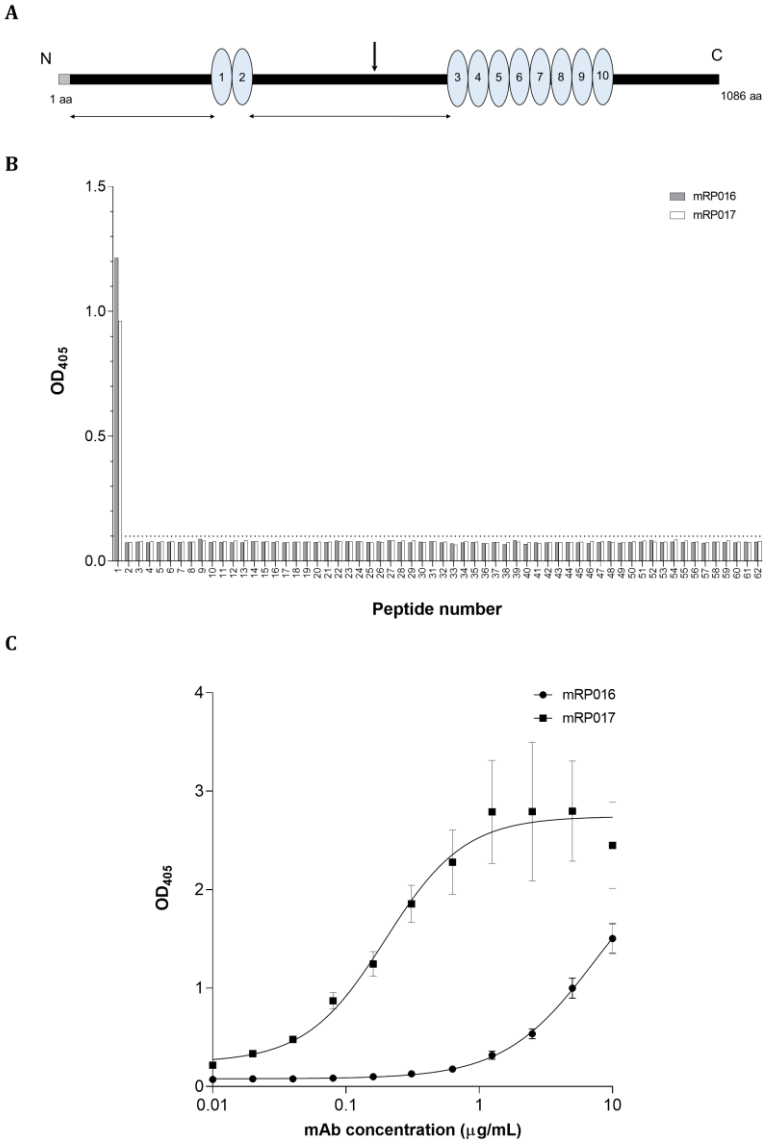


Figure 3.9 – PfRIPR Peptide screen for linear epitopes.
A) Schematic of the regions covered by the peptide screen. **B)** Peptide ELISA results for mRP016 and mRO017; both mAbs bind to peptide 1. Representative graph of two repeats shown. **C)** Titration curve of binding of mRP016 and mRP017 to peptide 1. Error bars in C are SD, points are median, N = mean of three replicate wells. each dataset fitted to a four-parameter dose-response curve.

3.5.2 Assessment of mouse mAb binding affinities by SPR

Although these mouse mAbs were non-functional in the GIA assay, likely due to binding non-functional epitopes, it was prudent to characterise the kinetic parameters of these mAbs to ensure that there was nothing unusual which may explain the lack of GIA activity, such as very low affinity. The mAb affinity, or equilibrium dissociation K_D, is reported in units of mol L^{-1} (M). K_D is the equilibrium point where the rate of mAb [A] and antigen [B] complex formation is equal to the rate of dissociation (Equation 3.1) in a simple 1:1 binding model. Antibody K_D values range from micromolar (10^{-6}) to nanomolar (10^{-9}). In addition to the K_D value, the K_{on} and K_{off} rates can be interrogated separately; it is possible that either K_{on} or K_{off} may be of particular interest for anti-merozoite malaria mAbs since there is only a short window of time during red blood cell invasion when mAbs can bind their target.

$$K_D = \frac{[A][B]}{[AB]} = \frac{K_{off}}{K_{on}}$$

Equation 3.1 – The relationship between K_D with K_{on} & K_{off}

The kinetic parameters of the non-functional mAbs were determined using the Biacore X100 evaluation software by fitting to a 1:1 Langmuir binding model. Initially each mAb was bound to a protein G chip then PfRIPR full-length antigen flowed over the mAb. This produced unclear results with high bulk volumes and sensorgram drift. This issue was largely attributed to problems with buffer-exchanging PfRIPR followed by concentration to the required level given that full-length PfRIPR protein is highly prone to aggregation with increasing concentration. This issue was circumvented by immobilising PfRIPR onto a CM5 chip to a RU of 1500, then flowing mAb over the chip as the antigen. SPR multicycle sensorgrams are shown in Figure 3.10 and a summary

of the results can be found in Table 3-3. All of the mAbs have high K_D values, often in the nanomolar range, with typical K_{on} and K_{off} values indicating that the affinity of these mAbs is unlikely to be responsible for the lack of GIA activity. Having ruled out kinetics as a reason for the negative GIA I then sought to investigate if these mAbs could bind the RCR complex *in vitro*.

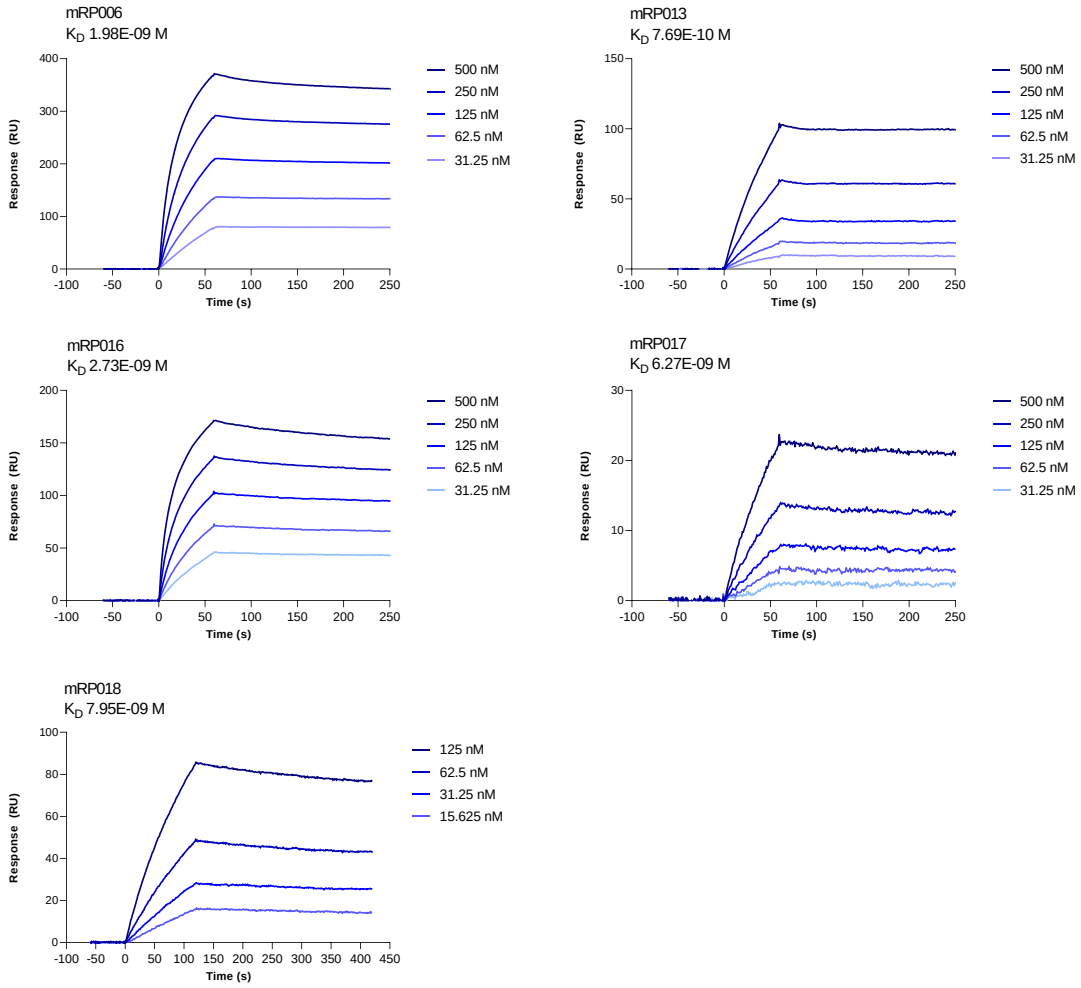


Figure 3.10 – Multi-cycle kinetic SPR sensorgrams of the five characterised non-functional anti-PfRIPR mAbs.
For mRP006, mRP013, mRP016 and mRP017 the following conditions were used: 60s contact time with mAb starting at 500nM and subsequently halving, a dissociation time of 240s followed by a glycine regeneration step of 30s (regeneration step not shown). For mRP018 the starting mAb concentration was lowered to 125 nM and the dissociation time extended to 300s to enable the software to calculate the kinetics. All samples were run in PBS + 0.05% P20. Calculated K_D values are displayed above each sensorgram.

3.5.3 Non-neutralising mAbs bind the RCR or prevent RCR formation

The mAb panel was so-far assessed for epitope binding region within PfRIPR and affinity. Another potential hypothesis related to antibody function is that neutralising/growth-inhibitory mAbs disrupt the interactions between PfRIPR, PfCyRPA and PfRH5 thereby forcing dissociation of the invasion complex and/or preventing complex formation. In contrast, non-neutralising mAbs may just bind the RCR complex without disrupting RCR protein-protein interactions. To test this hypothesis, an equimolar amount of mAb plus recombinant PfRIPR, PfCyRPA and PfRH5 proteins were incubated in different combinations and analysed by SEC. In addition, PfRIPR, PfCyRPA and PfRH5 were incubated to allow the RCR complex to form and then the mAb added after one hour followed by an incubation period before analysis by SEC. All mAbs bound PfRIPR in solution as expected, however variation was observed regarding mAb binding to the RCR complex (Appendix 8.2, representative examples shown in Figure 3.11).

mAbs mRP006, mRP013, and mRP016 could bind the full RCR complex but did not prevent its formation. mRP004 and mRP017 could bind to PfRIPR in complex with PfCyRPA but not the trimeric RCR complex, again these mAbs could not disrupt a preformed RCR complex. mRP003 only formed a complex with PfRIPR and prevented PfRIPR forming a complex with both PfCyRPA and PfRH5, again it failed to disrupt the preformed RCR complex. Notably, it was surprising that mRP016 and mRP017 had different binding characteristics given that they bound to the same peptide in the peptide ELISA screen.

Moreover, although some mAbs (mRP003, 004, 017 and 018) could prevent the RCR complex forming *in vitro,* none of them were able to displace PfRIPR from the RCR

complex if the RCR was pre-formed. These results indicate that preventing formation of the RCR complex is unlikely to be a mechanism of antibody mediated growth inhibition against the merozoite. These data wold also indicate that the RCR complex is presented on the merozoite surface preformed, thus preventing these antibodies from binding to their target epitopes. Experiments on neutralising antibodies isolated later in the project are reported in chapter V. In the meantime, a summary of the non-neutralising mAb characteristics is given in Table 3-3.

Table 3-3 – Summary of non-neutralising mAb data.

mAb	**Epitope type**	**PfRIPR Epitope/Binding Region**	**K_{on} (M^{-1} s^{-1})**	**K_{off} (s^{-1})**	**KD (M)**
mRP003	Not tested	EGF (1-2)	Not tested	Not tested	Not tested
mRP004	Not tested	EGF (1-2)	Not tested	Not tested	Not tested
mRP006	Conformational	EGF (3-4)	1.2E+05	2.38E-04	1.98E-09
mRP013	Conformational	Undefined	3.86E+05	2.97E-05	7.69E-10
mRP016	Linear	Non-EGF N-half	1.45E+05	4.09E-04	2.73E-09
mRP017	Linear	Non-EGF N-half	2.53E+04	1.59E-04	6.27E-09
mRP018	Linear	EGF (3-4)	5.48E+04	4.35E-04	7.95E-09

mAb	**mAb protein bindings**			
	PfRIPR	**PfRIPR + PfCyRPA**	**RCR complex**	**Pre-Formed RCR complex**
mRP003	✓	×	×	No disruption or binding
mRP004	✓	✓	×	No disruption or binding
mRP006	✓	✓	✓	Binds
mRP013	✓	✓	✓	Binds
mRP016	✓	✓	✓	Binds
mRP017	✓	✓	×	No disruption or binding
mRP018	✓	×	×	No disruption or binding

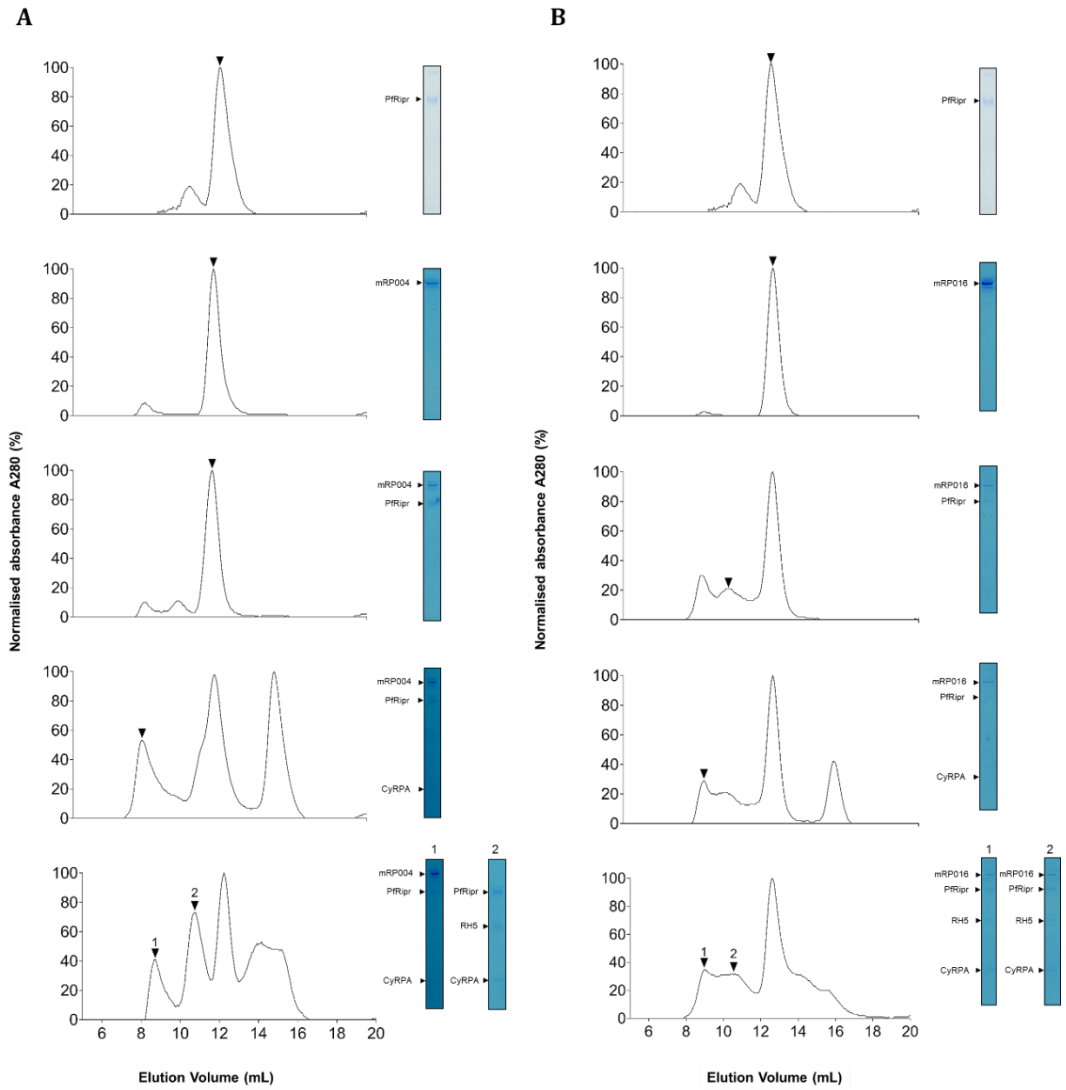


Figure 3.11 - Non-neutralising mAbs prevent formation of and bind the RCR complex. SEC profiles show PfRIPR, mAb, PfCyRPA, and PfRH5 run individually and in complex, SEC chromatogram peaks were run on an SDS-PAGE gel to visualise which proteins were present. Representative examples shown. **A)** mRP004 prevents the RCR complex forming. mRP004 binds to PfRIPR and, PfRIPR in complex with CyRPA, however does not form a quaternary mRP004-RCR complex (bottom panel). **B)** mRP016 can bind to the RCR complex forming a quaternary mRP016-RCR complex (bottom panel).

3.6 Investigating potential PfRIPR erythrocyte receptors

A common mechanism for antibody clones that inhibit cellular invasion processes is receptor blockade, indeed, many growth inhibitory clones that bind PfRH5 also block its interaction with basgin[156]. An erythrocyte surface receptor for PfRIPR, if one exists, is currently unknown. However, if such a receptor can be identified, then structural information of the PfRIPR-receptor complex can be used to identify potentially neutralising epitopes. It may also further aid our understanding of the function of PfRIPR within the RCR complex.

Whilst conducting this project, two putative PfRIPR receptors, Adhesion Molecule with Ig like Domain 2 (AMIGO2) and Semaphorin-7A (SEMA7A), were identified using a high throughput screen and reported by Nagaoka *et al.* [174]. I thus proceeded to investigate these newly reported interactions by initially seeking to produce the recombinant receptors in the HEK293 cell expression platform. Unfortunately, the AMIGO2 ectodomain could not be made to a high enough quality to perform any analysis, however SEMA7A fused to the CD4d3+4 solubility tag was straight-forward to produce and could be used in subsequent tests.

Recombinant SEMA7A and PfRIPR were next incubated at an equimolar ratio overnight before analysis by size exclusion chromatography. SEMA7A and PfRIPR, however, did not interact *in vitro* in this assay (Figure 3.12A) in contrast to the newly reported results[174]. In order to investigate further, a positive control was next produced, given Wright *et al.* had also reported that SEMA7A binds to a different merozoite protein– MTRAP[203]. Unfortunately, this result could also not be replicated

in this assay (Figure 3.12B). After communication with Dr Gavin Wright, the MTRAP construct was recloned without the CD4d3+4 solubility tag, as produced in the original study by Bartholdson *et al.*[203]. The MTRAP protein could still be expressed at high quality without this tag and upon analysis now formed a complex with SEMA7A after a 30-minute incubation at 4°C (Figure 3.12C). This result with the MTRAP positive control was reproducible and demonstrated that the SEMA7A protein behaved as expected, and called into question the reported interaction with PfRIPR.

In addition to analysis by SEC-FPLC, SEMA7A and PfRIPR binding was also investigated using SPR. PfRIPR was immobilised on a CM5 chip and SEMA7A used as the test antigen in the flow through. The results (Figure 3.13) showed no binding between SEMA7A and PfRIPR. In contrast, binding between PfCyRPA and PfRIPR (K_D 2.15E-06) was observed as expected, as well as between PfRIPR and the mRP006 mAb. Notably, the response observed with PfCyRPA was not large; this is likely due to the difficulty in detecting a mass shift when binding a small 43 kDa PfCyRPA protein to the large 124 kDa PfRIPR. In contrast, the SEMA7A-CD4d3+4 complex is 89 kDa, so should have been detectable if it occurred.

From these results it seemed extremely unlikely that PfRIPR forms a stable complex with SEMA7A as described by Nagaoka *et al.*[174]. It is possible that the WGCFS used to make the PfRIPR protein in the reported study produced a poorly folded protein that was 'sticky' and formed non-specific interactions with SEMA7A.

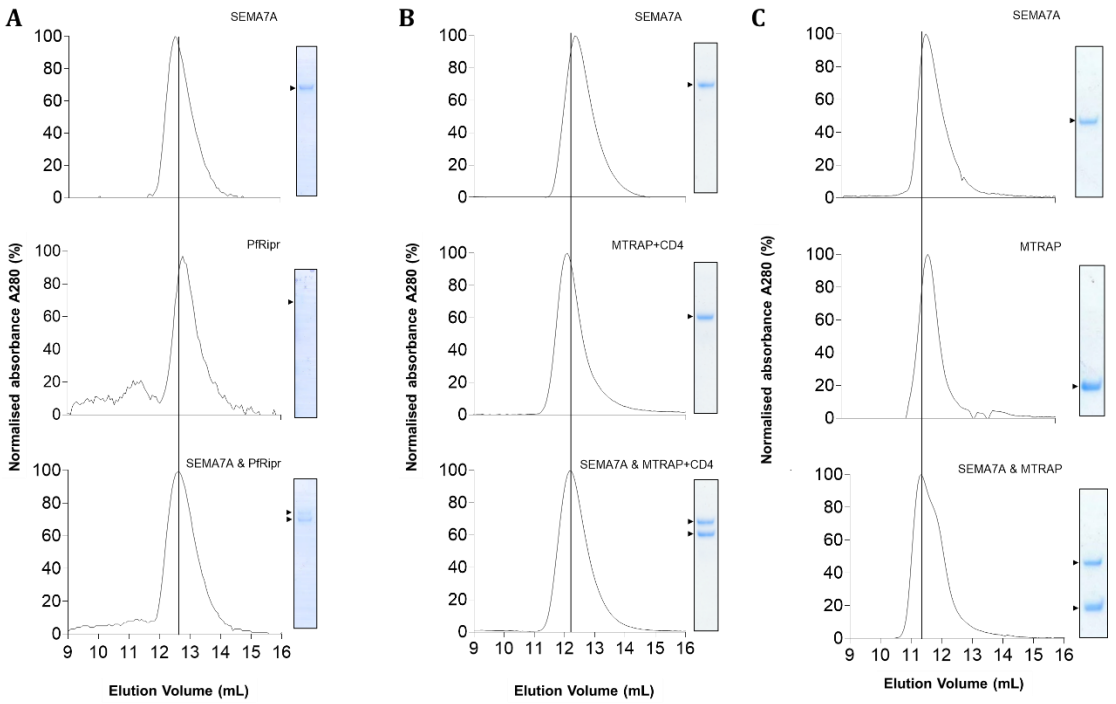


Figure 3.12 – Investigating the binding of PfRIPR to SEMA7A-CD4d3+4.
Each protein was incubated alone or in complex at an equimolar ratio. A gel of the SEC chromatogram peaks was run to determine which proteins were present. **A)** PfRIPR and SEMA7A alone and combined in solution (bottom panel). The two proteins do not interact which would have caused a shift of the peak to the left. **B)** MTRAP-CD4d3+4 and SEMA7A alone and combined in solution (bottom panel). MTRAP-CD4d3+4 and SEMA7A do not interact. **C)** MTRAP (without CD4d3+4) and SEMA7A alone and combined in solution. SEMA7A and MTRAP form a complex that runs at a larger size (elutes earlier) on SEC.

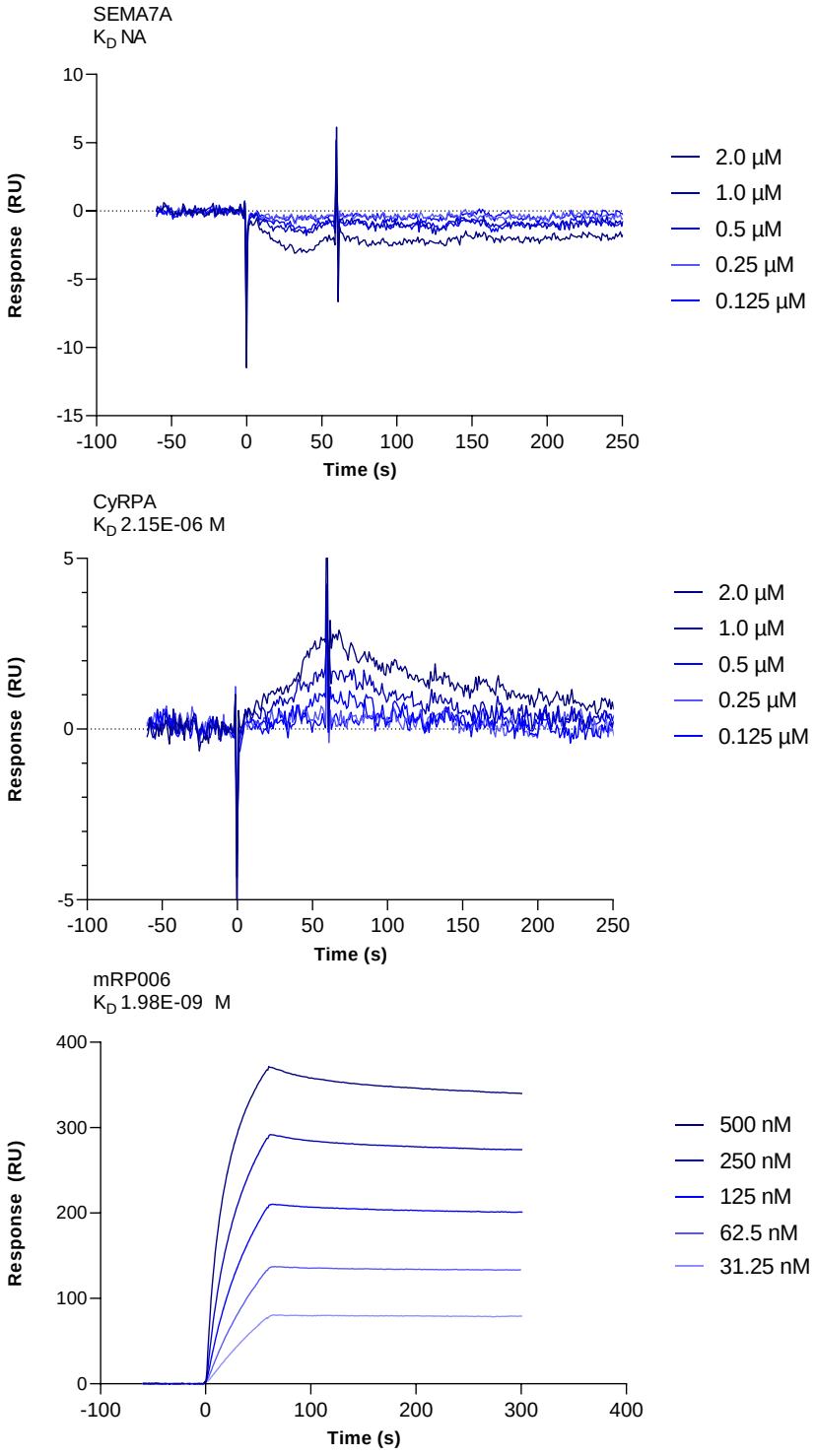


Figure 3.13 – Multi-cycle kinetic SPR sensorgrams using PfRIPR on a CM5 chip. SEMA7A (top, no K_D) and the positive control PfCyRPA (middle, K_D 2.15E-06 M) were run under the following conditions: 60s contact time with antigen starting at 2.0 µM and subsequently halving, a dissociation time of 240s followed by a glycine regeneration step of 30s (regeneration step not shown). The positive control mRP006 mAb (bottom, K_D 1.98E-09M) was run under the same conditions but starting at 500nM of mAb. RU, resonance unit, all samples were run in PBS + 0.05% P20.

3.7 Rabbit immunisations and identification of neutralising antibody epitopes on PfRIPR

In addition to monoclonal antibodies and structure guided approaches, neutralising antibody epitopes can be identified by antigen reversal of functional assay activity. In this case, the recombinant PfRIPR protein fragments can be used to deplete anti-PfRIPR pAb of antibodies against certain regions and the effect on GIA determined. Before the reversal assay can be performed, good quality anti-PfRIPR polyclonal antibodies that show strong GIA must be obtained.

3.7.1 Rabbit immunisations for antigen reversal

Four rabbits were initially immunised at Genscript Biotech (as detailed in section 2.1.14) to obtain sufficient anti-PfRIPR full-length pAb for the reversal GIA assay. However, surprisingly, the IgG purified from the serum of these rabbits yielded weak GIA (Figure 3.14A) with an EC_{50} value of 17.4mg/mL (interpolated, 95% CI not calculated), far above previously reported EC_{50} of <1 mg/mL[167]. However, despite the low GIA, each sample showed synergy with the anti-PfRH5 mAb R5.011 (Figure 3.14B) in agreement with the previous report from Alanine *et al.*, where this mAb was shown to slow the invasion of RBCs by merozoites[156] thereby giving more time for neutralising antibodies to act

Since the initial rabbit GIA assay data showed lower potency than expected for the anti-PfRIPR polyclonal IgG, the rabbit immunisations were repeated by collaborators at the NIH, USA and by another contract company in the UK, called CRB (section 2.1.14). Now, a 50 µg dose of recombinant PfRIPR in adjuvant was used as opposed to the 20 µg dose used in the Genscript study. The purified IgG samples from the 4

rabbits in the NIH study and 2 rabbits in the CRB study showed improved levels of GIA (Figure 3.15A & B), with an average EC_{50} of 2.1 mg/mL for the NIH samples (95% CI 1.90, 2.31) and 4.2 mg/mL for the CRB samples (95% CI 4.13, 5.92) with comparable results between different rabbits.

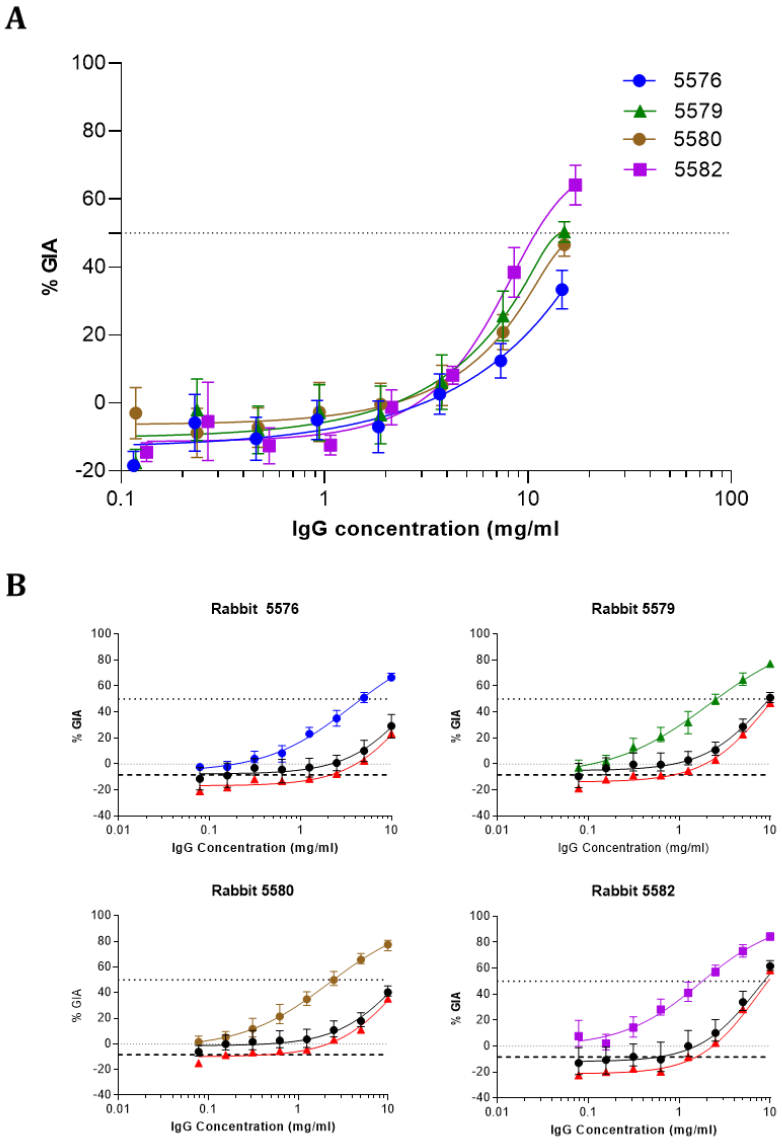


Figure 3.14 – GIA assay results using sera from rabbits immunised at Genscript.
A) IgG purified from sera were tested for GIA against 3D7 clone *P. falciparum* in a single-cycle assay. Titration curve for each of 4 rabbits is shown. **B)** Synergy analysis of the anti-PfRH5 mAb clone R5.011 with purified IgG from the four Genscript rabbits. R5.011 concentration was held at 2mg/mL for all test concentrations of rabbit sera (x-axis). Black line: Rabbit pAb (purified IgG) alone; red line: predicted Bliss additivity; coloured line: rabbit pAb + R5.011. Dashed black line shows fixed concentration of mAb R5.011 which is GIA negative (as expected). All error bars represent SEM, each dataset fitted with Richard's five-parameter dose-response curve with no constraints. Dotted line included to show 50% GIA on all graphs.

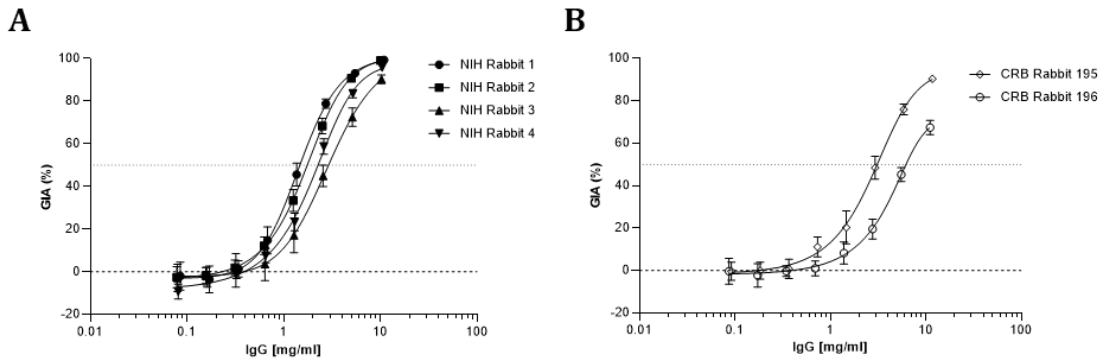


Figure 3.15 – GIA assay results from the NIH & CRB rabbits.
A) GIA titration curve of NIH rabbit purified IgG, mean EC_{50} for the four rabbits 2.1mg/mL. **B)** GIA titration curve of CRB rabbit purified IgG, mean EC_{50} for the two rabbits 4.2mg/mL. All error bars represent SEM, points are median values. Each dataset fitted with Richard's five-parameter dose-response curve with no constraints.

3.7.2 Antigen reversal GIA assays

Due to the substantial delay of immunising and testing new rabbits at NIH and CRB, initial antigen reversal GIA assays were carried out on the Genscript pAb whilst the second set of rabbit immunisations was ongoing. The reversal was initially conducted using two concentrations of the PfRIPR protein fragments, 0.5μM and 1.0μM (Figure 3.16A, B). Fragments such as EGF (3-6) and EGF (7-10) were only tested at 1.0μM due to low amount of protein available for testing. The full-length PfRIPR protein was used as the positive control and completely reversed the GIA as expected. Importantly, this protein had no effect on the GIA when included in the anti-PfRH5 IgG control. Each PfRIPR fragment was bound to the monoFc, as such the monoFc-GFP protein was included as a control. This control protein had no effect on the GIA. Each PfRIPR fragment was also tested in the absence of purified anti-RIPR IgG to ensure the addition of the protein fragments alone do not lead to GIA. None of the fragments gave GIA when tested without anti-PfRIPR purified IgG (data not shown).

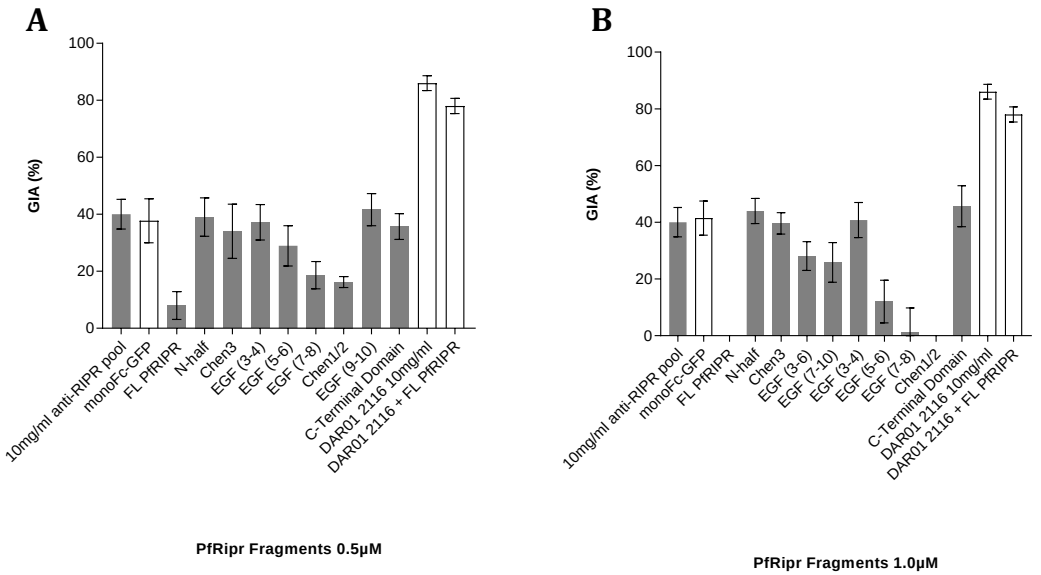


Figure 3.16 – Assessment of anti-PfRIPR full-length IgG GIA reversal using Genscript rabbit purified IgG.
A) Antigen reversal GIA assay with PfRIPR protein fragments held at 0.5µM. **B)** Antigen reversal with PfRIPR protein fragments held at 1.0µM. Rabbit purified IgG held at 10mg/mL in all experiments. Each protein fragment was fused to the monoFc fragment. White bars represent control samples, left to right: monoFc-GFP protein fragment antigen reversal, anti-RH5 purified IgG (DAR02 2116) at 10 mg/mL, anti-RH5 purified IgG (DAR02 2116) at 10 mg/mL and FL-PfRIPR protein. Grey bars represent test samples. All bars are mean with SD, n=3. Significance determine by Kruskal-Wallis test with Dunn's multiple comparisons test against the 10 mg/mL anti-PfRIPR pool, no significant differences were detected in the data.

In these experiments, the N-terminal half fragments of PfRIPR: N-half and Chen3, showed no GIA reversal. PfRIPR EGF (3-6) and EGF (7-10) showed a trend towards reversing the GIA at 1.0 µM but the result was not significant. However, strong reversal of GIA was seen at 0.5µM and 1.0µM for EGF (7-8), Chen1/2, and EGF (5-6) in the 1.0µM group only, however none of these reached statistical significance; this is likely due to the small sample size and large number of multiple comparisons. Despite the lack of statistical significance, the trend in the graph is clear.

In summary, these data indicated that a region encompassing EGF domains 6/7-8 could reverse the GIA afforded by anti-PfRIPR IgG. However, the lower limit of

quantification for the GIA assay is 20% GIA, and since the anti-PfRIPR pAb only generated 40% GIA, the sensitivity of this initial assay is likely to be low. Nevertheless, given the protein fragment EGF (7-8) yielded some very encouraging results, further experiments were conducted.

The antigen reversal experiments were repeated using anti-PfRIPR IgG purified from a pool of sera from the 4 NIH and 2 CRB rabbits. The first round of antigen reversal experiments using the new anti-PfRIPR pAb showed no reversal for any fragment (data not shown). It was likely that this was because there was insufficient amount of protein in the assay to reverse the anti-PfRIPR pAb held at 10mg/mL. To solve this, the anti-PfRIPR purified IgG was titrated against the protein fragments EGF (7-8) and Chen1/2 until a clear difference could be observed (Figure 3.17). A concentration of 3mg/mL was chosen as the most appropriate concentration for future reversal experiments, as this concentration gave 80% GIA under normal test conditions and could be reversed to 30% upon addition of 1μM EGF (7-8) or Chen1/2.

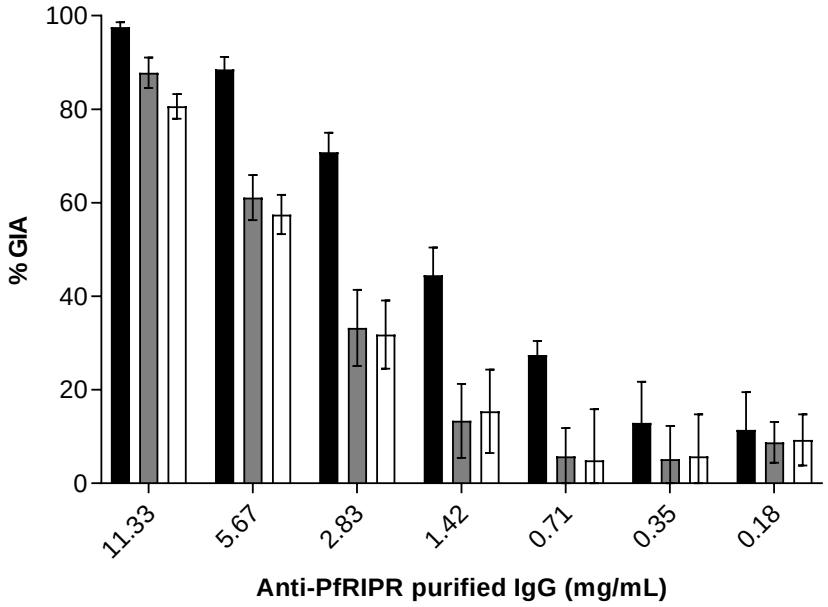


Figure 3.17 – Anti-PfRIPR purified IgG titration.
Titration of anti-PfRIPR pAb alone (black bars), with 1μM EGF (7-8) (grey bars), and Chen1/2 (white bars). All bars are mean with SD, n=3.

The repeat of the GIA reversal assay with the CRB rabbit pAb (Figure 3.18) gave very similar results to the initial experiment (Figure 3.16) with significant GIA reversal ($p<0.05$) being observed with the PfRIPR fragment EGF (7-8) and some non-significant reversal with EGF (5-6), EGF (6-7) and Chen1/2 (EGF 6-8). The small number of repeats and large number of multiple comparisons again likely reduced the statistical power.

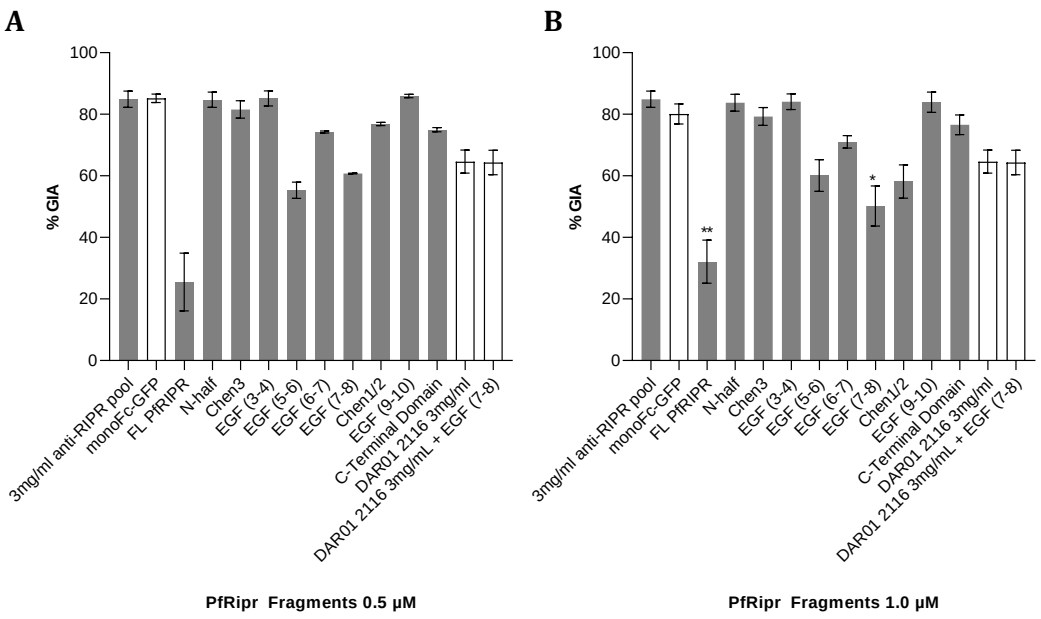


Figure 3.18 - Assessment of anti-PfRIPR full-length IgG GIA reversal using NIH and CRB rabbit purified IgG.

A) Antigen reversal GIA assay with PfRIPR protein fragments held at 0.5µM. **B)** Antigen reversal with PfRIPR protein fragments held at 1.0µM. Rabbit purified IgG held at 3mg/mL in all experiments. Each protein fragment was fused to the monoFc fragment.

White bars represent control samples, left to right: monoFc-GFP protein fragment antigen reversal, anti-RH5 purified IgG (DAR02 2116) at 3 mg/mL, anti-RH5 purified IgG (DAR02 2116) at 3 mg/mL and PfRIPR EGF (7-8) protein. Grey bars represent test samples. All bars are mean with SD, significance determine by Kruskal-Wallis test with Dunn's multiple comparisons test against the 10 mg/mL anti-RIPR pool, * is $p<0.05$, ** is $p<0.01$.

Given the antigen reversal trend seemed consistent across multiple studies but the statistics lacked power for a firm conclusion I conducted further antigen reversal titrations. These were carried out to test whether the GIA could be completely reversed using just one EGF-like domain protein fragment (Figure 3.19). Here, the GIA could be completely reversed with PfRIPR EGF (5-8), indicating that all neutralising epitopes are located within this relatively small section of the PfRIPR protein. The GIA could not be completely reversed with any other PfRIPR EGF domain fragment such as EGF (5-6), EGF (6-7), EGF (6-7) and EGF (7-8)

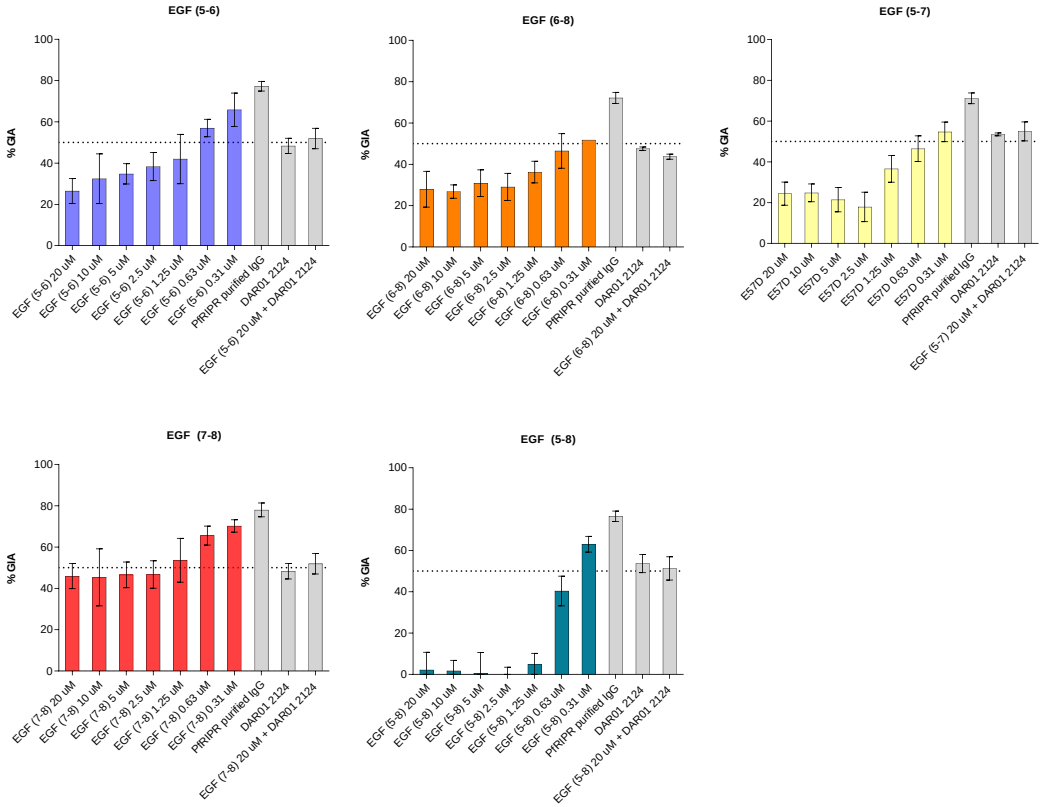


Figure 3.19 – Antigen reversal titrations using PfRIPR EGF-like domains.
Anti-PfRIPR purified IgG was held at 3mg/mL while each protein fragment was titrated from 20µM to 0.31µM. Coloured bars are test samples. Grey bars are controls: PfRIPR purified IgG held at 3 mg/mL, DAR01 2124: Purified anti-PfRH5 IgG held at 3 mg/mL. 20µM PfRIPR-EGF with DAR01 2124 anti-PfRH5 purified IgG held at 3 mg/mL. No EGF fragment reversed the GIA of the positive control anti-RH5 pAb. All bars are mean + SD, n=3 except for EGF (5-8) where n = 6.

3.8 Discussion

At the start of this project there was very little information known about PfRIPR other than its interaction with PfCyRPA in the RCR complex and that it plays an essential, if undefined, role in invasion of erythrocytes by *P. falciparum*.

This chapter details the production of PfRIPR protein fragments (that cover the majority of PfRIPR sequence) in a mammalian cell culture system. The production of many of these proteins was robust and scalable, however significant loss was noted during TEV protease cleavage. Alternative proteases or engineered versions of TEV could be used in the future to improve yields, however these were not examined as part of this thesis since the current TEV protocol was suitable for the in-house small-scale production. The sequence used for protein fragment production was a human codon optimised sequence with the N-linked glycan sites mutated as this was deemed the best sequence in expression trials. It was later discovered in the project that the N-half fragment could only be produced when the N-linked glycan sites were left intact and the glycans removed post-production by EndoH (see section 3.3). This result may explain why the N-half protein could not be produced from the codon harmonised sequence (Figure 3.2D) since the codon harmonised sequence has mutated N-linked glycan sites. In future, the codon harmonised version could be re-assessed, however good yields of most of the fragments could be achieved with the codon optimised sequence so further sequence exploration was deemed unnecessary.

These proteins fragments were used in a number of analyses. Firstly, I attempted to reconstitute the RCR complex using PfRIPR fragments, however unfortunately the RCR complex did not form with any of the protein fragments (section 3.4). Although

SEC is a crude method for detecting protein-protein interactions as compared to SPR, the full RCR complex can be detected with SEC consistently therefore the technique is not likely to be the limiting factor. A later study by Healer *et al.* reported that the N-half of the protein, prior to EGF (1-2), interacts with PfCyRPA[166]. This is consistent with our own mass spectrometry cross linking data which suggested an interaction between PfCyRPA and the PfRIPR motif 'EQKSL', just prior to EGF domains 1-2 (Robert Ragotte in collaboration with Intravacc, unpublished data). The N-half produced in this study was not well folded (Figure 3.2) with multiple bands observed on the SDA-PAGE gel, in addition attempts to produce this fragment in S2 cells failed. It is likely that misfolding of this protein fragment prevented binding to PfCyRPA. I suspect that Healer *et al*.[166] also suffered from the same issue since they did not report production of an N-half fragment, and they state that their C-half fragment aggregated badly.

I also explored whether PfRIPR could bind a newly identified erythrocyte receptor[174]. SEC experiments to verify SEMA7A as a potential binding partner for PfRIPR were unsuccessful (section 3.6), as was analysis by SPR. A re-analysis of the original paper[174] which identified SEMA7A as the receptor for PfRIPR identified numerous issues that cast doubt on the original result. Notably there is no quality control reported as to whether the PfRIPR produced in the wheat germ cell-free system was properly folded; indeed, proteins made using this system are often incorrectly folded. The paper reports that PfRIPR binds to PfRH5 with a KD of 4.8×10^{-10} M, this is four orders of magnitude stronger than the reported basigin-PfRH5 interaction (1×10^{-6} M). This is very strong for binding of a protein-protein complex, and very surprising given that previous papers reported no direct binding of PfRIPR-PfRH5[123,128]. The

strong binding kinetics and use of single cycle kinetics in SPR analysis, as opposed to the more traditional multi cycle kinetics, suggest that the PfRIPR is 'sticking' to multiple proteins non-specifically and not dissociating as would be expected from a protein-protein interaction. Single cycle kinetics experiments are normally used when the dissociation rate of a protein is very slow and not for this type of analysis. This spurious binding to PfRH5 then causes problems later in the paper. Potential PfRIPR receptors are screened using an "alpha-screen", with the PfRIPR-PfRH5 interaction as a positive control. Since the PfRH5-PfRIPR interaction is probably not real, it is difficult to then accept any conclusions from the alpha screen. A supplementary figure also shows that anti-SEMA7A antibodies have no GIA, this is unexpected if SEMA7A binds to PfRIPR and this interaction is required for invasion. Furthermore, it seems unlikely that both PfRIPR and MTRAP bind the same protein on the erythrocyte surface since this may lead to steric hindrance and therefore be sub-optimal for a merozoite that must invade a cell quickly.

The PfRIPR fragments were then used as tools for mapping the PfRIPR non-neutralising mAbs (section 3.5.1). All of the identified non-neutralising mAbs were located in the N-half of the protein and EGF (3-4). At this point, it was surprising that non-neutralising epitopes were found over such a wide range of domains/regions of PfRIPR. Given the size and essential nature of this protein, I suspected that there would be multiple functional domains that would be targets for neutralising mAbs and only a relatively small number of non-neutralising domains. This puzzle was amplified when it was found that the non-neutralising mAbs can bind the RCR complex, or prevent RCR complex formation (section 3.5.3) with no clear pattern. There are some potential explanations for this, such as accessibility of the epitopes on

the parasite – the epitopes may be buried on surfaces that are not visible to the immune system in a natural infection, or if they are visible then the presence of a mAb does not disrupt any essential functions of PfRIPR or the RCR complex. These questions will be difficult to answer without good quality structural information such as X-ray crystallography or CryoEM of PfRIPR in complex with the mAbs and/or the RCR complex. These data are likely to be difficult to gather given crystals of full-length PfRIPR may be impossible to produce due to its flexible nature.

This chapter also included the generation of purified anti-PfRIPR IgG from rabbits (section 3.7). Rabbits from the NIH and CRB yielded purified IgG that showed robust GIA responses, however the rabbits from Genscript did not. It is possible that 20μg PfRIPR was too low a dose of protein vaccine for a rabbit, given the NIH and CRB studies used 50μg. Alternatively the PfRIPR may have degraded in transport or been stored incorrectly during the Genscript study. Since these experiments were outsourced, it is very difficult to ascertain exactly why the GIA was low and/or the immunisation regimens performed relatively poorly. The robust responses from the other two studies give us confidence that the Genscript rabbit results were a case of bad luck.

The key finding of this chapter, and also the most surprising finding, was that all of the neutralising epitopes on PfRIPR are located within EGF-like domains 5-8 (section 3.7.2). Using antigen reversal GIA assay methodology, this neutralising epitope region was identified in a wide screen and then narrowed down using multiple protein fragment titrations. Since all the GIA was reversed by EGF (5-8) in multiple repeat experiments, we can be confident that no epitopes of significant importance were missed in the study. The variable nature of the antigen reversal screens (Figure 3.18)

due to variations in parasite growth between assays and sensitivity to IgG & protein fragment concentration, highlight the importance of assay repeats and reagent titrations to verify the results. Currently, very little information is known about this section of PfRIPR; it is not thought to bind to PfCyRPA[163] and could not be resolved in the referenced Cryo-EM structure, so both its function and location in the RCR complex remain a mystery. EGF-like domains are often found to play roles in adhesion or cell recognition, opening up the possibility that the EGF domains in the C-terminal half of PfRIPR bind a fourth merozoite protein or a red blood cell protein. The only protein with predicted structural homology to PfRIPR was TgMIC from *T. gondii*. TgMIC1 is an interesting protein that forms a complex with TgMIC4 and TgMIC6. This complex is also essential for cell invasion much like the RCR complex[211–213]. TgMIC1 performs several roles: it stabilises TgMIC6, performs a quality control function that enables the complex to be released from secretory organelles, and functions as an adhesin[211]. It is possible that PfRIPR acts in an analogous manner which may be worth exploring. Unfortunately, this is beyond the scope of this thesis.

Encouragingly, for the future work reported in this thesis, the EGF domains of PfRIPR were relatively easy to produce in HEK293 cells and therefore could be explored as vaccine candidates. If similar, or better, GIA can be generated from a construct encoding this small group of EGF domains, then production of a vaccine based on the full-length PfRIPR protein will be unnecessary. It is also possible that immunisation with the EGF domains will yield a better quality of antibody response, with proportionally more antibodies targeting neutralising epitopes. The investigation of RIPR EGF domains 5-8 as a vaccine candidate is further explored in Chapter 4.

Chapter 4 - PfRIPR vaccine development

4.1 Authorship statement

The GIA assays were carried out by two dedicated research associates: Dr Doris Quinket and Amelia Lias as described previously. HBsAg-SpyCatcher was provided by Dr Gaurav Gupta and Dr Yuanyuan Li. DLS was conducted at the Oxford Institute of Biomedical Engineering (IBME) with Dr David Pulido-Gomez's assistance. Rat standardised ELISAs were set up by Sarah Silk. Full length PfRIPR, PfRH5, and PfCyRPA protein was produced by either Dr David Pulido-Gomez or Hannah Davies. HBsAg RH5.1 and HBsAg PfCyRPA were produced by Dr David Pulido-Gomez. Rat immunisations were performed by Noble Life Sciences, USA. PfRH5 and PfCyRPA Standardised ELISAs and analysis were performed by Dr Lloyd King.

4.2 Introduction

Chapter 3 identified EGF like domains 5-8 as the target of neutralising antibodies against PfRIPR. The aim of this Chapter was to determine whether a smaller EGF like domain-based vaccine could elicit the same levels of neutralising antibodies and *in vitro* GIA as a vaccine based on the full length PfRIPR. A smaller vaccine subunit is likely to be easier to manufacture and more stable that the full length PfRIPR. This work also explores whether PfRIPR, PfRH5 and PfCyRPA can be co-immunised to improve anti-merozoite antibody neutralising activity. The work in this Chapter takes advantage of the recent advances in viral-like particle (VLP) vaccine design.

4.2.1 Virus-like particle vaccines

Recombinant subunit vaccines are sometimes poorly immunogenic. This can be for a variety of reasons; for example, a lack of B and T cell epitopes or small particle size leading to rapid clearance from the blood and lymphoid organs. Immunogenicity can be improved by the addition of a strong adjuvant; however, this can still be insufficient.

Some viral structural subunits, such as core and surface antigens, are able to self-assemble into virus-like particles (VLPs) that contain no viral genetic information; these particles are between 20 – 100nm in size and retain several key characteristics of viruses that induce a robust immune response. Commonly used VLP platforms include the hepatitis B virus surface antigen[62], human papillomavirus[214], and bacteriophages[215,216] however recently custom self-assembling nanoparticles are starting to be designed and used in pre-clinical studies[217] (Figure 4.1A). VLPs can improve the immunogenicity of a fused antigen in a number of ways. Firstly the size of the VLP, 20-200nm, enables rapid and free drainage of the VLPs to the lymph node where they are taken up by resident dendritic cells and presented to B-cells[218]. Secondly, the repeated geometric structure of the viral particle leads to enhanced cross-linking of B-cell receptors[219,220] which is a strong B-cell activator (Figure 4.1B). In contrast, protein antigens often do not cross link B-cell receptors and therefore fail to activate B-cells[221]. One of the most commonly used and clinically tested VLPs is the hepatitis B surface antigen (HBsAg)[62]. HBsAg is currently in use in the RTS,S and R21 malaria vaccines as a chimeric fusion HBsAg-CSP particle as discussed in the Chapter 1. It is also a licenced vaccine for hepatitis B in and of itself, HBsAg is included in the 6-in-1 vaccine; sold under the brand name Infanrix Hexa in the UK by GSK. The clinical

track record of HBsAg, alignment with R21 and its availability within the Jenner Institute made HBsAg the first choice for VLP vaccines in this project.

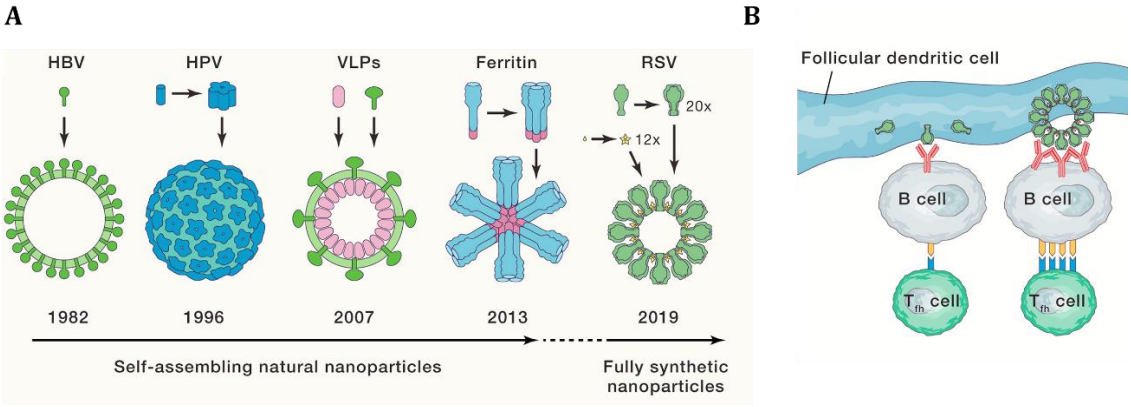


Figure 4.1 – Virus like particles and nanoparticles in vaccine design.
A) A timeline of nanoparticle use: HBV - hepatitis B virus; HPV - human papillomavirus; VLP, generic virus-like particle; Ferritin, ferritin-based nanoparticle; RSV – Custom *in silico* designed nanoparticle for RSV vaccination. **B)** VLPs promote clustering of B-cell and T-cell receptors leading to a more robust immune response. Image modified from Rappuoli *et al.* 2019[222].

4.2.2 SpyTag-SpyCatcher technology

One key challenge with chimeric VLP vaccines is the fusion of antigen to VLP subunit. Genetic fusion of antigen to VLP subunit is often very time consuming and problematic with the final fusion protein difficult or impossible to express at levels required for vaccination. Alternative strategies involve making the antigen and VLP subunit separately and then conjugating the two by chemical means or by using unnatural amino acids[223–225]. These strategies are difficult to control experimentally and lead to binding of the antigen at multiple orientations on the VLP and sometimes changing the antigen's fold to an immunologically less relevant conformation[226]. This reduces the overall efficacy of the vaccine. A new technology that overcomes many of these limitations is the SpyTag-SpyCatcher technology[227,228]. The technology was derived from the *Streptococcus pyogenes* fibronectin-binding protein FbaB[227]. This protein contains a domain, CnaB2, in which a spontaneous isopeptide bond forms

between Lys31 and Asp117. Rational design led to the domain being split into a 15 kDa "SpyCatcher" protein containing the lysine and a smaller 13 amino acid "SpyTag" peptide containing the aspartate residue. Mixing of the two components leads to peptide bond formation within minutes (Figure 4.2). The SpyTag is small enough to be added to the amino or carboxyl termini of a protein without affecting the native fold of the antigen and the gentle conjugation conditions, mixing the two components in TBS pH7.4, does not denature the antigen or VLP subunit. This technology has already been used to create chimeric VLP vaccines that give a robust immune response after a single dose without an adjuvant[228]. One VLP-SpyCatcher subunit can be used to create multiple different vaccines in a short space of time by conjugating the VLP to different SpyTagged antigens, this allows rapid testing of multiple antigens on a robust platform. These qualities made the system ideal for testing multiple PfRIPR-based vaccines in this project.

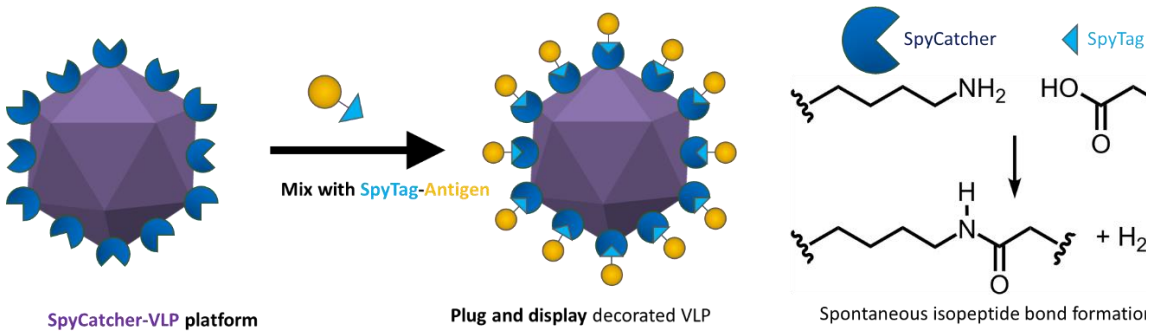


Figure 4.2 – SpyCatcher and SpyTag VLP platform.
The SpyCatcher-VLP platform is mixed with a SpyTag-Antigen to create a decorated VLP by spontaneous isopeptide formation between the SpyCatcher and SpyTag. Figure adapted from Brune *et al.* 2016[228]

The vaccine development work in this Chapter followed an iterative process. Given the length of time required to complete each immunisation study (~6 months from start of vaccine preparation to final analysis of GIA assay data), a number of studies

were run in parallel to address different questions. Given some data arising in each study was unexpected, subsequent study designs were adapted. The overall aim of this work was to generate a body of data that could lead to the rational design of a vaccine that improves on the current clinical benchmark for blood-stage malaria – RH5.1[110,229] . In particular, I aimed to:

i) Specifically define an optimal formulation of a PfRIPR-based vaccine in terms of dose, immunogen design, and delivery (soluble protein or VLP);
ii) Rank the relative potency of vaccines targeting PfRH5, PfCyRPA and PfRIPR;
iii) Assess the merits of combination vaccine approaches targeting the three antigens;
iv) Generate data to support a final strategy for optimal formulation, delivery and dose of each target antigen.

An initial experiment was performed in mice, however, at this point I switched to a rat immunisation model given mice provided too little sera to enable highly informed GIA assay analyses. Work in the rat model enabled me to address the above questions, however, in light of suspected under-dosing in the first two studies, further work necessitated repeat experiments at higher vaccine dose. A final study bringing all of these results together was unfortunately and significantly delayed by the Covid-19 pandemic, and remains in progress at the time of writing. However, the work performed has provided informative knowledge gain about the design, dosing, delivery and formulation of the three vaccine antigens that comprise the RCR complex, which I will discuss at the end of this Chapter.

4.3 PfRIPR vaccine design and production

In Section 4.2 I describe the novel vaccines that I produced for work conducted throughout this Chapter.

4.3.1 PfRIPR-based vaccines

Previously, in Chapter 3, I showed that all the targets of neutralising antibodies on PfRIPR are contained within EGF-like domains 5-8. The PfRIPR EGF-like domains are straightforward to produce in HEK293F cells as pairs or a quartet whilst fused to the monoFc domain. From these results I thus decided to manufacture and test six different PfRIPR vaccines based on the EGF-like domains; PfRIPR EGF (5-6), EGF (7-8), EGF (5-8), and HBsAg-PfRIPR EGF (5-6), (7-8), (5-8) were chosen for analysis.

A new expression plasmid was generated (Figure 4.3) that contained a C-terminal SpyTag sequence. Each of the three EGF-like domain combinations were cloned into this construct and expressed in HEK293F cells. These proteins were purified with a C-Tag column and then polished by size exclusion chromatography. Prior to conjugation, the N-terminal monoFc domain was removed by TEV protease and the final EGF-like domain re-purified by C-Tag affinity chromatography and SEC to remove the protease, cleaved monoFc and any undigested product. The purified PfRIPR EGF (5-6) SpyTag, EGF (7-8) SpyTag, and EGF (5-8) SpyTag were mixed at an equimolar ratio with HBsAg-SpyCatcher overnight to conjugate at 4°C; no precipitation was seen for any of the conjugations after 24 hours. The conjugated VLP was then purified by SEC. Three peaks were seen on the SEC trace (Figure 4.4A), an aggregate peak, HBsAg-PfRIPR fragment peak and an unconjugated PfRIPR fragment peak. The HBsAg-PfRIPR fragment peak was collected and concentrated to an appropriate level prior to quality control assessment.

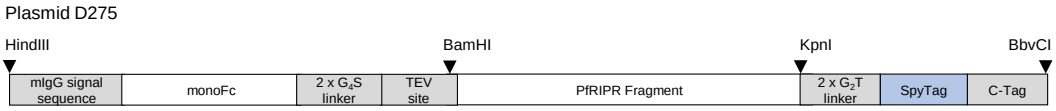


Figure 4.3 – Schematic of new SpyTag expression construct. Restriction sites are indicated by black arrows.

The quality of each VLP was assessed using dynamic light scattering (DLS). This technique measures the particle size distribution in solution. The average size of the HBsAg particle is 23.28 d.nm (diameter nm). Each conjugated VLP had a larger mean size than HBsAg particle (Figure 4.4B) indicating aggregation and a more heterogenous particle population; 32.94 d.nm for HBsAg-EGF (5-6), 27.65 d.nm for HBsAg-EGF (7-8), and 36.81 d.nm for HBsAg-EGF (5-8). More aggregation was seen in the conjugated VLPs relative to controls as expected. This aggregation is further reflected in the polydispersity index (Pdi, or $Đ$) of each of the VLP samples. The Pdi is a unitless measure of particle size distribution with 0 being a perfectly uniform particle size and 1 being completely heterogenous. Any sample with a Pdi of above 0.7 is considered have a very broad distribution and unsuitable for DLS analysis. The HBsAg particle control has a Pdi of 0.2, whereas the conjugated samples range from 0.2 to 0.29. These results gave confidence that the VLPs have formed correctly and are relatively uniform in size without gross aggregation. Some polydispersity is expected given the stochastic nature of the SpyTag-SpyCatcher conjugation system. Transmission electron microscopy (TEM) is also typically used to evaluate VLP quality. This was not conducted in this project as it is less informative that DLS and does not analyse the VLP product in its native solution.

The conjugation efficiency for each vaccine was determined by the relative intensities of HBsAg conjugated and unconjugated bands on a SDS-PAGE gel (Figure 4.4C) using

ImageJ software. The conjugation efficiencies were 73% for HBsAg-EGF (5-6), 75% for HBsAg-EGF (7-8), and 73% for HBsAg-EGF (5-8). These conjugation efficiencies were high given that no process development/optimisation had been carried out on the conjugation of these particular antigens. A minimum conjugation efficiency for immunisations had not been investigated therefore it was assumed that the high conjugation efficacy, *i.e.* greater than 50%, would be acceptable.

Each of the non-VLP EGF like-domain based protein vaccines were produced by cleaving the monoFc from either PfRIPR EGF (5-6), (7-8) or (5-8) by TEV protease followed by purification; proteins were then run on an SDS-PAGE gel to assess purity (Figure 4.4D). As before, each PfRIPR EGF fragment ran at a larger than expected size on the SDFS-PAGE gel. It was therefore decided to analyse each of the monoFc cleaved EGF domains by intact mass analysis to determine their exact size. The intact mass results confirmed that each protein was the correct size (Table 4-1). Each vaccine was quantified by BCA assay, tested for endotoxin levels, and sterile filtered (data not shown) prior to being stored at -80°C ready for animal immunisations.

Table 4-1 – Intact mass results from monoFc cleaved PfRIPR EGF fragments

Protein Fragment	Expected size (Da)	Actual size (Da)	ΔM (Da)
PfRIPR EGF (5-6)	12,567	12,553	-14
PfRIPR EGF (7-8)	10,270	10,256	-14
PfRIPR EGF (5-8)	22,123	22,164	41

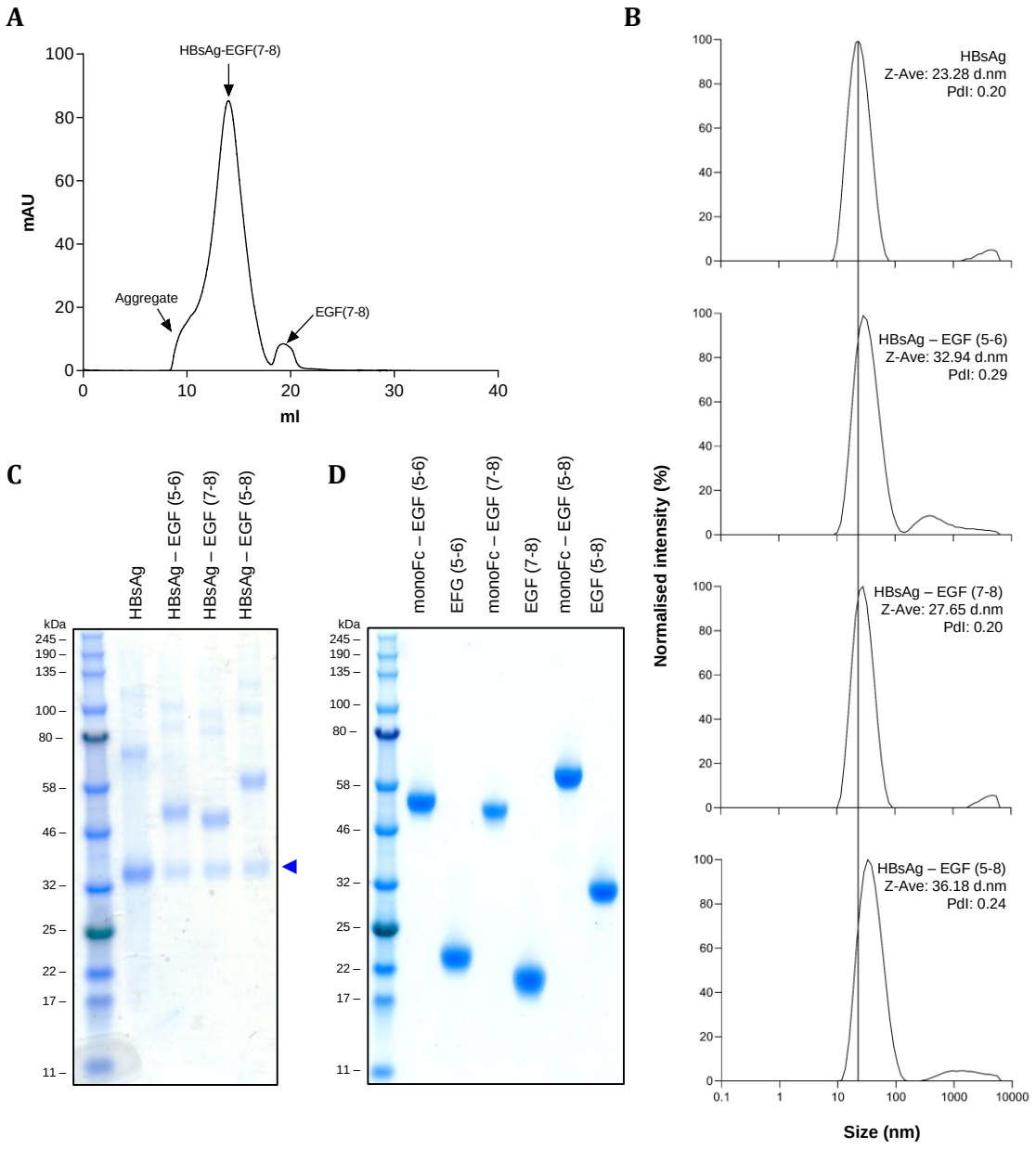


Figure 4.4 – Production and quality analysis of the PfRIPR based VLP vaccines.
A) SEC plot of HBsAg-EGF (7-8) after conjugation. Aggregate, conjugated and unconjugated peaks are indicated on the graph. **B)** Dynamic light scattering results for the three conjugated vaccines and HBsAg control. Normalised intensities are shown on each graph. larger particles have higher intensities therefore displaying intensities shows both the vaccine particle (large peak) and aggregated vaccine (small peak to the right). Note peak size does not indicate amount of each species present. Z-average (d.nm) and polydispersity index (PdI) are indicated for each VLP on the graph **C)** Reducing gel of HBsAg and conjugated vaccines. Unconjugated HBsAg is indicated by the blue arrow (expect MW 37 kDa, HBsAg dimers MW 74 kDa), larger bands are conjugated HBsAg-EGF antigen; expected MW – HBsAg-EGF (5-6): 51 kDA, HBsAg-EGF (7-8): 49 kDa, HBsAg-EGF (5-8): 61 kDa. **D)** TEV removal of monoFC fragment for protein EGF domain vaccines. Expected MW: monoFc-EGF (5-6): 38kDa, EGF (5-6): 12.5 kDa, monoFc-EFF (7-8): 36 kDa, EGF (7-8) 10 kDa, monoFc-EGF (5-8): 47 kDa, EGF (5-8) 22 kDa.

4.3.2 PfRIPR-PfCyRPA fusion vaccines

In addition to producing a PfRIPR-based vaccine, I wanted to investigate combining two or more blood-stage antigens into a single vaccine. This may lead to improved vaccine efficacy as compared to targeting one antigen alone. A combined PfRIPR and PfCyRPA vaccine may be able to complement the existing RH5.1 clinical vaccine[110], thereby creating a combination vaccine schedule that would target every protein in the essential RCR complex.

To investigate this question, I designed a fusion protein in which the previously identified PfRIPR EGF domains and full length PfCyRPA are fused with the SpyTag peptide in the middle of the two proteins flanked by repeating linker sequences (Figure 4.5A). The aim of placing the SpyTag peptide between the two proteins was to conjugate the construct to HBsAg-SpyCatcher in a 'V' formation ensuring both antigens are equally exposed on the VLP surface (Figure 4.5B). Initially only the PfRIPR EGF (7-8) – PfCyRPA fusion was generated for testing, this was designed when only the Genscript rabbit data were available (Chapter 3, Section 3.7.1). Subsequently, a PfRIPR EGF (5-8) – PfCyRPA fusion was generated after the data showed that PfRIPR EGF (5-8) contained all neutralising epitopes.

The PfRIPR-EGF-PfCyRPA proteins could be produced using the HEK293F transient expression system and purified on a C-Tag column. The monoFc was not required to produce the fusion proteins since PfCyRPA could be easily produced in HEK293F cells and therefore probably helped the solubility of the fused PfRIPR fragment. The anti-PfCyRPA mAb 3A7 which binds a conformational epitope was used to check the fusion had not altered the conformation of PfCyRPA. The mAb recognised both PfCyRPA and fusion PfCyRPA in a dot blot array (Figure 4.5C). No conformational mAbs targeting

PfRIPR EGF domains (7-8) or (5-8) was available to check the folding of the PfRIPR EGF construct, however the PfRIPR EGF (5-8) – PfCyRPA protein was able to completely reverse the GIA of anti-PfRIPR rabbit purified IgG (Figure 4.5D) indicating that all the targets of neutralising antibodies are present. PfRIPR EGF (5-8) – PfCyRPA protein could also able to completely reverse the GIA of anti-PfCyRPA rabbit purified IgG (data in appendix 8.3). Each protein was QC checked by SDS-PAGE (Figure 4.5E) and identity mass spectrometry & intact mass analysis (data not shown) to confirm the correct proteins were produced.

The fusion proteins were to be tested as protein alone and as VLP constructs. The PfRIPR EGF (7-8)-PfCyRPA and PfRIPR EGF (5-8)-PfCyRPA constructs were incubated in an equimolar ratio with HBsAg-SpyCatcher and incubated overnight at 4°C. The fusion VLPs were then purified by SEC as described for the HBsAg-PfRIPR vaccines in section 4.3.1. Conjugation efficiency was determined by comparison of band intensities on a reducing SDS-PAGE gel (Figure 4.4F). HBsAg-PfRIPR EGF (5-8) – PfCyRPA was 81% conjugated whereas a second batch of HBsAg – PfRIPR EFG (7-8) (not fused to PfCyRPA) produced at the same time was 56% conjugated. Each conjugated VLP was further analysed by DLS. The analysis showed that the fusion HBsAg-PfRIPR EGF (7-8) – PfCyRPA VLP was larger than the HBsAg-PfRIPR EGF (7-8), 42.6 d.nm and 27 d.nm respectively, as expected given the addition of a second antigen. A higher amount of aggregation was observed for the fusion VLP than the PfRIPR-only based VLPs as shown by a higher PdI value, an average of 0.4 and 0.24 respectively. Again, this was not a surprise since a much larger antigen was being fused to the HBsAg-SpyCatcher.

Once the vaccine candidates had passed the QC analysis they were stored at -80°C ready for a pilot mouse immunisation study.

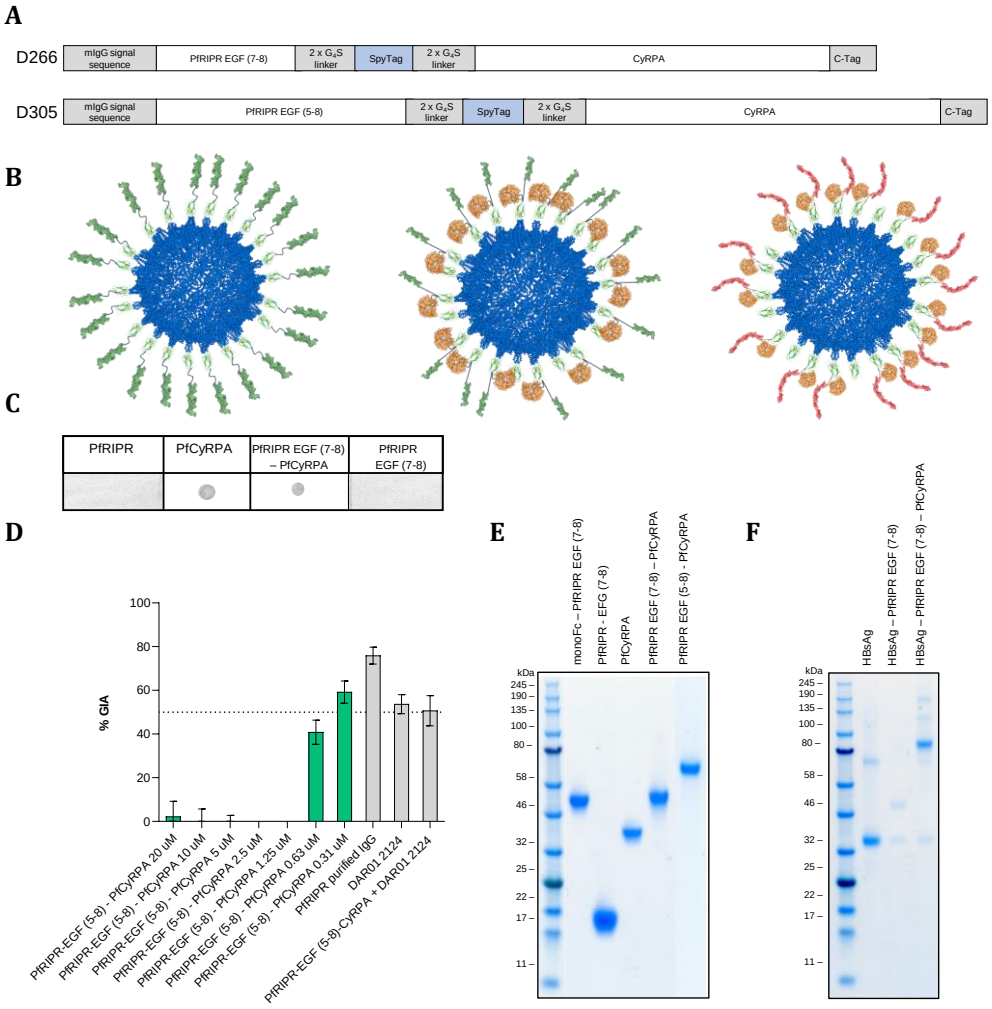


Figure 4.5 – Production and example quality analysis of PfRIPR – PfCyRPA fusion vaccines.

A) Schematic of the PfRIPR EGF – PfCyRPA fusion constructs with the SpyTag between the two proteins. **B)** Cartoon of the HBsAg VLP vaccines. From left to right: HBsAg-PfRIPR EGF (7-8), HBsAg-PfRIPR EGF (7-8) – PfCyRPA, HBsAg-PfRIPR (5-8) – PfCyRPA. Blue: HBsAg, green: PfRIPR EGF (7-8), red: PfRIPR EGF (5-8), orange: PfCyRPA. **C)** Dot blot array of PfCyRPA constructs with anti-PfCyRPA mAb 3A7 to check PfCyRPA folding. PfRIPR and PfRIPR EGF (7-8) included as negative controls. **D)** Antigen reversal of anti-PfRIPR pAb held at 3mg/mL with a titration of PfRIPR-EGF (5-8) – PfCyRPA fusion starting at 0.31µM. Grey bars are controls: PfRIPR purified IgG held at 3 mg/mL, DAR01 2124: Purified anti-PfRH5 IgG held at 3 mg/mL. 20µM PfRIPR-EGF (5-8)-PfCyRPA with DAR01 2124 anti-PfRH5 purified IgG held at 3 mg/mL. **E)** Protein gel of PfRIPR and fusion proteins prior to conjugation. Expected MW - monoFc-PfRIPR EGF (7-8): 36 kDa, PfRIPR EGF (7-8): 10 kDa, PfCyRPA: 43 kDA, PfRIPR EGF (7-8) – PfCyRPA: 52 kDa, PfRIPR EGF (5-8) – PfCyRPA: 64 kDa. **F)** Reducing gel of HBsAg and conjugated vaccines. Expected MW: HBsAg 37 kDa, HBsAg dimers: 74 kDa. Larger bands are conjugated antigens; expected MW – HBsAg-PfRIPR EGF (7-8): 61 kDa, HBsAg-PfRIPR EGF (7-8) - PfCyRPA: 89 kDa.

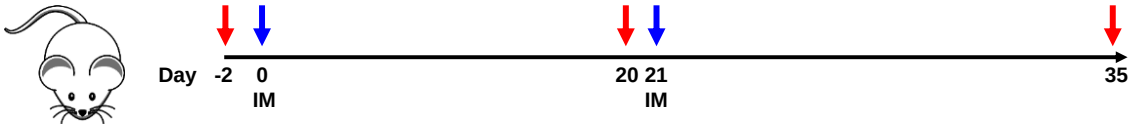
4.4 Pilot mouse vaccination study

With the production of several PfRIPR and PfRIPR-PfCyRPA fusion vaccines complete, a small pilot study was conducted in mice to examine the immunogenicity and *in vitro* GIA of each vaccine candidate. This study was small in order to fit the time frame for a grant application, but it also served as a useful first experiment to assess dosing for the different vaccines and the effect of conjugating an antigen onto a VLP on the antibody response. This initial functional immunogenicity study was conducted at the time when I only had the antigen reversal data from the Genscript rabbits (Chapter 3, Section 3.7.1); hence PfRIPR EGF (5-8) was not assessed. Instead, at this time, vaccines based on PfRIPR EGF (7-8) were the primary focus of my work. This experiment sought to compare the three full-length antigens alone versus PfRIPR (7-8) (protein alone vs VLP delivery) and a fusion antigen of PfCyRPA-PfRIPR EGF (7-8) as protein alone vs VLP delivery. The rationale being this could be a prime candidate to combine with RH5.1 in the future.

4.4.1 Study design

Seven antigens were tested (Figure 4.6) – three full-length proteins: PfRIPR, PfCyRPA, RH5.1. Two protein-only fragments and fusions: PfRIPR EGF (7-8), PfRIPR EGF (7-8) – PfCyRPA, and finally two VLP fusion vaccines: HBsAg – PfRIPR EGF (7-8) and HBsAg – PfRIPR EGF (7-8) – PfCyRPA. Full length PfRIPR, PfCyRPA, and RH5.1 were used as the positive controls. RH5.1 was additionally used as a benchmark to which the vaccines will be compared since this is the most studied antigen of the RCR complex. Each vaccine was tested at an equimolar amount to 2 μg of RH5.1, also accounting for conjugation efficiency in the VLP vaccines. Each antigen was formulated in the squalene oil-in-water adjuvant Addavax™, this adjuvant has been used extensively in

the group and was readily available at the time. Five female BALB/c mice were included in each group. Mice were immunised by intramuscular injection (IM) on day 0 and day 20. Blood samples were taken on day -2, day 30 and a final cardiac bleed on day 35.



Group	Antigen	Amount	Adjuvant
1	PfRIPR	2µg*	Addavax
2	PfCyRPA	2µg*	Addavax
3	PfRH5.1	2µg	Addavax
4	PfRIPR EGF (7-8)	2µg*	Addavax
5	HBsAg-PfRIPR EGF (7-8)	2µg*✞	Addavax
6	PfRIPR EGF (7-8) – PfCyRPA	2µg*	Addavax
7	HBsAg-PfRIPR EGF (7-8) – PfCyRPA	2µg*✞	Addavax

*Normalised to an equimolar amount of RH5.1

✞Also accounts for conjugation efficiency

Figure 4.6 – Mouse pilot study design.
Each group was composed of 5 mice. Mice were immunised on day 0 and day 21 (blue arrows), blood samples on day -2 and 20 (red arrows) with a final bleed on day 35.

4.4.2 Results

Serum samples from day 35 were evaluated by semi-quantitative ELISA. The ELISA results follow patterns typical of VLP immunisations (Figure 4.7). The anti-PfRIPR titres (Figure 4.7A) show that full-length PfRIPR gave the highest anti-PfRIPR response of the seven groups, this was to be expected as the other PfRIPR-based vaccines contain only domains EGF (7-8) and PfRIPR has been shown to be strongly immunogenic in rabbits (Chapter 3).

The PfRIPR EGF (7-8) protein vaccine gave very little anti-PfRIPR or anti-EGF (7-8) response (Figure 4.7A & B). This antigen may not immunogenic due to its small size, small immunogens may be less well retained by the lymph nodes, however there is

no strict correlation between size and immunogenicity and it is dependent on each antigen[230,231]. The anti-PfRIPR EGF (7-8) response is restored to, and exceeds, the anti-PfRIPR EGF (7-8) ELISA levels of full-length PfRIPR when the PfRIPR EGF (7-8) fragment is fused to PfCyRPA or conjugated to HBsAg.

Fusion of PfCyRPA to PfRIPR EGF (7-8) did not improve the immunogenicity of PfCyRPA, however conjugation of the PfRIPR EGF (7-8) – PfCyRPA fusion to HBsAg did lead to a small but non-significant increase in anti-PfCyRPA antibodies (Figure 4.7C). Importantly no immune competition was observed between antigens in the fusion PfRIPR EGF (7-8) - PfCyRPA vaccine as evidenced by the strong anti-PfRIPR and anti-PfCyRPA titres from the fusion vaccines. All of the controls behaved as expected in these ELISAs. The was no cross-reactivity between antigens except where a fusion vaccine was used. PfRH5 ELISAs were also run, only RH5.1 immunised mice showed a response to PfRH5. These data are not shown as comparisons of ELISA arbitrary units (AU) between antigens are not possible.

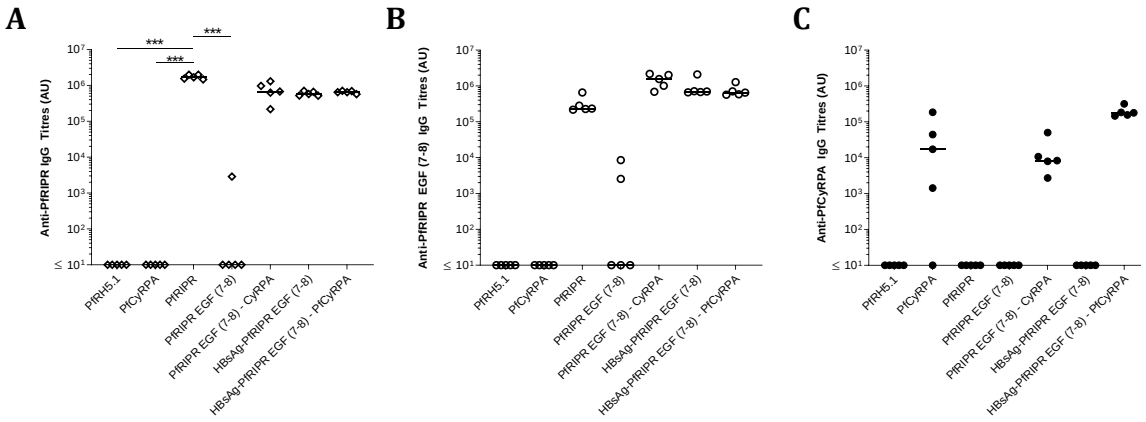


Figure 4.7 – End-point ELISA titre results mouse serum from day 35.

A) Anti-PfRIPR ELISA. Significance determined by Kruskal Wallis test with Dunn's multiple comparisons test. Non-significant results not indicated, *** represents $p \leq 0.001$. **B)** Anti-PfRIPR EGF (7-8) ELISA. **C)** Anti-PfCyRPA ELISA. Each symbol represents and individual animal with a line representing the median titres.

Mouse serum samples from day 35 were next pooled by group and the IgG purified. Samples were pooled to ensure enough IgG was purified for the GIA assay. Samples were then run on our in-house *in vitro* single cycle GIA assay. The best GIA result (Figure 4.8) came from RH5.1 with an EC_{50} of 0.36 mg/mL (95% CI could not be interpolated), in contrast full-length PfRIPR had an EC_{50} of 1.84 mg/mL and PfCyRPA an EC_{50} of 1.52 mg/mL.

The protein fragment PfRIPR EGF (7-8) gave no detectable GIA above the naïve control in line with its ELISA results. Encouragingly, the HBsAg-PfRIPR-EGF (7-8) antigen had an EC_{50} of 1.54mg/mL; better than the full-length PfRIPR (statistical analysis was not carried out due the pooled mouse serum resulting in group sizes of n=1 in the GIA assay). This validates the antigen reversal experiments in the preceding Chapter, and that a large proportion of the targets of neutralising antibodies can be found in PfRIPR EGF (7-8). It also shows that the VLP is an essential tool for small PfRIPR fragment-based vaccines.

The fusion protein vaccines gave improved GIA over their individual protein components with HBsAg-PfRIPR-EGF (7-8)-PfCyRPA yielding an EC_{50} of 0.82 mg/mL, a small improvement on the PfRIPR-EGF (7-8)-PfCyRPA protein alone vaccine but two-fold lower than RH5.1. A full list of EC_{50} values is given in Table 4-2. These values are a comparison of the total IgG EC_{50} rather than antigen specific IgG so are not a definitive comparison of antigens.

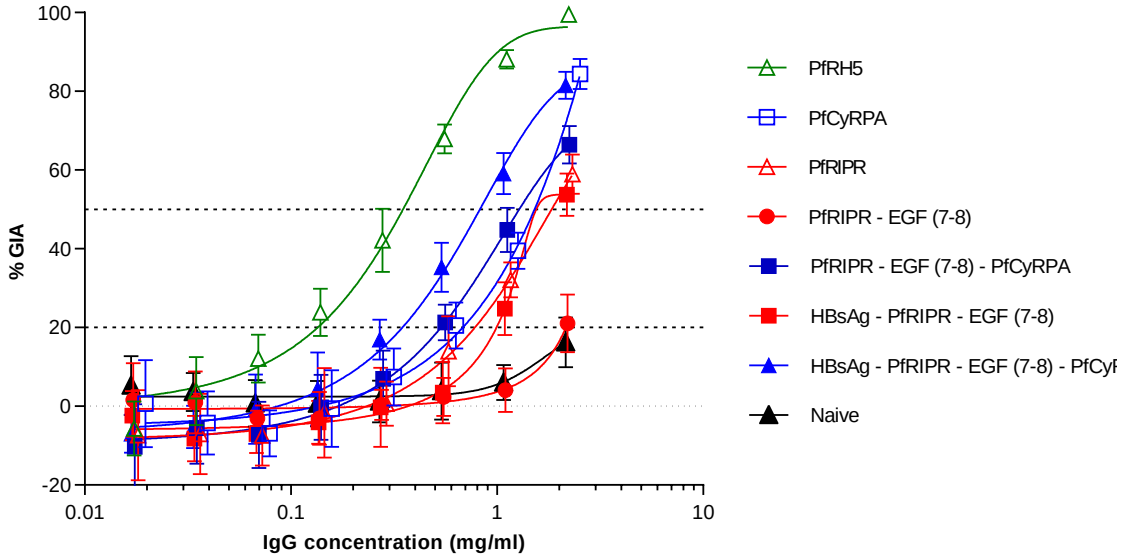


Figure 4.8 – Single cycle GIA assay with dilution curve of purified IgG from mice using *P. falciparum* clone 3D7.
Each antigen sample is a pool of serum from 5 mice. Each pool is tested using a dilution series of purified IgG. The dotted lines show 0% GIA. Dashed lines show 20% GIA (the accepted LLQ of the assay) and 50% GIA for comparison. Points are mean of 3 replicates, all error bars represent SD. Each dataset fitted with Richard's five-parameter dose-response curve with no constraints.

Table 4-2 – EC_{50} values of total purified serum IgG for each group in the mouse pilot study.
Values denoted with * could not be interpolated from the data.

Antigen	EC_{50} (mg/mL)	95% CI
RH5.1	0.36	NA*
PfCyRPA	1.52	NA*
PfRIPR	1.84	0.58, NA*
PfRIPR - EGF (7-8)	NA*	NA
PfRIPR - EGF (7-8) – PfCyRPA	1.29	0.10, NA*
HBsAg - PfRIPR - EGF (7-8)	1.55	NA*
HBsAg - PfRIPR - EGF (7-8) - PfCyRPA	0.82	NA*

The GIA data can also be presented plotted against the antigen-specific ELISA titres instead of total purified IgG. The antigen-specific titres are obtained by performing an ELISA on the purified IgG that is used in the GIA assay. The antigen-specific AU can then be used to convert the total IgG mg/mL in the GIA to antigen-specific IgG AU.

This ‘quality analysis’ gives a better idea of the GIA per AU of antibody. It can thus be used to distinguish which vaccine give a better quality of antibody for vaccines targeting the same antigen in the ELISA– quality here is taken as ability to block merozoite invasion.

The quality analysis of the HBsAg-PfRIPR-EGF (7-8) GIA (Figure 4.9A) shows a fourfold improvement in EC_{50} when compared to PfRIPR GIA (99,048 AU against 378,746 AU), indicating that the quality of antibody response is substantially better when a small domain of PfRIPR is used to vaccinate. The quality analysis of the PfRIPR-EGF (7-8) – PfCyRPA fusion vaccines could not, however, be deconvoluted as the antigen response is given in AU not μg/mL so the contribution of each antigen to the GIA could not be calculated.

Although none of the vaccines tested here were an improvement on RH5.1, the study does demonstrate that the antibody response against full length PfRIPR could be generated with a much smaller pair of EGF domains conjugated to HBsAg. In addition, the fusion of PfRIPR epitopes and full-length PfCyRPA make a viable vaccine candidate with no detected immune interference. This fusion vaccine gave only 2-3-fold lower GIA than RH5.1. RH5.1 has set the bar high for blood stage vaccine candidates so equalling the GIA by RH5.1 in one experiment was not expected. These experiments have, however, given us a new candidate to develop and test alongside / in combination with RH5.1 where we will hopefully see some additive or synergistic results.

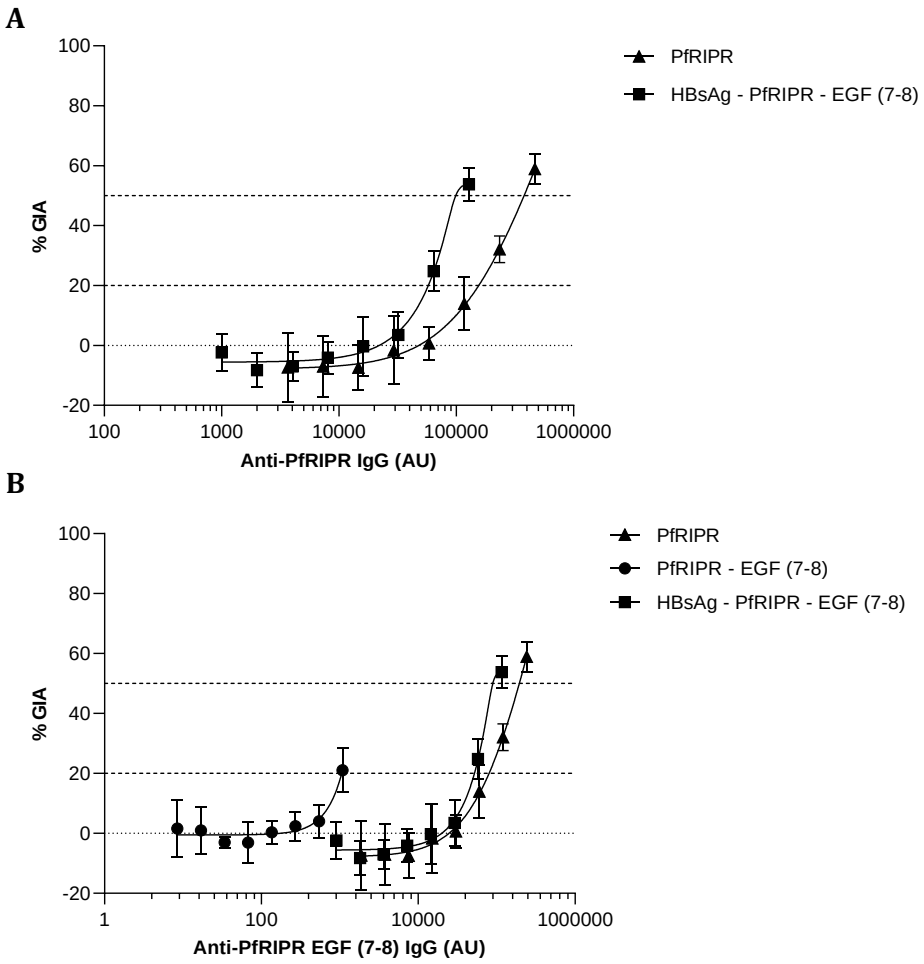


Figure 4.9 – Single cycle GIA using *P. falciparum* 3D7 clone with dilution curve of purified IgG. Graph plotted against antigen specific ELISA titres.
A) GIA plotted against anti-PfRIPR IgG AU. **B)** GIA plotted against anti PfRIPR EGF (7-8) IgG AU. The dotted lines show 0% GIA. Dashed lines show 20% GIA (the accepted LLQ of the assay) and 50% GIA for comparison. All points are mean, error bars represent SD, n=3. Each dataset fitted with Richard's five-parameter dose-response curve with no constraints.

Table 4-3 – Antigen specific EC_{50} values for each group in the mouse pilot study.
Values denoted with * could not be interpolated from the data. NA denotes no antigen-specific values.

Antigen	PfRIPR EC_{50} (AU)	95% CI	PfCyRPA EC_{50} (AU)	95% CI
CyRPA	NA	NA	65,168	13,792 – 65,168
PfRIPR	378,746	*	NA	NA
PfRIPR - EGF (7-8)	NA	NA	NA	NA
HBsAg - PfRIPR - EGF (7-8)	99,048	*	NA	NA

4.5 Pilot rat vaccination study

The mouse pilot study identified that:

i) The PfRIPR (7-8) immunogen looked more promising than full-length PfRIPR; and

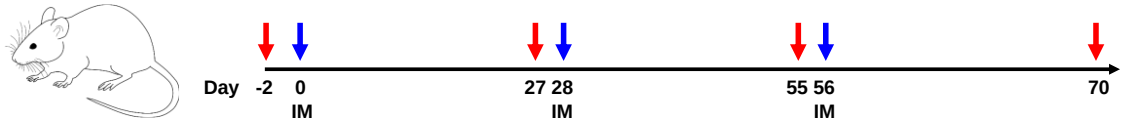
ii) There was no apparent immune competition when PfRIPR EGF (7-8) was fused to PfCyRPA.

These were both encouraging, however, ultimately the best vaccine did not outperform RH5.1. Moreover, the mouse serum samples were so limited, even when pooled, that it became apparent larger species needed to be immunised to provide more serum for more extensive analysis. During this work, I also discovered that all of the epitopes targeted by neutralising antibodies on PfRIPR were located in EGF (5-8) not just EGF (7-8) (Chapter 3, Section 3.7.2). In addition, as part of an ongoing collaboration with USAID, the Draper group switched from using BALB/c mice to Wistar rats for vaccine studies.

Consequently, in order to continue this work, I switched to using the rat immunisation model. Initially, I designed an experiment to determine the best immunogen and delivery platform for the PfRIPR-based vaccine component. Switching from mouse to rat also allowed the use of a standardised ELISA in conjunction with calibration free concentration analysis (CFCA) by surface plasmon resonance, previously developed in the Draper group, which provided quantitative ELISA results in a μg/mL readout – ultimately far more informative than the mouse semi-quantitative ELISAs.

4.5.1 Study design

As this was the first experiment to be conducted in rats with PfRIPR, several of the PfRIPR vaccines were tested again to assess head-to-head functional immunogenicity. Three protein-only EGF domain-based vaccines; PfRIPR EGF (5-6), PfRIPR EGF (7-8), and PfRIPR EGF (5-8), and three HBsAg-based vaccines; HBsAg PfRIPR EGF (5-6), HBsAg PfRIPR EGF (7-8), and HBsAg PfRIPR EGF (5-8) were tested and compared to full-length PfRIPR. Groups of 6 female rats were immunised IM with an equimolar amount of antigen normalised to 2 μg of full-length PfRIPR (Figure 4.10) in Matrix-M™ adjuvant, a clinical stage proprietary saponin-based adjuvant made by Novavax. A 2 μg dose was chosen based on the clinical experience with RH5.1/AS01$_B$, suggesting this protein dose was sufficient to reach maximal antibody responses in humans after three monthly immunisations (Minassian *et al.* 2021 Med. In press). Three immunisations were given at 4-week intervals with a terminal bleed on day 70. The primary aim of this study was to determine which of the PfRIPR EGF-based vaccines was the most potent in terms of growth inhibitory antibody induction. Rat immunisations were carried out by the contract research organisation (CRO) Noble Life Sciences in the USA.



Group	Antigen	Antigen size / kDa	Normalised dose / µg	Conjugation efficiency	Adjuvant
1	HBsAg (negative control)	37	2.00	N/A	Matrix-M™
2	PfRIPR	120	2.00	N/A	Matrix-M™
3	PfRIPR-EGF(5-6)	15	0.25	N/A	Matrix-M™
4	PfRIPR-EGF(7-8)	12	0.21	N/A	Matrix-M™
5	PfRIPR-EGF(5-8)	25	0.40	N/A	Matrix-M™
6	HBsAg-PfRIPR-EGF(5-6)	15	0.25*	73%	Matrix-M™
7	HBsAg-PfRIPR-EGF(7-8)	12	0.21*	75%	Matrix-M™
8	HBsAg-PfRIPR-EGF(5-8)	25	0.40*	75%	Matrix-M™

*accounts for conjugation efficiency

Figure 4.10 – Study design for rat immunisations.
Each group was composed of 6 Wistar rats except the negative control group which contained 3 rats. Rats were given three IM immunisations of 2 µg antigen (blue arrows). Blood samples (red arrows) were taken the day before each immunisation.

4.5.2 Results

Serum samples from each time point were analysed by PfRIPR standardised ELISA (Figure 4.11). The anti-PfRIPR ELISA titres generally reach a maximum level after just the first boost (Figure 4.11C) with only HBsAg-PfRIPR EGF (7-8) requiring the second boost to reach maximum titre. In the future a two-dose regime, rather than a three-dose regime, could be explored which would reduce the amount of vaccine required to achieve the same effect.

The ELISA results on the final bleed serum followed the same trend as the mouse pilot study. A strong anti-PfRIPR response was seen with full length PfRIPR and very little response to the protein only PfRIPR EGF domain antigens – sometimes these were below the lower limit of quantification (LLQ) after three immunisations. The three HBsAg conjugated antigens performed well, the reported ELISA titres were not significantly different to full length PfRIPR. As expected all of the conjugated vaccines

had an anti-HBsAg response similar to that of the HBsAg control (Figure 4.12). This result confirms the use of VLP delivery to increase the antibody response to a poorly immunogenic antigen. In this case conjugation to the VLP could 'restore' ELISA titre of the protein only PfRIPR EGF domain-based vaccines to the level set by the full-length PfRIPR.

It was noted that one rat in the HBsAg only group died during the experiment. Histopathology was performed by Noble Life Sciences and the findings suggested that the rat died from heart failure unrelated to the test articles and adjuvant.

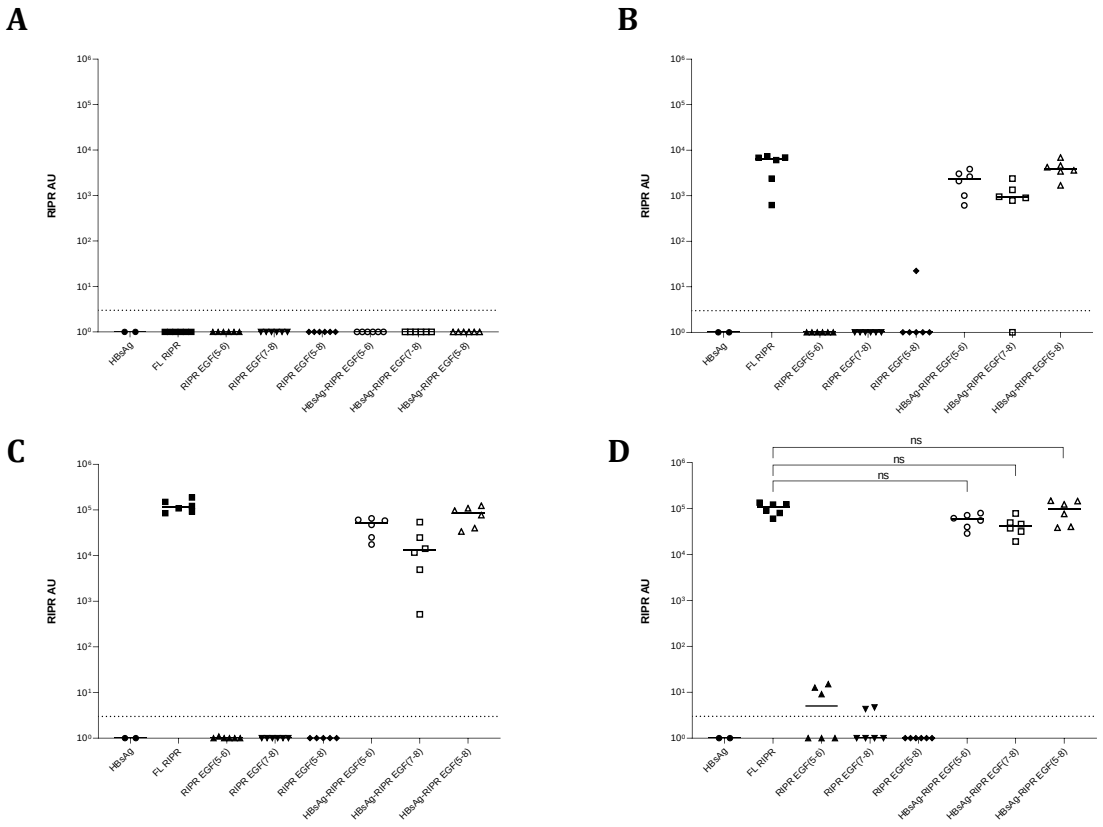


Figure 4.11 – Anti-PfRIPR standardised IgG ELISA titres.
A) Day -2 tires. **B)** Day 27 titres **C)** Day 55 titres **D)** Day 70 final bleed ELISA titres. Titres for the soluble EGF antigens was extremely low or below the LLQ for some rats. Anti-PfRIPR ELISA titres for the HBsAg groups were not significantly different to each other or full length PfRIPR. Each symbol represents an individual animal with a line representing the median titres. Significance determined by Kruskal Wallis with Dunn's multiple comparisons test, ns = non-significant.

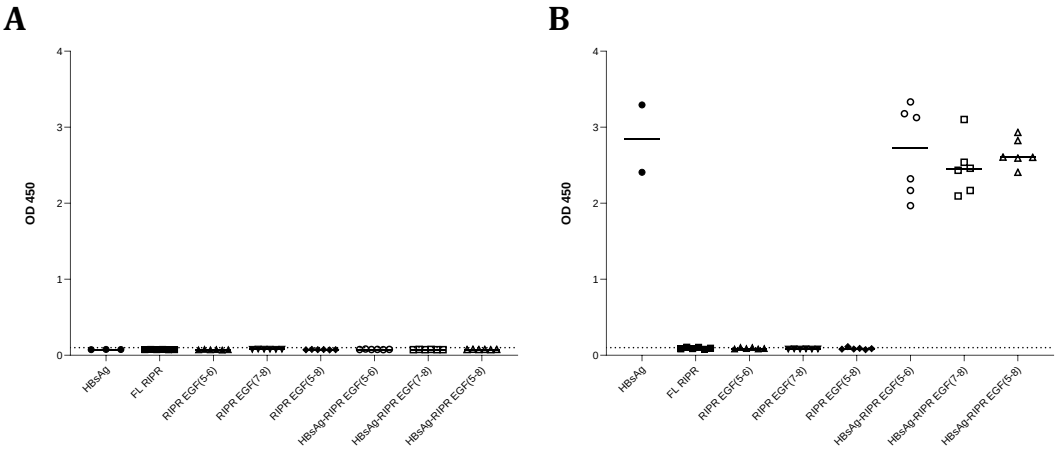


Figure 4.12 – Anti-HBsAg ELISA on day -2 and day 55. A) Day -2 B) Day 70.
Each symbol represents and individual animal with a line representing the median titres.

IgG was subsequently purified from each day 70 serum sample. Rat serum samples from each group were not pooled as enough purified IgG could be obtained from a single rat for a GIA assay. This improves the power of the data analysis of the data relative to pooled serum where a pool of serum is considered n=1.

The GIA results provided some interesting data but also some anomalous points that did not match the ELISA data (Figure 4.13). Notably the protein only PfRIPR-EGF vaccines, which had no detectable anti-PfRIPR antibodies by standardised ELISA (Figure 4.11D) showed strong GIA (Figure 4.13A); strangely the GIA from all three antigens was identical. It is suspected that this is a background effect however both the HBsAg negative controls and some HBsAg PfRIPR-EGF (5-6) samples were negative for GIA up to 10 mg/mL so it is unclear what caused this issue. The same results were obtained on a second set of purified serum IgG indicating that the problem was not specific to the one assay. The purified IgG was also tested on the standardised ELISA but again very little anti-PfRIPR signal was seen; this confirmed that samples were not mixed during the purification. The protein only PfRIPR EGF samples will therefore be ignored in the subsequent analysis until a solution is found and/or this can be repeated with independent samples.

The second strange results were found in the HBsAg PfRIPR-EGF (5-6) groups (Figure 4.13C); 4 out of 6 samples had little detectable GIA above baseline despite all three rats having very similar ELISA results. Only two rats immunised with HBsAg PfRIPR-EGF (5-6) behaved as expected. The EC_{50s} values for this group could not be interpolated due to the wide spread of data. IgG from each of the rat serum samples was purified twice, several months apart, and the ELISA and GIA analysis repeated to ensure that there was no sample mix up.

The full-length PfRIPR group (Figure 4.13B), HBsAg PfRIPR-(EGF 7-8) (Figure 4.13D), and HBsAg PfRIPR (EGF 5-8) (Figure 4.13E) groups all performed as expected. The mean EC_{50} for the full-length PfRIPR immunised group was 7.1 mg/mL total IgG (95% CI limit 6.2 – 8.4 mg/mL). HBsAg PfRIPR-(EGF 7-8) performed similarly with an EC_{50} of 6.5 mg/mL (95% CI limit 5.2 – 8.0 mg/mL). HBsAg PfRIPR-(EGF 5-8) showed a two-fold improvement on full-length PfRIPR with an EC_{50} of 3.9 mg/mL (95% CI limit 3.5 – 5.1 mg/mL). This confirms the findings in Chapter 3 that all of the targets of neutralising antibodies can be found in PfRIPR EGF (5-8) and suggests that an equimolar dose of PfRIPR EGF (5-8) can outperform full-length PfRIPR in a head-to-head study, although this is conditional on the immunogenicity of PfRIPR EGF (5-8) improving by either conjugation to HBsAg or a protein such as PfCyRPA.

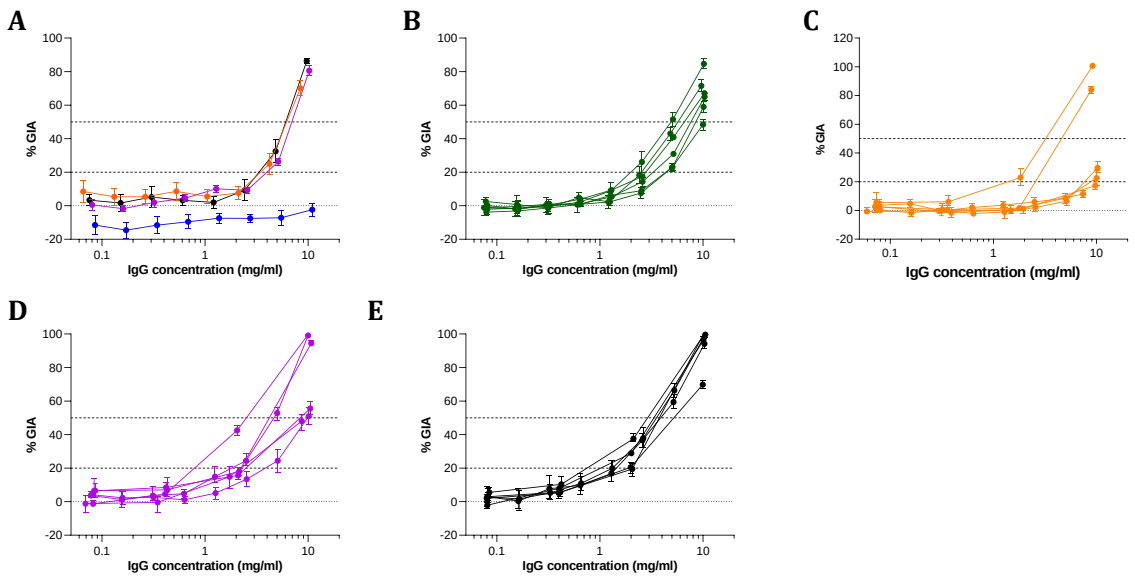


Figure 4.13 – Single cycle GIA assay results for the five antigen groups using *P. falciparum* clone 3D7. Dilution curves of purified IgG from rats.
A) Pools of purified IgG for the three protein only PfRIPR-EGF domain antigens [Black: PfRIPR EGF (5-8), orange: PfRIPR EGF (5-7), purple: PfRIPR EGF (7-8)]. and HBsAg negative control (blue). **B)** Full-length PfRIPR. **C)** HBsAg PfRIPR-EGF (5-6). **D)** HBsAg PfRIPR-EGF (7-8). **E)** HBsAg PfRIPR-EGF (5-8). The dotted lines show 0% GIA. Dashed lines show 20% GIA (the accepted LLQ of the assay) and 50% GIA for comparison. Each line represents a single animal, each point the mean and error bars are SEM. N = 3 per assay measurement.

Each purified IgG sample was further analysed by standardised ELISA; this produces an anti-PfRIPR specific AU readout per mg/mL total IgG for each sample. Using a conversion factor determined by CFCA, the PfRIPR specific AU per mg/mL can then be converted to anti-PfRIPR IgG in µg/mL. The GIA data can then be replotted against anti-PfRIPR IgG in µg/mL in a 'quality analysis'. This analysis gives a better picture of the GIA activity per µg of anti-PfRIPR antibody generated by each vaccine and thus enables me to determine whether one candidate vaccine generates better quality antibodies. The data from HBsAg PfRIPR-EGF (5-6) was excluded from this analysis as only two samples out of the six were positive for GIA. The protein only PfRIPR EGF (5-6), (7-8) and (5-8) were also excluded as the negligible/absent anti-PfRIPR

response on the ELISA means these data cannot be interpreted. An independent repeat of these groups is needed in the light of this unexplained data.

The quality analysis showed that immunisation with HBsAg PfRIPR EGF (7-8) or HBsAg PfRIPR EGF (5-8) led to an improvement in quality over full-length PfRIPR (Figure 4.14A). HBsAg PfRIPR EGF (7-8) had the lowest mean EC_{50}, 236 (95% CI: ± 129 μg/mL, however a large spread in the data was seen. The EC_{50} value for HBsAg PfRIPR EGF (5-8) was roughly half that of full-length PfRIPR, 270 ± 82 μg/mL vs 485 ± 116 μg/mL; indicating that the antibodies produce by the smaller EGF-like domain-based vaccines are superior to those produced by immunisation with full length PfRIPR (Figure 4.14B). Although a clear trend was observed, the data were not significantly different due to the broad spread of data points. A table of EC_{50} values is given in Table 4-4.

In summary, these data supported the on-going development of PfRIPR EGF (5-8) vaccines in the future. Notably, this immunogen, which is easier to make than full-length PfRIPR, could at least match its functional immunogenicity when delivered on a VLP, and the quality of the vaccine-induced IgG was ~2-fold improved. However, it was clear from this initial rat study that firm conclusions could not be drawn due to some unexplained outcomes in certain groups in the GIA assay. In addition, the rat IgG antigen-specific EC_{50}s determined in μg/mL were relatively high; suggesting need for on-going improvement.

Whilst undertaking this study, I performed another study in parallel that sought to rank the relative potencies of the three RCR complex antigens. This study is described next and confirms my observation here that relatively high antigen-specific IgG concentrations do appear necessary to provide functional GIA against PfRIPR.

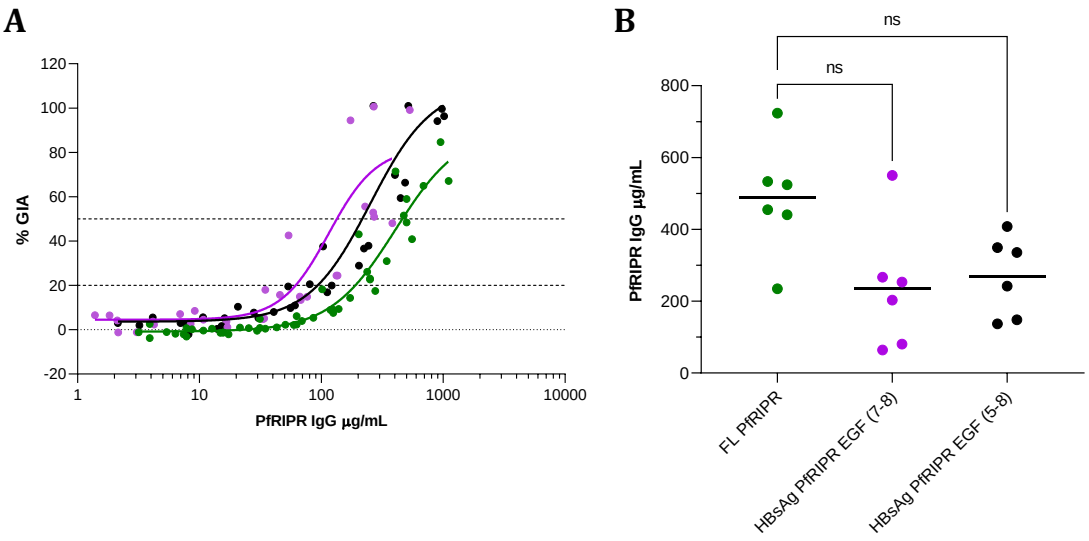


Figure 4.14 – Quality analysis of the different PfRIPR-based vaccines.
A) GIA data from full length PfRIPR (green), HBsAg PfRIPR-EGF (7-8) (purple) and HBsAg PfRIPR-EGF (5-8) (black) immunised animals plotted against anti-PfRIPR specific IgG. Points represent median GIA for each animal, each point a mean of 3 assay replicates. Each group of 6 animals was fitted with a 4-parameter dose response curve with no constraints. **B)** Interpolated EC_{50} values for full length PfRIPR, HBsAg PfRIPR-EGF (7-8), and HBsAg PfRIPR-EGF (5-8). The dotted lines show 0% GIA. Dashed lines show 20% GIA (the accepted LLQ of the assay) and 50% GIA for comparison. Each dot represents a single animal, black bar indicates median value. Significance determine by Kruskal Wallis with Dunn's multiple comparisons test, ns = non-significant.

Table 4-4 – EC_{50} values for the four PfRIPR-based vaccines.

Antigen	EC_{50} (µg/mL)	95% confidence limit
Full length PfRIPR	485.1	±116.1
HBsAg EGF (5-8)	270.0	±82.0
HBsAg EGF (5-6)	N/A	N/A
HBsAg EGF (7-8)	236.3	±128.5

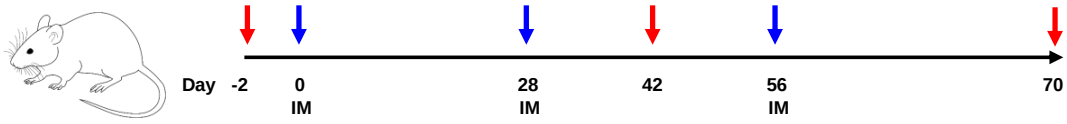
4.6 Comparing PfRIPR-based vaccines with PfRH5 and PfCyRPA-based vaccines

My development of the PfRIPR-based vaccines formed part of a larger body of work being undertaken by the Draper group to optimise vaccines targeting the three antigens that comprise the RCR complex. Consequently, in parallel to the above work with the HBsAg VLP strategy for the PfRIPR fragments, I also I sought to determine how PfRIPR compared to PfRH5 and PfCyRPA based vaccines.

4.6.1 Dose-Ranging Study – Recombinant Protein Approach, Single Component Protein Formulations

RH5.1 is the Draper group designation for the benchmark full-length PfRH5 protein vaccine (currently in clinical development[229]). Alongside RH5.1, full-length PfCyRPA and PfRIPR were used to immunise rats at a fixed 2 μg dose (Figure 4.15) in order to generate sera for ELISA development and give baseline GIA results for these antigens. 2 μg of PfCyRPA and PfRIPR was tested initially to allow inter-study comparison with the PfRIPR rat group described in section 4.4, which was conducted in parallel. The other rationale for using the 2 μg dose was based on the recent observations from the VAC063 clinical trial of RH5.1/AS01$_B$. Here healthy UK adult volunteers were vaccinated three times at monthly intervals with 2, 10 or 50 μg RH5.1/AS01$_B$, and responses were comparable regardless of dose[110]. Also, work performed by others in the group using RH5.1 in mice, suggested maximal serum IgG titres could still be achieved with three immunisations at doses < 100 ng (Pattinson, King, unpublished). Consequently, it was thought at the time that a 2 μg dose of any soluble protein vaccine in rats would be sufficient to achieve maximal responses, and in order to confirm this two extra groups were included for RH5.1 at 10-fold lower doses (0.2

and 0.02 µg). In this study, called "Study O1", each group was composed of six female Wistar rats and immunisations were given IM at days 0, 28 and 56. The rats were housed and vaccinated by the CRO Noble Life Sciences, USA; exactly as for the previous study (Section 4.4).



Group	Antigen	Dose (µg)	Group size	Strain	Adjuvant
1	RH5.1	2.00	6	Wistar	Matrix-M™
2	RH5.1	0.20	6	Wistar	Matrix-M™
3	RH5.1	0.02	6	Wistar	Matrix-M™
4	PfCyRPA	2.00	6	Wistar	Matrix-M™
5	PfRIPR	2.00	6	Wistar	Matrix-M™
6	Matrix-M Only (Baseline Control)	0	6	Wistar	Matrix-M™
7	Negative Control	0	3	Wistar	Matrix-M™

Figure 4.15 – Study O1 Design.
Each group was composed of 6 Wister rats except the negative control group which contained 3 rats. Rats were given three IM immunisations of antigen (blue arrows). Blood samples (red arrows) were taken on day -2, day 42 and day 70.

Serum samples at days -2, 42 and 70 were tested by antigen-specific standardised ELISA. All of the negative control and Matrix-M™ only animals tested negative for antigen-specific responses on day 70 (Figure 4.16A). In addition, each day 70 sample was tested against every antigen in the standardised ELISA to ensure that there was no error at either immunisation or blood sampling, e.g. PfRIPR immunised serum samples were tested against PfRH5 and PfCyRPA; all samples were negative as expected (data not shown). The standardised IgG ELISA results show that the magnitude of the humoral response depends on vaccine dose (in the case of RH5.1) and the number of immunisations (Figure 4.16).

The anti-PfRIPR serum IgG response (Figure 4.16C) followed the same pattern established in my previous PfRIPR rat study (Section 4.4.2); notably that the IgG response had mostly peaked after the first boost. A small but significant increase in IgG was seen once the second boost was given. This response profile was very different in animals immunised with PfCyRPA (Figure 4.16D). Some animals responded very poorly after two immunisations, so a third boost was necessary to reach peak response. The anti-RH5 ELISA results were broadly in line with expectations; with the 2 μg and 0.2 μg doses delivering similar levels of IgG, whereas animals immunised with 0.02 μg responded poorly after three immunisations. These initial ELISA results suggested that 2μg was an appropriate dose for rat immunisations when using RH5.1. However, it remained unclear whether this was definitely the case for PfCyRPA and PfRIPR.

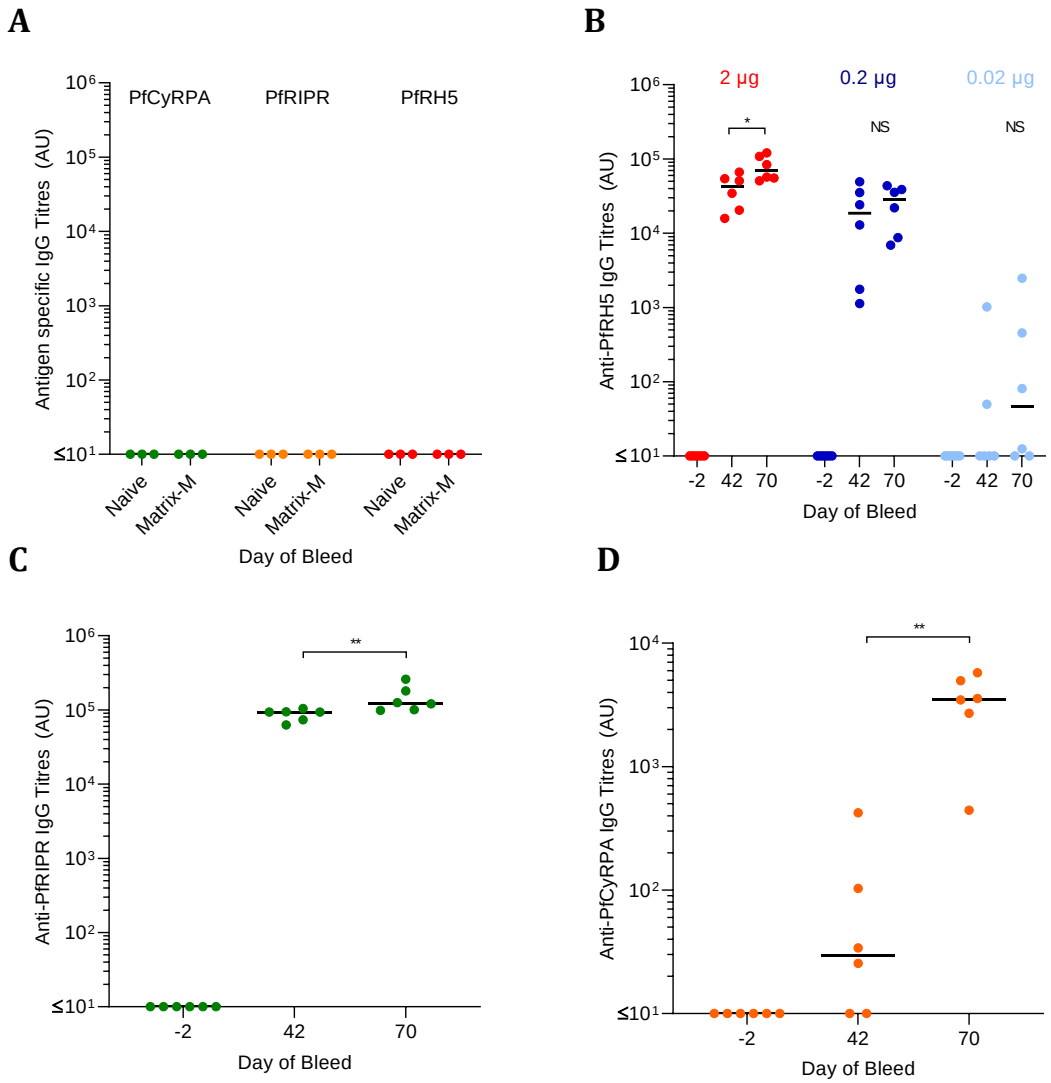


Figure 4.16 – Standardised IgG ELISAs for Study O1.

A) Anti-PfCyRPA, -PfRIPR, and -RH5 ELISA on day 70 samples from Matrix-M™ control and Naïve control rats. **B)** Anti-RH5 ELISA results for day -2, 42 and 70 from rats immunised with 2µg, 0.2 µg, and 0.02 µg RH5.1. **C)** Anti-PfRIPR ELISA day -2, 42 and 70 for rats immunised with 2 µg PfRIPR. **D)** Anti-PfCyRPA ELISA for day -2, 42 and 70 for rats immunised with 2 µg PfCyRPA. Each symbol represents an individual animal and black bars represent the median titres. Responses within the same group and between time-points were analysed by Wilcoxon signed rank test (paired analysis, two-tailed). N.S. represents Non-Significant, * represents $p \leq 0.05$, and ** represents $p \leq 0.01$.

Purified IgG from each individual rat serum sample was then tested for functional GIA. As expected, the naïve and Matrix-M™ control rats had no GIA at all concentrations of IgG (Figure 4.17A).

GIA from PfRH5 immunised rats showed a clear dose response (Figure 4.17B) with purified IgG from animals immunised with 2 μg consistently showing the highest GIA. Three samples of purified IgG from animals immunised with 0.02 μg showed no GIA, two samples followed a pattern similar to 0.2 μg but one sample showed very high GIA (>80 %), far exceeding all samples from 2 μg immunisations. The results from the 0.02 μg group are broadly reflective of the ELISA results, with the exception of the one outlier. From these results, immunisation with 2 μg of PfRH5 showed that it can provide robust and repeatable GIA data.

The GIA results from the PfRIPR immunised rats (Figure 4.17C) were in line with the results seen in Section 4.4.2 (Figure 4.13B). Given that much higher GIA has been seen in the rabbits immunised with PfRIPR (Chapter 3, Section 3.7.1), it was posited that 2 μg was too small a vaccine dose. These rabbits were immunised with 50 μg however the protein was formulated in either Montanide ISA720 or complete Freund's which is potentially a much stronger adjuvant.

This hypothesis was also supported by the PfCyRPA GIA data (Figure 4.17D). Despite measurable ELISA responses, no GIA was observed above the negative control baseline for PfCyRPA immunised animals. Two samples show a slight trend towards positive GIA at higher concentrations of purified IgG. In contrast, functional anti-PfCyRPA antibodies were obtained by me in mice (see Figure 4.8), and in rabbits by others and our collaborators at the NIH[164,167]. Notably, the earlier mouse experiment used a 2 μg dose in Matrix-M™, whereas the rabbits used a dose of 50 μg in

complete/incomplete Freund's adjuvant (C/IFA). I hypothesised my results here were therefore likely due to under-dosing of the protein vaccine in rats and/or use of an adjuvant that is less potent than C/IFA.

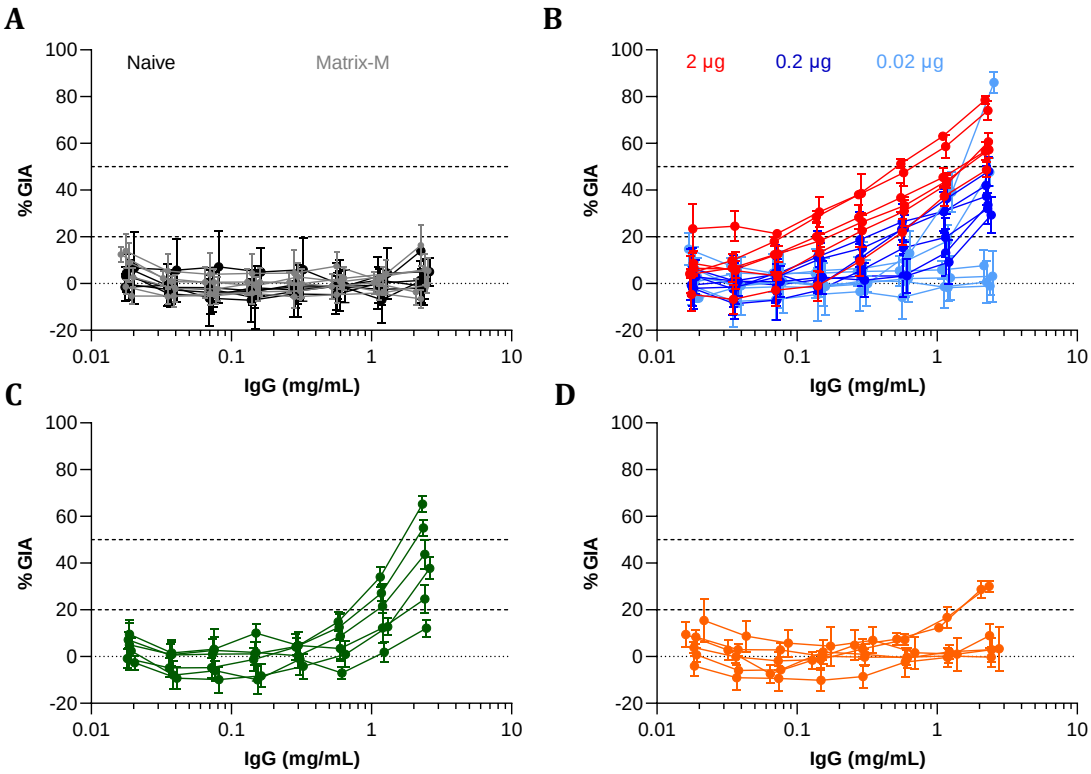


Figure 4.17 – Single cycle GIA assay with dilution curve of purified IgG from rats using *P. falciparum* clone 3D7.
A) Naïve and Matrix-M controls. **B)** GIA results from animals immunised with three different doses of PfRH5. Red: 2 µg, dark blue: 0.2 µg, light blue 0.02 µg. **C)** PfRIPR immunised animals. **D)** PfCyRPA immunised animals. The dotted lines show 0% GIA. Dashed lines correspond to 20% GIA (the accepted LLQ of the assay) and 50% GIA. Each line represents one animal, points are mean of three assay replicates with SD error bars.

Each purified IgG sample was next tested by standardised ELISA to determine the antigen-specific AU per mg of IgG. These data were used to replot the GIA results to show the GIA per µg antigen-specific IgG and therefore compare the quality of IgG response across doses of RH5.1, and between the three antigens (although at this stage data for PfCyRPA and PfRIPR were limited).

The PfRH5 data (Figure 4.18A) demonstrates that the dose of PfRH5 does not affect the quality of the IgG response, only the quantity. The 2 μg and 0.2 μg data merged into a single curve, indicating that the functional quality of the anti-RH5 IgG for each dose is the same. The 0.02 μg dose group was not analysed given the GIA data were negative.

In a similar manner, the somewhat variable GIA assay data for the PfRIPR group resolved into a single curve (Figure 4.18C), with an EC_{50} value of 523.6 μg/mL, very similar to my previous result EC_{50} of 485.1 μg/mL in Section 4.4.2. This suggested good reproducibility across these two independent rat studies using the 2 μg PfRIPR/Matrix-M™ formulation. These data thus indicated that different animals are producing different quantities of anti-PfRIPR IgG antibodies, not different qualities. Given higher overall levels of GIA had been observed in rabbits (using a 50 μg dose of PfRIPR protein in C/IFA adjuvant), like for PfCyRPA, these data suggested that increasing the dose of protein vaccine should be tested to try and improve the GIA.

Finally, a quality analysis could not be conducted on the PfCyRPA samples in isolation due to the low GIA. However, samples and data were available from a historical study by Illingworth *et al*[202]. where rats were immunised with 50 μg PfCyRPA in C/IFA[156]. When these historical data were overlaid onto data from this study, it was clear that the data from animals immunised with 2 μg PfCyRPA/Matrix-M™ follows the same trend as those immunised with 50 μg PfCyRPA in C/IFA (Figure 4.18B). This gave further confidence that 2 μg PfCyRPA, and likely 2 μg PfRIPR, was too low a dose for effective immunisation of Wistar rats when formulating in Matrix-M™. A summary table of antigen specific EC_{50} results is given in Table 4-5.

From these data, the decision was taken to continue to use 2 μg RH5.1 in future rat experiments – in line with robust GIA data being observed, and clinical experience to-date with this vaccine at this dose in humans. However, a new study was deemed necessary to test a 20 μg dose of PfCyRPA and PfRIPR. Nevertheless, the data obtained in this experiment suggested good reproducibility of the PfRIPR data between two independent experiments, and also gave preliminary evidence that the potency hierarchy of the three soluble full-length protein vaccine antigens is PfRH5 > PfCyRPA > PfRIPR. Notably, the HBsAg PfRIPR EGF domain VLPs in the previous study gave a potency/quality of IgG comparable to generated by PfCyRPA, suggesting the first step towards improving PfRIPR-based vaccine potency.

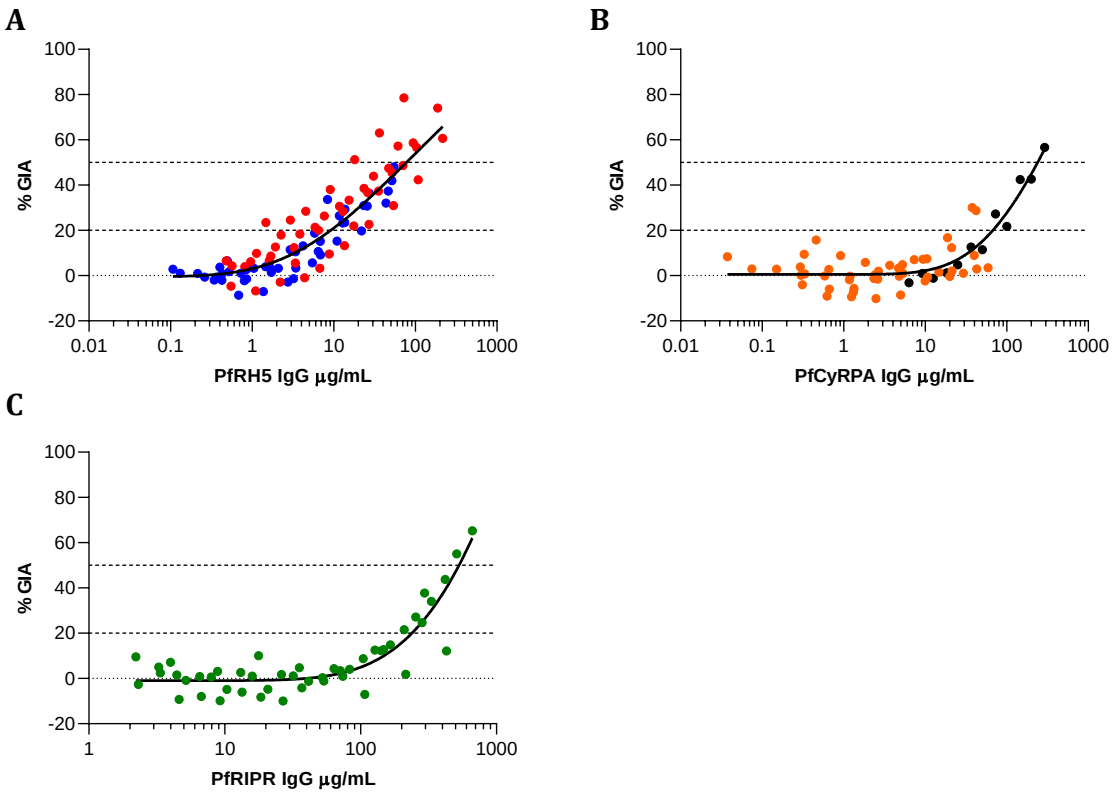


Figure 4.18 – Quality analysis of Study O1 GIA data.
A) GIA data of 2 µg (red) and 0.2 µg (blue) RH5.1/Matrix-M™ immunised animals plotted against anti-PfRH5 specific IgG measured in µg/mL. **B)** GIA data of 2 µg Matrix-M™ (orange) and 50 µg C/IFA historical data (black) PfCyRPA immunised animals plotted against PfCyRPA antigen specific IgG measured in µg/mL. **C)** GIA data of 2 µg PfRIPR/Matrix-M™ immunised animals plotted against PfRIPR specific IgG measured in µg/mL. The dotted lines show 0% GIA. Dashed lines show 20% GIA (the accepted LLQ of the assay) and 50% GIA for comparison. All points are mean, n=3. Each dataset fitted with Richard's five-parameter dose-response curve with no constraints.

Table 4-5 - Summary of interpolated EC_{50} values from each immunisation group.

Antigen	Dose (µg)	EC_{50} µg/mL	95% CI µg/mL
RH5.1	**2 & 0.2**	**60.4**	**51.9 to 74.0**
CyRPA	**2**	**N/A**	**N/A**
CyRPA - Historical	**50**	**231.9**	**N/A**
PfRIPR	**20**	**523.6**	**470.9 to 610.8**

4.6.2 Study O2 – Recombinant Protein Approach, Single and Multiple Component Protein Formulations

In light of the previous rat study data, a new Study O2 was designed. This had multiple aims:

i) To test the higher 20 μg doses of PfCyRPA and PfRIPR;

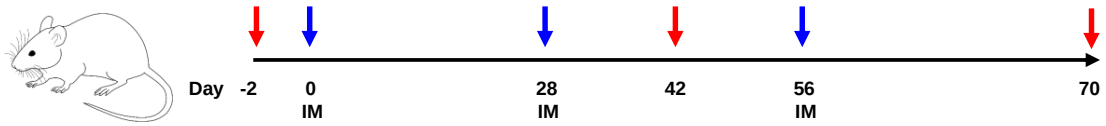
ii) To test PfRIPR EGF (5-8) at a ~10-fold higher dose than that used previously (Section 4.4.2);

iii) Generate preliminary data on functional immunogenicity of bi- and tri-valent antigen combinations.

Regarding the third aim, the three proteins PfRH5, PfCyRPA, and PfRIPR are not present on the merozoite as single antigens, rather they are formed into the RCR complex. It was therefore prudent to also test whether a mixture of the RCR antigens, or the whole RCR complex itself, could be used as a vaccine against blood stage malaria. Notably, my first pilot study in mice, which used a fusion PfRIPR-EGF (5-8)-PfCyRPA protein, suggested that a multi-component vaccine performed better than the single antigens alone (Figure 4.8). Study O2 sought to thoroughly explore this possibility *in vivo* using Wistar rats. Here, however, I elected to initially test soluble protein combinations, to avoid an excessive number of groups by also including fusion protein combinations at this stage. This study was designated Study O2.

Rats were immunised by the IM route on days 0, 28 and 56. Serum samples were taken on days -2, 28 and 56. Full immunisation details are given in Figure 4.19. Rat immunisations were carried out by the CRO Noble Life Sciences, USA. Groups 1 -3 were immunised with PfRH5, PfCyRPA and PfRIPR individual antigens at 2, 20 and 20 μg respectively. Groups 4-6 were immunised with pairwise combinations of the three

antigens. Group 7 was immunised with an equimolar ratio of the three antigens to a total dose of 20 µg. Group 8 was immunised with a combination of PfRH5, PfCyRPA and PfRIPR antigens at 2, 20 and 20 µg respectively. The antigens for groups 4 to 8 were all frozen and stored in isolation, the appropriate amounts of each antigen were then admixed immediately prior to immunisation by Noble Life Sciences. This was to minimise the formation of double & tripe complexes of protein prior to immunisation. Group 9 was immunised with 20 µg of the reconstituted RCR complex. The RCR complex was reconstituted *in vitro* by incubation of equimolar concentrations of PfRH5, PfCyRPA and PfRIPR for 1 hour at room temperature followed by SEC purification to remove any un-complexed antigens. The RCR complex was then stored at -80°C. Group 11 was immunised with PfRIPR-EGF (5-8) protein. The PfRIPR-EGF (5-8) dose chosen was an equivalent PfRIPR-EGF (5-8) molar amount to 20 µg full length PfRIPR, this was calculated to be 3.97 µg of PfRIPR-EGF (5-8) per dose. This ensured comparability between the PfRIPR and PfRIPR-EGF (5-8) groups, and was also 10x higher than that used in the initial rat study in section 4.4.



Group	Antigen	Antigen Doses					Total (µg)	Adjuvant
		PfRH5.1 (µg)	PfCyRPA (µg)	PFRIPR (µg)	RCR (µg)	Other (µg)		
1	PfRH5.1	2					2	Matrix-M™
2	PfCyRPA		20				20	Matrix-M™
3	PfRIPR			20			20	Matrix-M™
4	PfRH5.1 + PfRIPR	2		20			22	Matrix-M™
5	PfRH5.1 + CyRPA	2	20				22	Matrix-M™
6	PfRIPR + PfCyRPA		20	20			40	Matrix-M™
7	PfRH5.1 + PfCyRPA + PfRIPR (Equivalent Molar Ratio)	5.36	3.51	11.11			20	Matrix-M™
8	PfRH5.1 + PfCyRPA + PfRIPR	2	20	20			42	Matrix-M™
9	Reconstituted RCR				20		20	Matrix-M™
10	Matrix-M Only						NA	Matrix-M™
11	PfRIPR-EGF (5-8)					3.97	3.97	Matrix-M™

Figure 4.19 - Study O2 design.
Each group was composed of 6 Wistar rats except the negative control group which contained 3 rats. Rats were given three IM immunisations of antigen (blue arrows). Blood samples (red arrows) were taken on day -2, day 42 and day 70.

Serum samples taken from each animal on days -2, 42 and 70 were measured by antigen specific standardised ELISA. The results show a complex interaction between immunisation regime and ELISA titres. ELISA titres from immunisation with full length PfRIPR (Figure 4.20A) remained unchanged between Study O1 and O2 despite the increase in dose from 2 µg to 20 µg. In addition, only a small increase in ELISA titre is observed from the second to third dose in line with previous results. PfRIPR ELISA titres did not decrease when PfRIPR was co-immunised with either one or two additional antigens, whether admixed or in a pre-formed complex. There was also no difference seen in PfRIPR titres between the PfRH5-PfCyRPA-PfRIPR equimolar ratio mix (5.36, 3.51, 11.11 µg) and the PfRH5-PfCyRPA-PfRIPR (2,20,20 µg) mix. PfRIPR ELISA titres from PfRIPR-EGF (5-8) immunised rats were comparable to rats

immunised with full length PfRIPR. This contrasts with the first study using PfRIPR-EGF (5-8) where no ELISA titres were detected. This is most likely due to increasing the dose from 0.40 μg to 3.97 μg and suggests a higher dose can make this protein immunogenic.

Encouragingly, the increase in dose from 2 μg to 20 μg of PfCyRPA saw a close to 10-fold improvement in ELISA titre (Figure 4.20B). PfCyRPA has a more complex ELISA profile as co-immunisation with any antigen reducing the anti-PfCyRPA titre, this is especially pronounced in animals vaccinated with the PfRH5-PfCyRPA-PfRIPR equimolar ratio mix (5.36, 3.51, 11.11 μg) and RCR complex. This decrease is partly negated when the PfRH5-PfCyRPA-PfRIPR (2,20,20 μg) mix was used for immunisations.

A similar, but less pronounced trend is observed for PfRH5 (Figure 4.20C). PfRH5 ELISA titres were reduced when PfRH5 and PfRIPR were used in immunisations together, but not when PfRH5 and PfCyRPA were co-immunised. These data suggest that there is a gradient of immunodominance between the antigens with PfRIPR being the most immuno-dominant antigen followed by PfRH5. PfCyRPA is the least dominant and has reduced ELISA titres when immunised in conjunction with any of the three antigens.

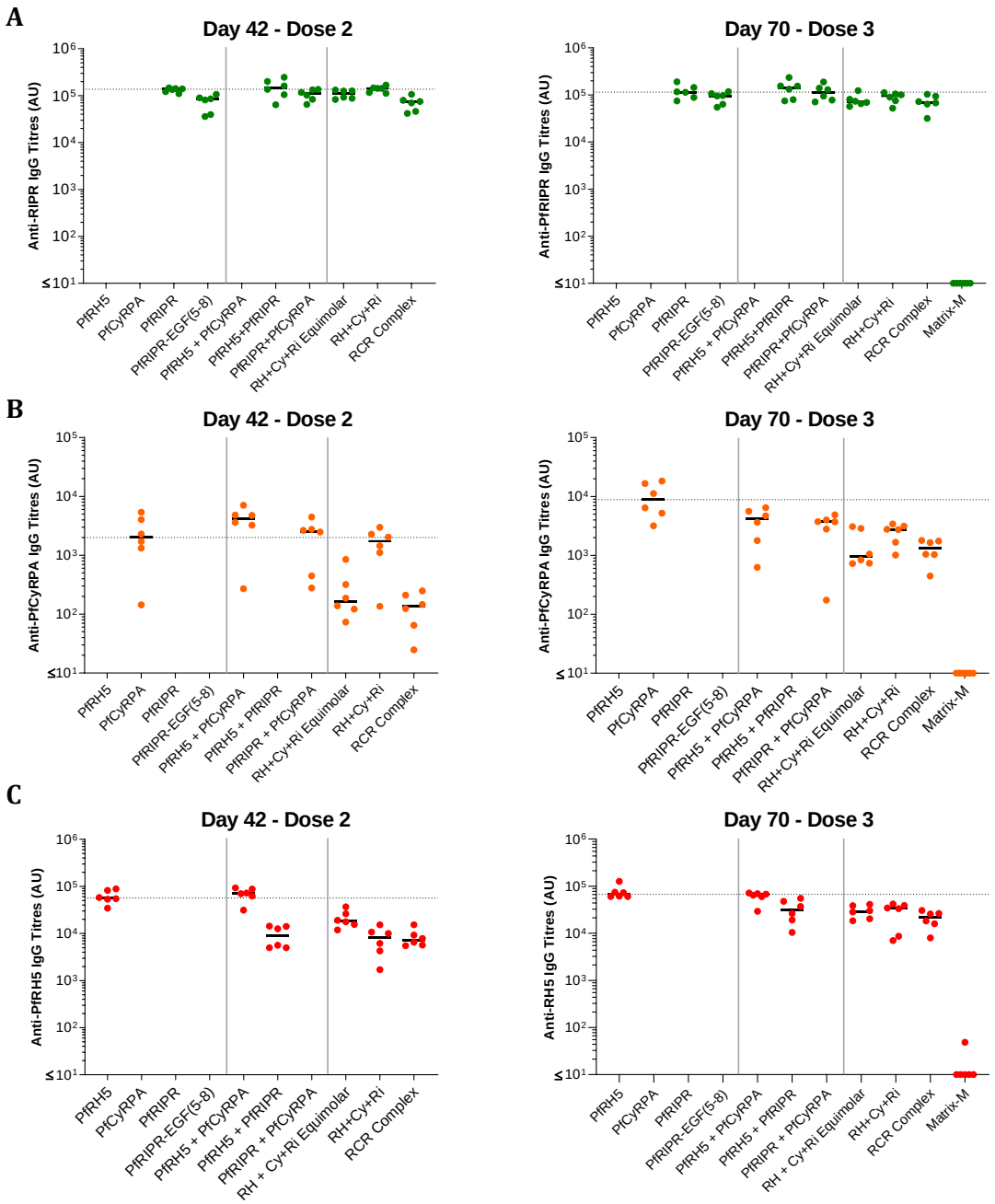


Figure 4.20 – Antigen-specific standardised ELISAs on Study O2 samples.

A) Anti-PfRIPR ELISA results for day 42 and 70. The dotted line corresponds to the median anti-PfRIPR IgG titres (AU) for the full-length protein. **B)** Anti-PfCyRPA ELISA results for day 42 and 70. The dotted line corresponds to the median anti-CyRPA IgG titres (AU) for the full-length protein. **C)** Anti-PfRH5 ELISA results for day 42 and 70. The dotted line corresponds to the median anti-PfRH5 IgG titres (AU) for the full-length protein. RH+Cy+Ri equimolar is the PfRH5-PfCyRPA-PfRIPR equimolar ratio mix (5.36, 3.51, 11.11 µg), RH+Cy+Ri is the PfRH5-PfCyRPA-PfRIPR (2,20,20 µg) mix. Grey vertical bars separate single antigens, pairs of antigens and triple antigen immunisations. Each dot represents a single animal, black bars are median, n = 6

The GIA results for the three full-length antigens; PfRH5, PfRIPR and PfCyRPA, follow a similar pattern to Study O1. The strongest GIA results were again seen from the 2μg dose of PfRH5 (EC_{50} 0.99 mg/mL ± 0.360) followed by PfRIPR (EC_{50} 3.64 mg/mL ± 0.46) and PfCyRPA (EC_{50} 4.47 mg/mL ± 3.2) (Figure 4.21A). However, GIA titres were improved for PfRIPR and PfCyRPA suggesting that 20 μg of protein is a more appropriate dose for these two antigens.

For simplicity, the full GIA curves of all groups can be found in appendix 8.3, however a comparison of the GIA from groups 1-9 and 11 at 5 mg/mL is given in Figure 4.21B. The results show that immunisations with pairs or three antigens gives higher GIA results than single antigens alone, with the highest GIA produced by the PfRH5-PfCyRPA-PfRIPR (2,20,20 μg) mix. These data bode well for improving overall vaccine-induced GIA as compared to RH5.1 alone, despite the fact some groups showed immune-interference, especially with the PfRH5 and PfCyRPA responses.

Each of the purified IgG samples was next analysed by antigen-specific standardised ELISA, so the "quality" or GIA potency per μg/mL of antigen-specific IgG could be compared. Notably here it was possible to sum responses against different antigens to calculate the total vaccine-induced antibody response. A full set of results is included in Table 4-6. The most potent antigen combination when accounting for the total concentration of antigen-specific IgG was 2μg of RH5.1 and 20 μg PfCyRPA, with an EC_{50} of 50.4 μg/mL. This was closely followed by the PfRH5-PfCyRPA-PfRIPR (2,20,20 μg) mix with an EC_{50} of 62.3 μg/mL.

When PfRIPR was immunised as a pair with either PfRH5 and PfCyRPA, the EC_{50} value was higher than immunisation with PfRH5 and PfCyRPA alone. Here, it is probable that the immunodominance of PfRIPR in these combinations is reducing the quality

or potency of the total antibody response, given the IgG raised against PfRIPR alone is the least potent (see section 4.6.1). This effect appears to be partly mitigated when all three antigens are used for immunisations. It is also probable that inter-antigen antibody interactions are occurring here (i.e. additivity and/or synergy), in that the levels of GIA are highly encouraging despite seeing reductions in antibody levels due to immune interference. However, given the primary focus of this Thesis is PfRIPR, I elected to further analyse the comparison of PfRIPR and PfRIPR EGF (5-8) protein immunisations.

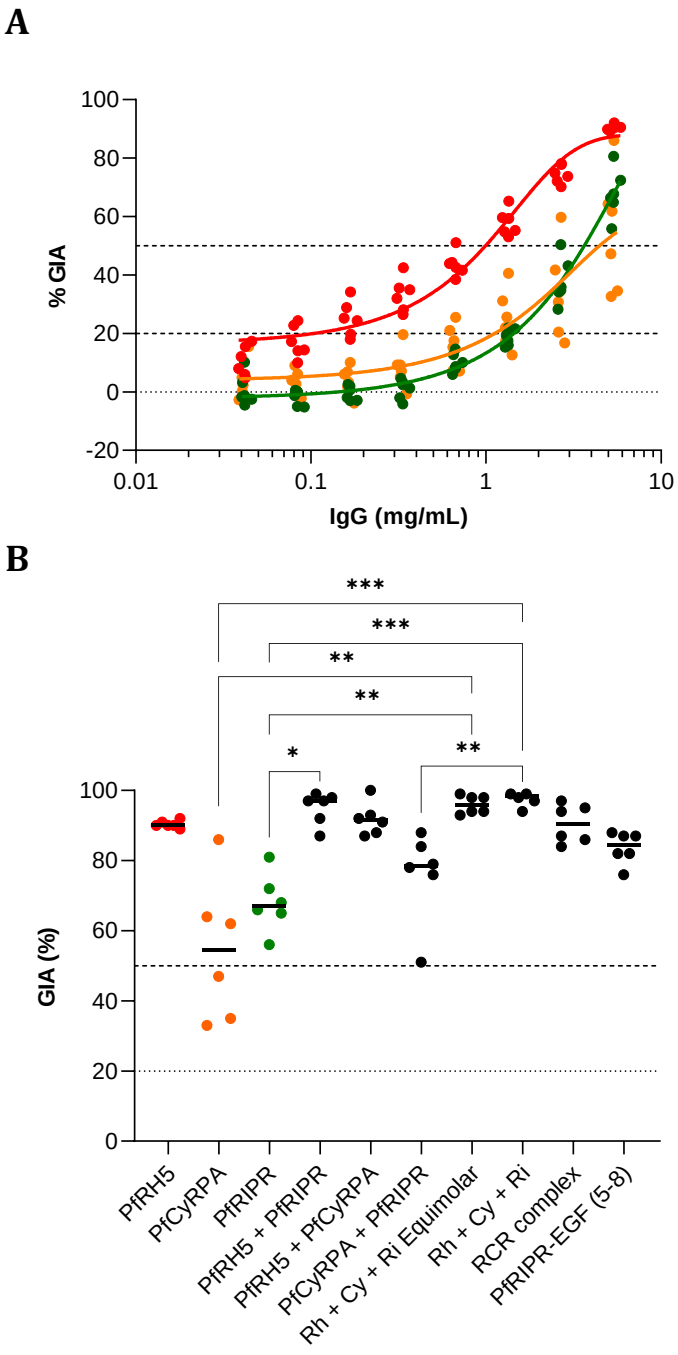


Figure 4.21 – Single cycle GIA assay with dilution curve of purified IgG from rats in Study O2 using *P. falciparum* clone 3D7.

A) GIA results from rats immunised with RH5.1 (red), PfCyRPA (orange) and PfRIPR (green). 6 animals per group, each dataset fitted with Richard's five-parameter dose-response curve with no constraints. **B)** GIA results at 5 mg/mL. RH5.1 (red), PfCyRPA (orange), PfRIPR (green) pairs and triple antigen immunisations in black. The dotted lines show 0% GIA. Dashed lines show 20% GIA (the accepted LLQ of the assay) and 50% GIA for comparison. Each point represents one animal, black bars represent the median GIA. Significance determined by Kruskal Wallis with Dunn's multiple comparisons test, * represents $p \leq 0.05$, ** $p \leq 0.01$, *** $p \leq 0.001$. non-significant values not shown. Significance values only displayed for comparisons of groups containing the same antigens e.g. PfRIPR vs PfRIPR + PfCyRPA, not PfRIPR vs PfCyRPA + PfRH5.

In this study, rats were immunised with 20 µg of full-length PfRIPR or 3.97 µg of PfRIPR EGF (5-8); 3.97 µg being an equimolar dose equivalent to 20 µg of full-length PfRIPR. Immunisation with PfRIPR EGF (5-8) showed a modest improvement in GIA compared with full length PfRIPR (Figure 4.22A & B) with GIA at 5 mg/mL improving from median value of 67% to 84%.

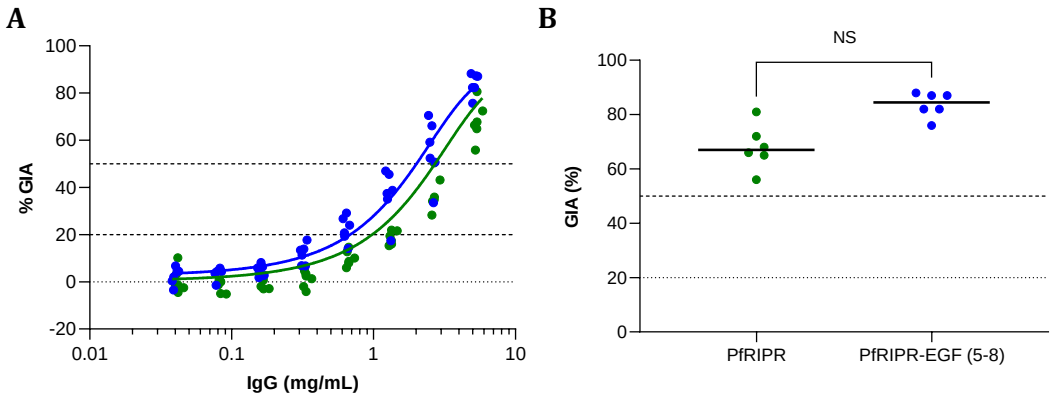


Figure 4.22 – Single cycle GIA assay with dilution curve of purified IgG from immunisations with full-length PfRIPR and PfRIPR EGF (5-8) protein in Study O2 using *P. falciparum* clone 3D7.

A) Full GIA curves of purified IgG from immunisations with full-length PfRIPR (green) and PfRIPR EGF (5-8) (blue). 6 animals per group. Each data set fitted with a Richard's five-parameter dose-response curve with no constraints. **B)** GIA at 5 mg/mL for PfRIPR and PfRIPR EGF (5-8). The dotted lines show 0% GIA. Dashed lines show 20% GIA (the accepted LLQ of the assay) and 50% GIA for comparison. Each point is a separate animal with black bars representing median values. Significance determined by Kruskal Wallis with Dunn's multiple comparisons test; NS represents not significant.

Each purified IgG sample was next analysed by PfRIPR specific standardised ELISA and the data re-plotted as GIA against anti-PfRIPR specific IgG in µg/mL (Figure 4.23A). The data show a large quality shift between PfRIPR and PfRIPR EGF (5-8) immunisations. This was expected since immunisations with PfRIPR and PfRIPR EGF (5-8) gave similar ELISA titres but the majority of antibodies from PfRIPR EGF (5-8) immunisations should have neutralising activity. There is a stark improvement in EC_{50}, 427.4 µg/mL vs 124.1 µg/mL (Figure 4.23B), confirming that immunisation with PfRIPR EGF (5-8) yields better GIA per µg of anti-PfRIPR antibody.

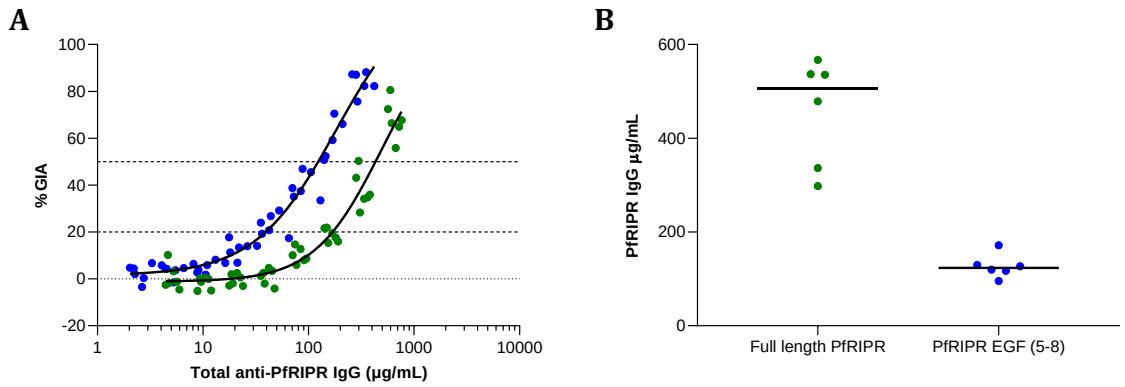


Figure 4.23 - Quality analysis of GIA data from immunisations with full-length PfRIPR and PfRIPR EGF (5-8) protein.
A) Full GIA curves plotted against anti-PfRIPR IgG. 6 animals per group, each data set fitted with a 4-parameter dose response curve. The dotted lines show 0% GIA. Dashed lines show 20% GIA (the accepted LLQ of the assay) and 50% GIA for comparison. **B)** Interpolated EC_{50} values (interpolated from panel A) from immunisations with PfRIPR and PfRIPR EGF (5-8). Each point represents one animal, black bars are median values.

Table 4-6 – Summary of interpolated total antigen-specific IgG EC_{50} values from each immunisation group.

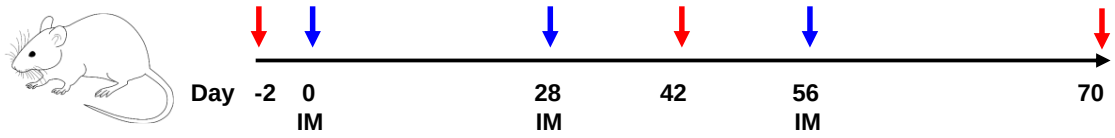
Group	Antigen	Dose (µg)	EC_{50} (µg/mL)	95% C.I. (µg/mL)
1	RH5.1	2	81.1	75.5 to 87.2
2	PfCyRPA	20	180.0	163.2 to 198.9
3	PfRIPR	20	427.4	394.4 to 461.3
4	RH5.1 + PfRIPR	2 + 20	96.3	85.9 to 108.4
5	RH5.1 + PfCyRPA	2 + 20	50.4	43.5 to 58.7
6	PfCyRPA + PfRIPR	20 + 20	329.7	310.4 to 350.4
7	RH+Cy+Ri Equimolar	5.36 + 3.51 + 11.11	132.4	120.0 to 146.5
8	RH+Cy+Ri	2 + 20 + 20	62.3	54.3 to 71.8
9	RCR Complex	20	100.8	92.9 to 109.5
10	Matrix-M™ only	NA	NA	NA
11	PfRIPR EGF (5-8)	3.97	124.1	116.0 to 132.9

4.6.3 VLP-Based Vaccine approaches

The previous study firmly established a higher dose of soluble PfRIPR EGF (5-8) as superior to full-length PfRIPR. In parallel to Study O2, a second study was also run in light of the earlier data. In particular, the need to repeat the experiment testing the HBsAg PfRIPR EGF (5-8) vaccine at a higher dose, and also an attempt to improve responses to PfCyRPA (after disappointing levels of GIA were seen in Study O1). For comparison, a test of RH5.1 also conjugated to HBsAg was included. This study was called Study O3.

Individual antigens RH5.1 and PfCyRPA were produced with a C-terminal SpyTag. These were conjugated to HBsAg-SpyCatcher and purified by SEC as described in sections 4.3.1 and 4.3.2. The development of HBsAg-PfRIPR was ongoing at this time however production of this VLP proved difficult due to the need to express a new PfRIPR full-length protein with terminal SpyTag, and this was challenging. Consequently, this vaccine was not progressed. However, HBsAg-PfRIPR EGF (5-8) had already been produced and was available from the previous work. Wistar rats were immunised IM on days 0, 28 and 56 with either 2, 0.2 or 0.02 μg of HBsAg-RH5.1 (to provide comparison to Study O1 with soluble RH5.1) or 20, 2, 0.2, or 0.02 μg of HBsAg-PfCyRPA or HBsAg-PfRIPR EGF (5-8) as detailed in Figure 4.24. Blood samples were taken on days -2 & 42 with a cardiac bleed at day 70 as in previous studies.

The doses of VLP were not normalised to be equivalent molar ratios rather, for example, 2 μg of VLP was given irrespective of antigen.



Group	Antigen	Dose (µg)	Conjugation efficiency	Group size	Adjuvant
1	HBsAg RH5.1	2	67%	6	Matrix-M™
2	HBsAg RH5.1	0.2		6	Matrix-M™
3	HBsAg RH5.1	0.02		6	Matrix-M™
4	HBsAg PfCyRPA	20	86%	6	Matrix-M™
5	HBsAg PfCyRPA	2		6	Matrix-M™
6	HBsAg PfRIPR-EGF (5-8)	20	44%	6	Matrix-M™
7	HBsAg PfRIPR-EGF (5-8)	2		6	Matrix-M™
8	HBsAg	20		6	Matrix-M™

Figure 4.24 - Study O3 design.
Each group was composed of 6 Wistar rats, given three IM immunisations of antigen (blue arrows). Blood samples (red arrows) were taken on day -2, day 42 and day 70.

Serum samples from each time point were analysed by antigen-specific standardised ELISA, in addition purified IgG samples were also tested for GIA as before. Only the HBsAg-PfRIPR EGF (5-8) samples will be discussed in this section, given the RH5.1 and PfCyRPA groups were analysed separately by Dr Lloyd King.

All rats were negative for PfRIPR specific antibodies at day -1, the only exception being a weak borderline response in one rat (Figure 4.25A). A single dose of 20 and 2 µg HBsAg-PfRIPR EGF (5-8) VLP generated a measurable anti-PfRIPR-specific response at day 14 (Figure 4.25B). The first boost resulted in an increased anti-PfRIPR responses at day 42 in all vaccinated groups no significant difference was observed between the 20 and 2 µg dose groups (Figure 4.25C). The second vaccination boost did not improve anti-PfRIPR titres consistent with the other studies of PfRIPR-based vaccines. Interestingly, although there was a trend dose-dependent anti-PfRIPR response, with higher vaccine doses inducing higher titres of antibody,

no significant differences were seen between the 20 and 2 µg dose groups at day 70, suggesting that a 2 µg dose of HBsAg PfRIPR EGF (5-8) is sufficient to deliver maximal IgG responses in rats.

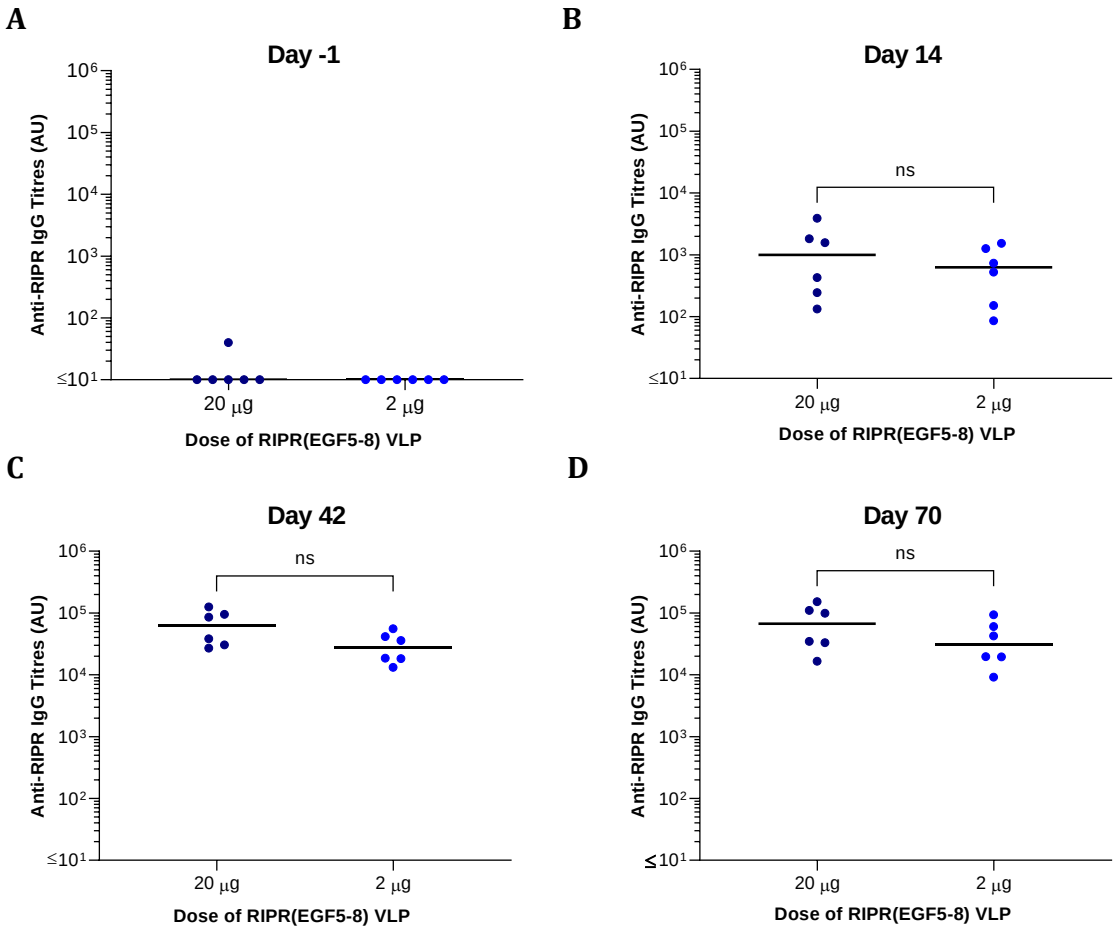


Figure 4.25 - Anti-PfRIPR specific standardised ELISA titres for HBsAg-PfRIPR EGF (5-8) immunised rats.

A) Day -1. **B)** Day 14. **C)** Day 42. **D)** Day 70. Each point represents an animal, black bars represent median titre. Significance determined by Mann-Whitney U test. 'ns' represents non-significant results.

The GIA results followed a similar pattern to the ELISA results. The two groups GIA readouts overlapped (Figure 4.26A) however GIA results over the 50% threshold were rarely seen. The data became clearer when the GIA was plotted against anti-PfRIPR specific IgG (Figure 4.26B). The 2 µg dose group produced substantially better

quality antibodies than the 20 μg dose group (EC_{50} 156 vs 694 μg/mL). This is more consistent with the GIA data produced from rats immunised with 0.4 μg HBsAg PfRIPR EGF (5-8) in Section 4.5.2 which gave a median EC_{50} of 270 μg/mL.

Disappointingly, however, the results are worse than the EC_{50} calculated from full-length PfRIPR (normally around 500 μg/mL) and PfRIPR EGF (5-8) soluble protein (124 μg/mL). These data would suggest, for now, that PfRIPR-based soluble protein vaccines may perform better than HBsAg VLP conjugated antigen, for reasons yet to be determined.

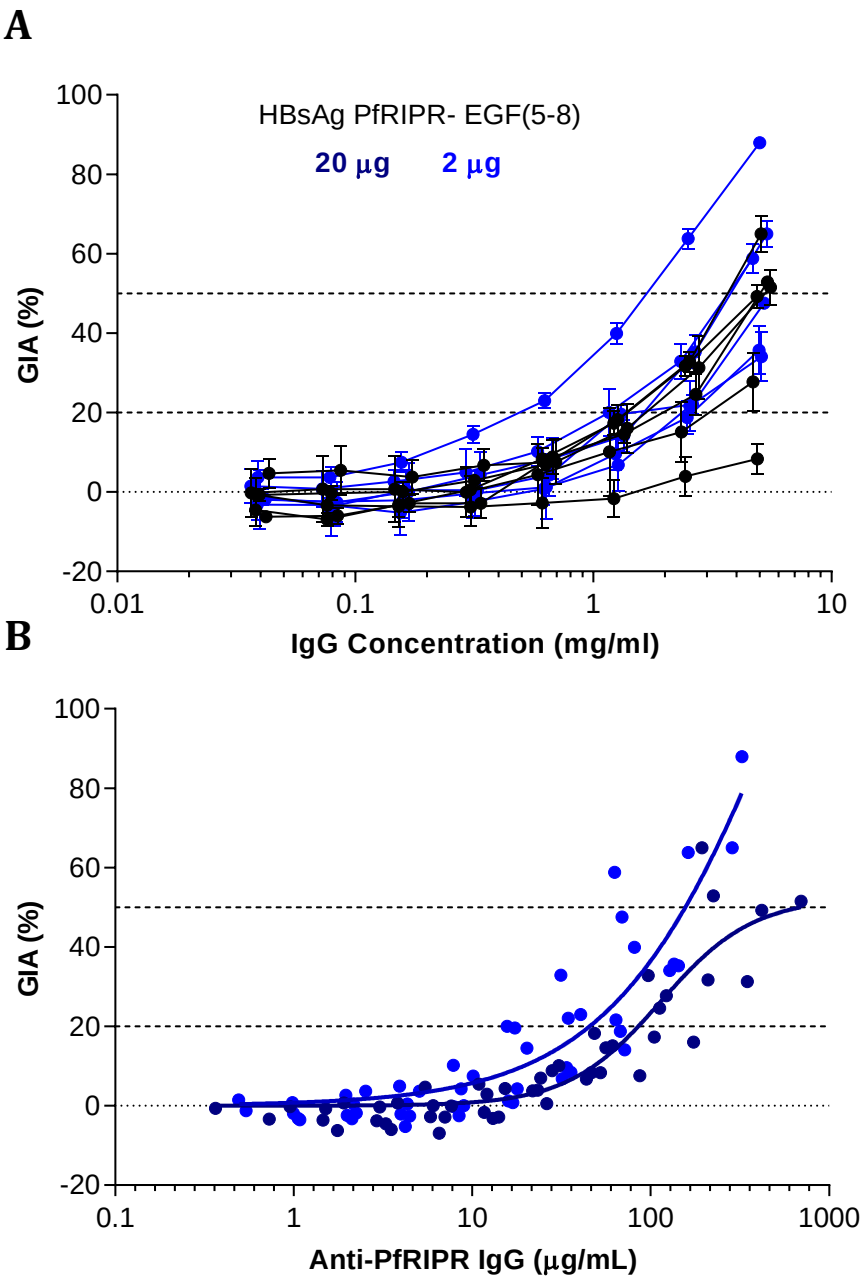


Figure 4.26 – GIA results from rats immunised with different doses of HBsAg PfRIPR EGF (5-8).

A) GIA plotted against total IgG (mg/mL) Each point is median and error bars SEM, n=3. Each line represents 1 animal. Dotted line corresponds to 0% GIA, hatched lines 20 & 50% GIA. **B)** GIA data plotted against PfRIPR specific IgG (µg/mL). Each group fitted with a 4-parameter dose response curve. lines. The dotted lines show 0% GIA. Dashed lines show 20% GIA (the accepted LLQ of the assay) and 50% GIA for comparison.

For completeness, I also compared these results to the RH5.1 and PfCyRPA VLPs (analysed separately by Dr Lloyd King). When HBsAg-RH5.1, HBsAg-PfCyRPA and HBsAg-PfRIPR EGF (5-8) are compared (Figure 4.27) it is clear that HBsAg-RH5.1 delivers superior GIA per µg of IgG than either HBsAg-PfCyRPA or HBsAg-PfRIPR EGF (5-8). Interestingly, however, HBsAg-PfCyRPA and HBsAg-PfRIPR EGF (5-8) both showed a dose response pattern (with the highest 20 µg dose leading to lower quality antibody responses) in contrast to HBsAg-PfRH5 where each dose performed the same. A summary of results from Study O3 is given in Table 4-7.

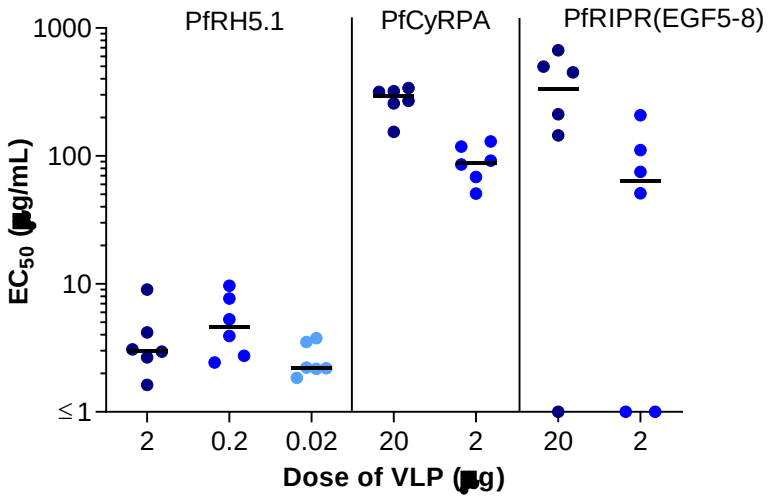


Figure 4.27 - Comparison of interpolated EC_{50} values from Study O3.
Each point represents an animal. Black bars are median.

Table 4-7. Summary of Study O3 GIA Assay Antigen-Specific Rat IgG EC_{50}

Antigen	Dose	EC_{50} µg/mL	95% C.I. µg/mL
RH5.1 VLP	2 µg	3.56	3.15 to 4.0
RH5.1 VLP	0.2 µg	4.95	4.37 to 5.63
RH5.1 VLP	0.02 µg	2.38	2.18 to 2.58
PfCyRPA VLP	20 µg	256	237 to 275
PfCyRPA VLP	2 µg	84	76 to 92
PfRIPR EGF (5-8) VLP	20 µg	694	-
PfRIPR EGF (5-8) VLP	2 µg	156	138 to 177

4.6.4 Summary of outcomes with different antigens used in rat immunisations

The four rat studies described above generated a lot of data regarding vaccination with PfRH5, PfCyRPA and PfRIPR. One informative way to compare each antigen is to use the antigen-specific EC_{50} value, since this gives a good indicator of the potency of the IgG generated by immunisation with each antigen(s). Results from each PfRIPR immunisation and representative results from RH5.1 and PfCyRPA are plotted in Figure 4.28.

The EC_{50} values from each of the three-independent full-length PfRIPR immunisations are remarkably consistent even at different doses, suggesting PfRIPR is highly immunogenic. However, PfRIPR has the highest EC_{50} values of the three antigens when immunised as soluble protein alone, nearly 10-fold worse than RH5.1. This is consistent with my earlier data suggesting all neutralising epitopes are in EGF domains 5-8 (accounting for just 16% of the total full-length antigen sequence). Accordingly, the development of a PfRIPR EGF (5-8) vaccine in this thesis led to an improved anti-PfRIPR antibody quality, bringing the antigen broadly in line with PfCyRPA when immunised as a soluble protein only at a dose of at least ~ 4 μg. Conjugation of PfRIPR EGF (5-8) to HBsAg gave mixed results compared with PfRH5 and PfCyRPA; both of these antigens saw a clear improvement in antibody quality when immunised as VLPs. Immunisations with HBsAg PfRIPR EGF (5-8) did not lead to an improvement in antibody response for reasons that currently remain unknown. Encouragingly, these data identify the RH5.1-HBsAg VLP as a clear improvement, and suggest that high doses of the PfCyRPA-PfRIPR EGF (5-8) fusion protein vaccine warrant testing. Given encouraging results were also seen with the combination

antigen study, the next steps could also include combining the RH5.1-VLP with the fusion protein. Due to the Covid-19 pandemic, this final study was delayed, but is now in progress at the time of writing.

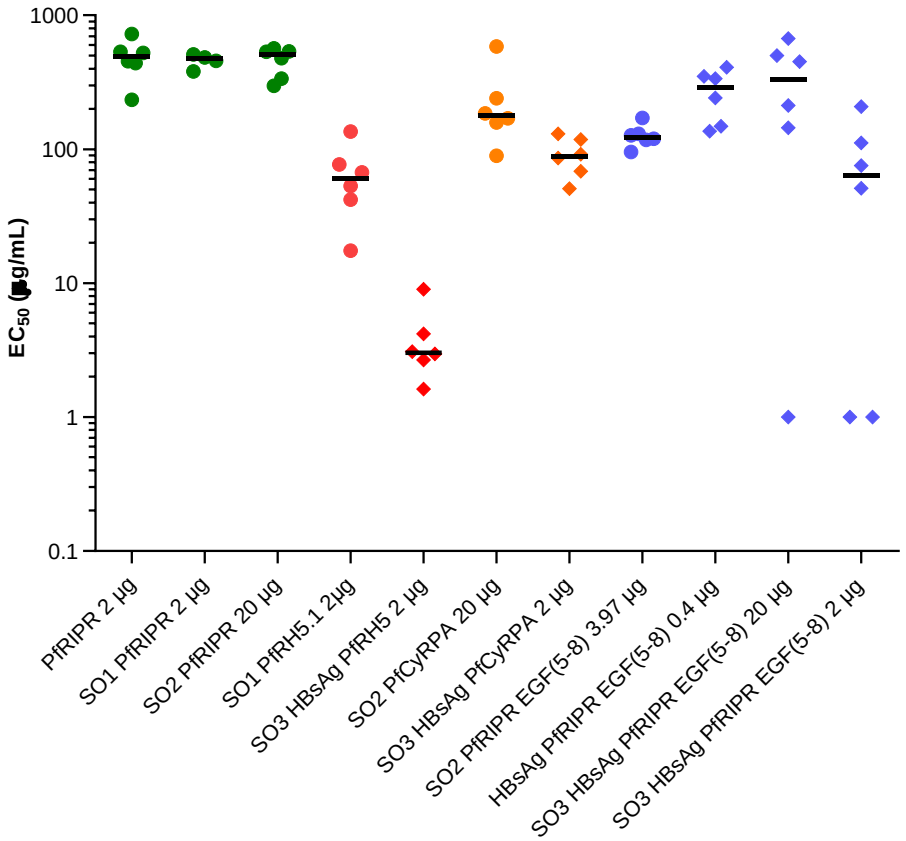


Figure 4.28 – Summary of interpolated EC_{50} values from the four rat studies in this Thesis.

Each point represents one animal with the black bar representing the median value. All PfRIPR and PfRIPR EGF (5-8) results are shown. Representative PfRH5 and PfCyRPA results are shown for comparison. Green circles: Full length PfRIPR. Red circles: RH5.1. Red Diamonds: HBsAg-RH5.1. Orange circles: PfCyRPA. Orange diamonds HBsAg-PfCyRPA. Blue circles PfRIPR EGF (5-8) protein. Blue diamonds: HBsAg PfRIPR EGF (5-8).

4.7 Discussion

In Chapter 3 I described how the targets of all neutralising antibodies against PfRIPR are localised in a just 16% of the PfRIPR protein corresponding to EGF like domains 5-8 in the C-terminal half of the protein. In this Chapter, I developed several vaccine candidates based on the PfRIPR EGF (5-8) protein and tested them head-to-head against full-length PfRIPR and also the other two members of the RCR complex: PfRH5 and PfCyRPA. This is the most extensive analysis of RCR-based vaccines conducted to date.

The vaccine candidates for the initial mouse study were designed based on the data gathered by the reversal of the GIA from rabbits immunised with PfRIPR at Genscript in Chapter 3. From these data, EGF like domains 7-8 were identified as the target of neutralising antibodies, making this the primary candidate for a PfRIPR-based vaccine. A fusion PfCyRPA-PfRIPR EGF (7-8) was also designed and produced to evaluate how multiple components performed *in vivo*. Both PfRIPR EGF (7-8) and PfCyRPA-PfRIPR EGF (7-8) were conjugated to HBsAg. Other VLP platforms are available such as IMX313[90] and the newly developed ADDomer[232] however the HBsAg-SpyCatcher system was readily available in the Oxford malaria vaccine programme and HBsAg has a strong clinical history, including use in the licensed hepatitis B vaccine and the RTS,S and R21 malaria vaccine candidates. The conjugations of antigen to HBsAg was successful in each of these cases. Each VLP was tested for conjugation efficiency and particle heterogeneity, however acceptable limits for each of these have not been developed, in part because there is scope to extensively optimise conjugation conditions for each antigen. It is unclear how particle heterogeneity or conjugation efficiency affect the vaccines' performance *in*

vivo, however, all analyses conducted showed no gross problems, with results in expected or typical ranges. As such we deemed it prudent to ensure all of these parameters are recorded for each experiment so that a retrospective analysis of the data could be conducted if it is found, for example, that particle heterogeneity has a profound effect on vaccine performance.

Conjugation efficacy may play an important role in vaccine efficacy. A recent study by Marcandalli *et al.* used a three-component synthetic nanoparticle for testing RSV glycoprotein vaccines[217]. By using three components they were able to accurately control the valency of the nanoparticle to either 33%, 67% or 100% conjugated. Anti-RSV IgG titres and RSV neutralisation was significantly increased with the higher valency nanoparticles. Conjugation efficiency was taken into consideration when designing each experiment in this Chapter so that an equal amount of antigen was used for immunisation, however it is still unclear whether, for example, 2 μg of 100% conjugated VLP vaccine gives the same response as 4 μg of 50% conjugation VLP. This will need carefully designed studies to untangle since the response may also be antigen dependent.

PfRIPR, PfRIPR EGF (7-8) and HBsAg PfRIPR (7-8) were tested against RH5.1 in a pilot study in mice. PfRIPR EGF (7-8) was not immunogenic and therefore gave no GIA however HBsAg PfRIPR (7-8) was superior to PfRIPR, thus in agreement with the results from Chapter 3. PfCyRPA-PfRIPR EGF (7-8), and HBsAg fusion, produced higher levels of functional antibodies, again suggesting that a multicomponent vaccine was viable. None of the new vaccine candidates surpassed RH5.1, however the fusion antigen VLP was almost comparable, suggesting a route to a combination of two high potency vaccines.

However, after the completion of this study it was found that the targets of neutralising antibodies in PfRIPR covered EGF like domains 5-8. This information, in conjunction with the group moving to rats for *in vivo* studies, forced a step back and a second pilot study. This study, in Wistar rats, sought to identify which of PfRIPR EGF (5-6), (7-8) or (5-8) was the most appropriate vaccine to take forward. This study was run in parallel with Study O1 which sought to formally compare the potency of RH5.1, PfCyRPA and PfRIPR by enabling µg/mL ELISA readouts of antigen-specific IgG.

Two main conclusions can be drawn from these two rat studies. Firstly, immunisation with HBsAg-PfRIPR EGF (5-8) generates equal GIA to full-length PfRIPR but also produces better quality antibodies, validating the design of PfRIPR EGF (5-8) based vaccines. Secondly, a 2µg dose of PfRIPR, equivalent PfRIPR EGF domains, and PfCyRPA in Matrix-M ™ was potentially too low. A subsequent study thus assessed the higher 20 µg or equivalent dose.

Study O2 sought to investigate immunisations with pairs of antigens and the three RCR antigens in combination alongside the higher doses of the individual antigens. Previous studies have shown synergistic interactions between the components of the RCR complex[167] particularly between PfRIPR and PfCyRPA. The study by Azasi *et al.*, and our own internal studies (unpublished), have performed these experiments by immunising rabbits with one component of the RCR complex and then mixing the purified IgG from one or more immunisations in the same GIA assay. Although this provides a result free from confounding factors (especially immune competition), it does not reflect what the immune response may be if two or more components are used to immunise the same animal at the same time. The components may synergise or they may compete leading to a worse overall vaccine.

Study O2 showed that immunisation with pairs or three antigens does improve the quality and quantity of GIA, however this is balanced by a reduced ELISA titre for certain antigens – notably PfRH5 and PfCyRPA. It seems that any immunisations that includes PfRIPR leads to PfRIPR dominating the humoral response, this is unfortunate as PfRIPR gives the lowest GIA potency. Due to the lowering ELISA responses but increasing GIA, it is possible that synergistic interactions are occurring between these antibody specificities but untangling these exact and complex interactions will require further work.

A vaccine with reduced PfRIPR immunodominance may improve the overall effectiveness of RCR-based vaccines; this may be achievable with PfRIPR EGF (5-8). In study O2, 3.97 μg PfRIPR EGF (5-8) protein gave a higher GIA at 5mg/mL IgG and also a four-fold improvement in antibody quality over PfRIPR. Although not tested in co-immunisation with other antigens, it may prove to be less immunodominant due to its smaller size. A more thorough examination of the PfRIPR EGF (5-8)-PfCyRPA fusion protein vaccine in rats, where the antigen specific standardised ELISA can be used, will shed light on this. This study was delayed by the pandemic but is now in progress.

Immunodominance is a complex phenomenon; a recent study by Angeletti *et al.* [233] investigated the immunodominance of the influenza hemagglutinin (HA) head against the HA stem. They found that immunodominance can be modulated by immunising with stem only constructs alongside full-length HA and that anti-stem antibody class switching is affected by these regimens. Such studies are possible with the three RCR antigens, however they would need to be carefully designed, since the number of antigen combinations and immunisation regimes could quickly become unfeasible.

The results from Study O3 using HBsAg PfRIPR EGF (5-8) were more mixed. A clear improvement over PfRIPR EGF (5-8) protein was not observed, and if anything, worse responses were seen. There may be several reasons for this. It is possible that improvements in immunogenicity between a protein only and HBsAg-conjugated vaccines is antigen-specific. Conjugation of PfRIPR EGF (5-8) to HBsAg may not give the same benefit as, for example, RH5.1 conjugated to HBsAg. Alternatively, it may be due to the quality of VLP produced, the conjugation efficiency was lower for the Study O3 batch of HBsAg PfRIPR EGF (5-8) than that used in the rat pilot study, 44% vs 75%, which may have reduced the potency. Alternatively, the orientation of the PfRIPR EGF (5-8) on the VLP is sub-optimal and does not present the neutralising epitopes appropriately. To examine this, I would need a panel of monoclonal antibodies against PfRIPR EGF (5-8) and good structural data on the protein.

A second question that has not been addressed, but which may impact PfRIPR vaccine effectiveness, is the expression of PfRIPR on the merozoite surface. It has been assumed that PfRIPR, PfCyRPA and PfRH5 are all expressed and presented at a 1:1:1 ratio. Although not unreasonable, it is possible that there is much more PfRIPR on the merozoite surface than PfRH5. *P. vivax* has been shown to evade anti-DBP humoral immunity by amplifying the copy number of the PvDBP gene[234] therefore it is also possible that anti-PfRIPR antibodies seem less effective than anti-RH5 antibodies because there is more PfRIPR on the merozoite surface. Sadly, this is beyond the scope of this Thesis to investigate, however there is a third, more tractable, question that can be investigated:

It is possible that by removing the majority of the PfRIPR protein I have removed important non-neutralising but synergistic epitopes. Non-neutralising but synergistic

epitopes have been found on PfRH5[156], so it is not unreasonable to assume that other similar epitopes may exist on different/related antigens. This is especially pertinent as it looks like PfRIPR EGF (5-8) is underperforming as compared to PfRIPR. PfRIPR EGF (5-8) is 16% of PfRIPR (184 of 1086 amino acids). If antibodies are generated equally across the PfRIPR protein, 1/6th of them would bind to PfRIPR EGF (5-8). Since PfRIPR EGF (5-8) generates the same ELISA titre as PfRIPR we would assume that the resulting antibody response would generate 6x better GIA. So far only 4x has been seen. In light of this, it therefore seemed prudent to fully explore the possibility of intra-protein synergy.

The next Chapter fully explores this possibility, using new anti-PfRIPR GIA positive monoclonal antibodies generated as part of this Thesis, with the aim of fully characterising this antigen as a vaccine candidate.

Chapter 5 - Using monoclonal antibodies to aid PfRIPR vaccine design

5.1 Authorship statement

The GIA assays were carried out by two dedicated research associates: Dr Doris Quinket and Amelia Lias as described previously. Dr Lea Barfod made the hybridomas for mRP003, mRP006, mRP013, mRP016, mRP017 and mRP018. The hybridoma 7B10H3 was produced by Cambridge Research Biochemicals (CRB). mRP012 was produced by Leidos Inc. Andrew Worth helped sort antigen specific B-cells. Full length PfRIPR, PfRH5, and PfCyRPA protein was produced by either Dr David Pulido-Gomez or Hannah Davies.

5.2 Introduction to monoclonal antibody discovery

Monoclonal antibodies are useful tools for structure-based vaccine design and they are powerful therapeutics in their own right[235]. At the start of this project no GIA-positive anti-PfRIPR mAbs had been identified by the Draper group; a panel of non-neutralising mAbs had been isolated, these were characterised in Chapter 3. The non-neutralising mAbs were found to bind to epitopes in the N-terminal half of the protein and EGF domains (3-4). This panel of mAbs was isolated at a time when our knowledge of the PfRIPR was more limited; work in Chapter 3 and Chapter 4 of this Thesis has demonstrated (by antigen-reversal GIA assay) that the neutralising epitopes of PfRIPR are located in EGF domains (5-8). Towards the end of this project two neutralising anti-PfRIPR mAbs were published by Healer *et al.*[166]. The mAbs,

1G12 and 5G6, had GIA EC_{50} values of 0.35 mg/mL and 0.8 mg/mL respectively; both of these mAbs bound to EGF domain 7, in agreement with the hypothesis developed during my project.

The difficulties encountered isolating neutralising anti-PfRIPR mAbs from mice immunised with full-length PfRIPR (Draper group, unpublished data) suggested that neutralising mAbs were rare. Now that the neutralising epitope region is known, a focused vaccination schedule using the HBsAg-PfRIPR EGF (5-8) VLP-based vaccines developed in Chapter IV should be able to induce neutralising mAbs with higher efficiency than immunisations with full-length PfRIPR protein.

Several approaches have been developed for mAb discovery; the most commonly used approach is based on the hybridoma technique developed in the 1970s by Köhler *et al.*[236]. The fusion of splenocytes from an immunised mouse with a mouse B-cell myeloma cell line leads to the generation of an immortalised 'hybridoma' cell that secretes IgG. Further advances to this technique include fully human hybridomas[237] and humanised mice[238] that enable the production of fully human antibodies from hybridomas. The hybridoma technique is available to the Draper group in-house and takes advantage of the ClonePix (molecular devices), an automated colony picker. Antibody discovery with hybridomas has numerous issues that mean it will soon be superseded by other techniques. Firstly, the fusion of B-cells to myeloma cells is inefficient and leads to the loss of potentially interesting clones. Secondly, screening of hybridoma colonies for antigen-specific mAbs is inefficient, often with less than 1% of colonies expressing antigen-specific IgG. Thirdly, hybridoma cells are unstable. Hybridomas often lose antibody expression over time, display inconsistent growth kinetics, and can produce a (problematic) mixed antibody product. A more efficient

method of isolating antibodies is to clone the antibody heavy and light chains directly from single antigen-specific B-cells[239]. Single B-cells are often sorted for antigen specificity by flow cytometry using fluorescent probes followed by RT-PCR. This technique has been developed in-house to isolate PfRH5-specific mAbs from clinical trial volunteers with great success[156]. Other groups have published similar protocols for use on mouse B-cells[186,240,241]. Isolating the heavy and light chains directly from B-cells circumvents all the disadvantages of hybridomas and allows recombinant mAbs to be produced in a controlled manner from CHO or HEK cell line systems. Single cell systems are also amenable to high throughput protocol design, enabling the screening of hundreds of B-cells in a single run. Further technological advances, in particular next-generation sequencing, are also starting to become mainstream with single cell deep phenotyping[242] and microfluidics combined with next-generation sequencing[243] being recently published.

Monoclonal antibodies can be used as tools for vaccine development in a number of ways. Antibodies can be used to determine if a vaccine candidate is folded in a biologically relevant conformation. Work with Respiratory Syncytial Virus (RSV) monoclonal antibodies showed that targets of neutralising antibodies were only present on the pre-fusion conformation of the F surface glycoprotein[178,179]. This pre-fusion state was found to be absent in the inactivated RSV vaccine, therefore a new stabilised pre-fusion F surface glycoprotein was designed that induces a neutralising antibody response[217]. In addition, mAbs can be used to map neutralising and non-neutralising epitopes on a particular protein, such as PfRH5[156]. This knowledge can then be used to generate second-generation vaccine candidates that induce a more focused immune response. Mapping of epitopes can be done crudely by producing

fragments of a protein and investigating mAb binding. I used this technique in Chapter 3 to identify regions of PfRIPR that were not targets of neutralising antibodies. A more detailed investigation requires structural techniques such as X-ray crystallography, cryo-EM or nuclear magnetic resonance (NMR) imaging. These techniques give atomic level detail of where the binding epitopes of more potent neutralising antibodies are located within PfRIPR. In addition, the structural information gleaned, such as antibody orientation, may provide hints as to a possible mechanism, such as preventing the RCR complex from contacting the erythrocyte surface.

A second use of monoclonal antibodies it to investigate intra-protein antibody synergy. When two neutralising antibodies bind to a protein, the combined response is often independent or additive, *i.e.* if two mAbs individually give 50% GIA at a given concentration, then their combined GIA would be 75% (50% for the first mAb plus 50% from the second mAb against the remaining 50% = 25%). However, if two mAbs act synergistically, then the total activity is greater than the sum of the two mAbs acting independently, *i.e.* if two mAbs individually give 50% GIA at a given concentration, then the combined GIA would be > 75%. In this case, by definition the action of one mAb must somehow improve the potency of the second mAb. Synergy between antibodies that bind different merozoite proteins (inter-antigen) has been firmly established[167,244] and synergy between PfRH5 mAbs (intra-antigen) was also recently idenitifed[156]. Notable in the study by Alanine *et al.* it was found that a mAb with no GIA, R5.011, could synergise with all neutralising mAbs. It did this by slowing the invasion of erythrocytes by merozoites, thereby allowing more time for neutralising mAbs to bind.

Since non-neutralising mAbs have been shown to have synergistic effects, it is possible that the PfRIPR EGF (5-8) vaccine candidate lacks important non-neutralising epitopes due to the design exclusively focusing on the target epitope regions of neutralising antibodies. This Chapter further explores PfRIPR as a vaccine candidate by developing new neutralising monoclonal antibodies against PfRIPR EGF (5-8), then using these antibodies to search for synergistic relationships between these and other anti-PfRIPR antibodies.

5.3 Monoclonal antibody discovery - hybridomas

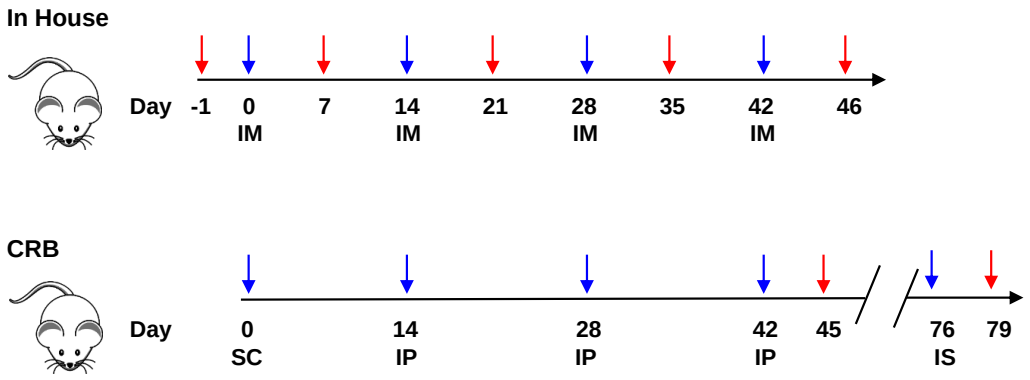
5.3.1 Antigen choice and immunisation strategies

With PfRIPR EGF (5-8) identified as the target of neutralising antibodies, I decided to use the VLP-based PfRIPR EGF (5-6), (7-8) and (5-8) vaccines to immunise mice for monoclonal antibody discovery. This was done to focus the immune response on the EGF-like domains and therefore increase the likelihood of identifying GIA positive monoclonal antibodies.

Two hybridoma programmes were run in parallel; the first was an in-house immunisation and hybridoma programme and the second was outsourced to Cambridge Research Biologics (CRB) (Figure 5.1A). CD1 and BALB/c mice were used for immunisations in house; these were immunised with either HBsAg-PfRIPR EGF (5-6) or HBsAg-PfRIPR EGF (7-8) at an equivalent equimolar dose to 2 μg of PfRH5. Animals were given four immunisations via intra-muscular injection at two-week intervals followed by a splenectomy four days post final boost. IgG titres were

monitored throughout the study by ELISA (Figure 5.2) to ensure the response had plateaued before the final boost.

Four BALB/c mice were immunised at CRB with 2 µg HBsAg PfRIPR EGF (5-8). Mice were initially immunised on day 0 by subcutaneous injection (SC) followed by intraperitoneal (IP) boosts on days 14, 28 and 42. Serum samples were then tested by ELISA and the highest responding mouse was then immunised with a fifth boost on day 76 by intrasplenic (IS) injection.



In house immunisations

Strain	Animal	Antigen	Dose (µg)	Adjuvant
Balb/c	1 – 3	HBsAg PfRIPR EGF (5-6)	0.47	Addavax™
	4 – 5	HBsAg PfRIPR EGF (7-8)	0.39	
CD1	1 – 3	HBsAg PfRIPR EGF (5-6)	0.47	
	4 – 5	HBsAg PfRIPR EGF (7-8)	0.39	

CRB immunisations

Strain	Group size	Antigen	Dose (µg)	Adjuvant
Balb/c	4	HBsAg PfRIPR EGF (5-8)	2.0	Complete & incomplete Freud's

Figure 5.1 – Mouse immunisation plan schedules.
In-house and CRB immunisation strategies for mAb production. Immunisations were intra-muscular (IM), sub-cutaneous (SC), intraperitoneal (IP) or intrasplenic (IS). Blue arrows represent immunisations and red arrows represent blood samples or splenectomy.

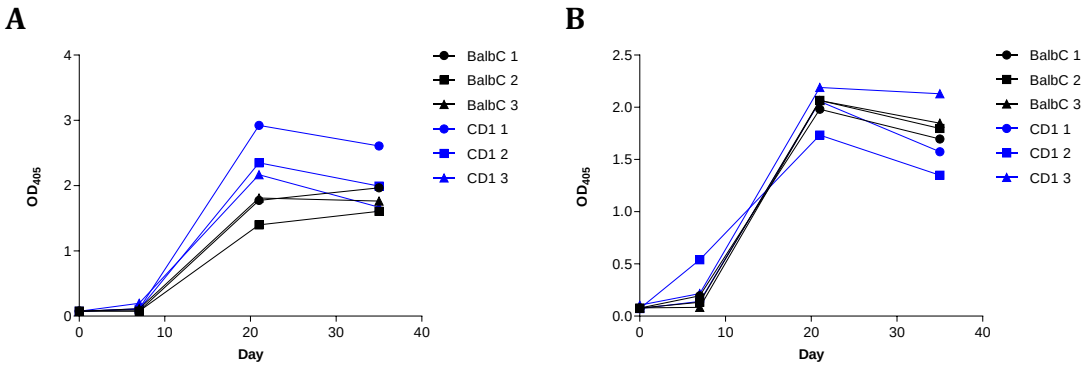


Figure 5.2 - OD ELISA titre for HBsAg-PfRIPR EGF (5-6) and HBsAg-PfRIPR EGF (7-8) immunised mice

A) OD ELISA titre for HBsAg-PfRIPR EGF (5-6) immunised mice up to day 35. **B)** OD ELISA titre for HBsAg-PfRIPR EGF (7-8) immunised mice up to day 35. Mouse serum samples all run at a 1:3000 dilution. Points represent mean OD_{405} of three repeats.

5.3.2 Hybridoma development and antibody production for in-house immunisations

With the immunisations complete, the animals were sacrificed and the spleens removed. B-cells were isolated using the STEMCELL™ technologies EasySep™ Mouse B Cell Isolation Kit. These B-cells were then fused to the SP2/0 mouse B-cell myeloma cell line using the STEMCELL™ technologies ClonaCell™-HY Hybridoma Kit. Cell fusions were plated out on semi solid media containing HAT (hypoxanthine-aminopterin-thymidine) selection medium and incubated for 10 days. B-cells that had successfully fused with SP2/0 cells grew into small colonies. The ClonePix was used to automate colony picking into 96 well plates containing growth media; in total 1,440 colonies were picked from two fusions. After a 3-day incubation supernatant from each plate was screened by ELISA against PfRIPR EGF (5-8). 42 colonies were identified as positive hits. These colonies were moved from the 96 well plates to 48 well plates. After a further 5 days of incubation the colonies were re-screened by ELISA against PfRIPR EGF (5-8) and also against monoFc-GFP to ensure that there was no cross reactivity with either the monoFc or the C-Tag. Only four positive

hybridomas remained after this screen; these were labelled mRi001, mRi009, mRi012 and mRi017. Each cell line was adapted to grow in media without HAT selection and moved into CELLine bioreactors for mAb production; supernatant from each CELLine was harvested weekly and stored prior to purification. Supernatant was purified monthly on a protein G column followed by a polishing step by SEC. It was discovered that only one hybridoma, mRi017, produced mAb that bound PfRIPR EGF (5-8); this mAb was re-labelled mRP021. mRi001, mRi009 and mRi012 were discarded.

The success rate for mAb production was surprisingly low, even for hybridomas. This was compounded by the loss of expression from three promising hybridoma clones. This emphasises the difficult in using hybridomas for high-throughput mAb discovery. The one mAb that was successfully generated, mRP021, was taken forward for further characterisation.

5.4 Monoclonal antibody discovery – single cell approaches

The hybridoma approach was successful in producing one new anti-PfRIPR antibody, however the process took over 6 months and had very poor yields. A more efficient method of antibody production, as outlined in the Introduction, is to clone the IgG genes out of antigen-specific single B-cells. This technique would allow 10s or 100s of antibodies to be isolated from a single spleen, circumventing the labour intensive hybridoma stages. As part of this PfRIPR monoclonal antibody development programme, I sought to set up a mouse single cell cloning approach to supersede the hybridoma approach.

5.4.1 Development of a flow cytometry protocol for antigen-specific mouse B-cells

The first step in the process was to reliably separate IgG producing mouse B-cells from vaccinated animals. B-cells were isolated from spleens and enriched using the EasySep™ Mouse Pan-B Cell Isolation Kit. Three cell markers were chosen to isolate IgG producing memory or follicular B-cells: the viability stain FVS780, anti-mouse IgG-FITC, and anti-B220-PECy7. B220, also known as CD45, is a B-cell surface receptor protein present on the majority of B-cell subsets. Using these three markers and a simple gating strategy (Figure 5.3) I could reliably sort single IgG producing B-cells.

Sorting single IgG producing B-cells allowed me to start developing the single cell PCR, however the primary challenge was the development of a probe that allowed sorting of antigen-specific B-cells.

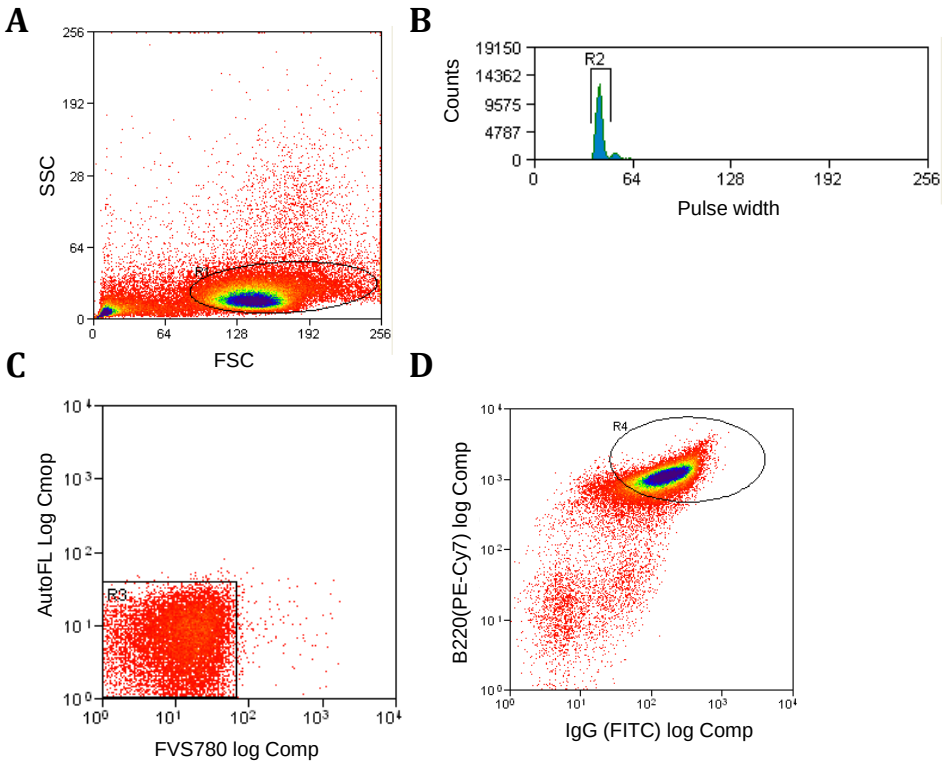


Figure 5.3 – Gating strategy for IgG producing B-cell isolation.
A) Side scatter (SSC) and forward scatter (FSC) of B-cell enriched samples. Circled population (R1) gated for analysis. **B)** Pulse width of R1. Gated population R2 taken forward. **C)** Viability stain FVS780 staining on R2. Gating performed on viable cells, R3. **D)** Representative flow cytometry gating of IgG-FITC and B220-PE-Cy7 positive cells.

The development of this single cell monoclonal antibody strategy was started early in the DPhil project; therefore, a fluorescently labelled PfRIPR EGF (7-8) probe was developed rather than a PfRIPR EGF (5-8) probe. To generate the probe, a biotin acceptor peptide (BAP) tag was cloned between the PfRIPR EGF (7-8) and the TEV protease site. The BAP tag is a 15 amino acid sequence that is targeted for biotinylation by the *E. coli* BirA biotin-protein ligase, this enzyme adds a single biotin molecule to the lysine in the BAP tag. The PfRIPR construct is then expressed in HEK293F cells alongside the enzyme BirA which mono-biotinylates the BAP tag. Biotinylated protein was then purified using the C-terminal C-Tag. Following purification, the monoFc domain was cleaved from the biotinylated protein using TEV protease as described in Chapter 3 Section 3.2. Probes could then be generated on the

day of flow cytometry by mixing a 4:1 ratio of mono-biotinylated PfRIPR EGF (7-8) to the streptavidin conjugated fluorophores PE or APC (Figure 5.4). This design is based on the probes used to single sort RH5 specific B-cells from human clinical trial samples[156].

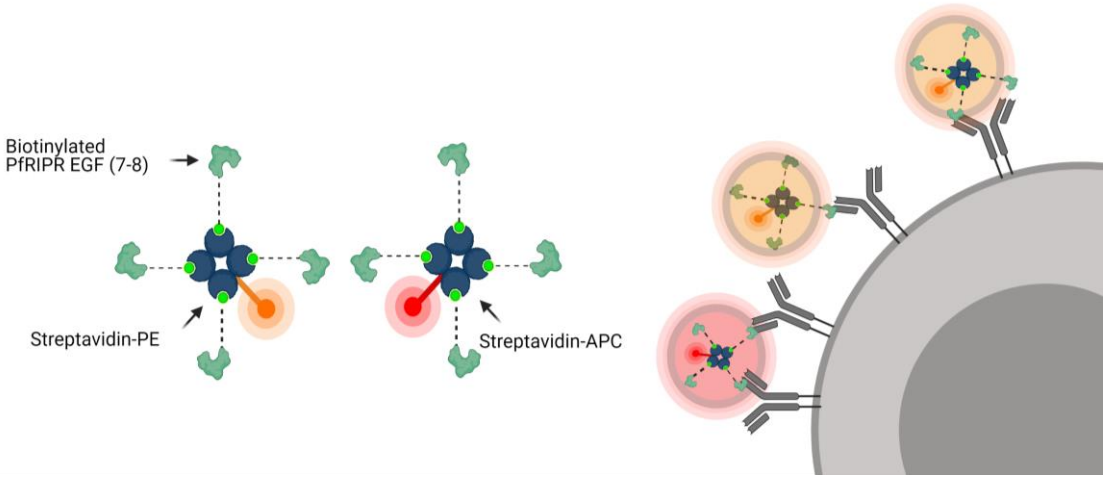


Figure 5.4 – Schematic of fluorophore conjugated PfRIPR EGF (7-8) probes.
Biotinylated PfRIPR EGF (7-8) forms tetramers with streptavidin bound fluorophores (left). Probes bind to antigen specific B-cells labelling them for dual colour sorting (right). Created with BioRender.com.

Probes were verified using mouse CompBeads bound to anti-PfRIPR EGF (7-8) purified IgG (Figure 5.5) to ensure the probes could bind antigen-specific IgG. A RH5-specific probe was used as a negative control. CompBeads contain two populations, one which binds mouse IgG and a second which does not. In Figure 5.5B & C it can be clearly seen that half of the bead population is stained with the appropriate PfRIPR EGF (7-8) APC or PE-Cy7 probe, indicating that my probes can bind antigen-specific IgG. No fluorescence was seen with either CompBeads with no IgG (Figure 5.5A) or CompBeads bound to anti-PfRH5 IgG (Figure 5.5D).

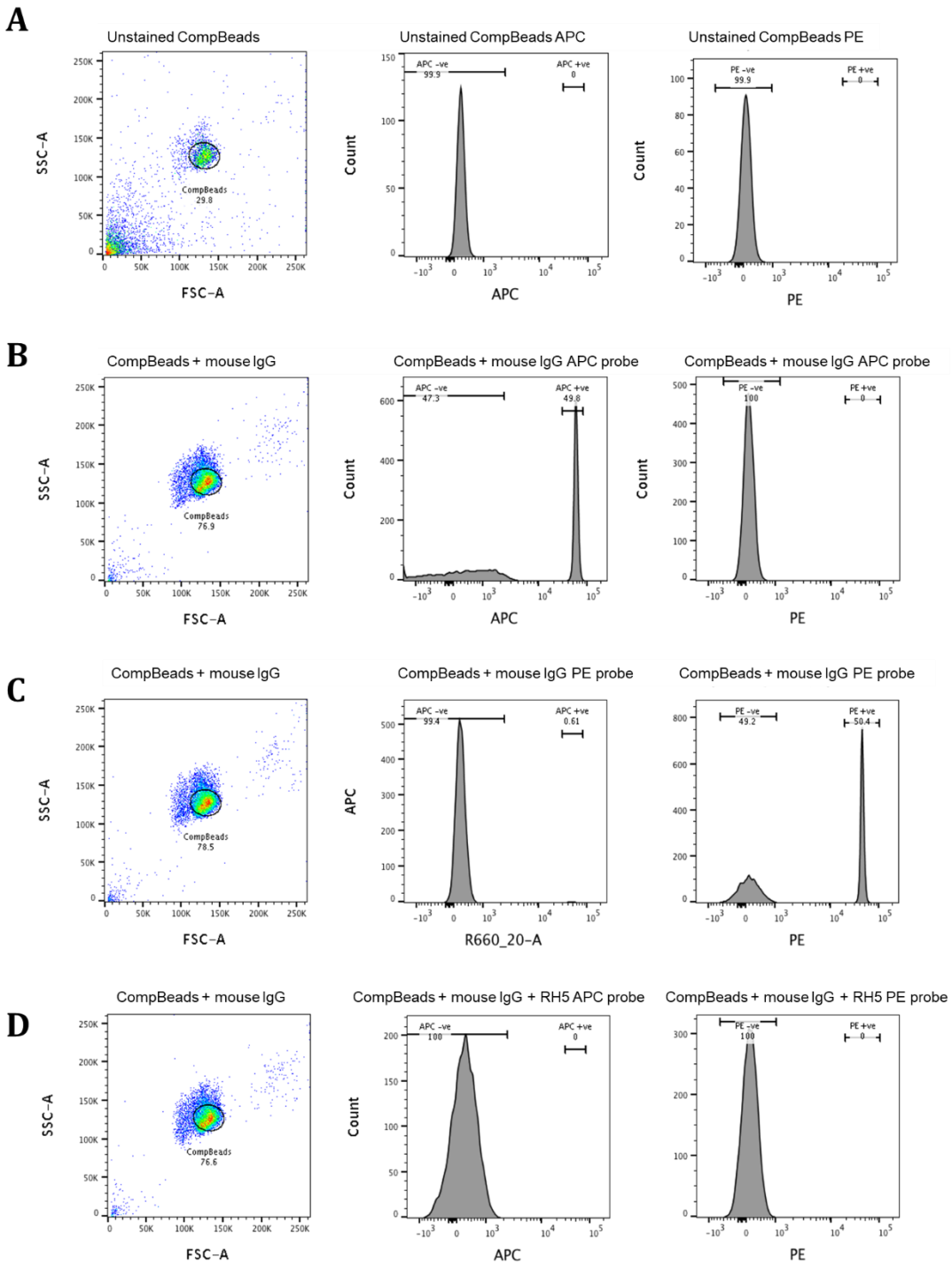


Figure 5.5 – PfRIPR EGF (7-8) probe verification on CompBeads bound to purified IgG from mice immunised with HBsAg PfRIPR EGF (7-8).

All panels from left to right: gating strategy on CompBeads, single channel gating on APC, single channel gating on PE-Cy7. **A)** Unstained controls. **B)** Mouse CompBeads stained with anti-PfRIPR EGF (7-8) purified IgG and PfRIPR EGF (7-8)-APC probe. **C)** Mouse CompBeads stained with anti-PfRIPR EGF (7-8) purified IgG and PfRIPR EGF (7-8)-PE probe. **D)** Mouse CompBeads stained with anti-PfRIPR EGF (7-8) serum, PfRH5-APC, and PfRH5-PE probes as a negative control.

Despite the PfRIPR EGF (7-8)-specific probes performing as expected with CompBeads, I had little success in recovering antigen-specific B-cells from an enriched B-cell population from an immunised mouse (Figure 5.6). No differences in APC & PE positive population frequency could be detected between HBsAg PfRIPR EGF (7-8) immunised mice and naïve mice suggesting that the probe was ineffective at identifying antigen specific B-cells in the immunised population. This strategy would require optimisation to consistently sort antigen-specific B-cells, however, due to the single cell PCR problems described in the next section this optimisation was halted.

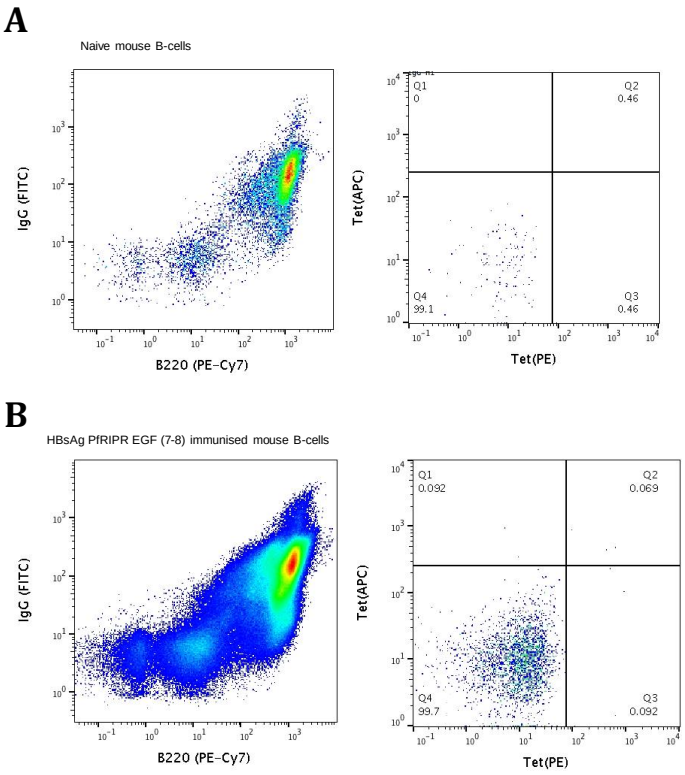


Figure 5.6 – Representative flow cytometry results.
A) Enriched B-cells from naïve mice stained for IgG and B220 (left panel). Naïve cells were used to set the gates for APC and PE negative cells (right panel). **B)** Enriched B-cells for HBsAg-PfRIPR EGF (7-8) immunised mice stained for IgG and B220 (left panel), gated for APC and PE (right panel). Cells negative for APC and PE staining present in Q4, single positive APC or PE cells in Q1 and Q3, APC & PE double positive cells in Q2.

5.4.2 Development of a single cell RT PCR for mAb isolation

The second key component of the single-cell mAb discovery platform is a robust single-cell PCR which can consistently amplify heavy and light chains. The PCR workflow was developed based on the successful workflow for isolating human anti-PfRH5 monoclonal antibodies from Alanine *et al.*[156]. This workflow takes a 96-well plate of sorted single B-cells through RNA extraction and reverse transcription to generate cDNA. The cDNA can then be stored at -20°C or used as a template for variable gamma heavy and kappa/lambda light chain region specific nested PCR. Nested PCR is required due to the small amount of starting cDNA from a single cell. Each PCR reaction can be run on an agarose gel and positive reactions cloned into our in-house expression vectors by standard restriction cloning. The in-house expression vectors contain the human constant heavy & light chains so resulting antibodies will be chimeric human-murine antibodies. Heavy and light chain pairs can then be co-transfected in HEK293F cells to test expression of each recombinant monoclonal antibody. A schematic of this process is shown in Figure 5.7.

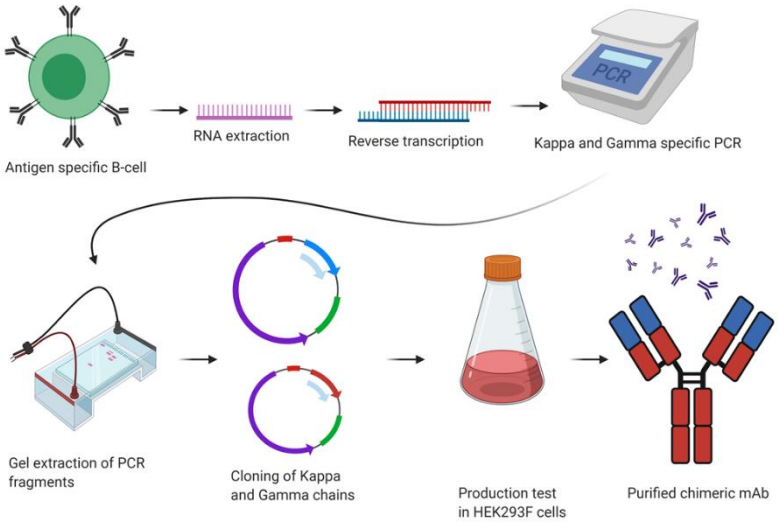


Figure 5.7 – Schematic representing the mAb cloning workflow.
From an isolated antigen specific B-cell to a purified chimeric monoclonal antibody. Created with BioRender.com.

The target of the single cell PCR is the variable heavy (V_H) and variable light (V_L) chains (Figure 5.8) on the Fab (fragment antigen binding) region. Once isolated, these sequences can then be cloned directly into a standard heavy / light chain constant region. Due to the high variability of the V_H and V_L regions, degenerate primers must be used in the PCR. Initially the primers and protocol from the Draper group's in-house hybridoma cloning protocol were tried, these primers were based on a publication by Crosnier *et al.*[241]. These primers were unsuccessful at amplifying the V_H and V_L regions from single cells. Subsequent attempts using the primers and protocols from Ho *et al.*[186] and the NIH (Elizabeth Potter, personal communication) also failed.

With large challenges still to be overcome in both the flow cytometry protocol and the single cell PCR, the focus of the project shifted to more promising avenues using the newly isolated anti-PfRIPR antibody mRP021.

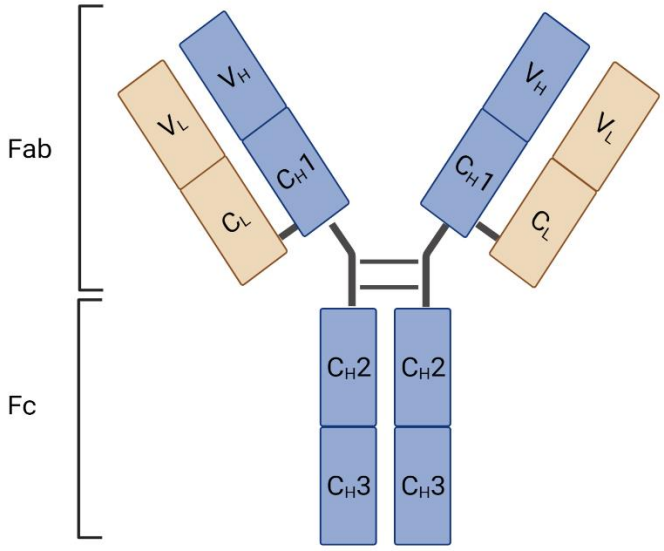


Figure 5.8 – Basic structure of an IgG molecule.
Created with BioRender.com.

5.4.3 Characterisation of mRP021

The new anti-PfRIPR mAb produced in-house using hybridoma technology, mRP021, and a second anti-PfRIPR mAb delivered by CRB, 7B10H3, were characterised by several methods. Both mAbs were tested for GIA, binding to PfRIPR protein fragments, binding to the RCR complex and antibody chain identity.

mRP021 was found to have a kappa light chain and murine IgG1 heavy chain using a Mouse Monoclonal Antibody Isotyping Kit (Sigma-Aldrich, data not shown). The EGF domains bound by mRP021 mAb were determined by a dot blot array against three overlapping EGF domain pairs and single EGF domains. mRP021 bound to EGF like domain 5 and did not bind denatured PfRIPR indicating that it binds a conformational epitope (Figure 5.9). mRP021 displayed positive GIA with an EC_{50} of 1.506 (± 0.841 mg/mL (Figure 5.10).

Disappointingly, 7B10H3 did not have any GIA (Figure 5.10B). In addition, no binding could be seen to either full-length PfRIPR or any PfRIPR fragment in a dot blot array (data not shown). This mAb was discarded and not used in further analyses.

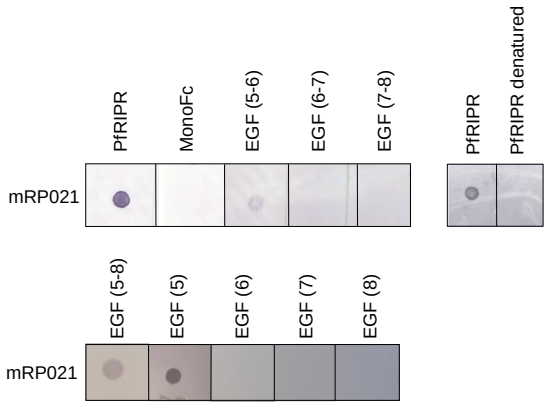


Figure 5.9 – Dot blot to determine the location of mRP021 binding.
mRP021 bound to EGF (5-6), this was narrowed down to EGF (5) once I produced single EGF domain reagents. mRP021 did not bind to denatured PfRIPR.

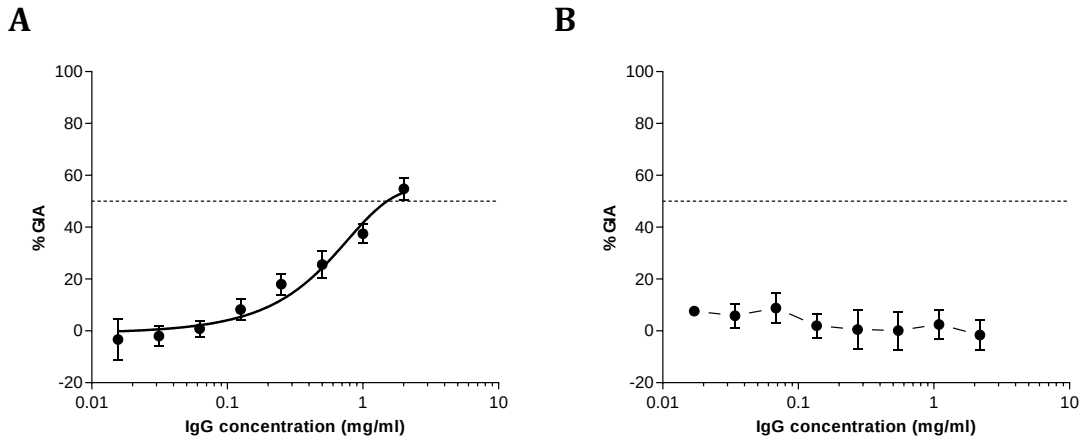


Figure 5.10 – Titration of the new anti-PfRIPR mAbs. Single-cycle growth inhibitory activity assay using *P. falciparum* 3D7 clone.

A) mRP021 **B)** 7B10H3. Each point is mean, all error bars represent SD. mRP021 dataset fitted with Richard's five-parameter dose-response curve with no constraints.

In preparation for structural studies, the binding of mRP021 to EGF (5) in solution was investigated using size exclusion chromatography; this was to ensure that a stable complex could be formed in a more experimentally relevant environment. mRP021 was incubated at an equimolar ratio with either PfRIPR EGF (5), (5-6) and (5-8) at room temperature for 1 hour before analysis by SEC. PfRIPR EGF (8) was used as a negative control.

Contrary to expectations, mRP021 did not bind to PfRIPR EGF (5) or PfRIPR EGF (5-6) in solution (Figure 5.11A & B) in SEC. This was not expected as mRP021 consistently bound to PfRIPR EGF (5) in dot blot arrays. To verify this finding, each SEC UV peak was checked by Western blot. The anti-Ctag antibody was used to detect the EGF domain proteins as this antibody is known to be very sensitive enabling the detection of very small amounts of protein that may not be visible via Coomassie staining. mRP021 was detected using a commercially available anti-mouse AP conjugated secondary. The results show that no bound EGF domains were detected in the shifted mRP021 peak. It is possible that a small difference in loading volume or flow rate caused a observed shift in the SEC UV peak; this, at first inspection, appeared to be a binding event but the Western blot showed to an artefact. mRP021 could, however, bind to PfRIPR EGF (5-8) in SEC, creating a reproducible shift in UV peak (Figure 5.12). PfRIPR EGF (5-8) was easily detected in the shifted mRP021 UV peak (Figure 5.12), this emphasises the need to run SDS-PAGE and Western blots of the UV peaks to verify the results obtained with SEC.

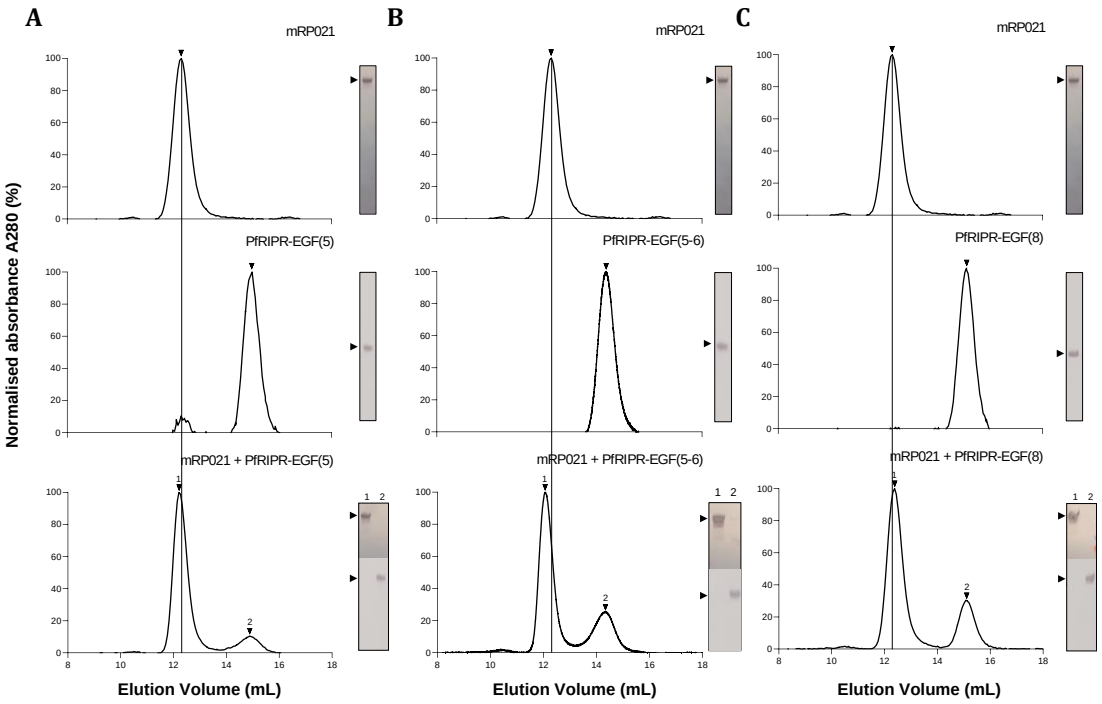


Figure 5.11 – SEC chromatograms of mRP021 binding to PfRIPR EGF (5), EGF (5-6), and EGF (8).

For all panels a solid black line is added from the mRP021 only peak to make the UV peak shift clearer. Black arrows indicate which UV peak was analysed by Western blot. **A)** Upper panel: mRP021 alone, SEC UV chromatogram and anti-mouse IgG western blot. Middle panel: PfRIPR EGF (5) alone, SEC UV chromatogram and anti-C-Tag western blot. Bottom panel: mRP021 and PfRIPR EGF (5), SEC UV chromatogram and merge of anti-mouse IgG anti-C-Tag western blots. **B)** Upper panel: mRP021 alone, SEC UV chromatogram and anti-mouse IgG western blot. Middle panel: PfRIPR EGF (5-6) alone, SEC UV chromatogram and anti-C-Tag western blot. Bottom panel: mRP021 and PfRIPR EGF (5-6), SEC UV chromatogram and merge of anti-mouse IgG anti-C-Tag western blots. **C)** Negative control. Upper panel: mRP021 alone, SEC UV chromatogram and anti-mouse IgG western blot. Middle panel: PfRIPR EGF (8) alone, SEC UV chromatogram and anti-C-Tag western blot. Bottom panel: mRP021 and PfRIPR EGF (8), SEC UV chromatogram and merge of anti-mouse IgG anti-C-Tag western blots.

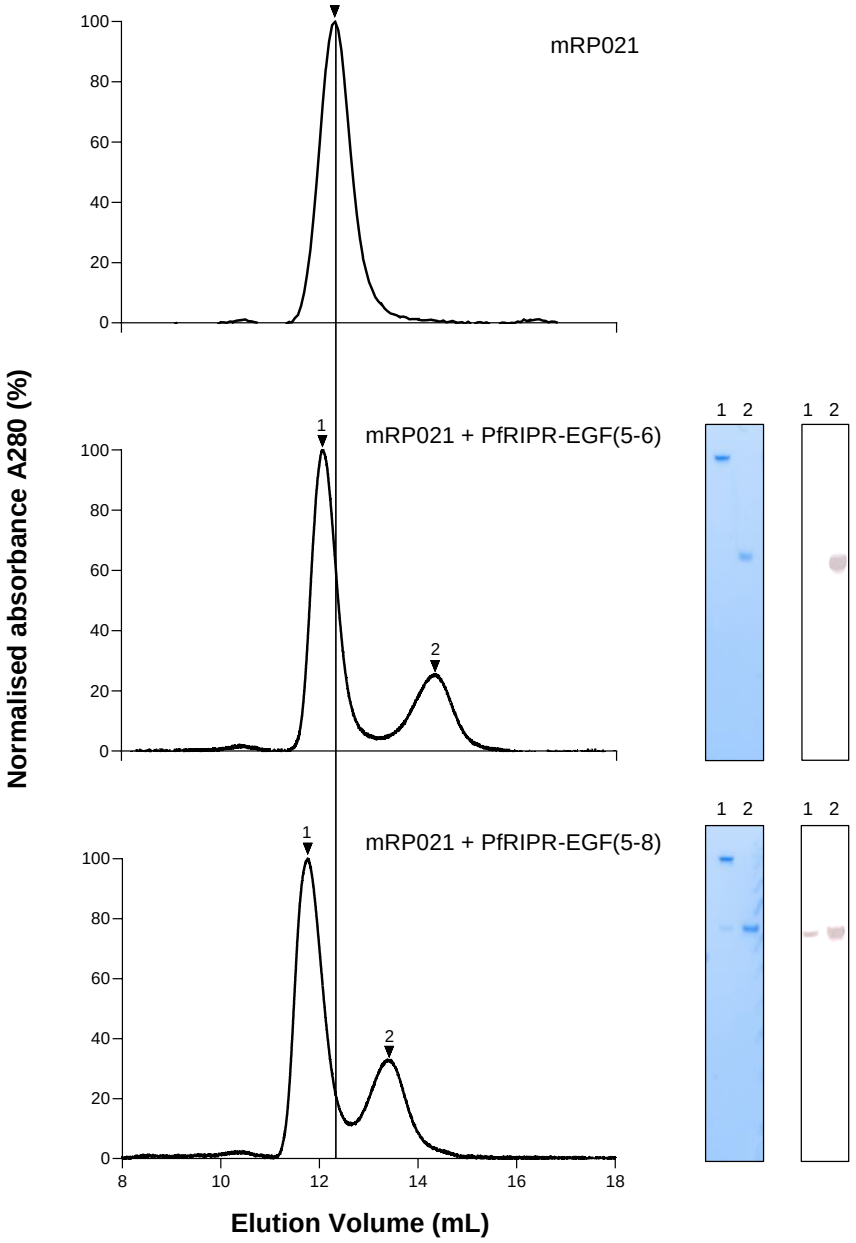


Figure 5.12 - SEC chromatograms of mRP021 binding to PfRIPR EGF (5-6) and PfRIPR EGF (5-8).

Upper panel: mRP021 alone, SEC UV chromatogram. Middle panel: mRP021 and PfRIPR EGF (5-6), SEC UV chromatogram, SDS-PAGE gel, and anti-C-Tag western blot to detect PfRIPR protein. Bottom panel: mRP021 and PfRIPR EGF (5-8), SEC UV chromatogram, SDS-PAGE gel, and anti-C-Tag western blot.

5.4.4 mRP021 and the RCR complex

Non-neutralising anti-PfRIPR mAbs were found to both bind the RCR complex and prevent the RCR complex forming in Chapter 3. In the same manner mRP021 was incubated overnight at 4°C with an equimolar ratio of PfRIPR, PfCyRPA and PfRH5. In addition, it was incubated overnight at 4°C with a pre-incubated mix of PfRIPR, PfCyRPA and PfRH5 which is known to have already formed the RCR complex. mRP021 bound the RCR complex forming a quaternary complex (Figure 5.13). This result suggests that disrupting the RCR complex is not a mechanism of protection against merozoite invasion of erythrocytes. This is consistent with data generated from both PfCyRPA and PfRH5 mAbs (Pulido & Ragotte, unpublished). It also suggests that only epitopes on PfRIPR that are exposed on the RCR complex are visible to the immune system *in vivo*.

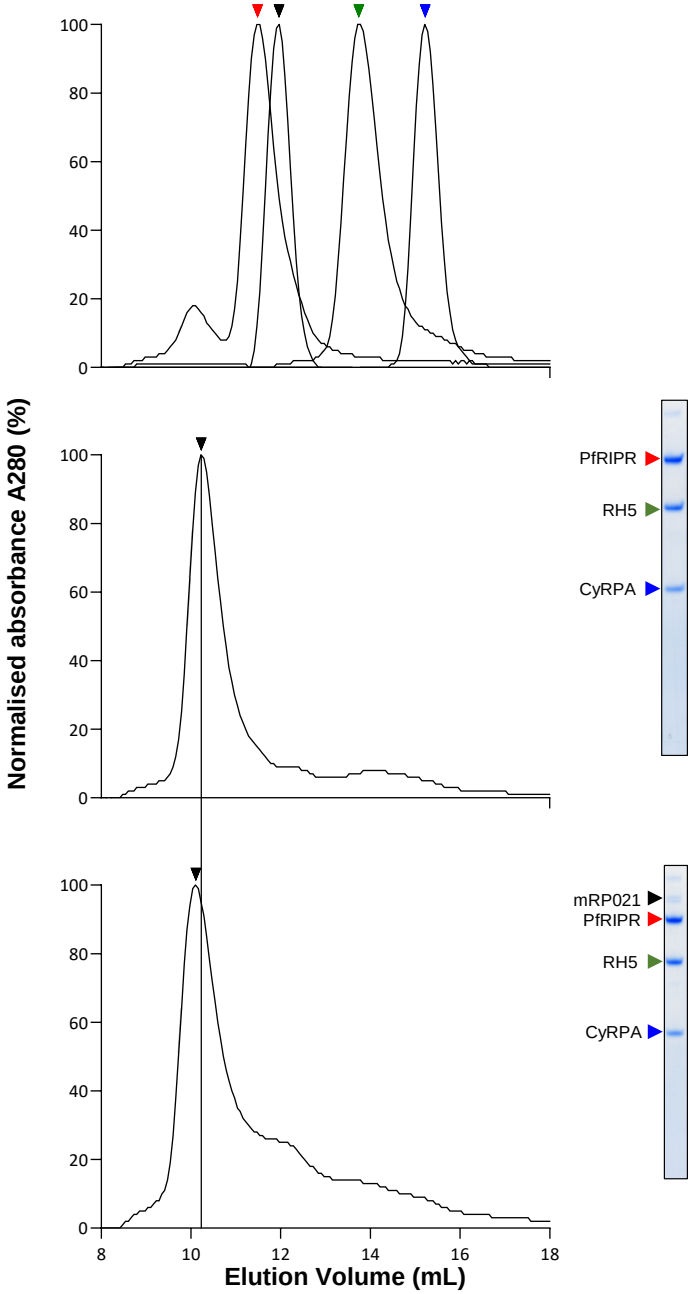


Figure 5.13 – SEC chromatograms of mRP021 binding to the RCR complex.
Top panel: Red arrow: PfRIPR, black arrow: mRP021, green arrow: PfRH5, blue arrow: PfCyRPA. Middle panel: The RCR complex reconstituted *in vitro*. SDS-PAGE gel with Coomassie staining of the indicated peak. Bottom panel: The quaternary complex of the RCR antigens and mRP021. SDS-PAGE gel with Coomassie staining of the indicated peak

5.4.5 mRP021 binding kinetics

The binding kinetics of mRP021 were determined using the Biacore X100 with a PfRIPR immobilised CM5 chip. mRP021 had a K_{on} of 2.92E+05 $M^{-1}s^{-1}$ which is in line with other PfRIPR mAbs (Chapter 3, Section 3.5.2), however the K_{off} was 0.026 s^{-1}, over 100-fold higher than the average non-functional PfRIPR mAb. This rapid dissociation is easily seen on the sensogram in Figure 5.14. The K_D for mRP021 is 8.92E-08 M, 10-fold lower than the average non-functional PfRIPR mAb. It is unusual that a GIA positive mAb has such a fast K_{off} as it was expected that a slow K_{off} rate is preferable as this would then block parasite entry to the erythrocyte for a longer period of time. On the other hand, a fast K_{on} rate may compensate for a fast K_{off} due to the speed of erythrocyte invasion as suggest by Alanine *et al.* in their analysis of PfRH5 mabs[156]. A rapid K_{off} rate was also seen for a CyRPA mAb; Cy.004 (Rob Ragotte, pending publication). It was found that K_D was improved by 35-fold (3.28E-8 M compared to 1.18E-6 M) by running the SPR in a calcium rich media, and the X-ray crystallography structure then showed that the Cy.004 epitope contains a calcium ion. mAbs that bind via ions are not unknown[245] but they are rare. Until Cy.004 no calcium dependent anti-malaria antibodies had been identified. Given the similarities in binding kinetics between mRP021 and Cy.004 I decided to examine the binding of mRP021 to PfRIPR in the presence of calcium. EGF domains are known to bind calcium ions so it was possible that calcium may be important in mAb binding or PfRIPR conformation. The results (Figure 5.14B) show that the addition of calcium had no effect on the K_D or K_{off}.

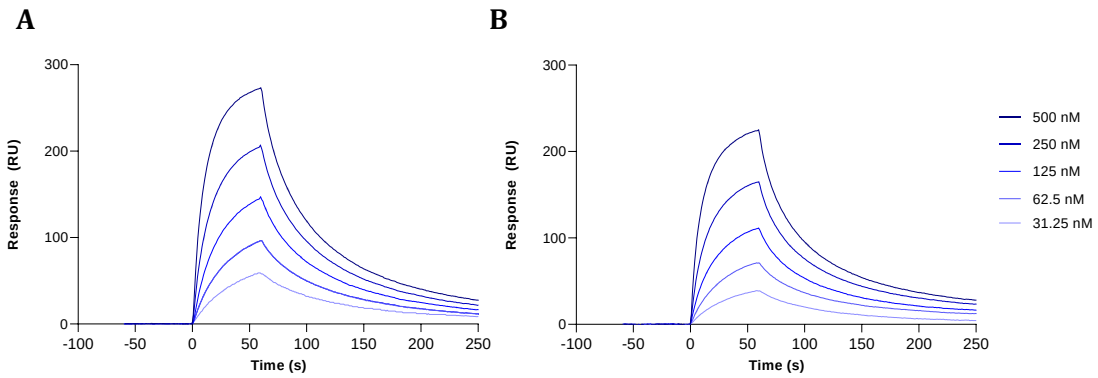


Figure 5.14 - Multi-cycle kinetic SPR sensorgrams of mRP021.
A) mRP021 run on a PfRIPR CM5 chip in PBS + 0.05% P20. **B)** mRP021 run on a PfRIPR CM5 chip in TRIS + 1mM $CaCl_2$ + 0.05% P20. The following conditions were used for each run: 60s contact time with mAb starting at 500nM and subsequently halving, a dissociation time of 240s followed by a glycine regeneration step of 30s (regeneration step not shown). K_D values calculated using a 1:1 Langmuir binding model.

5.5 Intra-PfRIPR synergistic antibody effects

It is known that monoclonal antibodies which have no GIA activity can potentiate the action of other antibodies[156] through mechanisms such as slowing down the merozoite invasion process thus giving neutralising antibodies more time to act. It is possible that there are epitopes on the PfRIPR protein that are non-neutralising but can synergise with neutralising mAbs. Two strategies were devised to look for intra-antigen synergistic interactions between non-functional epitopes and mRP021.

5.5.1 Failure of mRP021 hybridoma

mRP021 was going to be used to investigate synergy within the PfRIPR molecule. Unfortunately, when this experiment was attempted mRP021 gave no GIA at any concentration (Figure 5.15B). A second batch of mRP021 repeated in isolation also gave no GIA (Figure 5.15C). When compared, the original GIA positive mAb and new batch of mRP021 bound the same protein fragments in a dot blot array (data not shown) and gave the same K_D when assessed by SPR (Figure 5.15D & E). It is unclear why the new batch of mAb cannot prevent merozoite invasion whilst maintaining the

same binding characteristics in other assays. mRP021 could not be used in future assays since none of the original GIA positive batch was available.

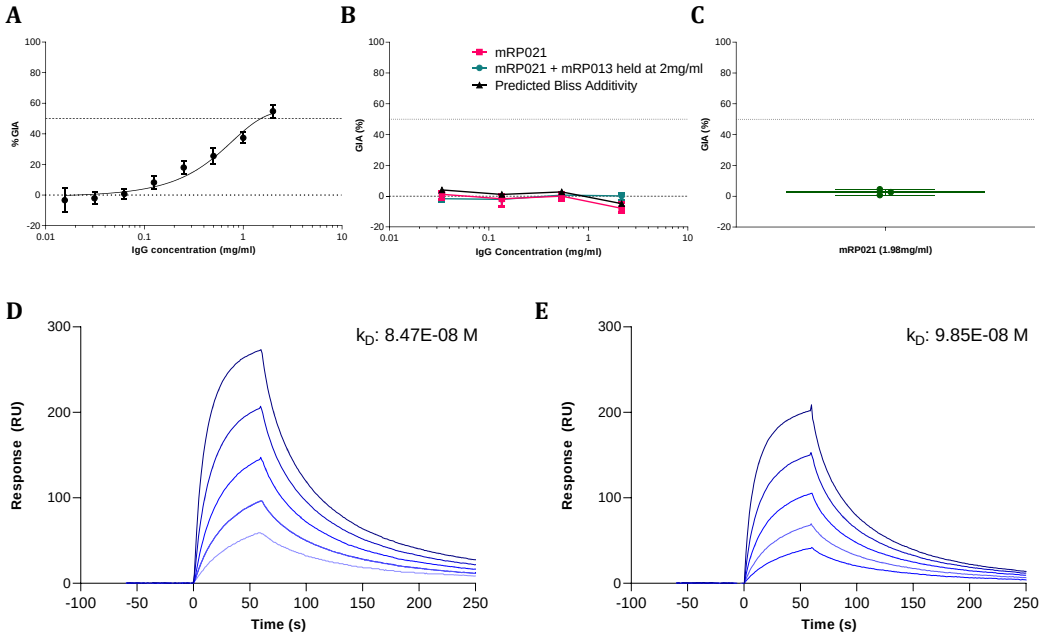


Figure 5.15 – Original and new mRP021 batches tested by GIA assay and SPR. mRP021 single-cycle GIA assay results with purified mAb with *P. falciparum* 3D7 clone**. A)** The original batch of mRP021 generated in late 2019 had an EC_{50} of 1.506 mg/mL. **B)** Initial dilution curve with the new batch of mRP021 and mRP013; mRP021 has no GIA at any concentration. **C)** The new batch of mRP021 tested at 1.98 mg/mL, no GIA was seen. **D)** SPR sensor trace of the new batch of mRP021 that has no GIA. **E)** SPR sensor trace of the original batch of mRP021 that had GIA. The following conditions were used for each run: 60s contact time with mAb starting at 500nM and subsequently halving, a dissociation time of 240 s followed by a glycine regeneration step of 30 s (regeneration step not shown). Buffer: PBS + 0.05% P20. K_D values calculated using a 1:1 Langmuir binding model.

In the meantime, a second GIA positive mAb, mRP012, was generated by Leidos Inc. as part of a separate collaboration. Using a dot blot array, I determined that this mAb bound to a linear epitope in the loop region between EGF 6 and EGF 7 (Figure 5.16A). The kinetic parameters of this mAb were determined by SPR using a PfRIPR CM5 chip (Figure 5.16B). This mAb has a K_{on} of 3.72E+05 M^{-1} s^{-1}, a K_{off} of 1.21E-04 s^{-1}, and a K_D of 3.24E+10 M. Despite the higher K_D and K_{off} than mRP021, the GIA activity of mRP012 is much lower; the EC_{50} value could not be determined due to the low GIA at

2mg/mL (Figure 5.16C). Despite the lower activity, mRP012 is still suitable for synergy studies since it has some positive GIA and can be made recombinantly ensuring consistency across batches.

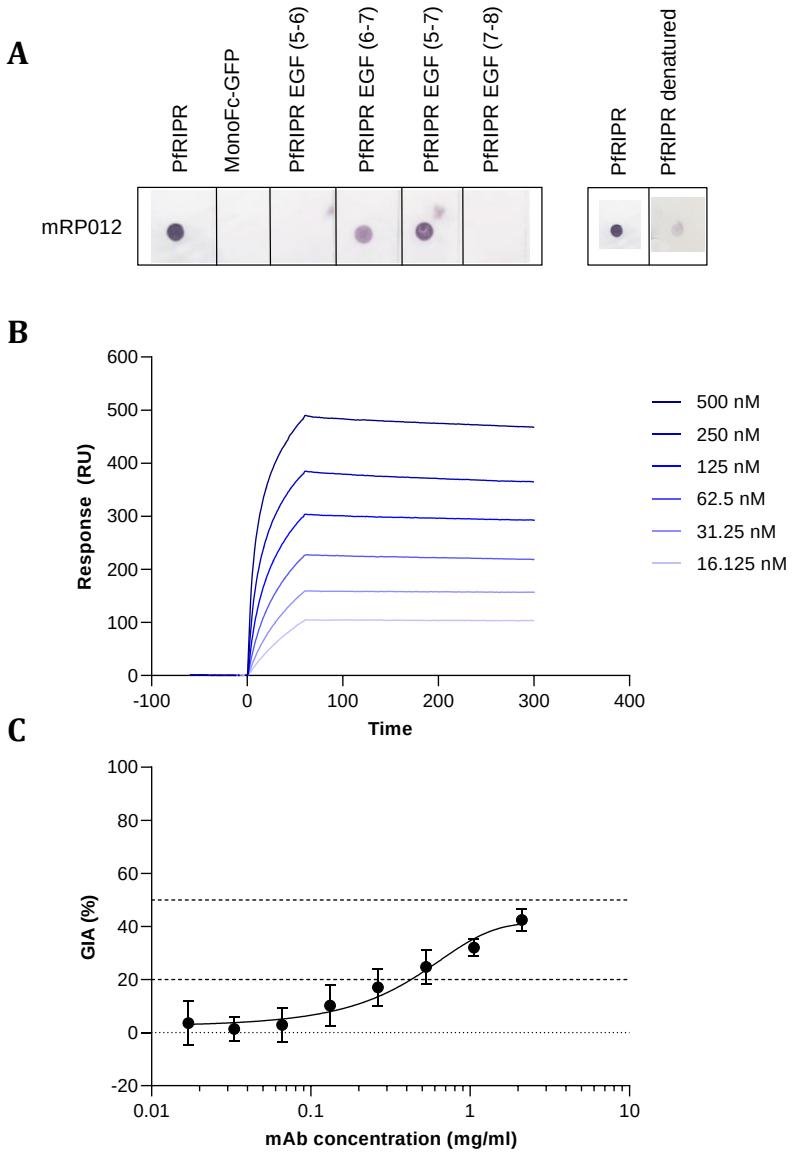


Figure 5.16 – Characterisation of anti-PfRIPR mAb mRP012.
A) Dot blot of mRP012 using PfRIPR protein fragments. MonoFc-GFP was used a negative control. PfRIPR was denatured by heating PfRIPR for 10 minutes at 90°C. **B)** SPR sensor trace of mRP012. The following conditions were used for each run: 60s contact time with mAb starting at 500nM and subsequently halving, a dissociation time of 240s followed by a glycine regeneration step of 30s (regeneration step not shown). Buffer: PBS + 0.05% P20. **C)** mRP021 titration in a single cycle GIA assay with *P. falciparum* 3D7 clone. Points are mean with SD, n=3. dataset fitted with Richard's five-parameter dose-response curve with no constraints.

5.5.2 Investigating synergy using non-functional PfRIPR monoclonal antibodies and mRP012

Intra-PfRIPR synergistic antibody effects were first investigated using the GIA-positive mAb mRP012 and five GIA-negative anti-PfRIPR mAbs: mRP006, mRP013, mRP016, mRP017 and mRP018. Each monoclonal was first assessed in isolation at close to 2 mg/mL to establish a baseline GIA result. mRP012 gave an average GIA result of 28% whereas each of the five GIA-negative mAbs gave no discernible GIA. From these two baseline results Bliss' additivity can be calculated for each mAb pair, this is the predicted additive (i.e. independent) GIA outcome of the two mAbs. mRP012 at 2 mg/mL was then mixed with 2 mg/mL of each of the GIA-negative mAbs in turn. Each mAb was only tested at a single concentration rather than at multiple concentrations due to a lack of reagents after the failed synergy experiment run with mRP021.

No synergistic activity was detected with any of the GIA-negative monoclonal antibodies in combination with mRP012 (Figure 5.17). This was not too surprising given the small sample size of GIA-negative mAbs and the lack of information surrounding the mAbs' epitopes. It is also likely that these non-neutralising mAbs cannot bind PfRIPR as it is presented by the merozoite *in vivo* (i.e. their epitopes are not exposed). mRP017 and mRP018 could not bind the RCR complex *in vitro* (Chapter 3, Section 3.5.3) making it extremely unlikely that they bind epitopes exposed *in vivo.* mRP003, mRP06 and mRP013 could bind the RCR *in vitro,* therefore the RCR may be presented in particular orientation *in vivo* occluding these mAbs epitopes or these mAbs may be truly non-functional. In the light of these results, a second broader approach was needed to investigate intra-PfRIPR antibody synergy.

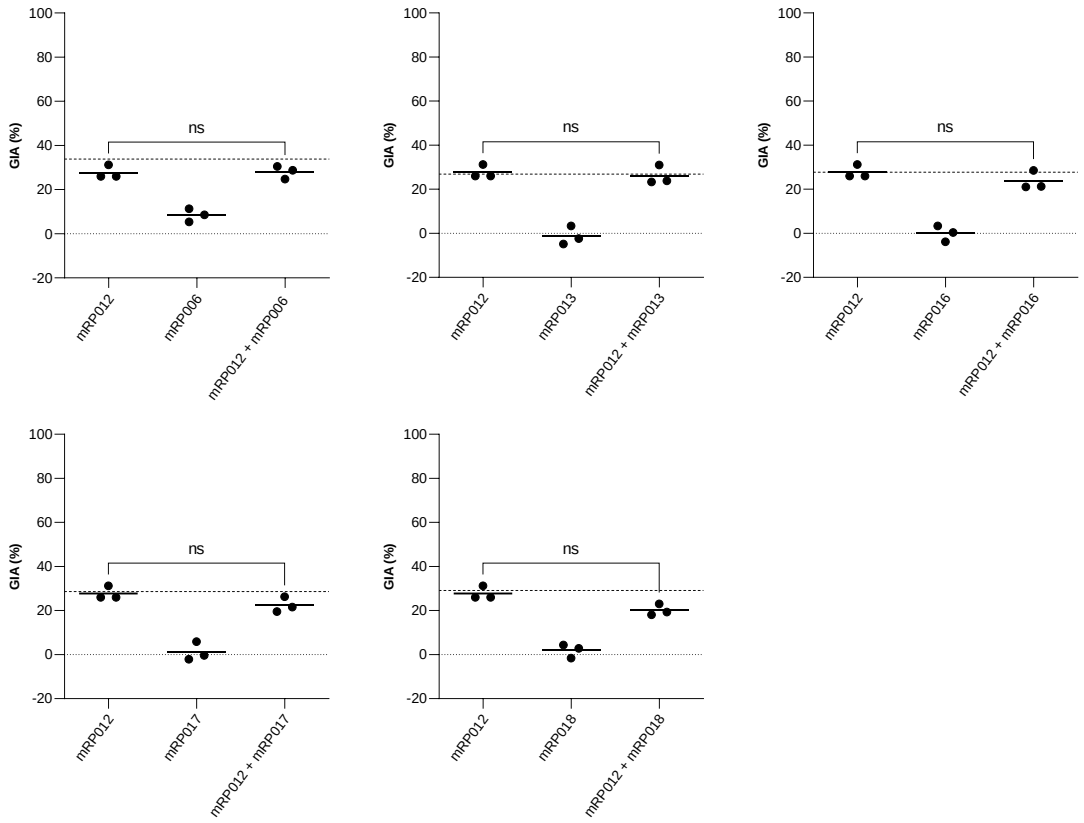


Figure 5.17 – GIA data of mRP012 tested in combination with non-neutralising anti-PfRIPR antibodies.

mRP012 was held at 2.1mg/mL and run in combination with the following non-neutralising mAbs: From left to right: mRP006, 2.11 mg/mL; mRP013, 2.02 mg/mL; mRP016, 1.89 mg/mL; mRP017, 2.25 mg/mL; and mRP018, 1.65 mg/mL. The hatched line on each graph shows the predicted Bliss' additivity for each combination. Each point is a single replicate, black bars indicate mean values. Significance was determined by Kruskal-Wallis with Dunn's correction for multiple comparisons, ns = non-significant. The data were analysed as a whole then split up for display for clarity.

5.5.3 Investigating synergy using PfRIPR EGF (5-8) depleted rabbit IgG and mRP012

Searching for synergy using monoclonal antibodies is akin to searching for a needle in a haystack. Since I had little success generating new monoclonal antibodies, a strategy was devised that may offer insight into synergy with non-neutralising epitopes, albeit at lower resolution. Purified IgG from rabbits immunised with full-

length PfRIPR in Chapter 3 could contain synergistic but GIA-negative antibodies against non-EGF (5-8) epitopes that were not detected in the protein fragment GIA-reversal studies. To isolate these non-neutralising antibodies, a PfRIPR EGF (5-8) affinity column was generated by coupling PfRIPR EGF (5-8) to a HiTrap NHS-Activated HP affinity column (Cytiva) via the amide groups on PfRIPR EGF (5-8) lysine moieties (Figure 5.18). The anti-PfRIPR EGF (5-8) antibodies can thus be removed from the purified IgG mixture using the affinity column leaving two polyclonal antibody pools; the PfRIPR EGF (5-8) depleted pool and the PfRIPR EGF (5-8)-specific pool.

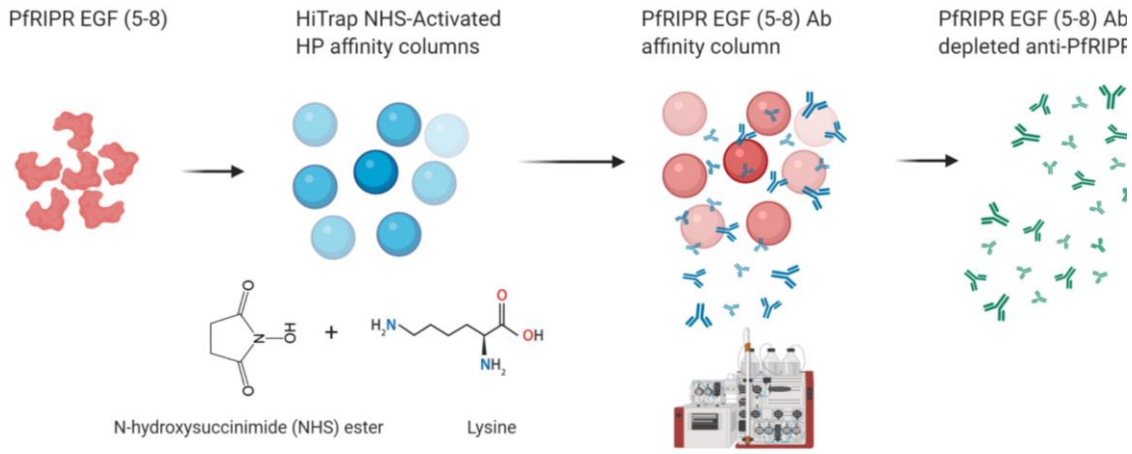
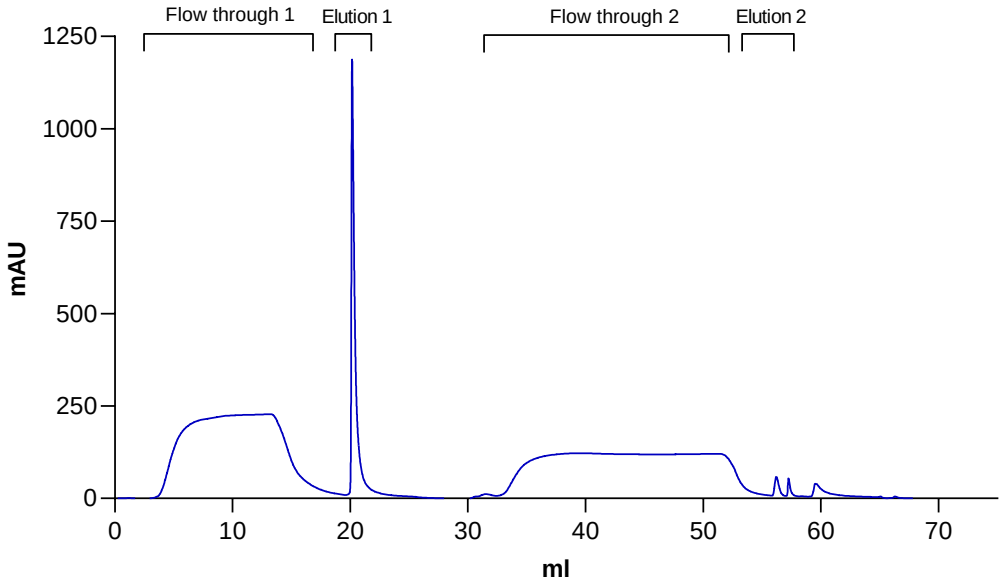


Figure 5.18 – Schematic of PfRIPR EGF (5-8) antibody depletion from polyclonal anti-PfRIPR antibodies.
PfRIPR EGF (5-8) was covalently bound to an activated NHS column by the formation of a stable amide bond with the primary amines of lysine residues. Anti-PfRIPR purified IgG (blue) is then flowed over the PfRIPR EGF (5-8) affinity column using the AKTA pure system. The unbound polyclonal antibody mix is thus depleted of any PfRIPR EGF (5-8) binding antibodies (green). Created with BioRender.com.

To ensure complete removal of PfRIPR EGF (5-8)-specific antibodies, the anti-PfRIPR polyclonal antibody mix was run over the column twice (Figure 5.19A). Very little antibody was collected in the second elution implying that the majority of the PfRIPR EGF (5-8) antibodies had been removed in the first round of purification. A dot blot array with full-length PfRIPR, PfRIPR EGF (3-4), EGF (5-8) and PfRIPR CTD was used

to check the specificity of the purification (Figure 5.19B). The PfRIPR EGF (5-8) IgG fraction cross reacted with a number of fragments implying either non-specific antibody binding or a contaminated preparation. The PfRIPR EGF (5-8) depleted IgG fraction, however, showed no binding to PfRIPR EGF (5-8) demonstrating that all PfRIPR EGF (5-8) binding, and hopefully therefore all GIA positive antibodies, had been removed from the polyclonal antibody mix.

A



B

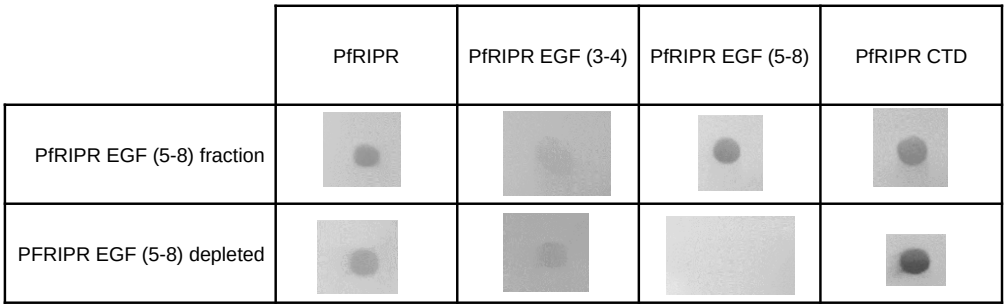


Figure 5.19 – Depletion and dot blot array of polyclonal antibody mixtures.
A) UV trace from the AKTA during antibody depletion. The flow through represents un-bound IgG and the elution peaks represent IgG bound to the PfRIPR EGF (5-8) column. **B)** Dot blot of the two polyclonal mixtures against full-length PfRIPR and fragments. PfRIPR, PfRIPR EGF (3-4) and PfRIPR CTD were included as controls.

mRP012 was once again used as the GIA-positive mAb in this set of experiments. Experimental conditions were set as similar as possible to the mAb synergy experiments by using 2 mg/mL of mRP012 and 2 mg/mL of purified IgG fractions. As expected the PfRIPR EGF (5-8) depleted rabbit IgG fraction gave no GIA (Figure 5.20), once again confirming that all of the targets of neutralising antibodies are contained within the EGF (5-8) fragment; mRP012 gave a baseline GIA of 28%. The combination of mRP012 and PfRIPR EGF (5-8) depleted IgG fraction resulted in a >2-fold increase in GIA to 67.4%. This result was significantly higher than the GIA result from PfRIPR EGF (5-8) fraction and not significantly different from the control anti-PfRIPR purified IgG. This suggests that intra-PfRIPR synergistic antibody interactions are playing a role in the inhibition of merozoite invasion mediated by anti-PfRIPR IgG. It is likely then that PfRIPR EGF (5-8) based vaccines are underperforming relative to a 'perfect' PfRIPR-based designer vaccine.

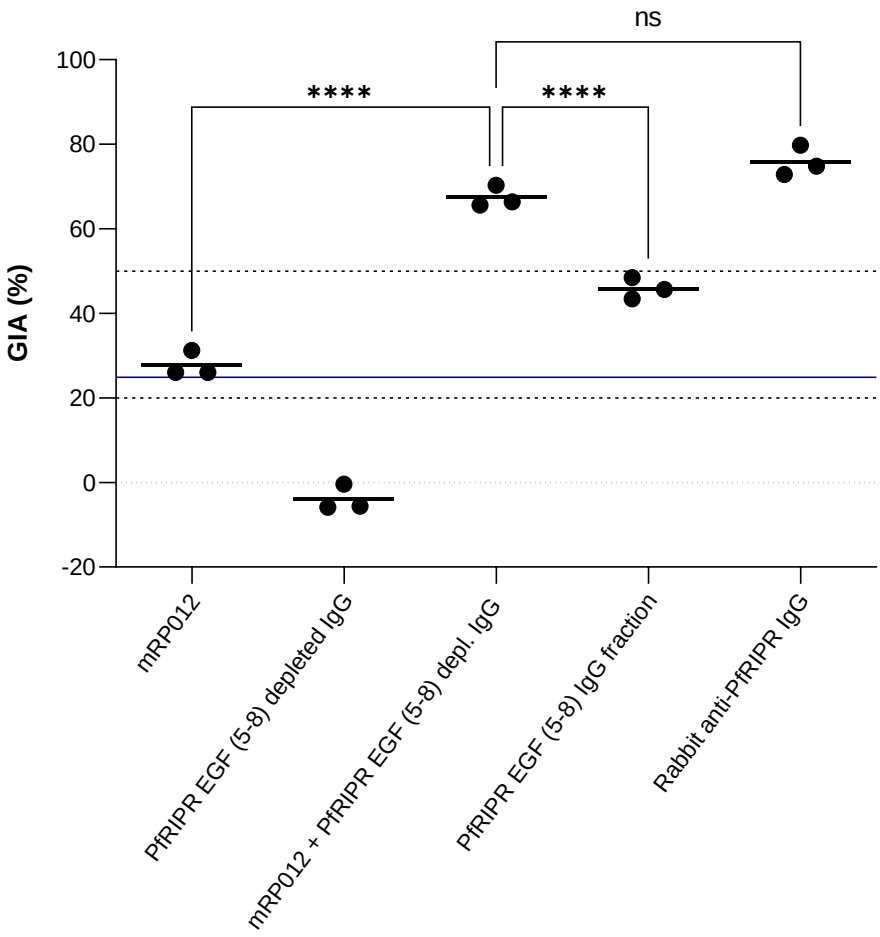


Figure 5.20 - GIA data of mRP012 tested in combination with PfRIPR EGF (5-8) depleted IgG.

mRP012 was held at 2.1 mg/mL for all experiments. PfRIPR EGF (5-8) depleted IgG and PfRIPR EGF (5-8) IgG fractions were run at 2.0 mg/mL. Rabbit anti-PfRIPR IgG was held at 3.0mg/mL. The blue line on the graph shows the predicted Bliss' additivity for mRP012 and the PfRIPR EGF (5-8) depleted IgG. Each point is a single replicate, black bars indicate mean values. Significance was determined by one-way ANOVA with Bonferroni's correction for multiple comparisons, ns = non-significant, **** = $p<0.0001$. Select statistical results are annotated for clarity.

5.6 Discussion

This Chapter had two primary aims: firstly, generate new GIA positive anti-PfRIPR monoclonal antibodies; secondly, investigate intra-PfRIPR antibody synergy with a view to improving the design of existing PfRIPR EGF (5-8)-based vaccines.

The development of new monoclonal antibodies against PfRIPR EGF (5-8) proved challenging with only one mAb, mRP021, successfully isolated. Even for a hybridoma based method this success rate is low compared to similar screens performed in the Draper group. It is unclear whether this was an experimental problem leading to low viability of B-cells or whether B-cells producing anti-PfRIPR EGF (5-8) antibodies are rare. A second hybridoma based antibody screen conducted at CRB also failed to deliver a functioning monoclonal antibody. It is possible that the immunisation regimen with a HBsAg conjugated antigen is sub-optimal for the generation of IgG producing B-cells, but this seems unlikely given that VLP vaccines are potent B-cell activators[219,220] and the VLP vaccines induced strong ELISA responses from vaccinated animals. It is possible that this was just a string of bad luck.

A second method for antibody generation based on single cell approaches was also investigated. The ability to sort individual antigen-specific B-cells should circumvent the problems of hybridoma manufacturing, such as the inefficient B-cell fusion step, and also allow the screening of hundreds of thousands of B-cells in a single experiment. This method suffered at two critical points. Firstly, more optimisation of the antigen-specific B-cell sort is required. The inability to sort antigen-specific cells suggests that too little of the tetrameric probe had formed or the concentration of probe in the assay was too low. Alternatively, there may have been a lack of antigen specific B-cells generated by the VLP based vaccine. There are suggestions that repeat

immunisations with VLP vaccines is sub-optimal for B-cell proliferation (Pulido & King– unpublished) therefore immunisation with a higher quantity of protein rather than VLP may be more successful for antibody generation. Secondly the single B-cell PCR required optimisation as neither the V_H or V_L chains could be amplified from the cDNA consistently. Since the assay requires a paired V_H and V_L to be amplified from the same sample, high PCR efficiency is key. Monoclonal antibodies are invaluable tools for structural biology and vaccine design, therefore the ability to quickly generate a panel of mAbs is highly advantageous. Optimising this single cell approach in mice will be critical for further investigations of PfRIPR-based vaccines. Unfortunately, there was insufficient time in this project to fully develop this workflow.

The one functional mAb developed in this project binds to PfRIPR EGF (5) and had reasonably weak GIA: EC_{50} of 1.5 mg/mL. The second mAb, mRP012, produced by Leidos Inc. bound PfRIPR EGF (6-7) and displayed weaker GIA with <50% GIA at 2 mg/mL. These mAbs confirm the overall hypothesis of this Thesis, that the targets of neutralising mAbs bind within EGF (5-8), however the GIA was lower than expected. Two previously published PfRIPR mAbs by Healer *et al*[166], 1G12 and 5G6 which bind EGF (7), had lower EC_{50} values of 0.35 and 0.8 mg/mL respectively; however these were analysed by two-cycle GIA so not directly comparable and this assay format can inflate or amplify the measured GIA. The PfRIPR specific EC_{50} of purified IgG from animals immunised with PfRIPR is around 0.5 mg/mL; it was unusual therefore that the neutralising mAbs (identified by us and others) all performed worse than the polyclonal IgG. This finding, and the underwhelming performance of PfRIPR EGF (5-

8) based vaccines in Chapter 4, led me to investigate if synergistic intra-antigen antibody interactions were important for PfRIPR.

No synergy was detected using the panel of GIA-negative monoclonal antibodies from Chapter 3. This was not unexpected due to the small number of antibodies assessed and the size of the PfRIPR protein. However, strong synergy was detected using PfRIPR EGF (5-8) depleted purified IgG. The resulting GIA was considered synergistic as it was greater than the predicted additive responses as calculated using the Bliss' additivity formula which assumes each antibody functions independently. This is an imperfect prediction because it can fail depending on the dose response curves of the antibodies tested leading to an antibody apparently synergising with itself. These dose effects have been seen with PfCyRPA antibodies where lower concentrations of anti-PfCyRPA antibodies show additive effects. However, the same combination of antibodies tested at a higher concentration demonstrated synergistic effects[167]. Due to a scarcity of reagents, each PfRIPR mAb combination and purified IgG combination was only tested at a single concentration. This may not give a complete picture of the synergistic relationship and lead to either an under or overestimation of the synergy. I am confident, however, that we are seeing synergy as each experiment contained one GIA-positive component and one GIA-negative, therefore the GIA should only, in theory, be affected by the dose of one component if the relationship was additive.

The data generated with mRP021 and mRP012 also add some clarity to the results in previous Chapters. mRP021, and the published GIA-positive anti-PfRIPR mAbs 1G12 and 5G6, all bind to the RCR complex forming a quaternary complex. This strongly supports the notion that anti-PfRIPR neutralising mAbs form complexes with the RCR likely due to those epitopes being exposed *in vivo*. This refutes the hypothesis that

merozoite invasion is prevented by the disruption of the RCR complex but sadly it does not present an obvious alternative hypothesis. The synergy data also help to understand the results obtained from the immunisations of multiple RCR proteins in Chapter 4. The results suggested synergistic interactions between antigens but this was not yet deconvoluted. The data presented here now suggest that in addition to published inter-protein synergy[167] and intra-PfRH5 syngery[156] there is also intra-PfRIPR synergy. These interactions will be difficult to untangle and harder to incorporate into a vaccine design but will hopefully yield a far more potent blood-stage vaccine that previously envisaged.

This Chapter has only scratched the surface of further investigations into non-neutralising epitopes of PfRIPR. Work has been slowed by the lack of good monoclonal antibodies and the Covid-19 pandemic, however the limited data generated here suggest that there is still plenty more to be investigated. These results highlight the importance of taking a step back and viewing the neutralising epitopes in the context of the protein and protein complex, rather than focusing exclusively on a narrow goal such as neutralisation.

Chapter 6 - Conclusions and future directions

6.1 Summary of output

The work described in this Thesis represents, to the best of my knowledge, the most thorough investigation of PfRIPR as a candidate blood-stage malaria vaccine to date. The tools developed in this work will aid future investigations into PfRIPR and the findings will hopefully lead to the clinical development of a next-generation blood-stage vaccine candidate. A summary of three key areas is given below.

6.1.1 Production of protein PfRIPR fragments

The production of multiple PfRIPR protein fragments in Chapter 3 provides an important set of tools for investigating PfRIPR. These proteins were used for mapping the binding of anti-PfRIPR antibodies and for GIA reversal studies. This work ultimately led to the discovery of PfRIPR EGF (5-8) as the target of neutralising antibodies. The use of the monoFc fusion construct was invaluable to this effort and the techniques developed have already been applied to other *Plasmodium* proteins in the Draper group (K. McHugh, personal communication).

6.1.2 Characterisation of anti-PfRIPR antibodies

GIA-negative monoclonal antibodies were found to bind primarily to the N-terminal half of PfRIPR, with two binding PfRIPR EGF (3-4). These antibodies could also bind the formed RCR complex or prevent its formation; however, none could disrupt the RCR complex once formed. Known GIA-positive antibodies exclusively bind within

PfRIPR EGF (5-8) and can form stable quaternary complexes with the RCR complex and do not block its *in vitro* formation.

6.1.3 PfRIPR does not bind PfSEMA7A

The hypothesised/reported binding of PfRIPR to PfSEMA7A[174] was not supported in this work using both SEC and SPR techniques. A binding partner or erythrocyte receptor for PfRIPR remains elusive; PII3 was identified as a binding partner of PfRH5 by AVEXIS[125] however PII3 cannot bind the full RCR complex implying that sequential binding of different RCR components may occur with the role of PfRIPR largely unknown. PfRIPR has not yet been screened by AVEXIS for binding partners, this technique may reveal candidates of interest. Alternatively, cross-linking mass spectrometry may be used to identify binding partners or closely associating proteins in the merozoite. This approach is being attempted (Ragotte, unpublished data) however, the low abundance of PfRIPR and the likelihood of PfRIPR binding being transient and conditional, perhaps on erythrocyte binding, has made the process challenging and problematic. A better approach may be to look at RIPR in other *Plasmodium* species to guide the search for interacting partners as discussed in Section 6.2.4.

6.1.4 Development of a PfRIPR EGF (5-8) based vaccine

The primary output from this work is the development of the PfRIPR EGF (5-8) vaccine candidate. My studies have shown that PfRIPR EGF (5-8) delivers a four-fold improvement in polyclonal antibody quality, as determined by GIA assay EC_{50}, and as compared to full-length PfRIPR. This immunogen can also be produced easily, at high quantities in HEK293F cells, and fused to other antigens such as PfCyRPA opening up the possibility of multi-antigen vaccines.

6.1.5 Development of GIA positive anti-PfRIPR antibodies

This project succeeded in delivering one GIA positive mAb that bound to PfRIPR EGF-like domain 5. Although problems were encountered with this mAb the results obtained, in combination with mRP012, helped clarify the role of anti-PfRIPR neutralising mAbs in the context of the RCR complex and provide a useful tool for future work.

6.1.6 Synergistic antibody interactions between the RCR complex proteins and within PfRIPR

This project has provided evidence for inter-antigen synergy between components of the RCR complex when co-immunised but also, for the first time, evidence of intra-antigen antibody synergy between PfRIPR epitopes.

6.2 Future work

6.2.1 Intra-PfRIPR antibody synergy

The work at the end of Chapter 5 shows that there may be considerable synergetic effects between neutralising and non-neutralising anti-PfRIPR antibodies. By focusing solely on PfRIPR EGF (5-8) these effects were likely lost in the new vaccine candidates. The identification of the synergistic epitopes should be prioritised as they may then be included in an updated PfRIPR EGF (5-8) vaccine. The mechanism of these synergistic antibodies may also deliver insights into the function of PfRIPR during erythrocyte invasion, a subject where information is sorely lacking. These antibodies may act by slowing invasion, like the anti-PfRH5 mAb clone R5.011[156], or by interfering with an as-yet undiscovered binding partner. Each presents a different opportunity for vaccine design.

6.2.2 Structural work

One goal of this Thesis, which was sadly interrupted by the COVID-19 pandemic, was the structural investigation of PfRIPR. There is currently no structural information regarding the C-terminal half of PfRIPR published and due to the protein's flexible nature a structure of the full molecule by X-ray crystallography is unlikely. However, with the key neutralising epitopes identified and GIA-positive mAbs available it may be possible to crystallise a portion, such as PfRIPR EGF (5-8), with a Fab fragment bound.

In addition, both GIA-positive and GIA-negative mAbs could be used to stabilise the protein, or whole RCR complex, for Cryo-EM. Although a lower resolution technique, the ability to identify epitopes within the context of the RCR complex may give important information as to how the RCR complex is presented *in vivo* and how each of the RCR complex's components interact. A low-resolution cryo-EM structure of the RCR complex has been published by Wong *et al.*[163] however the C-terminal portion of PfRIPR, which contains the neutralising epitopes, was conspicuously missing.

6.2.3 PfRIPR fusion vaccines

In Chapter 4 a fusion PfRIPR EGF (7-8) – PfCyRPA protein vaccine was developed and tested in mice. Although promising, the focus of this Thesis shifted away from fusion vaccines temporarily and returning to complete this work was also interrupted by the Covid-19 pandemic. In the future, a study in rats using variants of PfRIPR EGF (5-8) – PfCyRPA fusions should more thoroughly evaluate this candidate vaccine approach. Using rats will enable the use of the standardised ELISA, which was developed in-house, to allow better quantification of the contribution to GIA of antibodies against each antigen. Synergistic interactions could also be more fully explored, including

interactions between the fusion protein and the existing clinical RH5.1 vaccine. The development of an 'RCR-mini' construct is also currently underway, which is a complex of RH5.1 and the PfCyRPA-PfRIPR EGF (5-8) fusion. The results of these experiments are eagerly anticipated, given these constructs would provide a route to clinical development of such a vaccine targeting the entire invasion complex.

6.2.4 Understanding the role of PfRIPR in *P. falciparum*

The role of PfRIPR in *P. falciparum* merozoite invasion of erythrocytes has remained a mystery since its discovery in 2011[124]. The PfRH5-PfCyRPA-PfRIPR complex is thought to be unique to *P. falciparum*[146,172] and human erythrocyte invasion; however, this does not necessarily exclude a role of PfRIPR in other protein complexes. In *P. knowlesi*, PkRIPR forms a different trimeric complex with PkPTRAMP and PkCSS[172]. RIPR is also present in *P. vivax*[246] however its role has not yet been investigated. Two hypotheses can be put forward regarding PfRIPR: firstly, the role PfRIPR in *P. falciparum* has diverged significantly from other *Laverania* species and it is now functioning solely in the context of the PfRH5-PfCyRPA-PfRIPR complex. Alternatively, and perhaps more likely, PfRIPR now plays two or more roles in *P. falciparum*. One in the PfRH5-PfCyRPA-PfRIPR complex and a second role in a PfRIPR-PfPTRAMP-PfCSS or homologous complex. A more thorough understanding of these proteins and their biological functions should enable the design of better, more targeted, vaccine candidates that disrupt multiple critical pathways in merozoite invasion.

6.3 Prospects of PfRIPR as a blood-stage malaria vaccine candidate

For a number of years PfRH5 has been the leading blood-stage malaria vaccine candidate. It is currently being investigated in a number of clinical trials in the UK and Tanzania. Immunisation with RH5.1/AS01$_B$ recently showed the first *in vivo* impact (by any blood-stage vaccine candidate) on blood-stage *P. falciparum* parasite growth following CHMI result (Minassian *et al.*, In press 2021). PfRIPR is currently not in a position to dethrone PfRH5 for the title of lead blood-stage candidate antigen, however in this Thesis PfRIPR vaccines improved with each iteration. Chapter 5 showed that PfRIPR is still an order of magnitude behind PfRH5 in terms of antigen-specific antibody GIA EC_{50}, this gap may not be closed by PfRIPR alone but rather a combination PfRIPR-PfCyRPA vaccine has the potential to match it. A likely scenario is that PfRIPR and PfCyRPA will complement PfRH5 in a triple antigen vaccine; ideally one that is engineered to maximise both neutralisation but also synergy between components.

The second important step will be human immunisation. Promising vaccine candidates such as PfAMA1 have consistently failed to deliver sufficient malaria blocking serum antibody activity in humans[114,140,141] despite positive animal results. It is also possible, although unlikely, that immunisation of humans with PfRIPR is unsafe for unforeseen reasons. Unfortunately, this is the nature of vaccine discovery. I believe PfRIPR has a bright future as a blood-stage vaccine candidate although the road ahead may be long and difficult.

6.4 Final remarks

Vaccines and infectious disease research are currently enjoying a resurgence in public interest as news coverage of the COVID-19 pandemic continues. As a malaria researcher, it is hard not to feel jealous of the rapid development of vaccines with >70% efficacy and mAbs with nanomolar EC_{50} values – a testament to the efforts of dedicated researchers here in Oxford and around the globe (and $20 billion in US and UK federal funding alone). I trust that malaria, along with other the classic 'difficult' diseases such HIV, influenza, and TB, will also have their day in the spotlight once new efficacious vaccines are developed against these (arguably) more difficult-to-stop human pathogens. The challenges to creating an effective blood-stage malaria vaccine remain formidable, but I hope that the work in this Thesis moves the field one-step closer.

Chapter 7 - References

1. WHO | World malaria report 2019. *WHO* (2020).
2. Orem, J., Kirigia, J., Azairwe, R., Kasirye, I. & Walker, O. Impact of malaria morbidity on gross domestic product in Uganda. *Int. Arch. Med.* **5**, 12 (2012).
3. Phillips, M. A. *et al.* Malaria. *Nat. Rev. Dis. Prim.* **3**, 17050 (2017).
4. Bhatt, S. *et al.* The effect of malaria control on Plasmodium falciparum in Africa between 2000 and 2015. *Nature* **526**, 207–211 (2015).
5. Musiime, A. K. *et al.* Impact of vector control interventions on malaria transmission intensity, outdoor vector biting rates and Anopheles mosquito species composition in Tororo, Uganda. *Malar. J.* **18**, 445 (2019).
6. Ranson, H. & Lissenden, N. Insecticide Resistance in African Anopheles Mosquitoes: A Worsening Situation that Needs Urgent Action to Maintain Malaria Control. *Trends in Parasitology* vol. 32 187–196 (2016).
7. Dong, Y., Simões, M. L., Marois, E. & Dimopoulos, G. CRISPR/Cas9 -mediated gene knockout of Anopheles gambiae FREP1 suppresses malaria parasite infection. *PLoS Pathog.* **14**, (2018).
8. Wang, S. *et al.* Driving mosquito refractoriness to Plasmodium falciparum with engineered symbiotic bacteria. *Science (80-.).* **357**, 1399–1402 (2017).
9. Bilgo, E. *et al.* Improved efficacy of an arthropod toxin expressing fungus against insecticide-resistant malaria-vector mosquitoes. *Sci. Rep.* **7**, 1–8 (2017).
10. Noedl, H. *et al.* Evidence of Artemisinin-Resistant Malaria in Western Cambodia. *N. Engl. J. Med.* **359**, 2619–2620 (2008).
11. Ashley, E. A. *et al.* Spread of Artemisinin Resistance in *Plasmodium falciparum* Malaria. *N. Engl. J. Med.* **371**, 411–423 (2014).
12. Imwong, M. *et al.* The spread of artemisinin-resistant Plasmodium falciparum in the Greater Mekong subregion: a molecular epidemiology observational study. *Lancet. Infect. Dis.* **17**, 491–497 (2017).
13. Mbengue, A. *et al.* A molecular mechanism of artemisinin resistance in Plasmodium falciparum malaria. *Nature* **520**, 683–687 (2015).
14. Mukherjee, A. *et al.* Artemisinin resistance without pfkelch13 mutations in Plasmodium falciparum isolates from Cambodia. *Malar. J.* **16**, 195 (2017).
15. Reilly, H. B., Wang, H., Steuter, J. A., Marx, A. M. & Ferdig, M. T. Quantitative dissection of clone-specific growth rates in cultured malaria parasites. *Int. J. Parasitol.* **37**, 1599–1607 (2007).

16. Trampuz, A., Jereb, M., Muzlovic, I. & Prabhu, R. M. Clinical review: Severe malaria. *Critical Care* vol. 7 315–323 (2003).

17. Clark, I. A., Alleva, L. M., Budd, A. C. & Cowden, W. B. Understanding the role of inflammatory cytokines in malaria and related diseases. *Travel Med. Infect. Dis.* **6**, 67–81 (2008).

18. Chotivanich, K. *et al.* Parasite Multiplication Potential and the Severity of Falciparum Malaria. *J. Infect. Dis.* **181**, 1206–1209 (2000).

19. Deans, A. M. *et al.* Low multiplication rates of African Plasmodium falciparum isolates and lack of association of multiplication rate and red blood cell selectivity with malaria virulence. *Am. J. Trop. Med. Hyg.* **74**, 554–563 (2006).

20. Lee, W. C., Russell, B. & Rénia, L. Sticking for a cause: The falciparum malaria parasites cytoadherence paradigm. *Front. Immunol.* **10**, 1444 (2019).

21. Doumbo, O. K. *et al.* High levels of Plasmodium falciparum rosetting in all clinical forms of severe malaria in African children. *Am. J. Trop. Med. Hyg.* **81**, 987–993 (2009).

22. Moll, K., Palmkvist, M., Ch'ng, J., Kiwuwa, M. S. & Wahlgren, M. Evasion of immunity to Plasmodium falciparum: Rosettes of blood group a impair recognition of PfEMP1. *PLoS One* **10**, e0145120 (2015).

23. Rowe, J. A. *et al.* Blood group O protects against severe Plasmodium falciparum malaria through the mechanism of reduced rosetting. *Proc. Natl. Acad. Sci. U. S. A.* **104**, 17471–17476 (2007).

24. Cockburn, I. A. *et al.* A human complement receptor 1 polymorphism that reduces Plasmodium falciparum rosetting confers protection against severe malaria. *Proc. Natl. Acad. Sci. U. S. A.* **101**, 272–277 (2004).

25. McQuaid, F. & Rowe, J. A. Rosetting revisited: A critical look at the evidence for host erythrocyte receptors in Plasmodium falciparum rosetting. *Parasitology* vol. 147 1–11 (2020).

26. Frank, G. O., Stephen, B. T., Dominic, S. O. A., Kiptanui, C. & Bethwel, K. K. Platelet-mediated clumping adhesion phenotypes of P. falciparum-infected erythrocytes: A review. *Clin. Rev. Opin.* **8**, 14–18 (2017).

27. Chotivanich, K. *et al.* Platelet-induced autoagglutination of Plasmodium falciparum-infected red blood cells and disease severity in Thailand. *J. Infect. Dis.* **189**, 1052–1055 (2004).

28. Idro, R., Marsh, K., John, C. C. & Newton, C. R. J. Cerebral malaria: Mechanisms of brain injury and strategies for improved neurocognitive outcome. *Pediatric Research* vol. 68 267–274 (2010).

29. Combes, V. *et al.* Microvesiculation and cell interactions at the brain-endothelial interface in cerebral malaria pathogenesis. *Progress in Neurobiology* vol. 91 140–151 (2010).

30. Riggle, B. A., Miller, L. H. & Pierce, S. K. Desperately Seeking Therapies for Cerebral Malaria. *J. Immunol.* **204**, 327–334 (2020).

31. Pasternak, N. D. & Dzikowski, R. PfEMP1: An antigen that plays a key role in the pathogenicity and immune evasion of the malaria parasite Plasmodium falciparum. *International Journal of Biochemistry and Cell Biology* vol. 41 1463–1466 (2009).

32. Casares, S. & Richie, T. L. Immune evasion by malaria parasites: a challenge for vaccine development. *Current Opinion in Immunology* vol. 21 321–330 (2009).

33. Fowkes, F. J. I., Boeuf, P. & Beeson, J. G. Immunity to malaria in an era of declining malaria transmission. *Parasitology* **143**, 139–153 (2016).

34. Cohen, S., McGregor, I. A. & Carrington, S. Gamma-globulin and acquired immunity to human malaria. *Nature* **192**, 733–737 (1961).

35. Goel, S. *et al.* RIFINs are adhesins implicated in severe Plasmodium falciparum malaria. *Nat. Med.* **21**, 314–321 (2015).

36. Winter, G. *et al.* SURFIN is a polymorphic antigen expressed on Plasmodium falciparum merozoites and infected erythrocytes. *J. Exp. Med.* **201**, 1853–1863 (2005).

37. Niang, M. *et al.* STEVOR is a plasmodium falciparum erythrocyte binding protein that mediates merozoite invasion and rosetting. *Cell Host Microbe* **16**, 81–93 (2014).

38. Portugal, S., Pierce, S. K. & Crompton, P. D. Young Lives Lost as B Cells Falter: What We Are Learning About Antibody Responses in Malaria. *J. Immunol.* **190**, 3039–3046 (2013).

39. Akpogheneta, O. J. *et al.* Duration of naturally acquired antibody responses to blood-stage Plasmodium falciparum is age dependent and antigen specific. *Infect. Immun.* **76**, 1748–1755 (2008).

40. Portugal, S. *et al.* Malaria-associated atypical memory B cells exhibit markedly reduced B cell receptor signaling and effector function. *Elife* **4**, (2015).

41. Wykes, M. N., Horne-Debets, J. M., Leow, C.-Y. & Karunarathne, D. S. Malaria drives T cells to exhaustion. *Front. Microbiol.* **5**, 249 (2014).

42. Freitas do Rosário, A. P. *et al.* Gradual Decline in Malaria-Specific Memory T Cell Responses Leads to Failure to Maintain Long-Term Protective Immunity to Plasmodium chabaudi AS Despite Persistence of B Cell Memory and Circulating Antibody . *J. Immunol.* **181**, 8344–8355 (2008).

43. Loiseau, C., Cooper, M. M. & Doolan, D. L. Deciphering host immunity to malaria using systems immunology. *Immunol. Rev.* **293**, 115–143 (2020).

44. Ademolue, T. W. & Awandare, G. A. Evaluating antidisease immunity to malaria and implications for vaccine design. *Immunology* **153**, 423–434 (2018).

45. Jagannathan, P. *et al.* Loss and dysfunction of Vδ2+γδ T cells are associated with clinical tolerance to malaria. *Sci. Transl. Med.* **6**, 251ra117 (2014).

46. World Health Organisation. *World Malaria Report 2017*. http://apps.who.int/iris/bitstream/handle/10665/259492/9789241565523-eng.pdf?sequence=1 (2017).

47. World Health Organisation. *Malaria vaccine technology roadmap*. http://www.who.int/immunization/topics/malaria/vaccine_roadmap/TRM_update_nov13.pdf?ua=1 (2013).

48. Mulligan, H. W., Russell, P. F. & Mohan, B. N. Active Immunization of Fowls against Plasmodium gallinacemn by Injections of Killed Homologous Sporozoites. *J. Malar. Inst. India* **4**, (1941).

49. Richards, W. H. G. Active immunization of chicks against plasmodium gallinaceum by inactivated homologous sporozoites and erythrocytic parasites. *Nature* vol. 212 1492–1494 (1966).

50. Nussenzweig, R. S., Vanderberg, J., Most, H. & Orton, C. Protective immunity produced by the injection of X-irradiated sporozoites of plasmodium berghei. *Nature* vol. 216 160–162 (1967).

51. Hoffman, S. L. *et al.* Protection of Humans against Malaria by Immunization with Radiation-Attenuated Plasmodium falciparum Sporozoites . *J. Infect. Dis.* **185**, 1155–1164 (2002).

52. Rieckmann, K. H., Beaudoin, R. L., Cassells, J. S. & Sell, K. W. Use of attenuated sporozoites in the immunization of human volunteers against falciparum malaria. *Bull. World Health Organ.* **57**, 261–265 (1979).

53. Clyde, D. F., Most, H., McCarthy, V. C. & Vanderberg, J. P. Immunization of man against sporozoite induced falciparum malaria. *Am. J. Med. Sci.* **266**, 169–177 (1973).

54. Clyde, D. F., McCarthy, V. C., Miller, R. M. & Woodward, W. E. Immunization of man against falciparum and vivax malaria by use of attenuated sporozoites. *Am. J. Trop. Med. Hyg.* **24**, 397–401 (1975).

55. Clyde, D. F., McCarthy, V. C., Miller, R. M. & Hornick, R. B. Specificity of protection of man immunized against sporozoite induced falciparum malaria. *Am. J. Med. Sci.* **266**, 398–403 (1973).

56. Ishizuka, A. S. *et al.* Protection against malaria at 1 year and immune correlates following PfSPZ vaccination. *Nat. Med.* **22**, 614–623 (2016).

57. Epstein, J. E. *et al.* Live attenuated malaria vaccine designed to protect through hepatic CD8+ T cell immunity. *Science (80-.).* **334**, 475–480 (2011).

58. Jongo, S. A. *et al.* Increase of dose associated with decrease in protection against controlled human malaria infection by PfSPZ Vaccine in Tanzanian adults. *Clin. Infect. Dis.* (2019) doi:10.1093/cid/ciz1152.

59. Lyke, K. E. *et al.* Attenuated PfSPZ Vaccine induces strain-transcending T cells and durable protection against heterologous controlled human malaria infection. *Proc. Natl. Acad. Sci. U. S. A.* **114**, 2711–2716 (2017).

60. Epstein, J. E. *et al.* Protection against Plasmodium falciparum malaria by PfSPZ Vaccine. *JCI Insight* **2**, 89154 (2017).

61. Seder, R. A. *et al.* Protection Against Malaria by Intravenous Immunization with a Nonreplicating Sporozoite Vaccine. *Science (80-.).* **341**, 1359–1365 (2013).

62. Gordon, D. M. *et al.* Safety, immunogenicity, and efficacy of a recombinantly produced Plasmodium falciparum circumsporozoite protein-hepatitis B surface antigen subunit vaccine. *J. Infect. Dis.* **171**, 1576–85 (1995).

63. RTS, S. C. T. P. & Partnership, S. C. T. Efficacy and safety of RTS,S/AS01 malaria vaccine with or without a booster dose in infants and children in Africa: final results of a phase 3, individually randomised, controlled trial. *Lancet* **386**, 31–45 (2015).

64. Penny, M. A. *et al.* Public health impact and cost-effectiveness of the RTS,S/AS01 malaria vaccine: A systematic comparison of predictions from four mathematical models. *Lancet* **387**, 367–375 (2016).

65. Aide, P. *et al.* Four year immunogenicity of the RTS,S/AS02 A malaria vaccine in Mozambican children during a phase IIb trial. *Vaccine* **29**, 6059–6067 (2011).

66. Collins, K. A., Snaith, R., Cottingham, M. G., Gilbert, S. C. & Hill, A. V. S. S. Enhancing protective immunity to malaria with a highly immunogenic virus-like particle vaccine. *Sci. Rep.* **7**, (2017).

67. Venkatraman, N. *et al.* Phase I assessments of first-in-human administration of a novel malaria anti-sporozoite vaccine candidate, R21 in matrix-M adjuvant, in UK and Burkinabe volunteers. *medRxiv* 19009282 (2019) doi:10.1101/19009282.

68. Sultan, A. A. *et al.* TRAP is necessary for gliding motility and infectivity of Plasmodium sporozoites. *Cell* **90**, 511–522 (1997).

69. Ohashi, J., Suzuki, Y., Naka, I., Hananantachai, H. & Patarapotikul, J. Diversifying Selection on the Thrombospondin-Related Adhesive Protein (TRAP) Gene of Plasmodium falciparum in Thailand. *PLoS One* **9**, e90522 (2014).

70. McConkey, S. J. *et al.* Enhanced T-cell immunogenicity of plasmid DNA vaccines boosted by recombinant modified vaccinia virus Ankara in humans. *Nat. Med.* **9**, 729–735 (2003).

71. Gilbert, S. C. *et al. A protein particle vaccine containing multiple malaria epitopes*. *Nature Biotechnology* vol. 15 http://www.nature.com/naturebiotechnology (1997).

72. Prieur, E. *et al.* A Plasmodium falciparum candidate vaccine based on a six-antigen polyprotein encoded by recombinant poxviruses. *Proc. Natl. Acad. Sci. U. S. A.* **101**, 290–295 (2004).

73. Schneider, J. *et al.* Enhanced immunogenicity for CD8+ T cell induction and complete protective efficacy of malaria DNA vaccination by boosting with modified vaccinia virus Ankara. *Nat. Med.* **4**, 397–402 (1998).

74. O'hara, G. A. *et al.* Clinical Assessment of a Recombinant Simian Adenovirus ChAd63: A Potent New Vaccine Vector. *J. Infect. Dis.* **205**, 772–781 (2012).

75. Ogwang, C. *et al.* Safety and Immunogenicity of Heterologous Prime-Boost Immunisation with Plasmodium falciparum Malaria Candidate Vaccines, ChAd63 ME-TRAP and MVA ME-TRAP, in Healthy Gambian and Kenyan Adults. *PLoS One* **8**, e57726 (2013).

76. Tiono, A. B. *et al.* First field efficacy trial of the ChAd63 MVA ME-TRAP vectored malaria vaccine candidate in 5-17 months old infants and children. *PLoS One* **13**, e0208328 (2018).

77. Rampling, T. *et al.* Safety and high level efficacy of the combination malaria vaccine regimen of RTS,S/AS01B with chimpanzee adenovirus 63 and modified vaccinia Ankara vectored vaccines expressing me-trap. *J. Infect. Dis.* **214**, 772–781 (2016).

78. Rampling, T. *et al.* Safety and efficacy of novel malaria vaccine regimens of RTS,S/AS01B alone, or with concomitant ChAd63-MVA-vectored vaccines expressing ME-TRAP. *npj Vaccines* **3**, 1–9 (2018).

79. Kariu, T., Ishino, T., Yano, K., Chinzei, Y. & Yuda, M. CelTOS, a novel malarial protein that mediates transmission to mosquito and vertebrate hosts. *Mol. Microbiol.* **59**, 1369–1379 (2006).

80. Bergmann-Leitner, E. S. *et al.* Immunization with pre-erythrocytic antigen CelTOS from Plasmodium falciparum elicits cross-species protection against heterologous challenge with Plasmodium berghei. *PLoS One* **5**, e12294 (2010).

81. Longley, R. J. *et al.* Comparative assessment of vaccine vectors encoding ten malaria antigens identifies two protective liver-stage candidates. *Sci. Rep.* **5**, 1–13 (2015).

82. Espinosa, D. A. *et al.* The Plasmodium falciparum cell-traversal protein for ookinetes and sporozoites as a candidate for preerythrocytic and transmission-blocking vaccines. *Infect. Immun.* **85**, (2017).

83. Pirahmadi, S. *et al.* Cell-traversal protein for ookinetes and sporozoites (CelTOS) formulated with potent TLR adjuvants induces high-affinity antibodies that inhibit Plasmodium falciparum infection in Anopheles stephensi. *Malar. J.* **18**, 146 (2019).

84. Pirahmadi, S. *et al.* Combining monophosphoryl lipid A (MPL), CpG oligodeoxynucleotide (ODN), and QS-21 adjuvants induces strong and

persistent functional antibodies and T cell responses against cell-traversal protein for ookinetes and sporozoites (CelTOS) of plasmodium falciparum in BALB/c Mice. *Infect. Immun.* **87**, (2019).

85. Kaslow, D. C. *et al.* A vaccine candidate from the sexual stage of human malaria that contains EGF-like domains. *Nature* **333**, 74–76 (1988).

86. Rener, J., Graves, P. M., Carter, R., Williams, J. L. & Burkot, T. R. Target antigens of transmission-blocking immunity on gametes of plasmodium falciparum. *J. Exp. Med.* **158**, 976–981 (1983).

87. Wu, Y. *et al.* Phase 1 trial of malaria transmission blocking vaccine candidates Pfs25 and Pvs 25 formulated with montanide ISA 51. *PLoS One* **3**, e2636 (2008).

88. Ogun, S. A., Dumon-Seignovert, L., Marchand, J. B., Holder, A. A. & Hill, F. The oligomerization domain of C4-binding protein (C4bp) acts as an adjuvant, and the fusion protein comprised of the 19-kilodalton merozoite surface protein 1 fused with the murine C4bp domain protects mice against malaria. *Infect. Immun.* **76**, 3817–3823 (2008).

89. Li, Y. *et al.* Enhancing immunogenicity and transmission-blocking activity of malaria vaccines by fusing Pfs25 to IMX313 multimerization technology. *Sci. Rep.* **6**, 18848 (2016).

90. Brod, F. *et al.* Combination of RTS,S and Pfs25-IMX313 Induces a Functional Antibody Response Against Malaria Infection and Transmission in Mice. *Front. Immunol.* **9**, 2780 (2018).

91. MacDonald, N. J. *et al.* Structural and immunological characterization of recombinant 6-cysteine domains of the plasmodium falciparum sexual stage protein Pfs230. *J. Biol. Chem.* **291**, 19913–19922 (2016).

92. Lee, S. M. *et al.* Expression and purification optimization of an N-terminal Pfs230 transmission-blocking vaccine candidate. *Protein Expr. Purif.* **160**, 56–65 (2019).

93. Lee, S. M. *et al.* The Pfs230 N-Terminal fragment, Pfs230D1+: Expression and characterization of a potential malaria transmission-blocking vaccine candidate. *Malar. J.* **18**, 1–13 (2019).

94. KUMAR, N. Target antigens of malaria transmission blocking immunity exist as a stable membrane bound complex. *Parasite Immunol.* **9**, 321–335 (1987).

95. Vermeulen, A. N. *et al.* Sequential expression of antigens on sexual stages of plasmodium falciparum accessible to transmission-blocking antibodies in the mosquito. *J. Exp. Med.* **162**, 1460–1476 (1985).

96. Van Dijk, M. R. *et al.* A central role for P48/45 in malaria parasite male gamete fertility. *Cell* **104**, 153–164 (2001).

97. Ouédraogo, A. L. *et al.* Naturally acquired immune responses to Plasmodium falciparum sexual stage antigens Pfs48/45 and Pfs230 in an area of seasonal

transmission. *Infect. Immun.* **79**, 4957–4964 (2011).

98. Theisen, M. *et al.* A multi-stage malaria vaccine candidate targeting both transmission and asexual parasite life-cycle stages. *Vaccine* **32**, 2623–2630 (2014).

99. Singh, S. K. *et al.* Construct design, production, and characterization of Plasmodium falciparum 48/45 R0.6C subunit protein produced in Lactococcus lactis as candidate vaccine. *Microb. Cell Fact.* **16**, 97 (2017).

100. Lee, S. M. *et al.* A C-terminal Pfs48/45 malaria transmission-blocking vaccine candidate produced in the baculovirus expression system. *Sci. Rep.* **10**, 1–14 (2020).

101. Lennartz, F. *et al.* Structural basis for recognition of the malaria vaccine candidate Pfs48/45 by a transmission blocking antibody. *Nat. Commun.* **9**, 1–11 (2018).

102. Outchkourov, N. *et al.* Epitope analysis of the malaria surface antigen Pfs48/45 identifies a subdomain that elicits transmission blocking antibodies. *J. Biol. Chem.* **282**, 17148–17156 (2007).

103. Datta, D. *et al.* Comparative functional potency of DNA vaccines encoding Plasmodium falciparum transmission blocking target antigens Pfs48/45 and Pfs25 administered alone or in combination by in vivo electroporation in rhesus macaques. *Vaccine* **35**, 7049–7056 (2017).

104. Haynes, J. D., Moch, J. K. & Smoot, D. S. Erythrocytic malaria growth or invasion inhibition assays with emphasis on suspension culture GIA. *Methods Mol. Med.* **72**, 535–554 (2002).

105. Miura, K. *et al.* Anti-apical-membrane-antigen-1 antibody is more effective than anti-42-kilodalton-merozoite-surface-protein-1 antibody in inhibiting Plasmodium falciparum growth, as determined by the in vitro growth inhibition assay. *Clin. Vaccine Immunol.* **16**, 963–968 (2009).

106. Crompton, P. D. *et al.* In vitro growth-inhibitory activity and malaria risk in a cohort study in Mali. *Infect. Immun.* **78**, 737–745 (2010).

107. Ewer, K. J. *et al.* Progress with viral vectored malaria vaccines: A multi-stage approach involving 'unnatural immunity'. *Vaccine* **33**, 7444–7451 (2015).

108. Douglas, A. D. *et al.* A PfRH5-Based Vaccine Is Efficacious against Heterologous Strain Blood-Stage Plasmodium falciparum Infection in Aotus Monkeys. *Cell Host Microbe* **17**, 130–139 (2015).

109. Douglas, A. D. *et al.* A defined mechanistic correlate of protection against Plasmodium falciparum malaria in non-human primates. *Nat. Commun.* **10**, 1953 (2019).

110. Minassian, A. M. *et al.* Reduced blood-stage malaria growth and immune correlates in humans following RH5 vaccination. *Med* **0**, (2021).

111. Engwerda, C. R., Minigo, G., Amante, F. H. & McCarthy, J. S. Experimentally induced blood stage malaria infection as a tool for clinical research. *Trends in Parasitology* vol. 28 515–521 (2012).

112. Laurens, M. B. *et al.* A consultation on the optimization of controlled human malaria infection by mosquito bite for evaluation of candidate malaria vaccines. in *Vaccine* vol. 30 5302–5304 (2012).

113. Singh, S. *et al.* Immunity to recombinant Plasmodium falciparum merozoite surface protein 1 (MSP1): Protection in Aotus nancymai monkeys strongly correlates with anti-MSP1 antibody titer and in vitro parasite-inhibitory activity. *Infect. Immun.* **74**, 4573–4580 (2006).

114. Sheehy, S. H. *et al.* ChAd63-MVA-vectored blood-stage Malaria vaccines targeting MSP1 and AMA1: Assessment of efficacy against mosquito bite challenge in humans. *Mol. Ther.* **20**, 2355–2368 (2012).

115. Weiss, G. E., Crabb, B. S. & Gilson, P. R. Overlaying Molecular and Temporal Aspects of Malaria Parasite Invasion. *Trends in Parasitology* vol. 32 284–295 (2016).

116. Boyle, M. J. *et al.* Isolation of viable Plasmodium falciparum merozoites to define erythrocyte invasion events and advance vaccine and drug development. *Proc. Natl. Acad. Sci. U. S. A.* **107**, 14378–14383 (2010).

117. Weiss, G. E. *et al.* Revealing the Sequence and Resulting Cellular Morphology of Receptor-Ligand Interactions during Plasmodium falciparum Invasion of Erythrocytes. **11**, e1004670 (2015).

118. Das, S. *et al.* Processing of Plasmodium falciparum Merozoite Surface Protein MSP1 Activates a Spectrin-Binding Function Enabling Parasite Egress from RBCs. *Cell Host Microbe* **18**, 433–444 (2015).

119. Lin, C. S. *et al.* Multiple plasmodium falciparum merozoite surface protein 1 complexes mediate merozoite binding to human erythrocytes. *J. Biol. Chem.* **291**, 7703–7715 (2016).

120. Dent, A. E. *et al.* Temporal stability of naturally acquired immunity to merozoite surfacep protein-1 in kenyan adults. *Malar. J.* **8**, 162 (2009).

121. Cowman, A. F., Tonkin, C. J., Tham, W.-H. H. & Duraisingh, M. T. The Molecular Basis of Erythrocyte Invasion by Malaria Parasites. *Cell Host Microbe* **22**, 232–245 (2017).

122. Lopaticki, S. *et al.* Reticulocyte and erythrocyte binding-like proteins function cooperatively in invasion of human erythrocytes by malaria parasites. *Infect. Immun.* **79**, 1107–1117 (2011).

123. Reddy, K. S. *et al.* Multiprotein complex between the GPI-anchored CyRPA with PfRH5 and PfRipr is crucial for Plasmodium falciparum erythrocyte invasion. *Proc. Natl. Acad. Sci. U. S. A.* **112**, 1179–84 (2015).

124. Chen, L. *et al.* An egf-like protein forms a complex with pfrh5 and is required

for invasion of human erythrocytes by plasmodium falciparum. *PLoS Pathog.* **7**, (2011).

125. Galaway, F. *et al.* P113 is a merozoite surface protein that binds the N terminus of Plasmodium falciparum RH5. *Nat. Commun.* **8**, 1–11 (2017).

126. Sidik, S. M. *et al.* A Genome-wide CRISPR Screen in Toxoplasma Identifies Essential Apicomplexan Genes. *Cell* **166**, 1423-1435.e12 (2016).

127. Dasgupta, S. *et al.* Membrane-wrapping contributions to malaria parasite invasion of the human erythrocyte. *Biophys. J.* **107**, 43–54 (2014).

128. Volz, J. C. *et al.* Essential Role of the PfRh5/PfRipr/CyRPA Complex during Plasmodium falciparum Invasion of Erythrocytes. *Cell Host Microbe* **20**, 60–71 (2016).

129. Cao, J. *et al.* Rhoptry neck protein RON2 forms a complex with microneme protein AMA1 in Plasmodium falciparum merozoites. *Parasitol. Int.* **58**, 29–35 (2009).

130. Lamarque, M., Besteiro, S., Papoin, J., Roques, M. & Vulliez-Le Normand, B. The RON2-AMA1 Interaction is a Critical Step in Moving Junction-Dependent Invasion by Apicomplexan Parasites. *PLoS Pathog* **7**, 1001276 (2011).

131. Vulliez-Le Normand, B. *et al.* Structural and functional insights into the malaria parasite moving junction complex. *PLoS Pathog.* **8**, (2012).

132. Srinivasan, P. *et al.* Binding of Plasmodium merozoite proteins RON2 and AMA1 triggers commitment to invasion. *Proc. Natl. Acad. Sci. U. S. A.* **108**, 13275–13280 (2011).

133. Srinivasan, P. *et al.* Disrupting malaria parasite AMA1-RON2 interaction with a small molecule prevents erythrocyte invasion. *Nat. Commun.* **4**, 1–9 (2013).

134. Wang, G. *et al.* Structure–Activity Studies of β-Hairpin Peptide Inhibitors of the Plasmodium falciparum AMA1–RON2 Interaction. *J. Mol. Biol.* **428**, 3986–3998 (2016).

135. Baum, J. *et al.* A conserved molecular motor drives cell invasion and gliding motility across malaria life cycle stages and other apicomplexan parasites. *J. Biol. Chem.* **281**, 5197–5208 (2006).

136. Dutta, S. *et al.* High antibody titer against apical membrane antigen-1 is required to protect against malaria in the aotus model. *PLoS One* **4**, e8138 (2009).

137. Miura, K. *et al.* Overcoming allelic specificity by immunization with five allelic forms of Plasmodium falciparum apical membrane antigen 1. *Infect. Immun.* **81**, 1491–1501 (2013).

138. Duncan, C. J. A. *et al.* Impact on malaria parasite multiplication rates in infected volunteers of the protein-in-adjuvant vaccine AMA1-C1/alhydrogel+CPG 7909. *PLoS One* **6**, (2011).

139. Thera, M. A. *et al.* A Field Trial to Assess a Blood-Stage Malaria Vaccine. *N. Engl. J. Med.* **365**, 1004–1013 (2011).

140. Spring, M. D. *et al.* Phase 1/2a Study of the Malaria Vaccine Candidate Apical Membrane Antigen-1 (AMA-1) Administered in Adjuvant System AS01B or AS02A. *PLoS One* **4**, e5254 (2009).

141. Ouattara, A. *et al.* Lack of allele-specific efficacy of a bivalent AMA1 malaria vaccine. *Malar. J.* **9**, 175 (2010).

142. Srinivasan, P. *et al.* Immunization with a functional protein complex required for erythrocyte invasion protects against lethal malaria. *Proc. Natl. Acad. Sci. U. S. A.* **111**, 10311–6 (2014).

143. Spiegel, H. *et al.* Immunization with the malaria diversity-covering blood-stage vaccine candidate plasmodium falciparum apical membrane antigen 1 DiCo in complex with its natural ligand PfRon2 does not improve the in vitro efficacy. *Front. Immunol.* **8**, 743 (2017).

144. Baum, J. *et al.* Reticulocyte-binding protein homologue 5 – An essential adhesin involved in invasion of human erythrocytes by Plasmodium falciparum. *Int. J. Parasitol.* **39**, 371–380 (2009).

145. Crosnier, C. *et al.* Basigin is a receptor essential for erythrocyte invasion by Plasmodium falciparum. *Nature* **480**, 534–537 (2011).

146. Galaway, F., Yu, R., Constantinou, A., Prugnolle, F. & Wright, G. J. Resurrection of the ancestral RH5 invasion ligand provides a molecular explanation for the origin of P. falciparum malaria in humans. *PLOS Biol.* **17**, e3000490 (2019).

147. Otto, T. D. *et al.* Genomes of all known members of a Plasmodium subgenus reveal paths to virulent human malaria. *Nat. Microbiol.* **3**, 687–697 (2018).

148. Wanaguru, M., Liu, W., Hahn, B. H., Rayner, J. C. & Wright, G. J. RH5-Basigin interaction plays a major role in the host tropism of Plasmodium falciparum. *Proc. Natl. Acad. Sci. U. S. A.* **110**, 20735–20740 (2013).

149. Wright, K. E. *et al.* Structure of malaria invasion protein RH5 with erythrocyte basigin and blocking antibodies. *Nature* **515**, 427–430 (2014).

150. Patel, S. D. *et al.* Plasmodium falciparum Merozoite Surface Antigen, PfRH5, Elicits Detectable Levels of Invasion-Inhibiting Antibodies in Humans. *J. Infect. Dis.* **208**, 1679–1687 (2013).

151. Chiu, C. Y. H. *et al.* Association of antibodies to Plasmodium falciparum reticulocyte binding protein homolog 5 with protection from clinical malaria. *Front. Microbiol.* **5**, 1–8 (2014).

152. Tran, T. M. *et al.* Naturally Acquired Antibodies Specific for Plasmodium falciparum Reticulocyte-Binding Protein Homologue 5 Inhibit Parasite Growth and Predict Protection From Malaria. *J. Infect. Dis.* **209**, 789–798 (2014).

153. Weaver, R. *et al.* The association between naturally acquired IgG subclass

specific antibodies to the PfRH5 invasion complex and protection from Plasmodium falciparum malaria. *Sci. Rep.* **6**, 33094 (2016).

154. Bustamante, L. Y. *et al.* A full-length recombinant Plasmodium falciparum PfRH5 protein induces inhibitory antibodies that are effective across common PfRH5 genetic variants. *Vaccine* **31**, 373–379 (2013).

155. Douglas, A. D. *et al.* Neutralization of Plasmodium falciparum merozoites by antibodies against PfRH5. *J. Immunol.* **192**, 245–58 (2014).

156. Alanine, D. G. W. *et al.* Human Antibodies that Slow Erythrocyte Invasion Potentiate Malaria-Neutralizing Antibodies. *Cell* (2019) doi:10.1016/J.CELL.2019.05.025.

157. Douglas, A. D. *et al.* The blood-stage malaria antigen PfRH5 is susceptible to vaccine-inducible cross-strain neutralizing antibody. *Nat. Commun.* **2**, 601 (2011).

158. Chen, L. *et al.* Crystal structure of PfRh5, an essential P. falciparum ligand for invasion of human erythrocytes. *Elife* **3**, (2014).

159. Hjerrild, K. A. *et al.* Production of full-length soluble Plasmodium falciparum RH5 protein vaccine using a Drosophila melanogaster Schneider 2 stable cell line system. *Sci. Rep.* **6**, 30357 (2016).

160. Campeotto, I. *et al.* One-step design of a stable variant of the malaria invasion protein RH5 for use as a vaccine immunogen. *Proc. Natl. Acad. Sci. U. S. A.* **114**, 998–1002 (2017).

161. Payne, R. O. *et al.* Human vaccination against RH5 induces neutralizing antimalarial antibodies that inhibit RH5 invasion complex interactions. *JCI insight* **2**, (2017).

162. Dreyer, A. M. *et al.* Passive Immunoprotection of Plasmodium falciparum - Infected Mice Designates the CyRPA as Candidate Malaria Vaccine Antigen . *J. Immunol.* **188**, 6225–6237 (2012).

163. Wong, W. *et al.* Structure of Plasmodium falciparum Rh5–CyRPA–Ripr invasion complex. *Nature* 1 (2018) doi:10.1038/s41586-018-0779-6.

164. Favuzza, P. *et al.* Generation of Plasmodium falciparum parasite-inhibitory antibodies by immunization with recombinantly-expressed CyRPA. *Malar. J.* **15**, 1–14 (2016).

165. Chen, L. *et al.* Structural basis for inhibition of erythrocyte invasion by antibodies to Plasmodium falciparum protein CyRPA. *Elife* **6**, (2017).

166. Healer, J. *et al.* Neutralising antibodies block the function of Rh5/Ripr/CyRPA complex during invasion of *Plasmodium falciparum* into human erythrocytes. *Cell. Microbiol.* **21**, e13030 (2019).

167. Azasi, Y. *et al.* Bliss' and Loewe's additive and synergistic effects in Plasmodium falciparum growth inhibition by AMA1-RON2L, RH5, RIPR and

CyRPA antibody combinations. *Sci. Rep.* **10**, 1–12 (2020).

168. Favuzza, P. *et al.* Structure of the malaria vaccine candidate antigen CyRPA and its complex with a parasite invasion inhibitory antibody. *Elife* **6**, (2017).

169. Bustamante, L. Y. *et al.* Synergistic malaria vaccine combinations identified by systematic antigen screening. *Proc. Natl. Acad. Sci. U. S. A.* **114**, 12045–12050 (2017).

170. Ousterout, D. G. *et al.* Multiplex CRISPR/Cas9-based genome editing for correction of dystrophin mutations that cause Duchenne muscular dystrophy. *Nat. Commun.* **6**, 6244 (2015).

171. Favuzza, P. *et al.* Dual Plasmepsin-Targeting Antimalarial Agents Disrupt Multiple Stages of the Malaria Parasite Life Cycle. *Cell Host Microbe* **0**, (2020).

172. Knuepfer, E. *et al.* Divergent roles for the RH5 complex components, CyRPA and RIPR in human-infective malaria parasites. *PLOS Pathog.* **15**, e1007809 (2019).

173. Ntege, E. H. *et al.* Identification of Plasmodium falciparum reticulocyte binding protein homologue 5-interacting protein, PfRipr, as a highly conserved blood-stage malaria vaccine candidate. *Vaccine* **34**, 5612–5622 (2016).

174. Nagaoka, H. *et al.* Antibodies against a short region of PfRipr inhibit Plasmodium falciparum merozoite invasion and PfRipr interaction with Rh5 and SEMA7A. *Sci. Rep.* **10**, 6573 (2020).

175. Zenonos, Z. A., Rayner, J. C. & Wright, G. J. Towards a comprehensive Plasmodium falciparum merozoite cell surface and secreted recombinant protein library. *Malar. J.* **13**, 93 (2014).

176. KIM, H. W. *et al.* Respiratory syncytial virus disease in infants despite prior administration of antigenic inactivated vaccine. *Am. J. Epidemiol.* **89**, 422–434 (1969).

177. Halstead, S. B. Dengue Antibody-Dependent Enhancement: Knowns and Unknowns. in *Antibodies for Infectious Diseases* 249–271 (ASM Press, 2015). doi:10.1128/9781555817411.ch15.

178. Killikelly, A. M., Kanekiyo, M. & Graham, B. S. Pre-fusion F is absent on the surface of formalin-inactivated respiratory syncytial virus. *Sci. Rep.* **6**, 1–7 (2016).

179. McLellan, J. S. *et al.* Structure-based design of a fusion glycoprotein vaccine for respiratory syncytial virus. *Science (80-.).* **342**, 592–598 (2013).

180. Lin, X. *et al.* Self-assembling nanoparticles presenting receptor binding domain and 1 stabilized spike as next-generation COVID-19 vaccines. *bioRxiv* 2020.09.14.296715 (2020) doi:10.1101/2020.09.14.296715.

181. Hollingshead, S. *et al.* Structure-based design of chimeric antigens for multivalent protein vaccines. *Nat. Commun.* **9**, 1–10 (2018).

182. Ishino, T. *et al.* Engineering a monomeric Fc domain modality by N-glycosylation for the half-life extension of biotherapeutics. *J. Biol. Chem.* **288**, 16529–37 (2013).

183. Malkin, E. M. *et al.* Phase 1 clinical trial of apical membrane antigen 1: An asexual blood-stage vaccine for Plasmodium falciparum malaria. *Infect. Immun.* **73**, 3677–3685 (2005).

184. Rijal, P. *et al.* Therapeutic Monoclonal Antibodies for Ebola Virus Infection Derived from Vaccinated Humans. *Cell Rep.* **27**, 172-186.e7 (2019).

185. Predonzani, A., Arnoldi, F., López-Requena, A. & Burrone, O. R. In vivo site-specific biotinylation of proteins within the secretory pathway using a single vector system. (2008) doi:10.1186/1472-6750-8-41.

186. Ho, I. Y. *et al.* Refined protocol for generating monoclonal antibodies from single human and murine B cells. *J. Immunol. Methods* **438**, 67–70 (2016).

187. Pollack, Y., Katzen, A. L., Spira, D. T. & Golenser, J. The genome of Plasmodium falciparum. I: DNA base composition. *Nucleic Acids Res.* **10**, 539–46 (1982).

188. Nikbakht, H., Xia, X., Hickey, D. A. & Golding, B. The evolution of genomic GC content undergoes a rapid reversal within the genus Plasmodium. *Genome* **57**, 507–511 (2014).

189. Narum, D. L. *et al.* Codon optimization of gene fragments encoding Plasmodium falciparum merzoite proteins enhances DNA vaccine protein expression and immunogenicity in mice. *Infect. Immun.* **69**, 7250–7253 (2001).

190. Angov, E., Hillier, C. J., Kincaid, R. L. & Lyon, J. A. Heterologous Protein Expression Is Enhanced by Harmonizing the Codon Usage Frequencies of the Target Gene with those of the Expression Host. *PLoS One* **3**, e2189 (2008).

191. Pizzi, E. & Frontali, C. Low-Complexity Regions in Plasmodium falciparum Proteins. *Genome Res.* **11**, 218–229 (2001).

192. Feng, Z. P. *et al.* Abundance of intrinsically unstructured proteins in P. falciparum and other apicomplexan parasite proteomes. *Mol. Biochem. Parasitol.* **150**, 256–267 (2006).

193. Stephens, L. L., Shonhai, A. & Blatch, G. L. Co-expression of the Plasmodium falciparum molecular chaperone, PfHsp70, improves the heterologous production of the antimalarial drug target GTP cyclohydrolase I, PfGCHI. *Protein Expr. Purif.* **77**, 159–165 (2011).

194. Cottingham, M. G. *et al.* Preventing spontaneous genetic rearrangements in the transgene cassettes of adenovirus vectors. *Biotechnol. Bioeng.* **109**, 719–728 (2012).

195. von Itzstein, M., Plebanski, M., Cooke, B. M. & Coppel, R. L. Hot, sweet and sticky: the glycobiology of Plasmodium falciparum. *Trends Parasitol.* **24**, 210–218 (2008).

196. Tajik, S. *et al.* Characterization of Glycoproteins of Native 19kDa C-Terminal Merozoite Surface Protein-1 from Native Antigen of Plasmodium falciparum. *J. Arthropod. Borne. Dis.* **13**, 324–333 (2019).

197. Samuelson, J. *et al.* The diversity of dolichol-linked precursors to Asn-linked glycans likely results from secondary loss of sets glycosyltranferases. *Proc. Natl. Acad. Sci. U. S. A.* **102**, 1548–1553 (2005).

198. Aguiar, J. C. *et al.* High-throughput generation of P. falciparum functional molecules by recombinational cloning. *Genome Res.* **14**, 2076–2082 (2004).

199. Berkmen, M. Production of disulfide-bonded proteins in Escherichia coli. *Protein Expression and Purification* vol. 82 240–251 (2012).

200. Rodriguez, M., Lustigman, S., Montero, E., Oksov, Y. & Lobo, C. A. PfRH5: A novel reticulocyte-binding family homolog of Plasmodium falciparum that binds to the erythrocyte, and an investigation of its receptor. *PLoS One* **3**, e3300 (2008).

201. Dyring, C. Optimising the Drosophila S2 expression system for production of therapeutic vaccines. *Bioprocess. J.* **10**, 28–35 (2011).

202. Illingworth, J. J. *et al.* Functional Comparison of Blood-Stage Plasmodium falciparum Malaria Vaccine Candidate Antigens. *Front. Immunol.* **10**, 1254 (2019).

203. Bartholdson, S. J. *et al.* Semaphorin-7A Is an Erythrocyte Receptor for P. falciparum Merozoite-Specific TRAP Homolog, MTRAP. *PLoS Pathog.* **8**, e1003031 (2012).

204. Lambert, L. H. *et al.* Antigen reversal identifies targets of opsonizing IgGs against pregnancy-associated malaria. *Infect. Immun.* **82**, 4842–4853 (2014).

205. Jin, J. *et al.* Accelerating the clinical development of protein-based vaccines for malaria by efficient purification using a four amino acid C-terminal 'C-tag'. *Int. J. Parasitol.* **47**, 435–446 (2017).

206. Xu, C. & Ng, D. T. W. Glycosylation-directed quality control of protein folding. *Nature Reviews Molecular Cell Biology* vol. 16 742–752 (2015).

207. Yoko-o, T., Wiggins, C. A. R., Stolz, J., Peak-Chew, S. Y. & Munro, S. An N-acetylglucosaminyltransferase of the Golgi apparatus of the yeast Saccharomyces cerevisiae that can modify N-linked glycans. *Glycobiology* **13**, 581–589 (2003).

208. Hirose, S., Shimizu, K., Kanai, S., Kuroda, Y. & Noguchi, T. POODLE-L: a two-level SVM prediction system for reliably predicting long disordered regions. *Bioinformatics* **23**, 2046–53 (2007).

209. Romero, P. *et al.* Sequence complexity of disordered protein. *Proteins Struct. Funct. Bioinforma.* **42**, 38–48 (2001).

210. Shi, J., Blundell, T. L. & Mizuguchi, K. FUGUE: Sequence-structure homology

recognition using environment-specific substitution tables and structure-dependent gap penalties. *J. Mol. Biol.* **310**, 243–257 (2001).

211. Saouros, S. *et al.* A novel galectin-like domain from Toxoplasma gondii micronemal protein 1 assists the folding, assembly, and transport of a cell adhesion complex. *J. Biol. Chem.* **280**, 38583–38591 (2005).

212. Meissner, M. *et al.* A family of transmembrane microneme proteins of Toxoplasma gondii contain EGF-like domains and function as escorters. *J. Cell Sci.* **115**, 563–574 (2002).

213. Reiss, M. *et al.* Identification and characterization of an escorter for two secretory adhesins in Toxoplasma gondii. *J. Cell Biol.* **153**, 563–578 (2001).

214. Thrane, S. *et al.* A novel virus-like particle based vaccine platform displaying the placental malaria antigen VAR2CSA. *PLoS One* **10**, (2015).

215. Peabody, D. S. A viral platform for chemical modification and multivalent display. *J. Nanobiotechnology* **1**, 1–8 (2003).

216. Atcheson, E., Hill, A. V. S. & Reyes-Sandoval, A. A VLP for validation of the Plasmodium falciparum circumsporozoite protein junctional epitope for vaccine development. *npj Vaccines* **6**, 46 (2021).

217. Marcandalli, J. *et al.* Induction of Potent Neutralizing Antibody Responses by a Designed Protein Nanoparticle Vaccine for Respiratory Syncytial Virus. *Cell* **176**, 1420-1431.e17 (2019).

218. Manolova, V. *et al.* Nanoparticles target distinct dendritic cell populations according to their size. *Eur. J. Immunol.* **38**, 1404–1413 (2008).

219. Bachmann, M. F. & Jennings, G. T. Vaccine delivery: A matter of size, geometry, kinetics and molecular patterns. *Nature Reviews Immunology* vol. 10 787–796 (2010).

220. Bachmann, M. F. *et al.* The influence of antigen organization on B cell responsiveness. *Science (80-.).* **262**, 1448–1451 (1993).

221. Bachmann, M. F. & Zinkernagel, R. M. Neutralizing antiviral B cell responses. *Annu. Rev. Immunol.* **15**, 235–270 (1997).

222. Rappuoli, R. & Serruto, D. Self-Assembling Nanoparticles Usher in a New Era of Vaccine Design. *Cell* vol. 176 1245–1247 (2019).

223. Sapsford, K. E. *et al.* Functionalizing nanoparticles with biological molecules: Developing chemistries that facilitate nanotechnology. *Chemical Reviews* vol. 113 1904–2074 (2013).

224. Smith, M. T., Hawes, A. K. & Bundy, B. C. Reengineering viruses and virus-like particles through chemical functionalization strategies. *Current Opinion in Biotechnology* vol. 24 620–626 (2013).

225. Mateu, M. G. Virus engineering: functionalization and stabilization. *Protein*

Eng. Des. Sel. **24**, 53–63 (2011).

226. Taylor, K. M. *et al.* Influence of three-dimensional structure on the immunogenicity of a peptide expressed on the surface of a plant virus. *J. Mol. Recognit.* **13**, 71–82 (2000).

227. Zakeri, B. *et al.* Peptide tag forming a rapid covalent bond to a protein, through engineering a bacterial adhesin. *Proc. Natl. Acad. Sci.* **109**, E690–E697 (2012).

228. Brune, K. D. *et al.* Plug-and-Display: decoration of Virus-Like Particles via isopeptide bonds for modular immunization. *Sci. Rep.* **6**, 19234 (2016).

229. Jin, J. *et al.* Production, quality control, stability, and potency of cGMP-produced Plasmodium falciparum RH5.1 protein vaccine expressed in Drosophila S2 cells. **3**, 32 (2018).

230. Benne, N., van Duijn, J., Kuiper, J., Jiskoot, W. & Slütter, B. Orchestrating immune responses: How size, shape and rigidity affect the immunogenicity of particulate vaccines. *Journal of Controlled Release* vol. 234 124–134 (2016).

231. Jia, R., Guo, J. H. & Fan, M. W. The effect of antigen size on the immunogenicity of antigen presenting cell targeted DNA vaccine. *Int. Immunopharmacol.* **12**, 21–25 (2012).

232. Vragniau, C. *et al.* Synthetic self-assembling ADDomer platform for highly efficient vaccination by genetically encoded multiepitope display. *Sci. Adv.* **5**, eaaw2853 (2019).

233. Angeletti, D. *et al.* Outflanking immunodominance to target subdominant broadly neutralizing epitopes. *Proc. Natl. Acad. Sci. U. S. A.* **116**, 13474–13479 (2019).

234. Popovici, J. *et al.* Amplification of Duffy binding protein-encoding gene allows Plasmodium vivax to evade host anti-DBP humoral immunity. *Nat. Commun.* **11**, 1–9 (2020).

235. Julien, J. P. & Wardemann, H. Antibodies against Plasmodium falciparum malaria at the molecular level. *Nat. Rev. Immunol.* (2019).

236. Köhler, G. & Milstein, C. Continuous cultures of fused cells secreting antibody of predefined specificity. *Nature* **256**, 495–497 (1975).

237. Olsson, L. & Kaplan, H. S. Human-human hybridomas producing monoclonal antibodies of predefined antigenic specificity. *Proc. Natl. Acad. Sci. U. S. A.* **77**, 5429–5431 (1980).

238. Lee, E.-C. C. *et al.* complete humanization of the mouse immunoglobulin loci enables efficient therapeutic antibody discovery. *Nat. Biotechnol.* **32**, 356–363 (2014).

239. Tiller, T. *et al.* Efficient generation of monoclonal antibodies from single human B cells by single cell RT-PCR and expression vector cloning. *J. Immunol. Methods* **329**, 112–124 (2008).

240. Tiller, T., Busse, C. E. & Wardemann, H. Cloning and expression of murine Ig genes from single B cells. *J. Immunol. Methods* **350**, 183–193 (2009).

241. Crosnier, C. C., Staudt, N. & Wright, G. J. *A rapid and scalable method for selecting recombinant mouse monoclonal antibodies*. *BMC Biology* vol. 8 76 (2010).

242. Eyer, K. *et al.* Single-cell deep phenotyping of IgG-secreting cells for high-resolution immune monitoring. *Nat. Biotechnol.* **35**, 977–982 (2017).

243. Gérard, A. *et al.* High-throughput single-cell activity-based screening and sequencing of antibodies using droplet microfluidics. *Nat. Biotechnol.* 1–7 (2020) doi:10.1038/s41587-020-0466-7.

244. Williams, A. R. *et al.* Enhancing Blockade of Plasmodium falciparum Erythrocyte Invasion: Assessing Combinations of Antibodies against PfRH5 and Other Merozoite Antigens. *PLoS Pathog.* **8**, e1002991 (2012).

245. Liaw, P. C. Y., Ferrell, G. & Esmon, C. T. A monoclonal antibody against activated protein C allows rapid detection of activated protein C in plasma and reveals a calcium ion dependent epitope involved in factor Va inactivation. *J. Thromb. Haemost.* **1**, 662–670 (2003).

246. Kanjee, U., Rangel, G. W., Clark, M. A. & Duraisingh, M. T. Molecular and cellular interactions defining the tropism of Plasmodium vivax for reticulocytes. *Current Opinion in Microbiology* vol. 46 109–115 (2018).

Chapter 8 - Appendix

8.1 PfRIPR fragments do not form a complex with PfRH5 and PfCyRPA

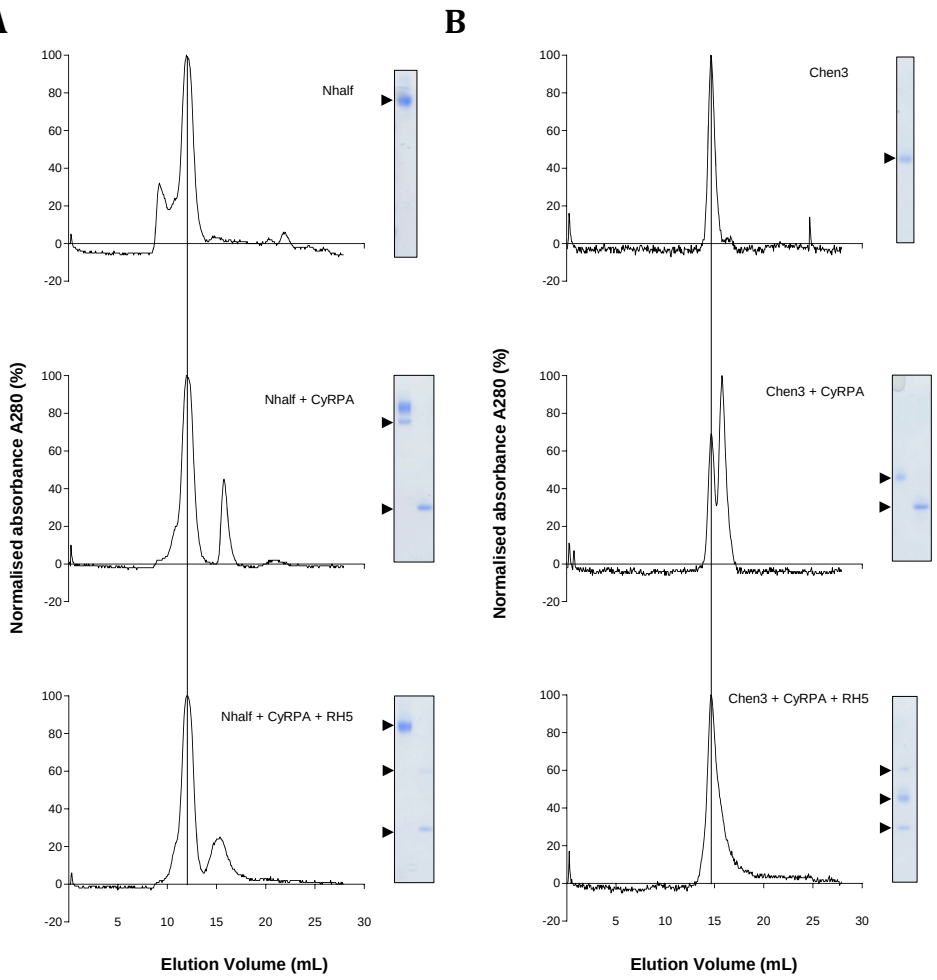


Figure 8.1 – SEC chromatograms of the Nhalf and Chen3 PfRipr fragments.
A) SEC trace of purified monoFc fused PfRIPR Nhalf individually and as a complex. SDS-PAGE gels are shown to the right. Top panel: PfRIPR Nhalf, expected MW 88 kDa. Middle panel: PfRIPR Nhalf (peak 1) and PfCyRPA (peak 2), expected bands 88 kDa and 42 kDa respectively. Bottom panel: PfRIPR Nhalf, PfCyRPA and PfRH5, expected band sizes 88 kDa, 42kDa and 58 kDa. **B)** SEC trace of purified monoFc fused PfRIPR Chen3 individually and as a complex. SDS-PAGE gels are shown to the right. Top panel: PfRIPR Chen3, expected MW 41 kDa. Middle panel: PfRIPR Chen3 (peak 1) and PfCyRPA (peak 2), expected bands 41 kDa and 42 kDa respectively. Bottom panel: PfRIPR Chen3, PfCyRPA and PfRH5, expected band sizes 41 kDa, 42kDa and 58 kDa. The shift in the bottom panel shows that CyRPA and RH5 interact as expected but not with PfRIPR Chen3. A straight line is added for clarity to show the peak of PfRIPR EGF (3-6) and Chen3, which does not shift in any experiment

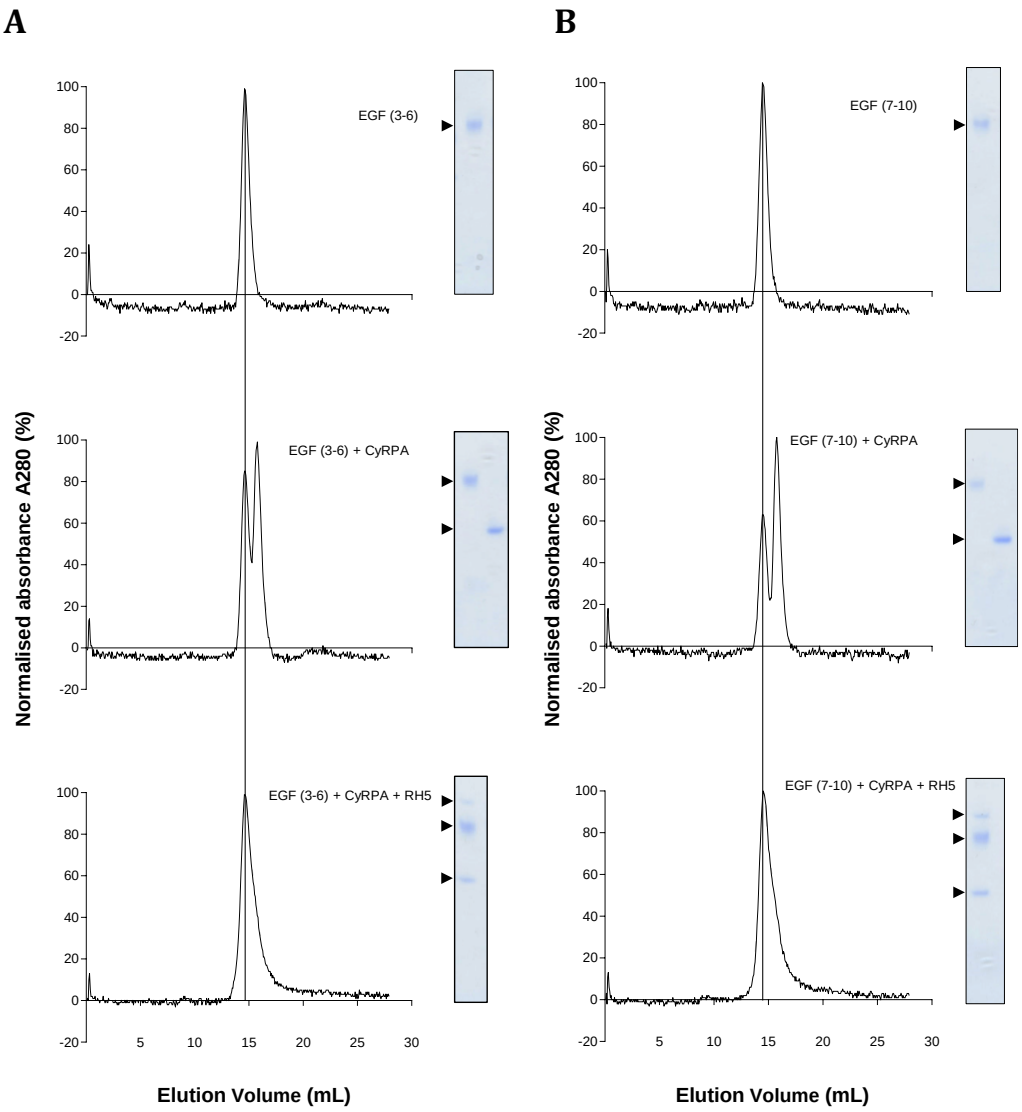


Figure 8.2 - SEC chromatograms of the EGF (3-6) and EGF (7-10) PfRipr fragments. **A)** SEC trace of purified monoFc fused PfRIPR EGF (3-6) individually and as a complex. SDS-PAGE gels are shown to the right. Top panel: PfRIPR EGF (3-6), expected MW 46 kDa. Middle panel: PfRIPR EGF (3-6) (peak 1) and PfCyRPA (peak 2), expected bands 46 kDa and 42 kDa respectively. Bottom panel: PfRIPR EGF (3-6), PfCyRPA and PfRH5, expected band sizes 46 kDa, 42kDa and 58 kDa. The shift in the bottom panel shows that CyRPA and RH5 interact as expected but not with PfRIPR EGF (3-6). A straight line is added for clarity to show the peak of PfRIPR EGF (3-6), which does not shift in any experiment. **B)** SEC trace of purified monoFc fused PfRIPR EGF (7-10) individually and as a complex. SDS-PAGE gels are shown to the right. Top panel: PfRIPR EGF (7-10), expected MW 44 kDa. Middle panel: PfRIPR EGF (7-10) (peak 1) and PfCyRPA (peak 2), expected bands 44 kDa and 42 kDa respectively. Bottom panel: PfRIPR EGF (7-10), PfCyRPA and PfRH5, expected band sizes 44 kDa, 42kDa and 58 kDa. The shift in the bottom panel shows that CyRPA and RH5 interact as expected but not with PfRIPR EGF (7-10). A straight line is added for clarity to show the peak of PfRIPR EGF (3-6), which does not shift in any experiment

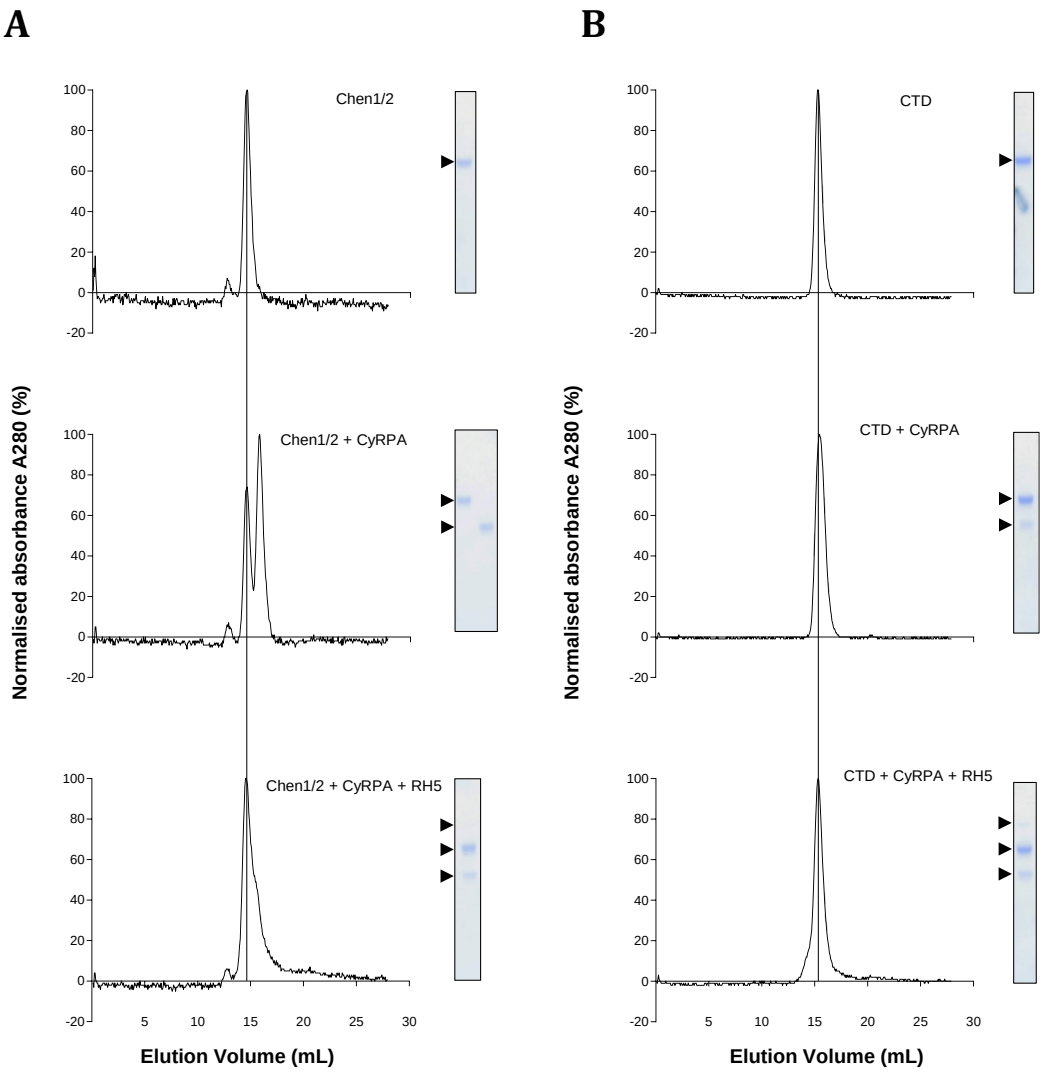


Figure 8.3 - SEC chromatograms of the Chen1/2 and C-terminal domain (CTD) PfRipr fragments.

Left: SEC trace of purified monoFc fused PfRIPR Chen1/2 individually and as a complex. SDS-PAGE gels are shown to the right. Top panel: PfRIPR Chen1/2, expected MW 39 kDa. Middle panel: PfRIPR Chen1/2 (peak 1) and PfCyRPA (peak 2), expected bands 39 kDa and 42 kDa respectively. Bottom panel: PfRIPR Chen1/2, PfCyRPA and PfRH5, expected band sizes 39 kDa, 42kDa and 58 kDa. **Right:** SEC trace of purified monoFc fused PfRIPR CTD individually and as a complex. SDS-PAGE gels are shown to the right. Top panel: PfRIPR Chen3, expected MW 39 kDa. Middle panel: PfRIPR CTD (peak 1) and PfCyRPA (peak 2), expected bands 39 kDa and 42 kDa respectively. Bottom panel: PfRIPR CTD, PfCyRPA and PfRH5, expected band sizes 39 kDa, 42kDa and 58 kDa. The shift in the bottom panel shows that CyRPA and RH5 interact as expected but not with PfRIPR Chen3. A straight line is added for clarity to show the peak of PfRIPR Chen1/2 and CTD, which does not shift in any experiment

8.2 Non-neutralising mAbs bind and disrupt the RCR complex

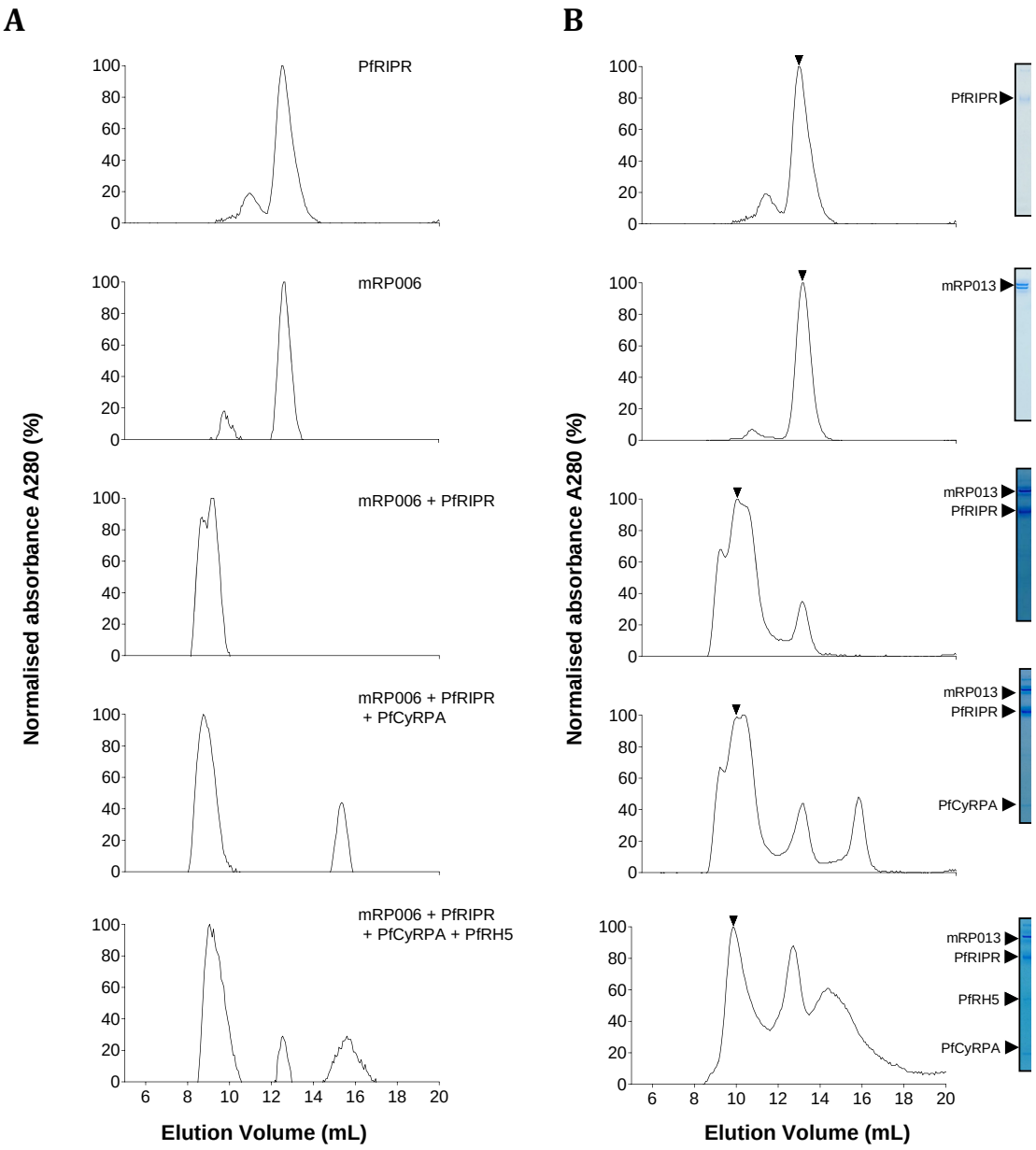


Figure 8.4 – mRP006 and mRP013 binding to the RCR complex.
SEC profiles show PfRIPR, mAb, PfCyRPA, and PfRH5 run individually and in complex, SEC chromatogram peaks were run on an SDS-PAGE gel to visualise which proteins were present. **A)** mRP006 binds the RCR complex forming. mRP006 binds to PfRIPR and, PfRIPR in complex with CyRPA, and forms a quaternary mRP004-RCR complex (bottom panel). **B)** mRP013 can bind to the RCR complex forming a quaternary mRP016-RCR complex (bottom panel).

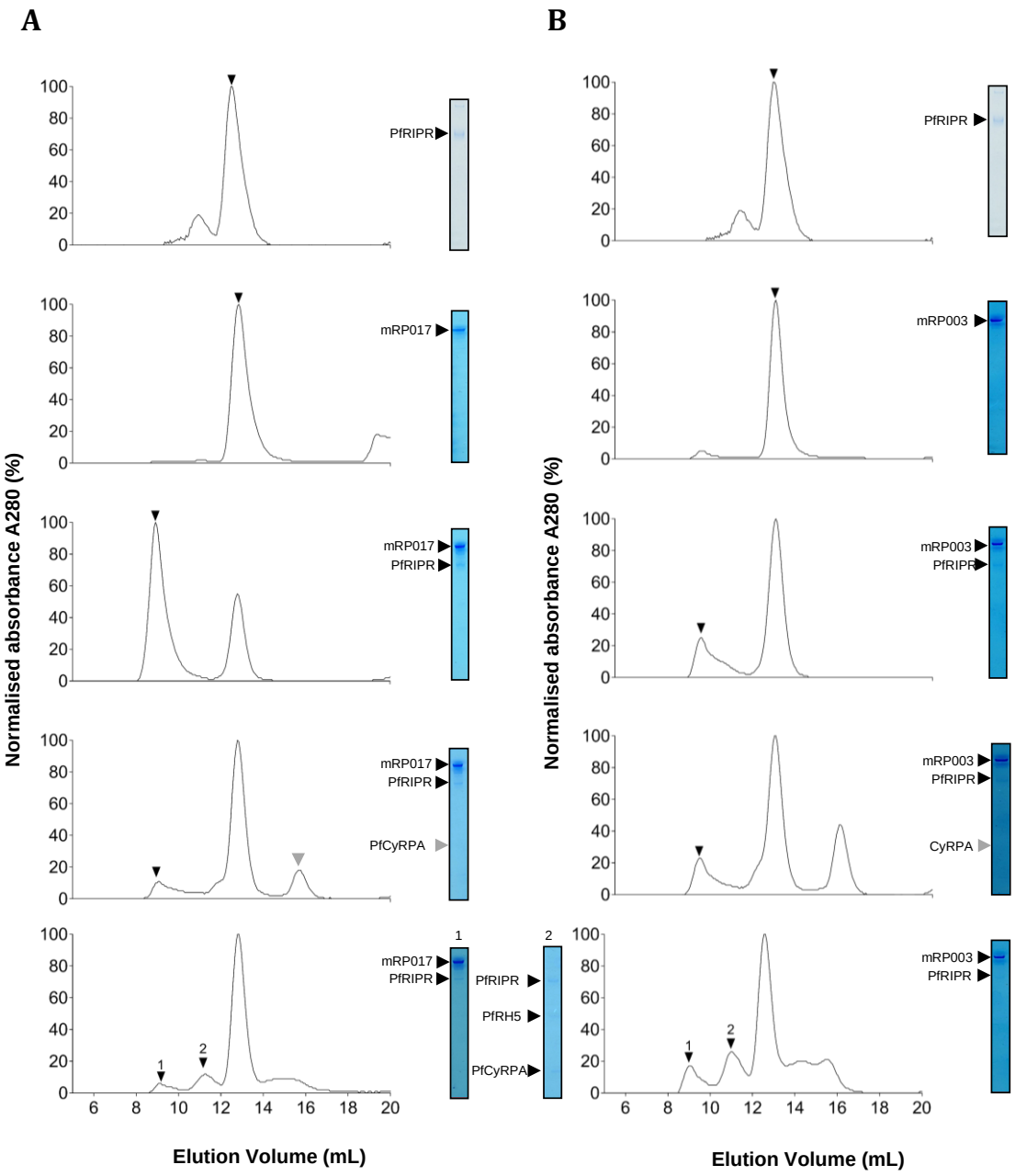


Figure 8.5 - mRP017 and mRP003 binding to the RCR complex.
SEC profiles show PfRIPR, mAb, PfCyRPA, and PfRH5 run individually and in complex, SEC chromatogram peaks were run on an SDS-PAGE gel to visualise which proteins were present. **A)** mRP017 prevents the RCR complex forming. mRP017 binds to PfRIPR and, PfRIPR in complex with CyRPA, but cannot form a quaternary mRP017-RCR complex (bottom panel). **B)** mRP003 can bind to PfRIPR but cannot form any higher order complexes.

8.3 Antigen reversal GIA using PfRIPR EGF (5-8) – PfCyRPA fusion protein

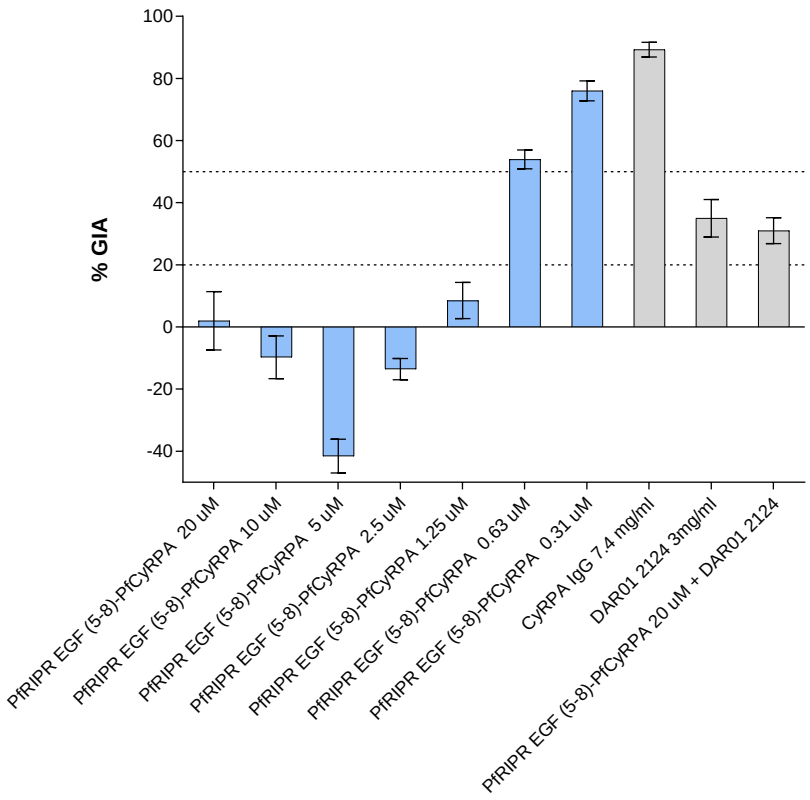


Figure 8.6 - Antigen reversal of anti-PfCyRPA purified IgG held at 7.4mg/mL with a titration of PfRIPR-EGF (5-8) – PfCyRPA fusion starting at 0.31µM
Antigen reversal of anti-CyRPA purified IgG held at 7.4mg/mL with a titration of PfRIPR-EGF (5-8) – PfCyRPA fusion starting at 0.31µM. Grey bars are controls: PfCyRPA purified IgG held at 7.4 mg/mL, DAR01 2124: Purified anti-PfRH5 IgG held at 3 mg/mL. 20µM PfRIPR-EGF (5-8)-PfCyRPA with DAR01 2124 anti-PfRH5 purified IgG held at 3 mg/mL. Dashed lines at 20% GIA (the LLQ of the assay) and 50% GIA for reference.

8.4 Full GIA results from Study O2

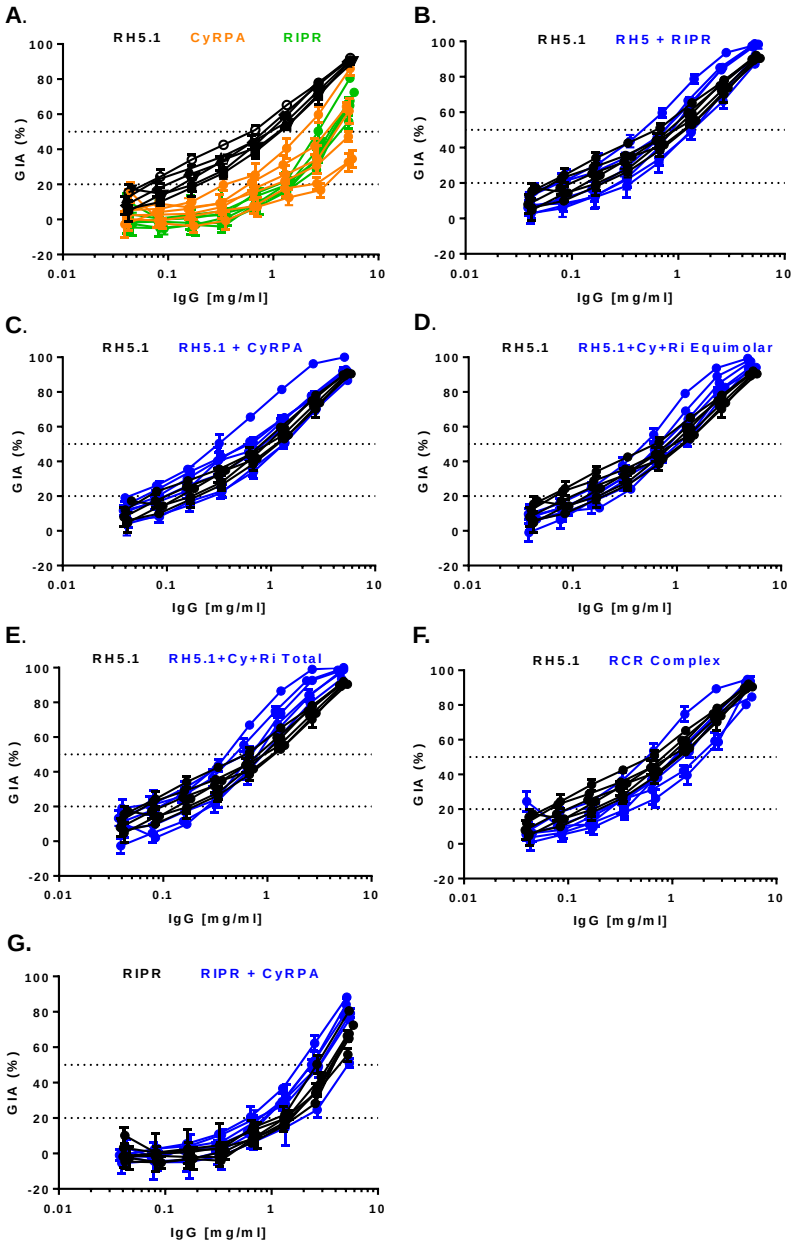


Figure 8.7 - Single cycle GIA assay results for Study O2 groups using *P. falciparum* clone 3D7.

Dilution curves of purified IgG from day 70 terminal bleeds. **A)** RH5.1 vs PfCyRPA vs PfRIPR; **B)** RH5.1 vs RH5.1+ PfRIPR; **C)** RH5.1 vs RH5.1+ PfCyRPA; **D)** RH5.1 vs RH5.1+ PfCyRPA + PfRIPR (Equimolar Dosing); **E)** RH5.1 vs RH5.1+ PfCyRPA + PfRIPR; **F)** RH5.1 vs RCR Complex; and **G)** PfRIPR vs PfCyRPA + PfRIPR. Each line represents an individual animal and each point represents the mean of three technical replicates, with the bars depicting the mean +/- the standard deviation. Dotted lines are shown at 20% and 50% GIA. Results are considered GIA negative if the % GIA is less than 20%.